MECHANISTIC INSIGHT INTO ELECTROCATALYTIC HYDROGENOLYSIS/HYDROGENATION OF ARYL ETHERS OVER SKELETAL NICKEL SURFACE IN AQUEOUS PHASE

BY

Yuting Zhou

A DISSERTATION

Submitted to
Michigan State University
in partial fulfillment of the requirement
for the degree of

Chemistry—Doctor of Philosophy

2021

ABSTRACT

MECHANISTIC INSIGHT INTO ELECTROCATALYTIC HYDROGENOLYSIS/HYDROGENATION OF ARYL ETHERS OVER SKELETAL NICKEL SURFACE IN AQUEOUS PHASE

BY

Yuting Zhou

Catalytic strategies to complete the cycle of carbon and energy are urgently needed, as they are the key to mitigating the severe challenges of climate change and surface water pollution, while addressing the world's energy needs. To replace conventional petroleum-derived chemical products and energy, utilization of renewable carbon resources in biomass is critical and simple procedures to break down persistent organic pollutants are also needed. This dissertation presents a mild (ambient pressure at 60 °C) and effective heterogeneous catalytic strategy that uses skeletal nickel cathodes to electrocatalytically upgrade a variety of aryl ethers and alkyl aryl ethers into simplified, higher energy species by converting them into more valuable smaller aromatic monomers. To successfully breakdown the C-O ether bonds in water insoluble aryl ether substrates, we surveyed different organic co-solvents to achieve the optimal electrocatalytic hydrogenolysis/hydrogenation (ECH) conditions. Importantly, based on the combined observations from rate comparisons, substrate competitions, substituent studies, isotope labeling experiments, and regioselectivity investigations several distinct C-O cleavage mechanisms of these structurally varied aryl ethers were identified. These efforts and insights not only offer guidance to enable rational design of future catalytic approaches, but also reveal the electrocatalyst's ability to achieve the defluorinations of fluorinated aryl ethers bearing sp^2 or sp^3 C-F bonds.

ACKNOWLEDGEMENTS

With gratitude, I want to thank many individuals in the beginning; this work would not have been achieved without the guidance and contributions from them. First, I want to thank my advisor, Dr. James (Ned) E. Jackson. Ned has been a rock of support of everything since I the day that I joined the lab. I am so appreciated to have Ned as my doctoral advisor who is willing to give his student maximum degree of freedom in their research. Every conversation with Ned always led to more ideas and more understandings towards the results that I observed. I am beyond grateful for the wide latitude that Ned encouraged me to hypothesize and as well as to examine. This embedded the curious mindset in me, and I believe no matter where I end up landing at, no matter how old I am, I will always carry this curiosity through my entire career/life.

I want to thank my committee members Dr. William Wulff, Dr. Christopher Saffron, Dr. Angela Wilson and Dr. Greg Swain for their willingness to listen and answer my questions. Many thanks to every committee member, who spent their time in reading all the page proofs for this dissertation.

I acknowledge with gratitude Dr. Eric Hegg from Department of Biochemistry and Molecular Biology and Dr. Christopher Saffron from Department of Biosystems and Agricultural Engineering for funding these projects. I am grateful for the collaborations with both Dr. Hegg and Dr. Saffron, without their numerous supports, these projects will not proceed as they were.

I want to thank my first-year graduate courses instructors Dr. William Wulff and Dr. Babak Borhan for their willingness to care and listen. As a first-year graduate student who do not have any research experience in chemistry, Dr. Wulff and Dr. Borhan have helped me in developing

passion in learning organic reactions and as well as to appreciate the beauty of synthesis. I am beyond grateful for all the wise suggestions and patient listens that Dr. Wulff has offered me.

I would also like to acknowledge Dr. Dan Holmes, Dr. Dan Jones and Dr. Cassandra Johnny who helped me with NMR and mass spec facilities, and Dr. Jackson (Ned) for his computational supports. I want to thank Dr. Hadi Gholami, Dr. Yukari Nishizawa-Brennen and Dr. Pengchao Hao for mentoring and guiding me in experimental set up and synthesis during my first year in graduate research.

During my time in Michigan State University, I'm lucky to have all the company and support from my friends and group members in Jackson lab. I want to thank the Jackson lab for the wonderful time and memories: Dr. Gracielou Klinger, Dr. Zhen Fang, Dr. Pengchao Hao, Dr. Mahlet Garedew, Dr. Mikhail Redko, Dr. Tayeb Kakeshpour, Dr. Benjamin Appiagyei, Sophie Bedford, Bill Killian, Monique Noel and Cesar Plascencia. Most importantly, I want to Ned for holding us together and making everything such memorable. I would also like to thank my friends: Katarina Keel, Mengxia Sun, Jose Montero, Seokjoo Lee, Kiyoto Tanemura, Zhilin Hou, Alex Oconnell and Saeedeh Torabikohlbouni for the great company and support, graduate school will be very different without my dear friends.

Lastly, I want to thank my parents Xiancheng Zhou, Runlan Zhang and my younger brother Shibin Zhou for their understanding and supports. I have been in a different country for near ten years, more than one third of my life. Words cannot describe how they feel and how I feel, but their understanding is priceless for me.

TABLE OF CONTENTS

LIST OF TABLES

LIST OF FIGURES

KEY TO SYMBOLS AND ABBREVIATIONS

4-O-5	phenoxyphenol
5-5	biphenyl
α-O-4/β-5	phenylcoumaran
β-β	pinoresionol
β-1	diaryl propane
β-O-4	β-aryl ether
CTH	catalytic transfer hydrogenolysis
DAE	diaryl ether
DCM	dichloromethane
DDQ	2,3-dichloro-5,6-dicyano-1,4-benzoquinone
DFT	density functional theory
DPE	diphenyl ether
ECH	electrocatalytic hydrogenolysis/hydrogenation
GC-MS	gas chromatography-mass spectrometry
GPC	gel permeation chromatography
HSQC	heteronuclear single quantum coherence spectroscopy
IPA	isopropyl alcohol/2-propanol
NMR	nuclear magnetic resonance spectroscopy
POP	persistent organic pollutant
RVC	reticulated vitreous carbon
SEM	scanning electron microscopy
TEM	transmission electron microscopy

Chapter 1 Introduction to Catalytic Cleavage of Aryl Ethers

1.1 Importance of Aryl Ethers: Applications and Motivations for Cleavage

1.1.1 Aryl Ether --- Linkages in Lignin --- Road to Biomass Utilization

In recent years, the increasing frequency of large wildfires across continents has been a critical indicator of the progressively more severe global warming, largely triggered from the rise in atmosphere carbon dioxide level.[1-4] Meanwhile, ongoing consumption of fossil resources has introduced another global crisis, shortages of energy and carbon resources. Researchers are therefore searching for renewable and sustainable sources to replace the conventional petroleum-based production of energy and chemicals.[5-7] Utilization of biomass is the key to achieve the goal of mitigating the global climate change and addressing the demand for renewable energy and carbon resources (Figure 1.1).

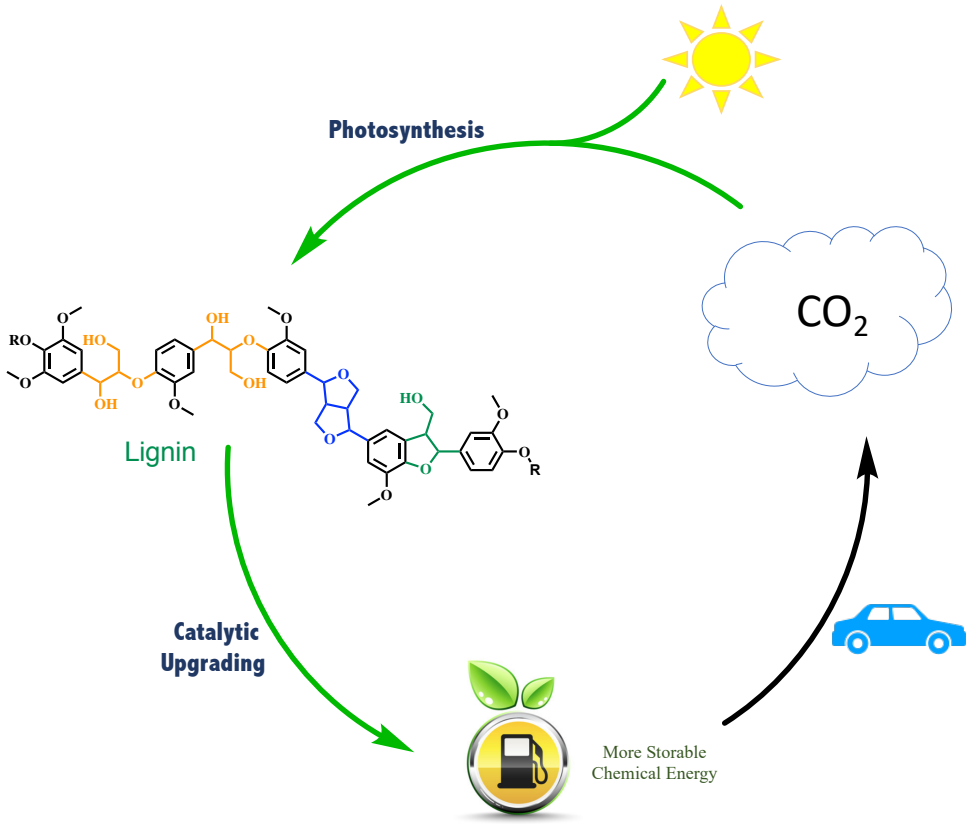

Figure 1.1 Cycle of carbon and energy

Lignin accounts for 15-30 wt% of total biomass, and its high carbon content (~30%) ensures its high heating value for energy conversion.[5, 8] With its varied, crosslinked methoxyphenolic moieties, lignin is also an ideal natural source for the production of small chemical building blocks.[6, 7, 9-12] As shown in Figure 1.1, to utilize this carbon-rich and energy-dense natural resource and to complete the cycle of energy and carbon, new catalytic tools are urgently needed.

Historically treated as waste product from pulp industry, lignin's recalcitrant crosslinked aromatic phenylpropanoid subunits make the depolymerization process energy intensive and costly. In the biosynthesis of lignin, three phenylpropanoid subunits with varied degree of methoxylation – p-coumaryl (H), coniferyl (G), and sinapyl (S) – are linked via radical couplings to produce the complex heterogeneous aromatic polymeric structure (Figure 1.2). The highly conjugated pi system of the phenylpropanoids enables the formation of different free radicals,

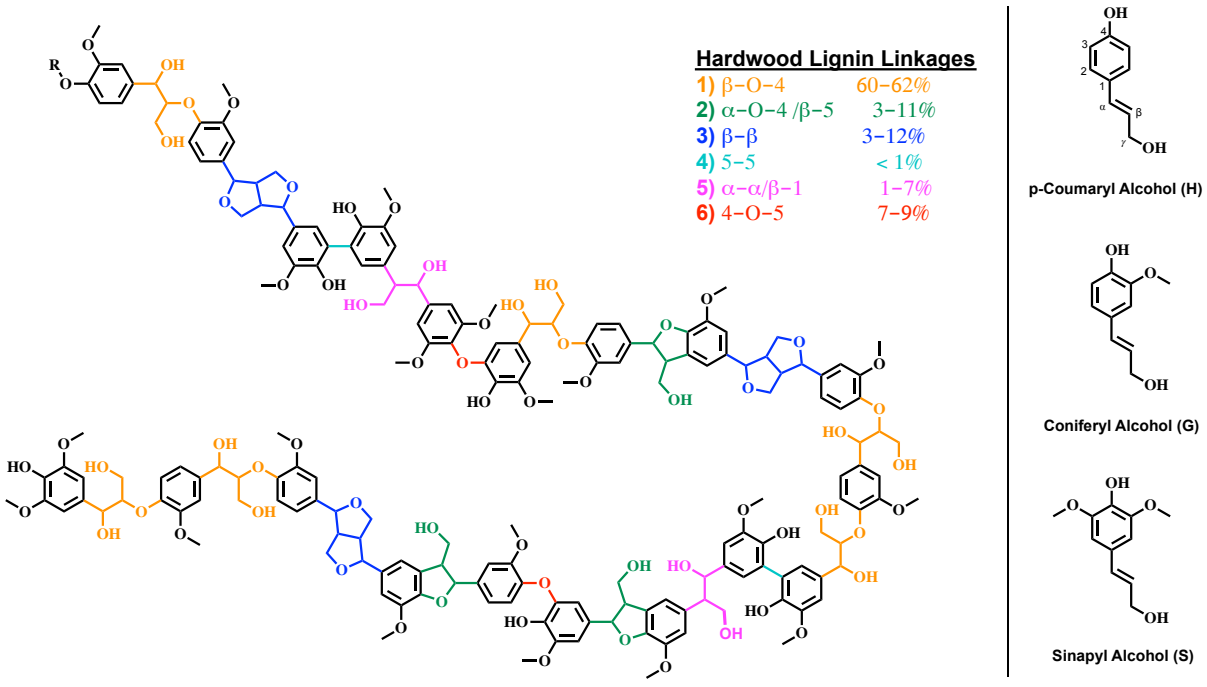

Figure 1.2 (Left) Structure of poplar lignin with linkages highlighted in colors; (Right) the three aromatic monomers.

leading to formation of roughly six different lignin linkages (β-O-4, α-O-4/ β-5, β-β, 5-5, β-1, and 4-O-5, as depicted in Figure 1.2). Among these six linkages, β-O-4 (alkyl aryl ether) composes as much as 60% (hardwood lignin) of the total linkages in this hetero-polymer. At the same time, compared with the other five linkages, the relatively weaker alkyl aryl ether bond in β-O-4 also makes it the easiest and highest priority target to achieve the successful depolymerization of lignin.

Although the high abundance of the β-O-4 linkage gives it a crucial role in the depolymerization of the lignin polymer, other linkages are also important. The amount of monomer production is also highly dependent on the deconstructions of the minor linkages.[13] Compared with the stronger C-C bonds in β-β and β-1 linkages, the relatively weaker C-O bonds in the second most abundant α-O-4 and 4-O-5 linkages are also desirable targets to cleave. Therefore, new chemical tools that enables the successful cleavage of these aryl ethers are the focus in efforts to address today's challenges in energy, sustainability, and environmental sciences.

1.1.2 Aryl Ethers -- Intractable Moieties in Persistent Organic Pollutants -- Pollution Mitigation

Aryl ethers are not only a crucial problem in biomass utilization; they are also among the most troublesome compounds contributing to the alarmingly escalating water contamination (Figure 1.3). Several organic molecules containing specific aromatic ether units that spread widely in the environment have been identified as persistent organic pollutants (POPs), sometimes also known as "forever chemicals". POPs often are introduced to the environment through agrochemicals, pharmaceuticals, and industrial products. Among the varied types of persistent organic pollutants, the diaryl ether-derived compounds (such as polyhalogenated diaryl ethers) are especially disturbing due to their high stability, high toxicity, carcinogenicity, and their broad range of applications.

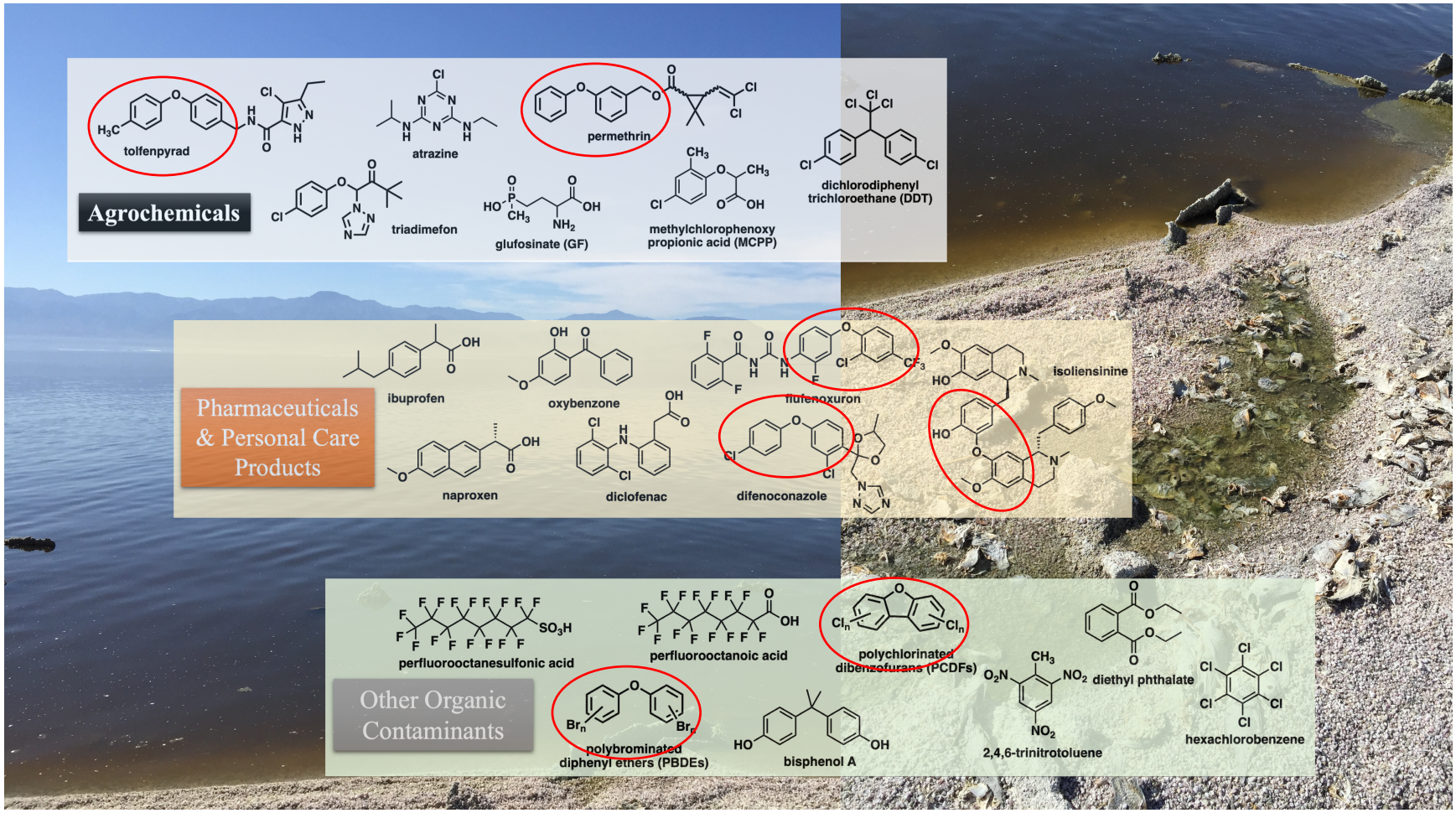

Figure 1.3 Surface water contamination from persistent organic pollutants (POPs). Pictures taken from heavily polluted lake (near large agricultural farming land) in southern California.

Diaryl ethers are recently recognized as the second most popular functional scaffold in the synthesis and discovery of agrochemicals.[14] The outstanding physical properties (cell wall permeability, lipophilicity and hydrophobicity) and chemical stability of these moieties make them resistant to degradation. With their excellent cell wall permeability, these hydrophobic aromatic headgroup are often coupled with other chemically active substituents (alkyl groups, halides, per-halogenated alkyl groups, and acidic/basic groups). Thus, DAE-derived organic molecules have been intensely researched and commercialized for pharmaceutical and agrochemical applications over the past decade.[14, 15] Unfortunately, the accumulation of these agrochemicals and drugs in the environment (soil, animals, surface and ground waters) has also raised significant concerns regarding their breakdown products, which have been identified as a new category of persistent organic pollutants (POPs).[16-19]

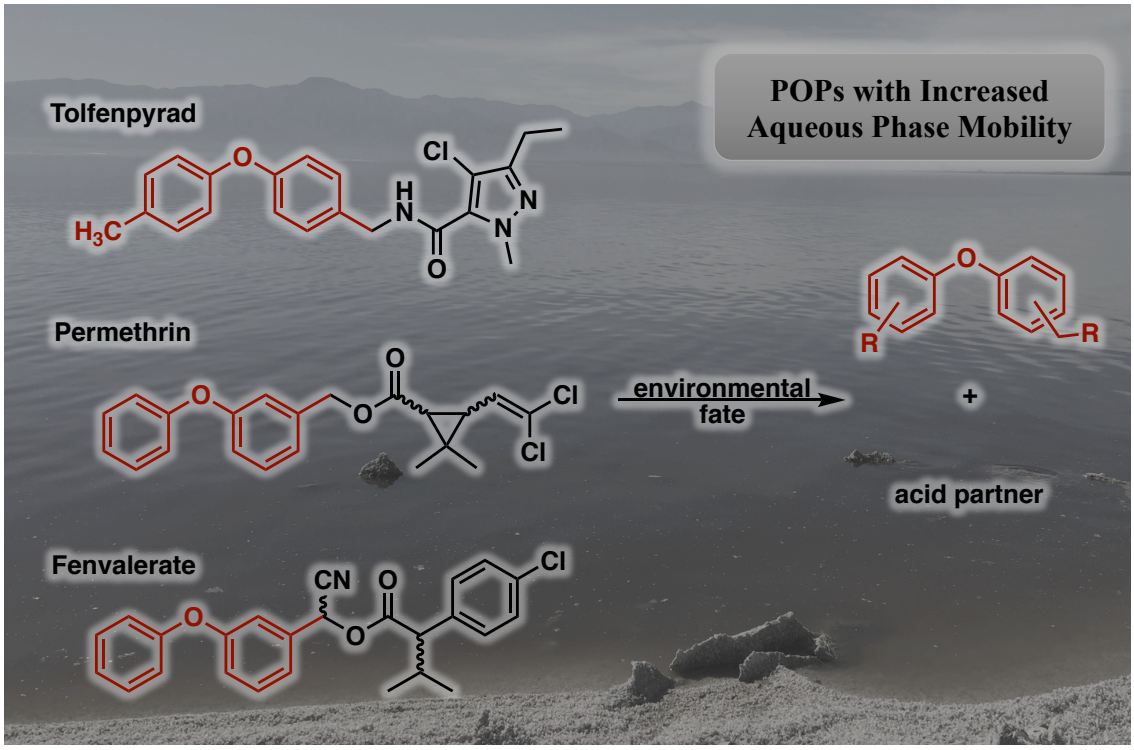

Figure 1.4 The common environmental breakdown products of three representative agrochemicals show enhancing mobility in aqueous system.

As shown in Figure 1.4, different from their hydrophilic polar pendants which commonly contain relatively weaker ester or amide linkages, the carbon rich aromatic diphenyl ether headgroups are often found to resist environmental degradations.[20] A good example is Tolfenpyrad, a recently developed pesticide approved for usage in the US since 2014. It can be partially metabolized in nature via multiple degradation pathways. The methyl group can be oxidized into carboxylic acid or benzyl alcohol through metabolism in animals' bodies, plants, or microorganisms. The amide bond that links together the diaryl ether headgroup and the pyrazole pendant can also undergo hydrolysis in water to form the more polar amino-DAE and corresponding carboxylic acid.[18, 21] However, as summarized in the report,[22] none of the 25 identified environmental fates have successfully broken down the sp^2 C-O bond inside the diphenyl ether headgroup; instead, the increased hydrophilicity from the newly formed functional groups further enhances their environmental mobility.[22] Therefore, catalytic conversion to breakdown aryl ethers is not only important in addressing the climate change issue, it also plays a central role in water pollution mitigation.

1.2 Challenges in the Method Development of Aryl Ethers Cleavage: Water & Selectivity

In recent decades, driven by escalating global crises (energy and drinking water shortages), a series of chemical strategies and processing technologies have been developed by the scientific community for biomass upgrading and for wastewater treatment to remove various persistent organic pollutants. However, among the challenges that still need to be addressed is the development of catalytic methods to break down the aryl ether moieties in biomass and persistent pollutants.

Due to the highly crosslinked and stabilized aryl ether bonds inside the lignin polymer, it resists most depolymerization methods; harsh reaction conditions (high temperature and high pressure) and acid promoted chemical processes often introduce additional crosslinking (formation of stronger C-C bonds) upon the depolymerization.[23, 24] To avoid this additional crosslinking, while still breaking the β-O-4 ether bonds, many efforts have focused on development of mild reaction conditions. Different chemical and catalytic methodologies have been explored to avoid the condensation of those oxygen enriched lignin linkages. But these reactive methodologies that enable the C-O cleavage under mild conditions are usually accompanied with reactive species (e.g. molecular metal complexes[25-28]), which are often sensitive to water and air. However, water is an unavoidable compound in both biomass processing and pollution mitigation. Thus, valorization methods should at least satisfy two boundary conditions: first, it should be able to run at mild reaction condition; second, it should be compatible with water.

Another important challenge for the catalytic development of aryl ether cleavage is the control of reaction selectivity. Notably, the homolytic bond dissociation energies of sp^3 C-O (74 kcal/mol) and sp^2 C-O (86 kcal/mol) ether bonds in these aryl ethers were high.[29] It can therefore require high energy inputs to successfully cleave these ether bonds, as in the case of classical catalytic hydrogenation/hydrogenolysis at high temperatures and high pressures. These catalytic strategies generally have very low reaction selectivity, which significantly limits the economic valorization of these carbon resources.

1.3 Homogeneous Molecular Catalysis Methods of Cleaving Aryl Ethers

Aryl ethers are often found as important synthetic intermediates; for example, methoxy is a good directing group for many C-H functionalization processes (Friedel-Crafts, electrophilic

aromatic substitutions, and ortho-metalation). The critical role of ether substituents as directing functionalities has prompted studies to achieve the selective cleavage of aryl ethers using single metal molecular catalysts. In 2010, Martin and co-workers reported the first nickel metal complex that could catalyze reductive cleavage of methoxy groups from different aromatic systems (Figure 1.5), which opened the door for homogeneous catalytic cleavage of aryl ether C-O bonds.[25] Later, Hartwig and co-workers demonstrated the successful reductive cleavage of sp^2 C-O bonds in a diaryl ether system using $Ni(COD)_2$ with a N-heterocyclic carbene ligand.[26] Moving beyond Ni, Ellman and co-workers reported a tandem catalytic strategy using a ruthenium complex $RuH_2(CO)(PPh_3)_3$ to accomplish the cleavage of the sp^3 C-O ether bond in 2-phenoxy-1-

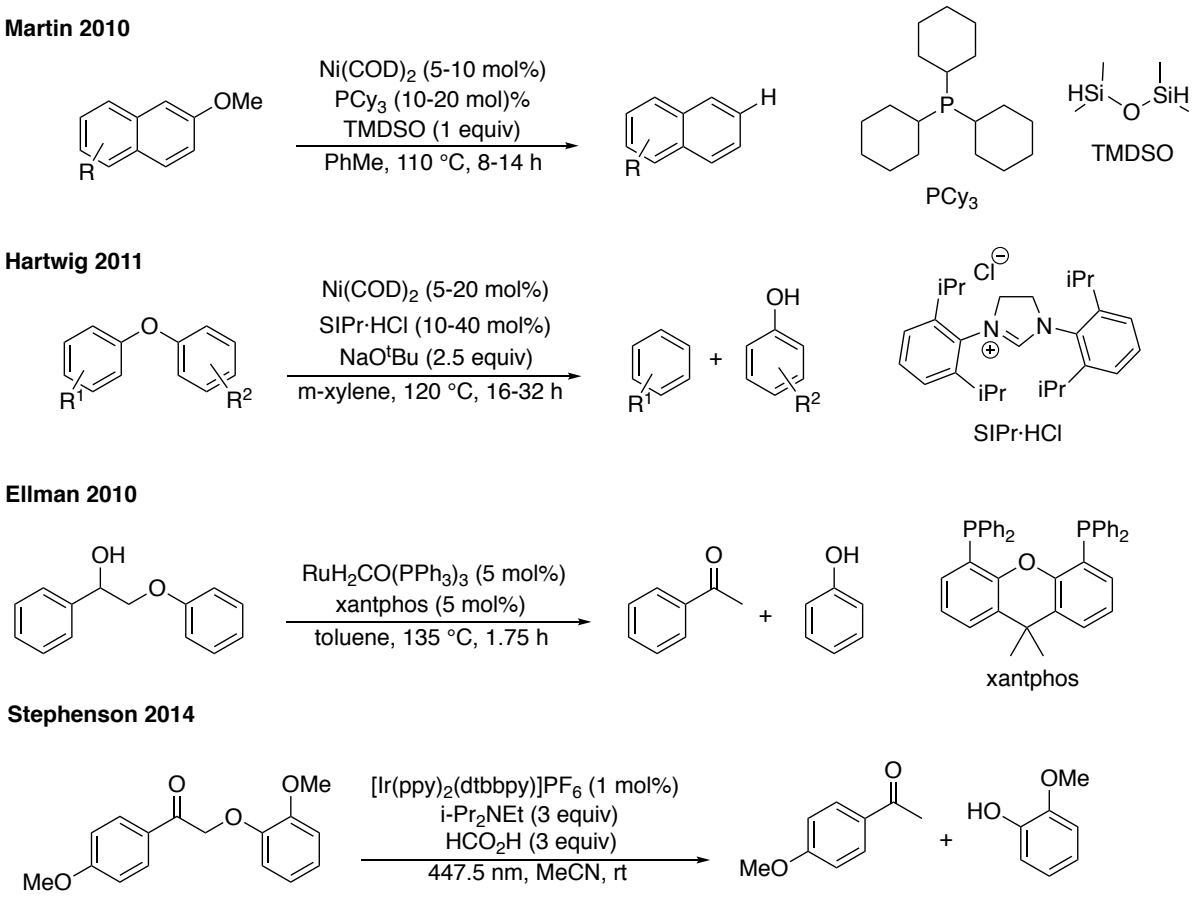

Figure 1.5 Different reported homogeneous catalytic strategies for aryl ether cleavages.

phenylethan-1-ol, a model compound representating the β-O-4 linkage in the lignin polymer.[27] Single transition-metal complexes can also be use as photocatalysts to enable the degradation of lignin ether linkage; Stephenson and co-workers presented a visible-light activated cleavage approach to successfully break down the C-O ether bond via usage of $[Ir(ppy)_2(dtbbpy)]PF_6$ complex.[30]

The above homogeneous organometallic methods do provide good selectivity and excellent reduction control in ether bond cleavage. However, the transition metal complexes used in these methodologies tend to be sensitive to air and water, typically requiring dry organic solvents and inert atmosphere conditions. Meanwhile, some also required specialized ligands to coordinate their metal centers, which demand extra synthetic procedures both to build these unique precursors and in assembling the active catalysts. Importantly, biomass and organic pollutants are both surrounded by water and distributed in the non-inert natural environment. Although these homogeneous catalytic methods have outstanding reaction selectivities, water is still the number one issue for the practical application of these methodologies in both biomass utilization and pollution mitigation.

1.4 Heterogeneous Catalytic Methods in Cleaving Aryl Ethers

As discussed, interaction with water is unavoidable in biomass processing and wastewater treatment. Compared to the delicate molecular metal complexes, the more robust heterogeneous solid catalysts are better options for lignin depolymerization and pollution mitigation in the presence of water. Due to its greater compatibility with aqueous system, tremendous efforts has been directed toward the development of heterogeneous catalysis of lignin depolymerization, especially focusing on the relatively weaker β-O-4 linkages. Classic hydrogenation methods offer

simplicity and efficiency in breakdown of aryl ether C-O bonds. However, owing to the high bond strengths of these aryl ethers, these classic hydrogenation/hydrogenolysis methods often run at temperatures in the range of (200-300 °C) to overcome the energy barrier for the C-O bond activation. They also typically require high pressures (40-65 bar) to enable the H_2 dissociation on the solid metal surface.[31-33]

To avoid the handling of high pressure flammable gas at high temperatures, milder hydrogenolysis approaches have been pursued. In order to reduce the applied molecular hydrogen pressure, precious metals (Pd, Ru and Pt) with better H_2 activation ability were chosen for the next generation aryl ether hydrogenolysis and hydrogenation. In 2016, Hartwig and co-workers reported a redox-neutral cleavage approach for the fragmentation of β-O-4 ether linkages of lignin.[34] By using commercially available palladium nanoparticles (10 wt% Pd/C) as the solid catalyst, 2-phenoxy-1-phenylethan-1-ol (alcohol model of β-O-4 linkage) was cleaved under ambient pressure (Figure 1.6).[34] Later, Li and Yang demonstrated the successful cleavage of the stronger sp^2 C-O bond in diphenyl ether under reduced hydrogen pressure (10 bar) and lower reaction temperature (110 °C) via the usage of a bimetallic metal catalyst composed of Ru and Pd nanoparticles.[35] It is not only the precious metals that can bring down the energy cost for these cleavages; more economical transition metals such as Ti, Co, and W have also been developed for such catalytic processes, but these solid catalysts were usually prepared via pyrolysis at high temperature (500-800 °C) or required calcination followed by reduction using H_2 under high temperature (600 °C).[36-39]

Catalytic transfer hydrogenolysis (CTH) is a recently developed new approach to achieve the cleavage of aryl ether bond. This approach avoids the direct usage of hydrogen gas which itself is commercially produced from fossil feedstocks (Figure 1.6). Instead, 2-propanol was used as the

H-donor in the metal catalyzed hydrogenolysis of aryl ethers under relatively mild temperatures (120-180 °C).[40-42] The noble metal ruthenium was found to be an efficient solid nanoparticle for CTH process, Han and co-workers reported the successful cleavage of diphenyl ether under 120 °C with 2-propanol as the hydrogen source.[40] To lower the cost of the catalyst, the earth abundant metal nickel was also used as the CTH catalyst. However, applied pressure (10 bar N_2) was still required owing to the lower reactivity of Ni when compared with the more reactive noble metal Ru towards H reception from the donor 2-propanol.[41, 42].

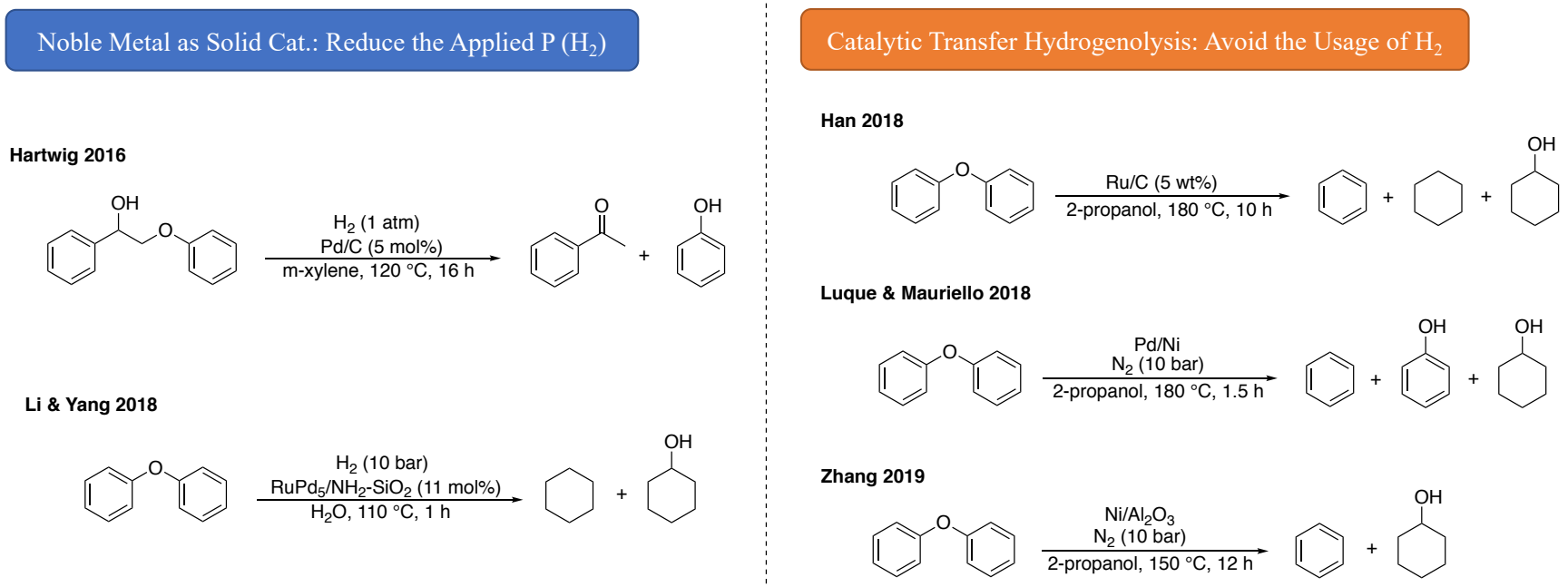

Figure 1.6 Literature reported heterogeneous hydrogenolysis/hydrogenation strategies for aryl ether cleavages: Usage of Noble Metal vs. Catalytic Transfer Hydrogenolysis.

As noted above, one important motivation for choosing a heterogeneous solid metal catalyst is to obtain compatibility with water. Thus, the ultimate goal for the catalytic method development for biomass upgrading and pollution mitigation is to enable ether cleavage in water (Figure 1.7). In 2012, Lercher and co-workers demonstrated that a SiO_2-supported Ni metal catalyst can cleave lignin linkages like aryl ethers in water under mild conditions (120 °C and 6 bar H_2).[43] Later, in 2018, Dyson and co-workers reported that introduction of noble metals such as Ru or Rh to the Ni catalyst enabled the resulting bimetallic nanoparticles to achieves the same C-O ether cleavage under even milder condition (ambient H_2 pressure and 95 °C).[44]

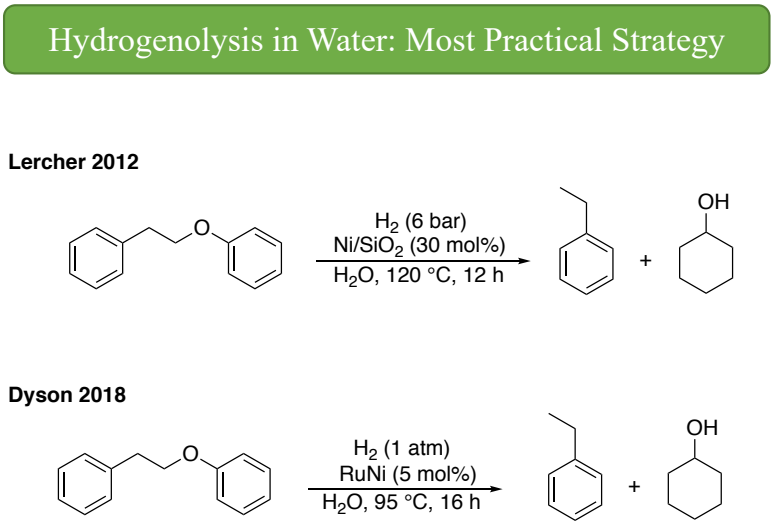

Figure 1.7 Reported Hydrogenolysis Examples of β-O-4 type aryl ether in water via heterogeneous solid nickel catalyst.

1.5 Why is Mechanistic Understanding Always Lacking for Solid Metal Catalyzed Ether Cleavages?

Although these novel studies have uncovered aryl ether C-O cleavage under mild conditions with robust and low-cost heterogeneous catalysts, they did not further explore the mechanisms of these reactions. The biggest concern regarding these cleavage methods is their lack of reaction selectivity; for instance, over reduction of phenolic products is often seen. Mechanistic insight is the key for selectivity control, but unlike the case of molecular metal catalysts, mechanistic investigation of heterogeneous catalysts faces large barriers due to their complexity involving the non-uniform solid phase metal surface, liquid solvent phase, and the gas phase of H_2.

Mechanistic investigation is difficult to conduct on the heterogeneous surface, particularly with the limitations of spectroscopic tools for probing such complicated interfaces. Quantum chemical models might offer insight; they are widely and successfully used to shed light on organic reaction mechanisms. In studying heterogeneous catalysis, DFT calculations are generally limited to molecular interactions in vacuum between small aromatic monomers (phenol, benzene, guaiacol)[45-48] and well-defined metal surfaces. However, most metal surfaces that catalyze lignin cleavage were under solvent, especially polar solvents. Meanwhile, the choice of solvent in these catalytic systems has been found to exert significant influence in both chemoselectivity and catalyst activity.[49] Importantly, among all the common solvents that have been used in reductive hydrogenations, water, the "greenest" biomass upgrading solvent is actually most difficult to simulate.

Powerful spectroscopic tools can be used to analyze catalytic metal surfaces, but, as with DFT simulations, they are largely limited to idealized systems. Electron microscopy (TEM, SEM) often carried out under ultra-high vacuum, is only able to reveal the topological and compositional

features of a catalytic surface. Infrared spectroscopy is useful for in situ investigation of solid-liquid interfaces, but typically requires structurally simple non-polar solvents (cyclohexane[50], *n*-hexane[51]). A new tool, tip enhanced Raman spectroscopy, can probe substrate-metal interactions in aqueous media under applied current, but an atomically level catalyst surface is still required.[52] Tools for understand complicated surface reactions are still developing. Despite these challenges, there is substantial need for guiding principles to understand and predict molecular interactions in these complex heterogeneous systems catalyze surface reactions.[53, 54]

1.6 Electrocatalytic Hydrogenation (ECH) of Aryl Ethers

Going back to our original motivation which is to complete the cycle of energy and carbon, a heterogeneous catalytic approach for both biomass upgrading and pollution mitigation appears attractive based on the above advantages. Compared to conventional catalytic hydrogenation strategies which utilize fossil-derived H_2, electrocatalytic hydrogenation/hydrogenolysis (ECH) is an excellent alternative to achieve the cleavage of aryl ethers under extremely mild reaction conditions and without the direct handling of gaseous hydrogen. Furthermore, electrocatalysis is typically performed in aqueous media which satisfies the first boundary condition of lignin valorization and pollution mitigation that the catalytic method needs to be compatible with water. Most importantly, the biggest advantage of electrocatalysis is that electricity can be produced from renewable energy, and via the catalytic upgrading of biomass carbon, it can be transformed into stored chemical energy (Figure 1.8).

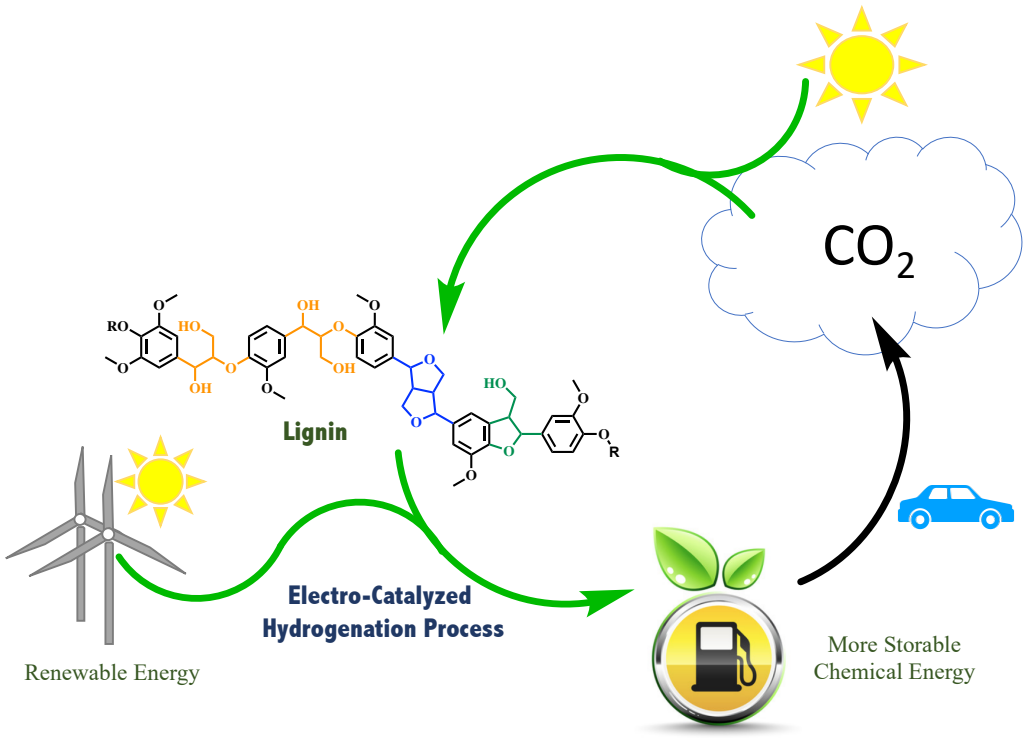

Figure 1.8 Cycle of carbon and energy: capture, storage, and usage.

Lessard and co-workers demonstrated among several commercially available solid transition metal catalysts (Ni_2B, Rh/C, Ru/C, Pt/C, Pd/C, Pd/Al_2O_3, Rh/Al_2O_3, $Pd/BaSO_4$ and RaNi), that only palladium powder and active Raney® nickel powder plated electrodes showed good reactivity towards the cleavage of lignin aryl ether linkages.[55, 56] These papers did explore the electrocatalytic hydrogenolysis (ECH) of representative β-O-4 linkage models and 4-O-5 linkage model (4-phenoxyphenol), but they mainly presented single-point product mixture analyses after a fixed period of ECH, and they offered little in the way of mechanistic insight into the actual mechanisms of bond activation and cleavage. In 2015, Lam from this lab reported the ECH pathway of guaiacol (the simplest lignin monomeric units) using RaNi plated electrode.[57] As shown in Figure 1.9, guaiacol first undergoes demethoxylation to become phenol, followed by aromatic ring reduction which converts phenol into cyclohexanol. Later, Hao also from our lab

illustrated the reduction sequence of eugenol (lignin monomer with the corresponding propenyl chain), similar as guaiacol, eugenol can be demethoxylated into 4-propylphenol.[58] However, the propyl chain that para to the hydroxyl group largely slowdown the reduction of the methoxy group (slowed the cleavage of this sp^2 C-O ether bond).

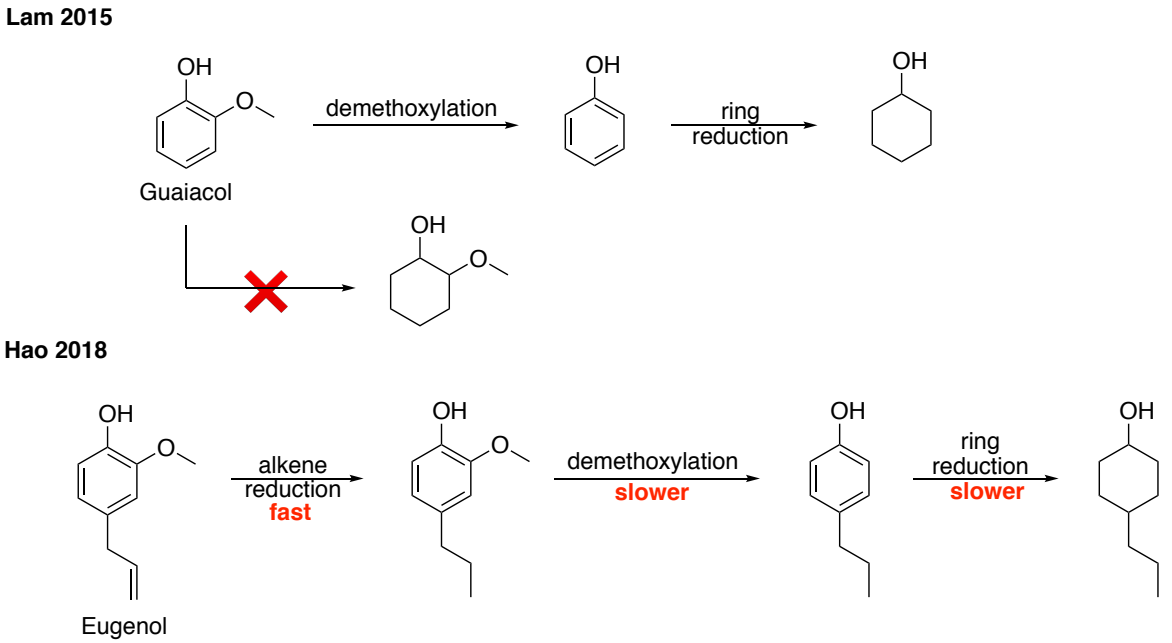

Figure 1.9 Reduction pathways of guaiacol and eugenol reported by Lam and Hao. Demethoxylation and ring reduction of eugenol is much slower than guaiacol.

Based on the observations from the above two monomer studies, different substituents have significant impacts on the reduction of aryl ethers. And looking back at the structure of the lignin polymer (Figure 1.2) and those different diaryl ether based organic pollutants, substituents are another critical factor that cannot be neglected. Most work in this area (aryl ether cleavage), including the above discussed examples, have focused on methods development aimed at lignin cleavage and upgrading. Relatively little mechanistic analysis has been presented in the context of heterogeneous catalytic cleavage, partly because much of the work is focused on empirical

prospecting for catalysts and conditions. Meanwhile, in compounds relevant to either biomass utilization or pollution remediation, these aryl ether groupings always carry a variety of substituents. These issues matter; as demonstrated herein, substituents grossly alter the reactivity and selectivity landscapes in these cleavage processes. Thus, studies to unravel the cleavage mechanisms of aryl ethers are critical to achieve both excellent selectivity control and to understand the impacts of substituents in pursuing further development in biomass valorization and pollution mitigation.

REFERENCES

REFERENCES

1. Gurney, K. R.; Liang, J.; Roest, G.; Song, Y.; Mueller, K.; Lauvaux, T., Under-reporting of greenhouse gas emissions in U.S. cities. *Nature Communications* **2021,** *12* (1), 553-553.

2. Reiner, D. M., Europe's 'green deal' and carbon dioxide removal. *Nature* **2021,** *589* (7840), 19-19.

3. Touma, D.; Stevenson, S.; Lehner, F.; Coats, S., Human-driven greenhouse gas and aerosol emissions cause distinct regional impacts on extreme fire weather. *Nature Communications* **2021,** *12* (1), 212-212.

4. Gillett, N. P.; Kirchmeier-Young, M.; Ribes, A.; Shiogama, H.; Hegerl, G. C.; Knutti, R.; Gastineau, G.; John, J. G.; Li, L.; Nazarenko, L.; Rosenbloom, N.; Seland, O.; Wu, T.; Yukimoto, S.; Ziehn, T., Constraining human contributions to observed warming since the pre-industrial period. *Nature Climate Change* **2021**.

5. Cox, P. M.; Betts, R. A.; Jones, C. D.; Spall, S. A.; Totterdell, I. J., Acceleration of global warming due to carbon-cycle feedbacks in a coupled climate model. *Nature* **2000,** *408* (6809), 184-187.

6. Zakzeski, J.; Bruijnincx, P. C. A.; Jongerius, A. L.; Weckhuysen, B. M., The Catalytic Valorization of Lignin for the Production of Renewable Chemicals. *Chemical Reviews* **2010,** *110* (6), 3552-3599.

7. Isikgor, F. H.; Becer, C. R., Lignocellulosic biomass: a sustainable platform for the production of bio-based chemicals and polymers. *Polymer Chemistry* **2015,** *6* (25), 4497-4559.

8. Boerjan, W.; Ralph, J.; Baucher, M., Lignin biosynthesis. *Annual Review of Plant Biology* **2003,** *54*, 519-546.

9. Crestini, C.; Melone, F.; Sette, M.; Saladino, R., Milled Wood Lignin: A Linear Oligomer. *Biomacromolecules* **2011,** *12* (11), 3928-3935.

10. Karkas, M. D.; Matsuura, B. S.; Monos, T. M.; Magallanes, G.; Stephenson, C. R. J., Transition-metal catalyzed valorization of lignin: the key to a sustainable carbon-neutral future. *Organic & Biomolecular Chemistry* **2016,** *14* (6), 1853-1914.

11. Schutyser, W.; Renders, T.; Van den Bosch, S.; Koelewijn, S. F.; Beckham, G. T.; Sels, B. F., Chemicals from lignin: an interplay of lignocellulose fractionation, depolymerisation, and upgrading. *Chemical Society Reviews* **2018,** *47* (3), 852-908.

12. Xu, C. P.; Arancon, R. A. D.; Labidi, J.; Luque, R., Lignin depolymerisation strategies: towards valuable chemicals and fuels. *Chemical Society Reviews* **2014,** *43* (22), 7485-7500.

13. Zaheer, M.; Kempe, R., Catalytic Hydrogenolysis of Aryl Ethers: A Key Step in Lignin Valorization to Valuable Chemicals. *ACS Catalysis* **2015,** *5* (3), 1675-1684.
14. Chen, T.; Xiong, H.; Yang, J.-F.; Zhu, X.-L.; Qu, R.-Y.; Yang, G.-F., Diaryl Ether: A Privileged Scaffold for Drug and Agrochemical Discovery. *Journal of Agricultural and Food Chemistry* **2020,** *68* (37), 9839-9877.

15. Le, T. G.; Kundu, A.; Ghoshal, A.; Nguyen, N. H.; Preston, S.; Jiao, Y. Q.; Ruan, B. F.; Xue, L.; Huang, F.; Keiser, J.; Hofmann, A.; Chang, B. C. H.; Garcia-Bustos, J.; Wells, T. N. C.; Palmer, M. J.; Jabbar, A.; Gasser, R. B.; Baell, J. B., Structure-Activity Relationship Studies of Tolfenpyrad Reveal Subnanomolar Inhibitors of Haemonchus contortus Development. *Journal of Medicinal Chemistry* **2019,** *62* (2), 1036-1053.

16. Manzetti, S.; van der Spoel, E. R.; van der Spoel, D., Chemical Properties, Environmental Fate, and Degradation of Seven Classes of Pollutants. *Chemical Research in Toxicology* **2014,** *27* (5), 713-737.

17. Jones, K. C.; de Voogt, P., Persistent organic pollutants (POPs): state of the science. *Environmental Pollution* **1999,** *100* (1-3), 209-221.

18. Yamaguchi, K.; Hikiji, W.; Takino, M.; Saka, K.; Hayashida, M.; Fukunaga, T.; Ohno, Y., Analysis of Tolfenpyrad and its Metabolites in Plasma in a Tolfenpyrad Poisoning Case. *Journal of Analytical Toxicology* **2012,** *36* (7), 529-537.

19. Rodrigo, M. A.; Oturan, N.; Oturan, M. A., Electrochemically Assisted Remediation of Pesticides in Soils and Water: A Review. *Chemical Reviews* **2014,** *114* (17), 8720-8745.

20. Yang, Q.; Cai, S.; Dong, S. W.; Chen, L. L.; Chen, J. F.; Cai, T. M., Biodegradation of 3-methyldiphenylether (MDE) by Hydrogenophaga atypical strain QY7-2 and cloning of the methy-oxidation gene mdeABCD. *Scientific Reports* **2016,** *6*, 10.

21. Dong, M. F.; Wen, G. Y.; Tang, H. X.; Wang, T.; Zhao, Z. H.; Song, W. G.; Wang, W. M.; Zhao, L., Dissipation and safety evaluation of novaluron, pyriproxyfen, thiacloprid and tolfenpyrad residues in the citrus-field ecosystem. *Food Chemistry* **2018,** *269*, 136-141.

22. Ambrus, A. TOLFENPYRAD (269) Report, Food and Agriculture Organization of the United Nations. http://www.fao.org/fileadmin/templates/agphome/documents/Pests_Pesticides/JMPR/Evaluation13/Tolfenpyrad.pdf (accessed 05/29/2021).

23. Lahive, C. W.; Deuss, P. J.; Lancefield, C. S.; Sun, Z. H.; Cordes, D. B.; Young, C. M.; Tran, F.; Slawin, A. M. Z.; de Vries, J. G.; Kamer, P. C. J.; Westwood, N. J.; Barta, K., Advanced Model Compounds for Understanding Acid-Catalyzed Lignin Depolymerization: Identification of Renewable Aromatics and a Lignin-Derived Solvent. *Journal of the American Chemical Society* **2016,** *138* (28), 8900-8911.

24. Deuss, P. J.; Scott, M.; Tran, F.; Westwood, N. J.; de Vries, J. G.; Barta, K., Aromatic Monomers by in Situ Conversion of Reactive Intermediates in the Acid-Catalyzed Depolymerization of Lignin. *Journal of the American Chemical Society* **2015,** *137* (23), 7456-7467.

25. Alvarez-Bercedo, P.; Martin, R., Ni-Catalyzed Reduction of Inert C-O Bonds: A New Strategy for Using Aryl Ethers as Easily Removable Directing Groups. *Journal of the American Chemical Society* **2010,** *132* (49), 17352-17353.

26. Sergeev, A. G.; Hartwig, J. F., Selective, Nickel-Catalyzed Hydrogenolysis of Aryl Ethers. *Science* **2011,** *332* (6028), 439-443.

27. Nichols, J. M.; Bishop, L. M.; Bergman, R. G.; Ellman, J. A., Catalytic C-O Bond Cleavage of 2-Aryloxy-1-arylethanols and Its Application to the Depolymerization of Lignin-Related Polymers. *Journal of the American Chemical Society* **2010,** *132* (36), 12554-12555.

28. Chan, J. M. W.; Bauer, S.; Sorek, H.; Sreekumar, S.; Wang, K.; Toste, F. D., Studies on the Vanadium-Catalyzed Nonoxidative Depolymerization of Miscanthus giganteus-Derived Lignin. *ACS Catalysis* **2013,** *3* (6), 1369-1377.

29. P.J. Linstrom and W.G. Mallard, Eds., **NIST Chemistry WebBook, NIST Standard Reference Database Number 69**, National Institute of Standards and Technology, Gaithersburg MD, 20899, https://doi.org/10.18434/T4D303.

30. Nguyen, J. D.; Matsuura, B. S.; Stephenson, C. R. J., A Photochemical Strategy for Lignin Degradation at Room Temperature. *Journal of the American Chemical Society* **2014,** *136* (4), 1218-1221.

31. Dong, L.; Xin, Y.; Liu, X. H.; Guo, Y.; Pao, C. W.; Chen, J. L.; Wang, Y. Q., Selective hydrodeoxygenation of lignin oil to valuable phenolics over Au/Nb2O5 in water. *Green Chemistry* **2019,** *21* (11), 3081-3090.

32. Zhao, C.; Kou, Y.; Lemonidou, A. A.; Li, X. B.; Lercher, J. A., Hydrodeoxygenation of bio-derived phenols to hydrocarbons using RANEY (R) Ni and Nafion/SiO2 catalysts. *Chemical Communications* **2010,** *46* (3), 412-414.

33. Zhao, C.; Lercher, J. A., Upgrading Pyrolysis Oil over Ni/HZSM-5 by Cascade Reactions. *Angewandte Chemie-International Edition* **2012,** *51* (24), 5935-5940.

34. Gao, F.; Webb, J. D.; Sorek, H.; Wemmer, D. E.; Hartwig, J. F., Fragmentation of Lignin Samples with Commercial Pd/C under Ambient Pressure of Hydrogen. *ACS Catalysis* **2016,** *6* (11), 7385-7392.

35. Guo, M.; Peng, J.; Yang, Q. H.; Li, C., Highly Active and Selective RuPd Bimetallic NPs for the Cleavage of the Diphenyl Ether C-O Bond. *ACS Catalysis* **2018,** *8* (12), 11174-11183.

36. Guo, H. W.; Miles-Barrett, D. M.; Zhang, B.; Wang, A. Q.; Zhang, T.; Westwood, N. J.; Li, C. Z., Is oxidation-reduction a real robust strategy for lignin conversion? A comparative study on lignin and model compounds. *Green Chemistry* **2019,** *21* (4), 803-811.

37. Liu, X. H.; Xu, L. J.; Xu, G. Y.; Jia, W. D.; Ma, Y. F.; Zhang, Y., Selective Hydrodeoxygenation of Lignin-Derived Phenols to Cyclohexanols or Cyclohexanes over Magnetic CoNx@NC Catalysts under Mild Conditions. *ACS Catalysis* **2016,** *6* (11), 7611-7620.

38. Liu, X. H.; Jia, W. D.; Xu, G. Y.; Zhang, Y.; Fu, Y., Selective Hydrodeoxygenation of Lignin-Derived Phenols to Cyclohexanols over Co-Based Catalysts. *ACS Sustainable Chemistry & Engineering* **2017,** *5* (10), 8594-8601.

39. Molinari, V.; Giordano, C.; Antonietti, M.; Esposito, D., Titanium Nitride-Nickel Nanocomposite as Heterogeneous Catalyst for the Hydrogenolysis of Aryl Ethers. *Journal of the American Chemical Society* **2014,** *136* (5), 1758-1761.

40. Wu, H. R.; Song, J. L.; Xie, C.; Wu, C. Y.; Chen, C. J.; Han, B. X., Efficient and Mild Transfer Hydrogenolytic Cleavage of Aromatic Ether Bonds in Lignin-Derived Compounds over Ru/C. *Acs Sustainable Chemistry & Engineering* **2018,** *6* (3), 2872-2877.

41. Jiang, L.; Guo, H. W.; Li, C. Z.; Zhou, P.; Zhang, Z. H., Selective cleavage of lignin and lignin model compounds without external hydrogen, catalyzed by heterogeneous nickel catalysts. *Chemical Science* **2019,** *10* (16), 4458-4468.

42. Mauriello, F.; Paone, E.; Pietropaolo, R.; Balu, A. M.; Luque, R., Catalytic Transfer Hydrogenolysis of Lignin-Derived Aromatic Ethers Promoted by Bimetallic Pd/Ni Systems. *Acs Sustainable Chemistry & Engineering* **2018,** *6* (7), 9269-9276.

43. He, J. Y.; Zhao, C.; Lercher, J. A., Ni-Catalyzed Cleavage of Aryl Ethers in the Aqueous Phase. *Journal of the American Chemical Society* **2012,** *134* (51), 20768-20775.

44. Bulut, S.; Siankevich, S.; van Muyden, A. P.; Alexander, D. T. L.; Savoglidis, G.; Zhang, J. G.; Hatzimanikatis, V.; Yan, N.; Dyson, P. J., Efficient cleavage of aryl ether C-O linkages by Rh-Ni and Ru-Ni nanoscale catalysts operating in water. *Chemical Science* **2018,** *9* (25), 5530-5535.

45. Mittendorfer, F.; Hafner, J., Hydrogenation of benzene on Ni(111) - a DFT study. *Journal of Physical Chemistry B* **2002,** *106* (51), 13299-13305.

46. Delle Site, L.; Alavi, A.; Abrams, C. F., Adsorption energies and geometries of phenol on the (111) surface of nickel: An ab initio study. *Physical Review B* **2003,** *67* (19), 3.

47. Chiu, C. C.; Genest, A.; Borgna, A.; Rosch, N., Hydrodeoxygenation of Guaiacol over Ru(0001): A DFT Study. *ACS Catalysis* **2014,** *4* (11), 4178-4188.

48. Lee, K.; Gu, G. H.; Mullen, C. A.; Boateng, A. A.; Vlachos, D. G., Guaiacol Hydrodeoxygenation Mechanism on Pt(111): Insights from Density Functional Theory and Linear Free Energy Relations. *ChemSusChem* **2015,** *8* (2), 315-322.

49. Varghese, J. J.; Mushrif, S. H., Origins of complex solvent effects on chemical reactivity and computational tools to investigate them: a review. *Reaction Chemistry & Engineering* **2019,** *4* (2), 165-206.

50. de Castro, I. B. D.; Graca, I.; Rodriguez-Garcia, L.; Kennema, M.; Rinaldi, R.; Meemken, F., Elucidating the reactivity of methoxyphenol positional isomers towards hydrogen-transfer reactions by ATR-IR spectroscopy of the liquid-solid interface of RANEY (R) Ni. *Catalysis Science & Technology* **2018,** *8* (12), 3107-3114.

51. Chen, M. M.; Maeda, N.; Baiker, A.; Huang, J., Molecular Insight into Pt-Catalyzed Chemoselective Hydrogenation of an Aromatic Ketone by In Situ Modulation-Excitation IR Spectroscopy. *ACS Catalysis* **2012,** *2* (9), 2007-2013.

52. Jiang, S.; Chen, Z.; Chen, X.; Nguyen, D.; Mattei, M.; Goubert, G.; Van Duyne, R. P., Investigation of Cobalt Phthalocyanine at the Solid/Liquid Interface by Electrochemical Tip-Enhanced Raman Spectroscopy. *Journal of Physical Chemistry C* **2019,** *123* (15), 9852-9859.

53. Zhang, X. H.; Sewell, T. E.; Glatz, B.; Sarupria, S.; Getman, R. B., On the water structure at hydrophobic interfaces and the roles of water on transition-metal catalyzed reactions: A short review. *Catalysis Today* **2017,** *285*, 57-64.

54. Zaera, F., Probing Liquid/Solid Interfaces at the Molecular Level. *Chemical Reviews* **2012,** *112* (5), 2920-2986.

55. Dabo, P.; Cyr, A.; Lessard, J.; Brossard, L.; Menard, H., Electrocatalytic hydrogenation of 4-phenoxyphenol on active powders highly dispersed in a reticulated vitreous carbon electrode. *Canadian Journal of Chemistry* **1999,** *77* (7), 1225-1229.

56. Cyr, A.; Chiltz, F.; Jeanson, P.; Martel, A.; Brossard, L.; Lessard, J.; Menard, H., Electrocatalytic hydrogenation of lignin models at Raney nickel and palladium-based electrodes. *Canadian Journal of Chemistry* **2000,** *78* (3), 307-315.

57. Lam, C. H.; Lowe, C. B.; Li, Z. L.; Longe, K. N.; Rayburn, J. T.; Caldwell, M. A.; Houdek, C. E.; Maguire, J. B.; Saffron, C. M.; Miller, D. J.; Jackson, J. E., Electrocatalytic upgrading of model lignin monomers with earth abundant metal electrodes. *Green Chemistry* **2015,** *17* (1), 601-609.

58. Hao, P., Electrocatalytic Hydrogenation of Monomeric, Dimeric, and Polymeric Lignin Model Compounds with Raney Nickel: Chemistry, Mechanistic, and Product Toxicity Studies. Michigan State University, East Lansing, MI, 2018.

Chapter 2 ECH Catalytic Methodology Studies & Aryl Ether Synthesis*

2.1 Introduction

2.1.1 ECH Catalytic Methodology

Any practical process to convert substrates as diverse as biomass and persistent organic pollutants (POPs) must meet four criteria: it must tolerate water, run at modest temperatures and pressures, and be composed of relatively low-cost materials. To this end, we performed catalytic methodology studies of ECH over skeletal Ni cathodes. Water is the greenest solvent for both biomass processing and pollution mitigation, but the low solubility in water of some of the ether substrates calls for a water-miscible organic co-solvent.

Classic heterogeneous catalytic hydrogenation is sometimes criticized for its low selectivity control as it often leads to over reduction of aromatics. Considering the challenge of cleaving these strong aryl ether bonds, a process offering control of product selectivity would be especially valuable, not only to upgrade or to mitigate these feedstocks, but also to convert them into simple mixtures of small-molecule products. Regardless of high laboratory selectivities, a water-sensitive molecular catalyst that requires inert atmosphere conditions and dry organic solvents is of limited applicability. Therefore, with the lessons from the mechanistic analyses (for details see chapters 3-4), we sought to optimize and generalize our ECH method for mild and selective cleavage of water-soluble and -insoluble aryl ethers.

*This chapter is adapted from both Zhou, Y. T.; Klinger, G. E.; Hegg, E. L.; Saffron, C. M.; Jackson, J. E., Multiple Mechanisms Mapped in Aryl Alkyl Ether Cleavage via Aqueous Electrocatalytic Hydrogenation (ECH) over Skeletal Nickel. *J. Am. Chem. Soc.* **2020,** *142*, 4037-4050.

2.2 Results and Discussion

2.2.1 Effects of Co-solvent on Reduction Selectivities

Though smaller monomers such as guaiacol could be studied in purely aqueous electrolyte solution, more hydrophobic species such as 2-phenoxyacetophenone a β-O-4 ketone model and diphenyl ether model (4-O-5 linkage) required an organic co-solvent to achieve homogeneous solution. Water-miscible organic solvents, such as methanol, ethanol, isopropyl alcohol (IPA) and acetone, are good organic co-solvents for dissolving substrates that have low solubility in water. Meanwhile, introduction of organic co-solvent can not only help dissolving the water insoluble substrate into the aqueous electrolyte, but also significantly impact both cleavage rate and product selectivity.

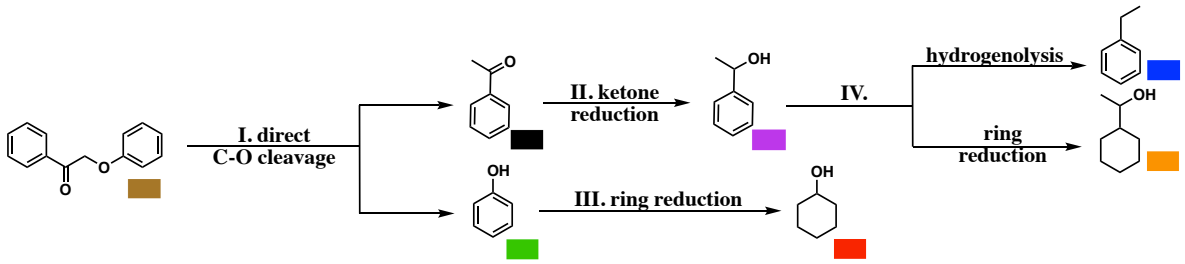

Figure 2.1 Major reduction pathway of 2-phenoxyacetophenone

2.2.1.1 Co-solvent Effects of Alkyl Aryl Ethers (β-O-4 model Linkages)

When used as co-solvents, all three alcohols gave similar ECH results: complete C-O cleavage of the 2-phenoxyacetophenone (Figure 2.1 I), and reduction of aromatic products (Figure 2.1 II and III). Summarized in Figure 2.2, compared to methanol, the more hydrophobic ethanol and IPA favored formation of 1-cyclohexyl-ethanol (orange). To ensure homogeneity in the liquid phase for kinetic measurements, 33% v/v was used as the standard co-solvent content for all ether substrate studies.

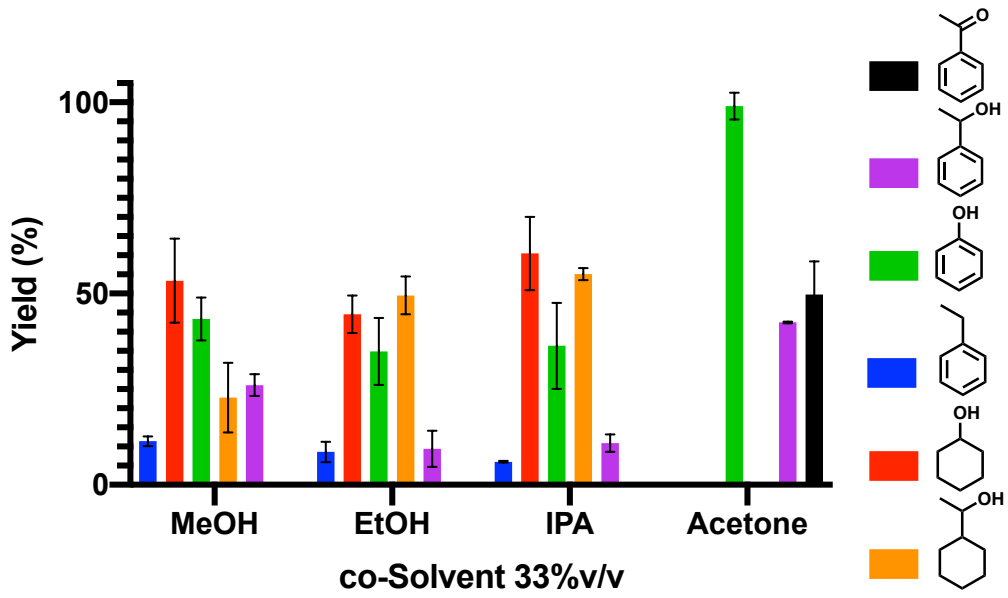

Figure 2.2 Co-solvent influence on ECH of ketone **1**. Reaction conditions: isopropyl alcohol treated Ni electrode, constant current at 50 mA, co-solvent content 33% by volume, mixed with 67% pH 8 borate buffer, ECH for 9 hours at 60 °C. The yields of cyclohexanol and 1-cyclohexylethanol were corrected for extraction losses. The yields of phenol and 1-phenylethanol were corrected for extraction losses. No yield correction was applied on ethylbenzene.

Lower alcohol concentrations (10% v/v) also gave generally good ECH results (Figure 2.3), but their borderline substrate solubilities led to less reliable analytical quantification. The more hydrophobic alcohol *t*-BuOH was also tested, but was found to be immiscible with 0.1 M pH 8 borate buffer. Ultimately, IPA was chosen as the co-solvent in the substrate mapping and in the mechanistic studies (chapters 3-4) because it is the most amphiphilic of the three, and because previous work had found it to extend the lifetime of the catalyst by preventing buildup of surface oxide.[1] In higher temperature Ni-catalyzed hydrogenolyses, IPA is also known to serve as a hydrogen transfer agent which can supply hydrogen to the catalytic surface, forming acetone as byproduct.[2,3]

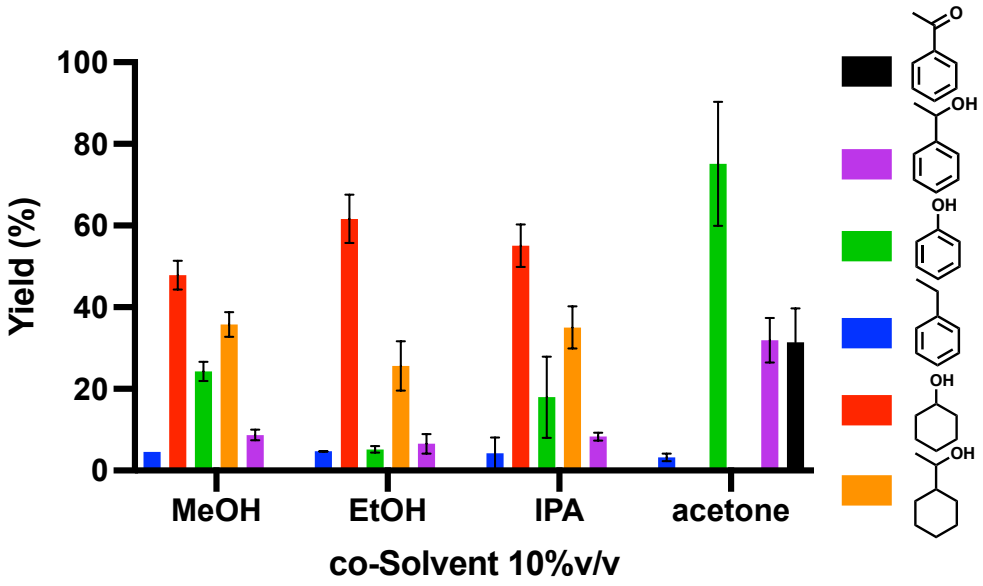

Figure 2.3 Co-solvent influence on electrocatalytic hydrogenation (ECH). Reaction conditions: isopropyl alcohol treated Ni electrode, constant current at 50 mA, co-solvent content 10% by volume, mixed with 90% pH 8 borate buffer. ECH for 9 hours at 60 °C. No product yield correction was applied in 10% by volume co-solvent studies, the actual yield may be larger than the reported numbers here due to extraction/evaporation losses.

When acetone was used as the organic co-solvent at 33%, significantly different results were obtained than with the alcohols (Figure 2.2). Specifically, no ring saturation products were observed. The ketone β-O-4 ether still underwent 100% C-O cleavage, but the aromatic saturation process was completely inhibited. This change may be understood by noting nickel's high affinity for the carbonyl functionality (reported in the mechanistic findings, see chapter 3 and chapter 4); with acetone as co-solvent, the catalyst is exposed to a carbonyl rich environment, placing aromatic ring reduction into competition with acetone reduction. Even at 10% v/v acetone content (Figure 2.3), the aromatic ring saturation is inhibited. However, in both 10% and 33% v/v cases, the ketone β-O-4 dimer was 100% cleaved and about 50% of the acetophenone was reduced to 1-phenylethanol. Thus, despite the competition between acetone and aromatic reduction, aromatic ketones can compete with acetone. These results suggest a hierarchy of surface-active site binding

affinities for different reduction intermediates from the starting aryl dimers to the downstream alcohols (Figure 2.4).

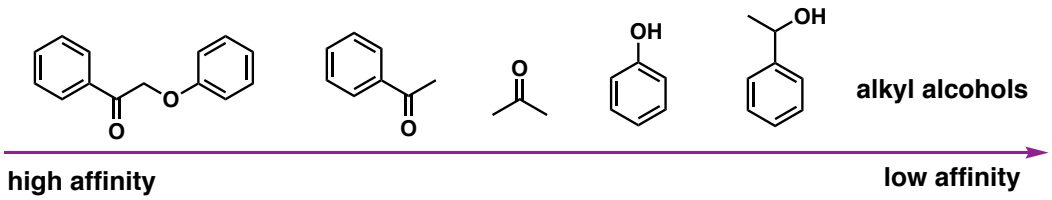

Figure 2.4 Suggested substrate affinities towards Ni catalyst surface

2.2.1.2 Co-solvent Effects on Cleavage of Diaryl Ethers (4-O-5 model Linkages & POPs)

To achieve the cleavage of insoluble diaryl ethers, a water miscible organic co-solvent was required. As with the β-O-4 model system above, methanol, ethanol, isopropyl alcohol (IPA) and acetone were tested as co-solvents to aid in solubilizing and cleaving diphenyl ether. Due to this substrate's high hydrophobicity, even at high co-solvent/buffer ratios, neither methanol nor ethanol could achieve a homogeneous liquid phase at 60 °C. The more amphiphilic isopropyl alcohol (IPA), however, at a 1:2 alcohol:buffer ratio (i.e. 33% IPA by volume), was found to be optimal, and was also used at the standard conditions for the diaryl ether cleavages in the mechanistic analysis (chapter 4). Solutions with less than 33% IPA remained inhomogeneous, and at 50% (Table 2.1, Entry 3), the higher electrical resistance slowed the cleavage rate (direct rate comparison plots, Figure 2.5 d) by inhibiting current flow.

Though 2-propanol was identified as the generally optimal co-solvent for mild electrocatalytic cleavage of water-insoluble diaryl ethers, it was not always the fastest. For water-soluble hydroxylated substrates, introducing the organic co-solvent slowed down the rates of both the cleavage (Table 2.1, Entries 5-8) and phenol hydrogenation, compared with 100% buffer (Entries 5, 8).

Table 2.1 co-Solvent Study of Diaryl Ethers: Water Solution and Water Insoluble Substrate.

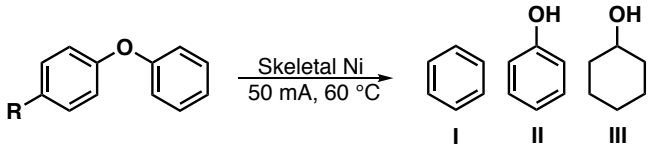

entry	R	co-solv.	conv.	time	yields of products (%)		
					I	II	III
1	H	33%IPA	>99%	9 h	13%	48%	50%
2	H	33%EtOH	>99%	9 h	26%	47%	35%
3	H	50%IPA	95%	9 h	17%	64%	30%
5	OH	100%buffer	>99%	1 h	--	90%	82%
6	OH	10%IPA	>99%	2 h	--	85%	75%
7	OH	10%EtOH	>99%	2 h	--	66%	102%
8	OH	33%IPA	>99%	3 h	--	117%	40%

The values over 100% reflect the fact that in the case of the phenoxyphenols, cleavage of one ether forms two copies of the product phenol. Note that compared to its formation rate, the faster evaporation rate of benzene (b.p. 80 °C) made it difficult to retain in the heated (60 °C) polar aqueous system (evaporation studies see Figure 2.8b).

Full ECH Time Courses for Diphenyl Ether (DPE) and 4-phenoxyphenol (Hydroxylated DPE) using Different Organic Co-Solvents at ***Different Time Scales***

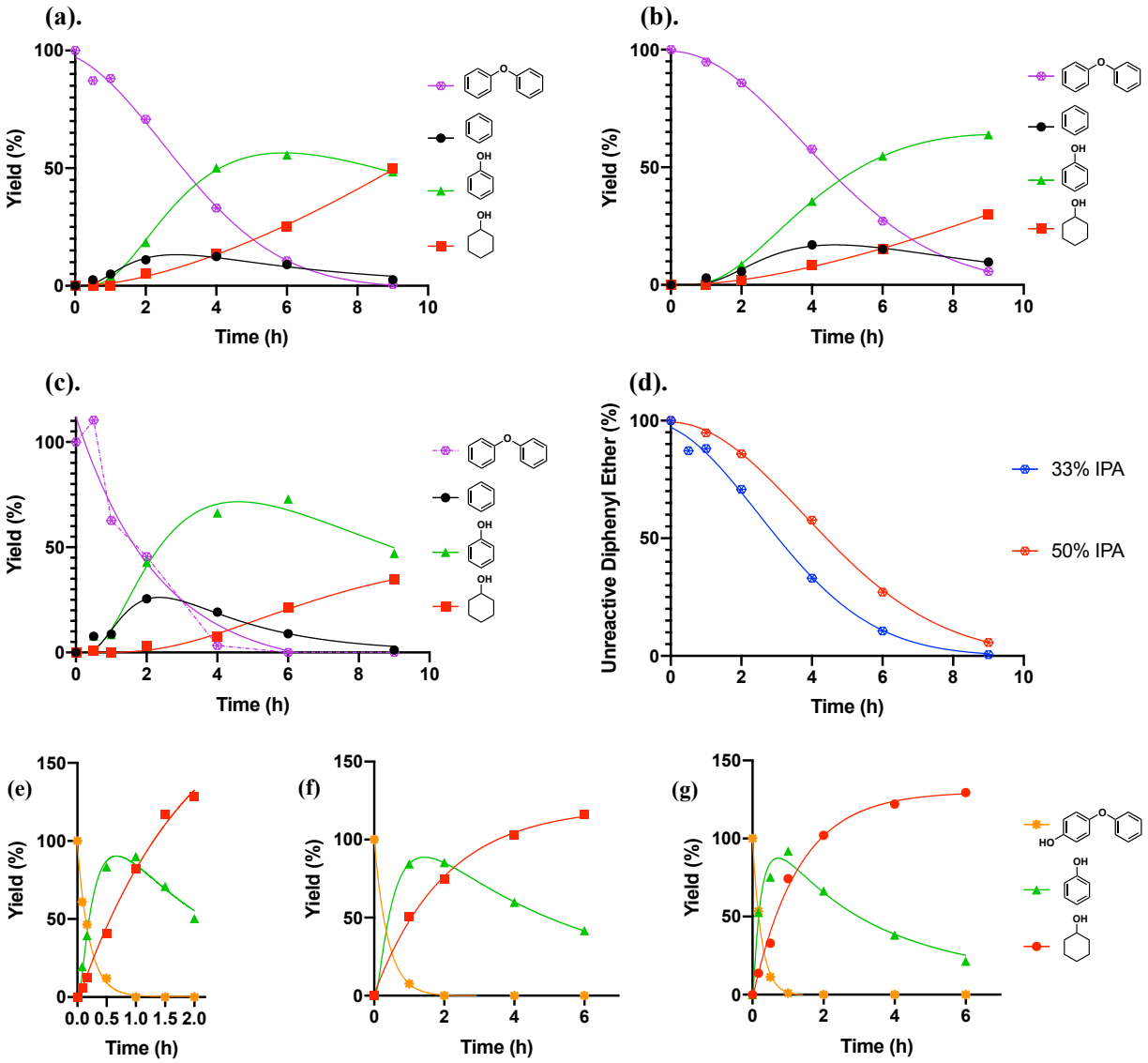

Figure 2.5 Full ECH measurements under standard conditions (50 mA, 60 °C) of (a) diphenyl ether with 33% v/v IPA as co-solvent, (b) diphenyl ether with 50% v/v IPA as co-solvent, (c) diphenyl ether with 33% v/v EtOH as co-solvent, (d) plot of diphenyl ether cleavage rate comparison between 33% v/v IPA and 50% v/v IPA, (e) 4-phenoxyphenol with 100% pure buffer, (f) 4-phenoxyphenol with 10% v/v IPA as co-solvent, (g) 4-phenoxyphenol with 10% v/v EtOH as co-solvent.

2.2.2 The Role of Applied Current

Skeletal Ni electrodes were prepared via (a) by electroplating a stainless steel mesh (window screen) in a stirring aqueous suspension of powdered Ni/Al (1:1) alloy in nickel(II)-ammonia solution; and (b) then activating the Nis through treatment with a 30 wt% NaOH solution to etch out the Al.[4] The Al etching process generates a large amount of H_2 gas, some of which is captured by the skeletal Ni surface, preloading some reducing capacity in the catalyst. This preloading can affect the ECH selectivity by adding extra reducing equivalents to the system apart from those brought by the applied current. Based on the acetone finding, freshly prepared skeletal Ni electrodes were immersed for 24 hours in acetone to discharge the preloaded reducing capacity, leaving electric current to fine tune surface H formation and adjust the reduction selectivity.

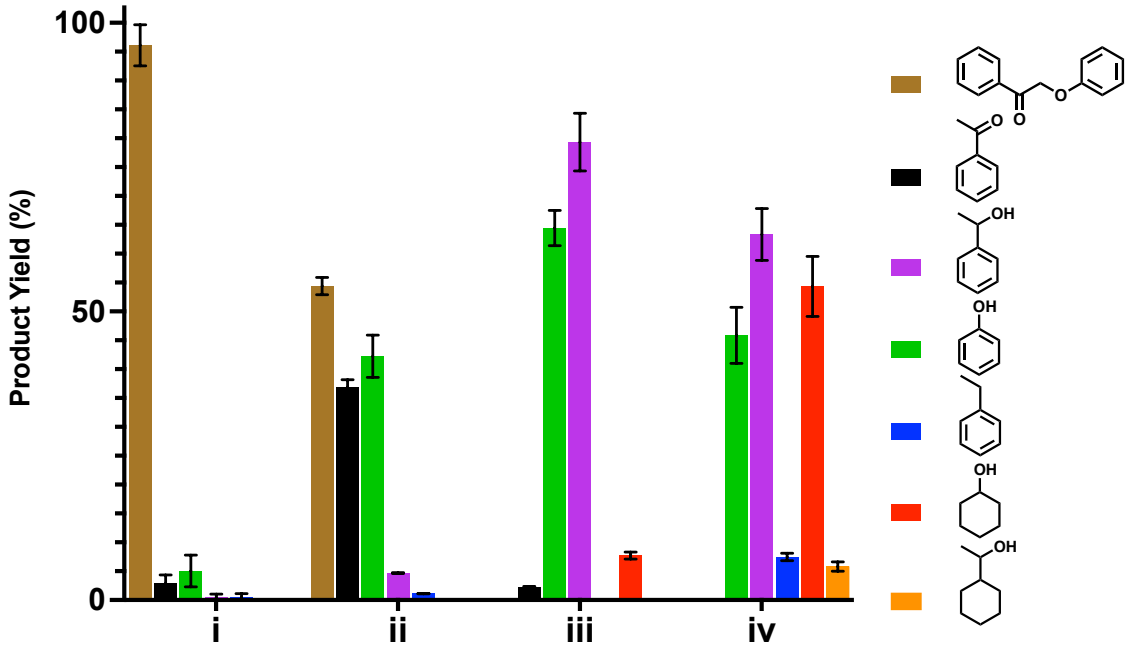

Figure 2.6 Hydrogenation of 2-phenoxyacetophenone with acetone treated electrode (discharged cat.) for 9 hours under different current levels (0-50 mA). (i) Control trial: discharged catalyst at 0 mA. (ii) Discharged catalyst, pre-charged prior to substrate addition for 1 h at 50 mA (8 mA/cm^2), followed by substrate reduction at 0 mA. (iii) Discharged catalyst, ECH for 9 h at 10 mA (1.6 mA/cm^2). (iv) Discharged catalyst, ECH for 9 h at 50 mA (8 mA/cm^2). All trials used 33% v/v isopropyl alcohol (IPA) as co-solvent and reduction ran at 60 °C under ambient pressure.

Figure 2.6 shows variable charge and current treatments of 2-phenoxyacetophenone over the discharged electrodes. As shown in the control where no charge was passed experiment (Figure 2.6 i), essentially no transformation has occurred, confirming that the acetone treatment successfully discharged the skeletal Ni's pre-loaded reducing capacity. Even 2-phenoxyacetophenone, the most susceptible β-O-4 model, was not cleaved as long as no current was passed. When current was applied for only 1 hour before adding the substrate (pre-charging), approximately 50% of the ketone dimer was cleaved (Figure 2.6 ii) upon contacting the catalyst. Thus, the highly porous and skeletal Ni surface can also function as a hydrogen reservoir. With longer current flow applied (Figure 2.6 iii-iv), the 2-phenoxyacetophenone was cleaved completely while the aromatic monomers began reduction to the ring saturated end products. Thus, by using the combination of acetone treatment and current control, selectivity to aromatic or saturated products via skeletal Ni catalyzed ECH can be finely tuned.

2.2.3 Broadening the Scope and Applications of Skeletal Ni ECH: Hydrodefluorination

As summarized in Table 2.2, a range of different substituted DAEs was examined via skeletal Ni electrode catalyzed ECH under standard conditions (ambient pressure, 60 °C, 50 mA). The skeletal Ni electrode was also able to cleave not only DAE's with classic donor substituents, but also those with electron withdrawing functionalities (Table 2.2, Entries 3-7).

Noteworthily, hydrodefluorination of 4-fluoro- and 4-trifluoromethyl diphenyl ethers was observed, highlighting the ability of the skeletal Ni electrode to activate carbon-fluorine bonds (both sp^2 C-F and sp^3 C-F), some of the strongest single bonds in organic chemistry. Nickel-catalyzed hydrodefluorination of a fluorophenol at high H_2 pressure had been previously reported,[5] but to our knowledge, this is the first report of electrocatalytic hydrodefluorination of a perfluoroalkyl substituted diphenyl ether. This finding opens the door to the use of electrodes made from earth abundant nickel to catalyze aqueous-phase defluorination of aliphatic C-F sites, suggesting a new strategy for PFAS mitigation, as well as potentially useful organic transformations.

Table 2.2 Substrate Scope of Diphenyl Ether ECH Cleavage

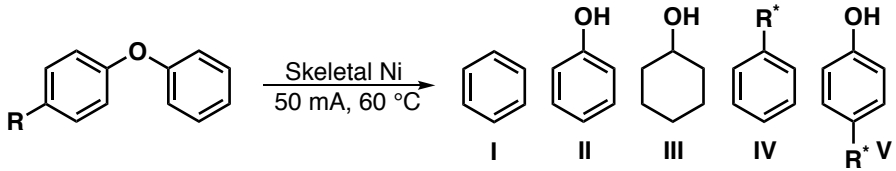

entry	R	R*	time (h)	conv. (%)	$t_{1/2}$ (min)	yields of products (%)				
						I	II	III	IV	V
1	Me	Me	9	99	219	3%	34%	45%	35%	8%
2	OMe	OMe	9	>99	200	5%	48%	42%	67%	2%
3	CHO	CH_2OH	9	>99	257	9%	50%	18%	--	--
4[a]	$COCH_3$	$CH(OH)CH_3$	9	98	295	8%	51%	15%	76%	5%
5	CN	CH_2NH_2	3	>99	70.0	1%	87%	3%	--	--
6[b]	CF_3	CH_3	9	90	774	5%	20%	16%	20%	5%
7	F	H	6	>99	189	13%	55%	48%	--	--
8	Et	Et	9	96	234	1%	26%	49%	14%	9%
9	OH	OH	9	>99	76.0	--	117%	40%	--	--
10	$CH(OH)CH_3$	$CH(OH)CH_3$	9	98	419	9%	34%	18%	50%	1%

The electron withdrawing substituent (Entries 2-7) R will undergo fast reduction to R^* prior to ether C-O cleavage. Additional information on intermediates and reaction processes is presented in chapter 4 (for additional time courses and product analyses, see Figures 4.72-4.80).

2.2.4 Volatile Product Evaporation Accounts for Major Loss in the Mass Balance

In situ formation of surface H creates a potentially powerful hydrogenation method; however, water reduction also generates a large amount of hydrogen gas. Under ambient pressure and with an open system, volatile and water insoluble products such as alkylbenzenes were sparged by this bubbling, making them hard to capture, causing incomplete mass balance. Meanwhile, to ensure the homogeneity for kinetic measurements of water insoluble ether substrates, 33% v/v isopropanol (IPA) was used, which resulted in extraction losses of alcohol end products.

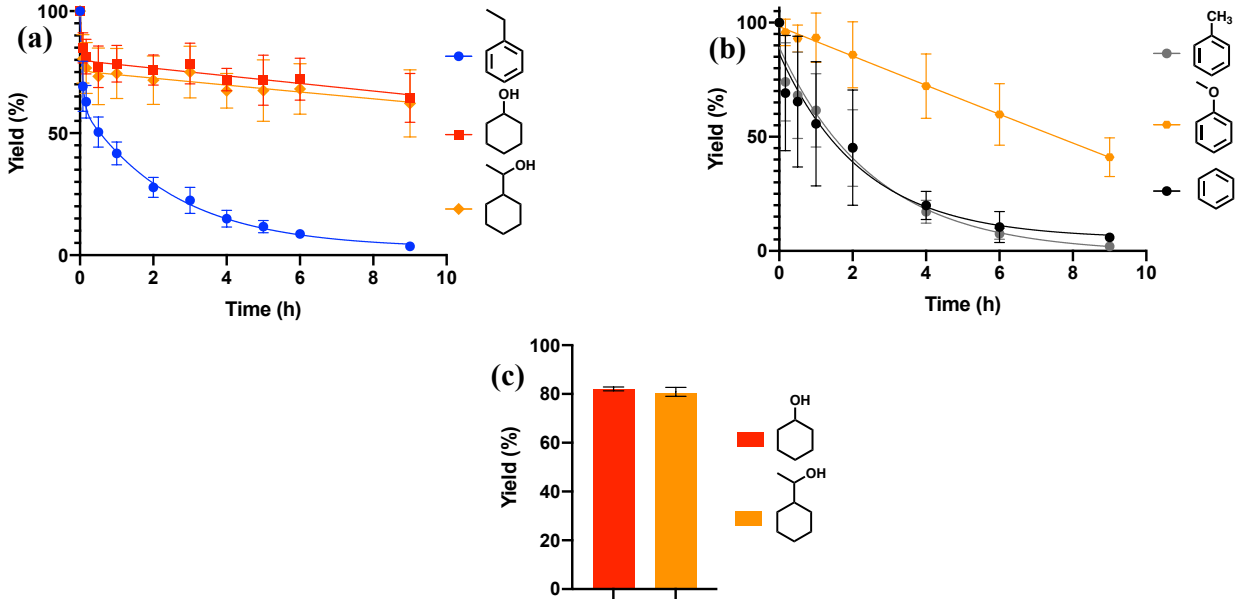

Figure 2.7 (a) Kinetic evaporation curves of ethylbenzene, cyclohexanol and 1-cyclohexylethanol (non-reducible products) under standard ECH condition, 60 °C, 50 mA and 33% IPA as co-solvent. (b) Kinetic evaporation curves of toluene, anisole, and benzene (non-reducible products) under standard ECH condition, 60 °C, 50 mA and 33% IPA as co-solvent. (c) Extraction efficiency of cyclohexanol and 1-cyclohexylethanol in pH 8 borate buffer with 33% IPA.

In the evaporation curves Figure 2.7 a-b, benzene, toluene, and ethylbenzene (low water solubility) almost completely evaporated after 9 hours of ECH. The slightly more polar anisole also evaporated, but more slowly than the non-polar alkyl benzenes. Cyclohexanol and 1-

cyclohexylethanol suffered less evaporation loss in this period (~20%), but the extraction process of both alcohols caused ~20% loss (Figure 2.7 c). The evaporation curves of cyclohexanol and 1-cyclohexylethanol were used to correct the yields in the ECH kinetics. The correction process is described below. However, due to their volatility, corrections for the alkylbenzenes could not be reliably applied to the kinetic data, because their rates of evaporation are faster than their rates of formation. Though slower than the alkyl benzenes, anisole's evaporation was still faster than its formation. Thus, evaporation corrections for anisole were also unable to be applied in the kinetic data. Therefore, the actual yields of alkylbenzene and anisole were larger than the reported numbers. Note that water condensers were equipped in both ECH and evaporation studies, but the recoveries of alkyl benzenes were still low.

End Products Evaporation in Different Co-solvent

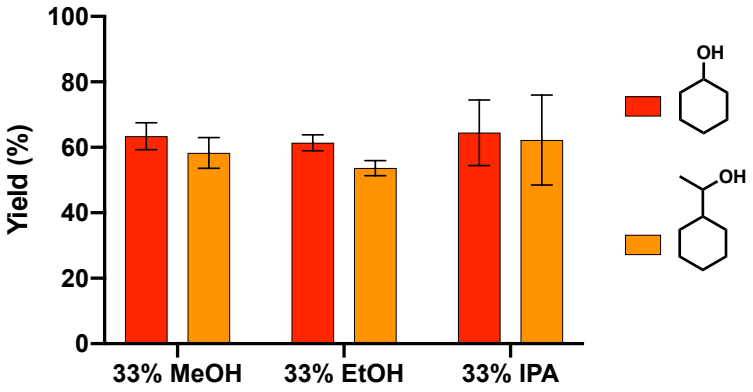

Figure 2.8 Cyclohexanol and 1-cyclohexylethanol evaporation efficiencies in different co-solvent (33% v/v) mixtures after 9 hours of ECH at 60 °C with 2-propanol treated electrode under 50 mA.

In the co-solvent studies, methanol and ethanol were also used as co-solvents (Figure 2.2). The ECH in both alcohols also generated the aromatic reduction products cyclohexanol and 1-cyclohexylethanol. Evaporation corrections for these two products in 33% v/v methanol and ethanol were also performed to correct the corresponding quantified yields.

Aromatic Intermediates Extraction Efficiency in Different Co-Solvent

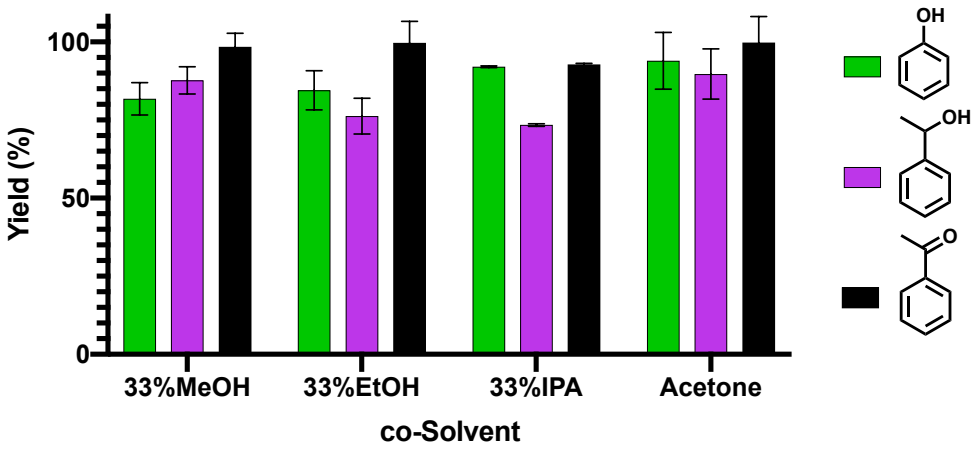

Figure 2.9 Extraction efficiencies of aromatic intermediates phenol, 1-phenylethanol and acetophenone in different co-solvents (33% v/v). Standard deviations shown are from triplicate measurements.

For the three reducible aromatic intermediates, phenol, 1-phenylethanol and acetophenone, only extraction corrections were applied to the quantified yield. Phenol and acetophenone both could be efficiently extracted out of the buffer mixture. However, in 33% v/v ethanol and isopropyl alcohol the extraction efficiency of 1-phenylethanol is lower. All extraction efficiency experiments performed in triplicate; their standard deviations are shown in Figure 2.9. The lower extraction efficiency of 1-phenylethanol is likely due to the high content of organic co-solvent, since 1-phenylethanol can be efficiently extracted out of the pure buffer system, as shown in Figure 2.10.

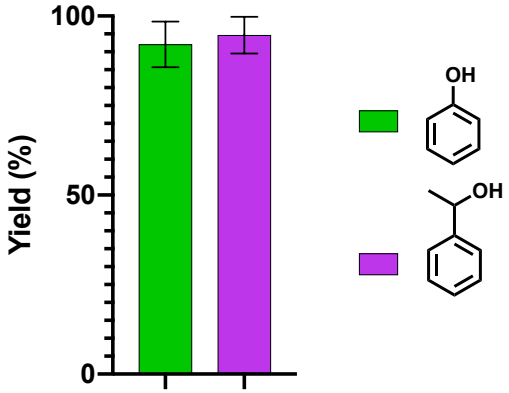

Figure 2.10 Extraction efficiencies of phenol and 1-phenylethanol for **100% pH 8 borate buffer**. Note, acetophenone is not soluble in 100% borate buffer.

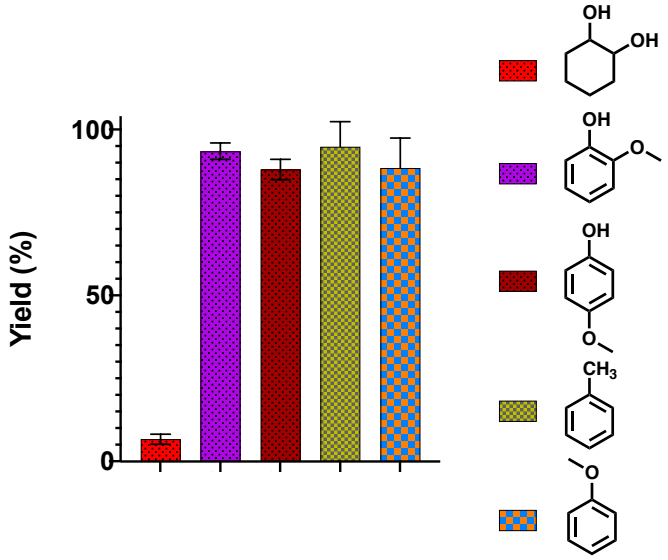

Figure 2.11 Extraction efficiencies of 1,2-dihydroxycyclohexane, 2-methoxyphenol, 4-methoxyphenol, toluene and anisole in 33% v/v IPA borate buffer solution.

The extraction efficiencies of the aromatic intermediates were used to correct the yields of the intermediates in the kinetic data as described in the example below. The extraction solvent is dichloromethane as described in the quantitative analysis section below.

2.2.5 Evaporation and Extraction Correction Application Examples

Figure 2.12 illustrates the application of yield corrections for evaporation and extraction losses of the corresponding products. The applied corrections only influence the yield values, not the kinetic reduction results. Figures 2.12a and 2.12b both show the same kinetic pattern; the ketone dimer undergoes direct cleavage to become the corresponding aromatic monomer first. Phenol competes with 1-phenylethanol in aromatic reduction, with formation of cyclohexanol faster than 1-cyclohexylethanol, as already observed in the quantified Figure 2.12a. But without the extraction correction, the buildup and decay of 1-phenylethanol looks similar to that of phenol, which is not matched with the slower formation of 1-cyclohexylethanol.

As reported in Figure 2.9, the extraction efficiency of 1-phenylethanol is lower than that of phenol in 33% v/v 2-propanol. After the extraction correction, the reported formation and decay of 1-phenylethanol is more consistent with the slower formation of 1-cyclohexylethanol.

Yield Correction Example: β-O-4 type Model Compound

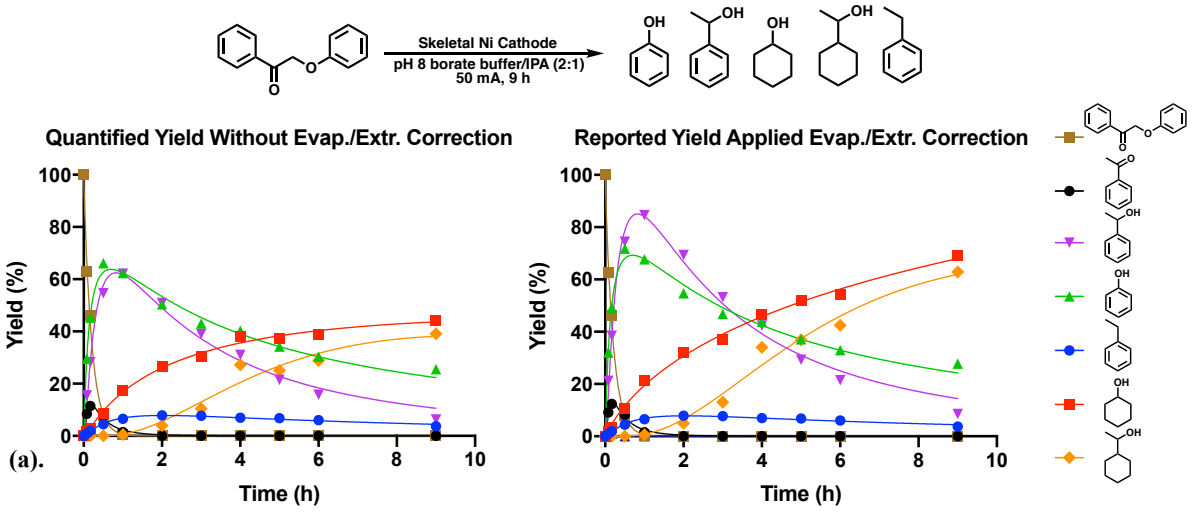

Figure 2.12 (a) ECH kinetic measurements of 2-phenoxyacetophenone, quantified yields without any correction. (b) ECH kinetic measurements of 2-phenoxyacetophenone, reported yields with evaporation/extraction corrections. ECH performed at standard condition, 50 mA, 60 °C and IPA treated electrode with 33% v/v IPA.

All yield corrections in the kinetic measurements of β-O-4 type aryl ether models follow the method described below. Due to the low solubility and high vapor pressure of alkylbenzene products in the aqueous system, the rate of evaporation is faster than the rate of formation. Therefore, quantified yields of alkylbenzenes had no correction, and the actual yield should be higher than the reported numbers. No yield corrections were used for the nonpolar aryl ethers (starting materials) as their volatility is low and extraction efficiency is high. The reported numbers were based on the gas chromatographic (GC) analyses. For reducible aromatic intermediates such as phenol, 1-phenylethanol and acetophenone, the quantified GC yields were only corrected for extraction losses. For non-reducible end products, such as cyclohexanol and 1-cyclohexylethanol, the quantified GC yield was corrected for evaporation, which included the extraction losses.

Extraction Correction:

$$Yield\ (reported) = \frac{Yield\ (quantified)}{Extraction\ Efficiency} \qquad [1]$$

Example: Phenol Sample at 9 hours (Figure 2.12)

$$Yield\ (reported) = \frac{Yield\ (quantified)}{Extraction\ Efficiency} = \frac{26\%}{0.92} = 28\%$$

- Extraction Efficiency of phenol in 33% v/v IPA buffer mixtures is 0.92 (Figure 2.9)

Evaporation Correction:

$$Yield\ (reported) = \frac{Yield\ (quantified)}{Evaporation\ Efficiency} \qquad [2]$$

Example: Cyclohexanol Sample at 9 h (Figure 2.12)

$$Yield\ (reported) = \frac{Yield\ (quantified)}{Evaporation\ Efficiency} = \frac{44\%}{0.64} = 69\%$$

- Evaporation Efficiency of Cyclohexanol after 9 hour ECH at 50 mA is 0.64 (Figure 2.7a)

Yield Correction Example: 4-O-5 Type Model Compound (diaryl ethers)

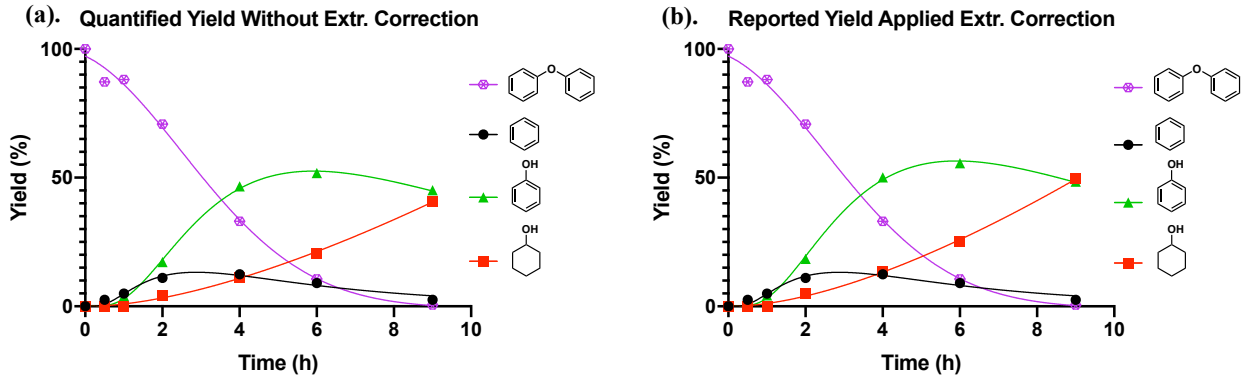

Figure 2.13 (a) ECH reaction profile of diphenyl ether, showing quantified yields from GC-MS measurements. (b) ECH reaction profile of diphenyl ether, showing reported yield after extraction corrections for cyclohexanol and phenol.

No yield corrections were applied for benzene or diphenyl ether. ECH performed at standard conditions, 60 °C, 50 mA and 33% v/v 2-propanol (IPA) as co-solvent.In the case of diaryl ethers, due to their much slower ether cleavage rates (compared with the β-O-4 models), only extraction corrections for the more stable polar products were applied. Extraction correction was performed following the above equation [1].

2.3 Experimental Details

2.3.1 General Information

All purchased chemicals were tested for purity using ^{1}H NMR prior to use. All ECH reactions were performed followed below experiment procedures. All electrodes were prepared followed the described procedures. Column chromatographic purification of reaction mixtures was performed using Silicycle (Quebec City, Canada) SiliaFlash P60 silica gel (40-63 μm). Thin layer chromatography (TLC) analysis of reaction mixtures was performed using Sigma Aldrich (St. Louis, MO) plastic silica gel 60 F-254 plates and the bands were visualized using UV light (254 nm). Nuclear magnetic resonance (NMR) spectra were acquired on Agilent 500/54 premium shielded instruments at the Michigan State University Max T. Rogers NMR facility. ^{1}H and ^{13}C chemical shifts are reported in ppm downfield of tetramethylsilane and referenced to residual solvent peak ($CHCl_3$; $\delta H = 7.26$ ppm). GC-MS analyses were performed on an Agilent 7890A GC/ single quadrupole mass spectrometer with 5975C inert XL MSD (Agilent, Santa Clara, CA) equipped with Agilent J&W VF-5ms column (30 m x 0.25 mm x 0.25 mm) (Agilent, Santa Clara, CA). GC-MS yields were determined based on external standards with prepared concentrations (0.125 mM - 4 mM) to form a 6-point calibration curve for each compound of interest. Each GC-MS analysis sequence included a freshly prepared external standard sequence.

2.3.2 Preparation of Plating Solution:

Following Reported Procedures.[6, 7] To a 1 L volumetric flask, 213 g of $NiCl_2 \cdot 6H_2O$ and 30 g of NH_4Cl were added, 500 mL of deionized water was then added, followed by 200 mL of NH_4OH solution

(28~30% NH_3) to keep the plating bath pH between 9-10. Deionized water was then added to make a total volume of 1 L plating solution.

2.3.3 Preparation of pH 8 Borate Buffer (0.1 M):

Following Reported Procedures.[6, 7] To a 500 mL volumetric flask, 3.00 g of H_3BO_3 (0.097 M) and 1.00 g of $K_2B_4O_7 \cdot 4H_2O$ (0.0066 M) were added, the chosen water/co-solvent mixture (most commonly 2:1 v/v H_2O/IPA) was added to make a buffer with 500 mL total volume. Depending on measured pH, if needed, KOH was added to adjust pH to 8.

2.3.4 Preparation of pH 7 Phosphate Buffer (0.1 M):

Following Reported Procedures.[6, 7] To a 1 L volumetric flask, 5.30 g of KH_2PO_4 (0.039 M) and 10.8 g of K_2HPO_4 (0.062 M) was added, deionized water was added to make a buffer solution with 1 L total volume.

2.3.5 Preparation of Skeletal Nickel Cathode Electrode

To achieve maximum surface area that contains the most potential active sites, a square piece of stainless-steel wire mesh was subjected to nickel electroplating to trap the aluminum-nickel powder. 1.5 g of Aluminum-nickel (1:1) alloy purum was placed in 50 ml of the above nickel-ammonia plating solution with stirring at 350 rpm. A square of stainless steel 314 screen (50 mesh, 2.5 x 2.5 cm) connected to the cathode was positioned facing parallel to a plain nickel bar as a sacrificial anode. Application of electrical current effects direct deposition of nickel on the mesh, trapping the nickel-aluminum powder during the reduction of nickel ions. The plating

current was maintained at 0.6 A for approximately 1~2 hours, and the cathode was turned 180° every 30 minutes to ensure even deposition of the nickel-aluminum particles on both sides. The plated skeletal nickel cathode was then activated in 30 wt% NaOH solution at 75 °C for 6 hours to etch out the aluminum. After the etching process, the activated skeletal Ni electrode was washed with deionized water to wash off the surface base and stored in 2-propanol (IPA) for a minimum of 24 hours before the next use.

As reported in the previous studies[7], 2-propanol (IPA) was found to be a good storage solvent to maintain low surface oxide levels on the Ni catalyst.

2.3.6 Preparation of CoP Anode[8]

The Kanan-Nocera[8] cobalt phosphate (Co-P) water splitting anode electrode was formed in-situ during the electro-catalytic process before the injection of the organic substrate in the cathode half-cell. A flat square of stainless steel (8 mesh, 12 cm x 4 cm) was rolled up into a cylinder shape with a cross-section of 2.5 cm x 2.5 cm and immersed in the electrolyte in the anode half-cell in 30 ml of 0.1 M potassium phosphate buffer with 30 mg of $Co(NO_3)_2 \cdot 6H_2O$. Under application of electrical current, the Co-P deposited on the stainless-steel surface as a black thin coating, which enabled oxygen evolution and proton production via water oxidation.

2.3.7 General Procedure of Electrocatalytic Hydrogenation (ECH)[7]

The electrocatalytic hydrogenation/hydrogenolysis (ECH) of all aryl ethers followed a previously reported procedure.[7] The two half cells were separated by a Nafion 117 membrane. The cathode half-cell was equipped with a water condenser to prevent evaporative loss of the buffer solution. The skeletal Ni cathode was placed in the cathode side with 20 mL of 0.1 M pH 8

potassium borate buffer with the addition of 8 mL 2-propanol as co-solvent. A small stir bar was also placed inside the cathode half-cell (stirring at 300 rpm). An additional 2 ml of 2-propanol was used to dissolve the weighed aryl ether substrate (0.25 mmol) in a 4-mL glass vial, in preparation for its addition to the cathode solution. The Co-P coated stainless steel anode was placed in 30 mL of 0.1 M pH 7 potassium phosphate buffer. The entire set up was placed in a water bath where the temperature was maintained at 60 °C. The divided cell containing both electrodes was equilibrated for 30 mins to obtain a constant current at 50 mA (current density 8 mA/cm^2, ~10 V). The vial with the 2 mL of 2-propanol and the aryl ether substrate was then added into the cathode solution and subjected to ECH for 9-12 hours at 60 °C under ambient pressure.

For the co-solvent studies, the ECH procedure is the same as above, but with modifications in the choice of the organic co-solvent and the ratio of co-solvent to buffer.

2.3.8 Quantitative Analysis Preparation:

At each desired time point, 0.25 mL of cathode solution was syringed into a 1.7 mL conical vial for extraction. To extract the organics, 3 drops of diluted HCl solution (1 M) were added to the conical vial to acidify the cathode solution, following by 3 drops of saturated NaCl solution and 1 mL of dichloromethane (DCM). The conical vial was then vortexed, and the bottom DCM layer was carefully pipetted into a GC vial. The sample was analyzed through GC-MS and quantified using calibration curves based on the corresponding external standard of each compound. Every sequence of the GC-MS analyses included a set of freshly prepared external standard calibration samples.

2.3.9 Aryl Ether Synthesis

To study the cleavage mechanism of β-O-4 type alkyl aryl ether and diaryl ethers, model compounds with different functional moieties are needed. Lignin is composed of aromatic units containing hydroxyl, methoxy and alkyl substituents. Most of the diaryl ether persistent organic pollutants also contain different substituted aromatic units (Figure 2.14). Therefore, synthetic methods with practical and economically feasible approaches were selected to synthesize model aryl ethers representing these substitution classes.

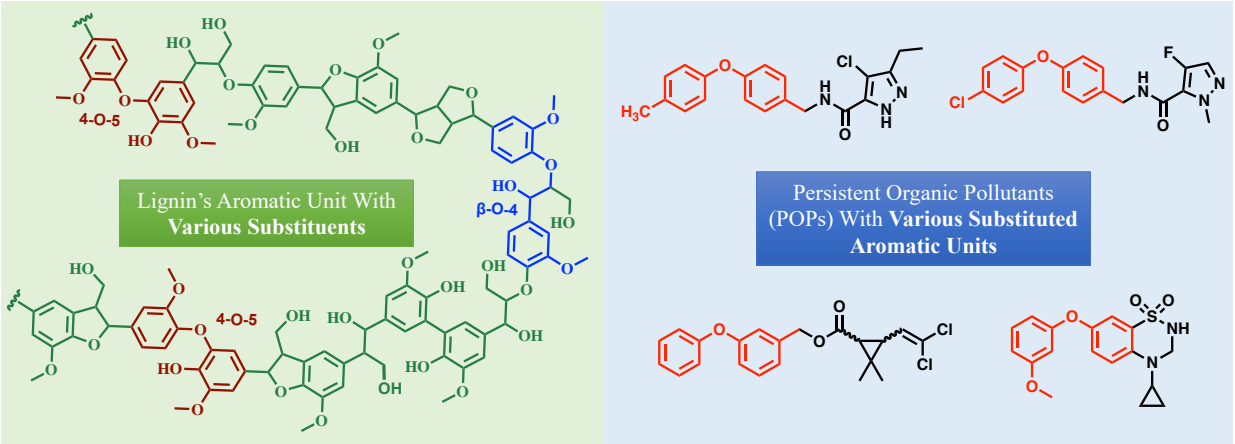

Figure 2.14 Representation of lignin structure and persistent organic pollutants (POPs) with common aromatic units highlighted in color.

2.3.10 Dimer Synthesis Procedures

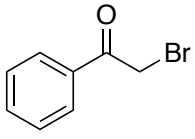

2-bromo-1-phenylethanone: This compound was prepared following a literature procedure with modification.[9] Acetophenone (6.0 g, 50 mmol) was added into 70 mL of $CHCl_3$ in a 250 mL round bottom flask. To this mixture, bromine (8.4 g, 52.5 mmol) dissolved in another 70 mL of $CHCl_3$ was added dropwise over 2 hours at room temperature. After the completion of the reaction, the reaction mixture was washed with saturated $Na_2S_2O_3$ and brine solution. The organic layer was dried over anhydrous Na_2SO_4

and concentrated under vacuo. The crude product was directly carried forward to the next step without purification. ^{1}H NMR (500 MHz, $CDCl_3$) δ 7.99 (dd, *J* = 8.3, 1.4 Hz, 2H), 7.67 – 7.58 (m, 1H), 7.56 – 7.47 (m, 2H), 4.47 (s, 2H). Spectral data are consistent with those reported in the literature.[10]

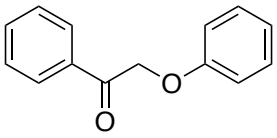

2-phenoxyacetophenone: This compound was prepared following a literature procedure.[9] Potassium carbonate (5.23 g, 37.8 mmol) and phenol (3.55 g, 37.8 mmol) were stirred in acetone (75 mL) at room temperature for 30 minutes. 2-bromo-1-phenylethanone (5 g, 25.2) dissolved in another 75 mL of acetone was added dropwise to the mixture and stirred overnight at room temperature. The reaction was filtered, and dried over anhydrous Na_2SO_4 and concentrated under vacuo. The solids were recrystallized from ethanol producing a white crystal (3.96 g) in 75% yield. ^{1}H NMR (500 MHz, $CDCl_3$) δ 8.02 (dd, *J* = 8.4, 1.3 Hz, 2H), 7.66 – 7.61 (m, 1H), 7.52 (dd, *J* = 8.4, 7.1 Hz, 2H), 7.33 – 7.28 (m, 2H), 7.00 (tt, *J* = 7.4, 1.1 Hz, 1H), 6.96 (dt, *J* = 7.8, 1.0 Hz, 2H), 5.29 (s, 2H). Spectral data are consistent with those reported in the literature.[9]

2-phenoxy-1-phenylethan-1-ol: This compound was prepared following a literature procedure.[9]

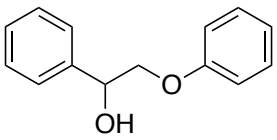

2-phenoxyacetophenone (2.25 g, 10.6 mmol) was added to MeOH (80 mL). To this mixture, $NaBH_4$ (0.6 g, 15.9 mmol) was added in small portions and stirred overnight at RT. After the completion of the reaction, saturated NH_4Cl (100 mL) solution was added and the mixture was extracted with CH_2Cl_2 and washed with deionized water. The organic layer was dried over anhydrous Na_2SO_4 and concentrated under vacuum, giving 97% yield of the pure product (2.2 g). ^{1}H NMR (500 MHz, $CDCl_3$) δ 7.50 – 7.46 (m, 2H), 7.44 –

7.38 (m, 2H), 7.38 – 7.33 (m, 1H), 7.33 – 7.28 (m, 2H), 6.99 (tt, *J* = 7.5, 1.1 Hz, 1H), 6.95 – 6.91 (m, 2H), 5.15 (dt, *J* = 8.9, 2.8 Hz, 1H), 4.13 (dd, *J* = 9.5, 3.1 Hz, 1H), 4.02 (t, *J* = 9.3 Hz, 1H), 2.77 (d, *J* = 2.4 Hz, 1H). Spectral data are in accordance with those previously reported.[9]

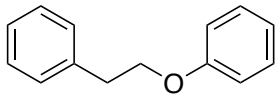

1-phenyl-2-phenoxyethane: This compound was prepared following a literature procedure with modification.[9] Potassium carbonate (3.6 g, 26.0 mmol) and phenol (2.45 g, 26.0 mmol) were stirred in DMF (45 mL) at room temperature for 30 minutes. 2-bromo-1-phenylethane (3.7 g, 20.0 mmol) was added dropwise to the mixture and stirred overnight at room temperature. After the completion of the reaction, cold water was added into the reaction mixture. The aqueous mixture was extracted with diethylether (2×60 mL). The combined organic extracts were washed with brine, dried over Na_2SO_4 and concentrated in vacuo. The crude product was purified by column chromatography (Pentane/DCM, 4:1) to give 2-phenoxy-1-phenylethane as an oil (0.97 g) in 24% yield. ^{1}H NMR (500 MHz, $CDCl_3$) δ 7.38 – 7.23 (m, 7H), 6.95 (td, *J* = 7.3, 1.1 Hz, 1H), 6.92 (dt, *J* = 7.9, 1.0 Hz, 2H), 4.19 (t, *J* = 7.1 Hz, 2H), 3.12 (t, *J* = 7.2 Hz, 2H). Spectral data are in accordance with those previously reported.[9]

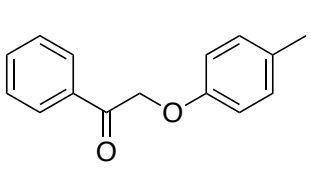

1-phenyl-2-(p-tolyloxy)ethan-1-one: This compound was prepared following a literature procedure.[11] A 250 mL round bottom flask connected with a dropping funnel was charged with *p*-cresol (6.5 g, 60 mmol) and K_2CO_3 (11 g, 79 mmol) in acetone (50 mL) and stirred at room temperature. To this solution, 2-bromoacetophenone (7.9 g, 40 mmol) in acetone (50 mL) was added dropwise at room temperature. The resulting suspension was stirred at room temperature overnight; the suspension was filtered and concentrated *in vacuo*. The crude product was purified by column chromatography

using EtOAc/hexane (1:9) to give 1-phenyl-2-(*p*-tolyloxy)ethan-1-one as a white solid (4.8 g) in 53% yield after solvent removal. ^{1}H NMR (500 MHz, $CDCl_3$) δ 8.01 (dd, *J* = 8.4, 1.3 Hz, 2H), 7.69 – 7.58 (m, 1H), 7.51 (t, *J* = 7.8 Hz, 2H), 7.13 – 7.05 (m, 2H), 6.86 (d, *J* = 8.6 Hz, 2H), 5.26 (s, 2H), 2.29 (s, 3H). Spectral data are in accordance with those previously reported.[11]

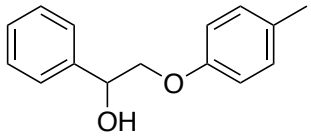

1-phenyl-2-(p-tolyloxy)ethanol: This compound was prepared following a literature procedure.[9] 1-phenyl-2-(p-tolyloxy)ethan-1-one (0.87 g, 3.84 mmol) was added to MeOH (40 mL). To this mixture, $NaBH_4$ (0.5 g, 13.2 mmol) was added in small portions and stirred overnight at RT. After the completion of the reaction, saturated NH_4Cl (100 mL) solution was added and the mixture was extracted with CH_2Cl_2 and washed with deionized water. The organic layer was dried over anhydrous Na_2SO_4 and concentrated under vacuum. The crude product was purified by column chromatography using EtOAc /hexane (1:4) to give 1-phenyl-2-(*p*-tolyloxy)ethanol as a white solid (0.59 g) in 67% yield after solvent removal. ^{1}H NMR (500 MHz, $CDCl_3$) δ 7.48 – 7.45 (m, 2H), 7.40 (ddd, *J* = 7.7, 6.3, 1.3 Hz, 2H), 7.37 – 7.32 (m, 1H), 7.14 – 7.06 (m, 2H), 6.83 (d, *J* = 8.5 Hz, 2H), 5.13 (dd, *J* = 9.0, 3.1 Hz, 1H), 4.10 (dd, *J* = 9.6, 3.1 Hz, 1H), 3.99 (t, *J* = 9.3 Hz, 1H), 2.30 (s, 3H). Spectral data are in accordance with those previously reported.[11]

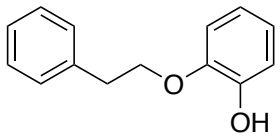

2-(2-phenylethoxy)phenol: Potassium carbonate (1.6 g, 11.6 mmol) and catechol (1.27 g, 11.5 mmol) were stirred in DMF (45 mL) at 90 °C for 30 minutes. 2-bromo-1-phenylethane (1.85 g, 10.0 mmol) was added dropwise to the mixture and stirred overnight at 90 °C. After the completion of the reaction, cold water was added into the reaction mixture. The aqueous mixture was extracted with diethylether

(2×60 mL). The combined organic extracts were washed with brine, dried over Na_2SO_4 and concentrated in vacuo. The crude product was purified by column chromatography (Hexane/EtOAc, 9:1) to give 2-(2-phenylethoxy)phenol as an oil (0.39 g) in 18% yield. ^{1}H NMR (500 MHz, $CDCl_3$) δ 7.34 (t, *J* = 7.4 Hz, 2H), 7.30 – 7.24 (m, 3H), 6.87 (m, *J* = 22.0, 18.0, 7.6, 1.8 Hz, 4H), 5.48 (s, 1H), 4.26 (t, *J* = 6.8 Hz, 2H), 3.13 (t, *J* = 6.8 Hz, 2H). Spectral data are in accordance with those previously reported.[12]

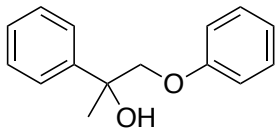

1-phenoxy-2-phenyl-2-propanol: This compound was prepared following a literature procedure.[9] To a stirring solution of 2-phenoxyacetophenone (0.5 g, 2.36 mmol) in anhydrous THF (15 mL), 2 mL of methyllithium (0.6 M in Et_2O) was added dropwise at 0 °C, under argon. The reaction mixture was stirred for 10 hours where the temperature slowly warmed up to room temperature. The reaction was quenched with saturated ammonium chloride solution (15 mL). The aqueous layer was extracted with diethylether (3×20 mL). The combined organic extracts were washed with brine, dried over Na_2SO_4 and concentrated in vacuo. The crude product was purified by column chromatography (pentane/DCM 7:3) to give 1-phenoxy-2-phenyl-2-propanol (0.192 g) in 36% yield. ^{1}H NMR (500 MHz, $CDCl_3$) δ 7.57 – 7.52 (m, 2H), 7.39 (ddd, *J* = 8.1, 6.9, 1.8 Hz, 2H), 7.33 – 7.27 (m, 3H), 7.00 – 6.95 (m, 1H), 6.93 – 6.89 (m, 2H), 4.13 (dd, *J* = 9.0, 1.8 Hz, 1H), 4.04 (dd, *J* = 9.0, 1.8 Hz, 1H), 2.82 (d, *J* = 1.8 Hz, 1H), 1.68 (d, *J* = 1.8 Hz, 3H). Spectral data are consistent with those reported in the literature.[9]

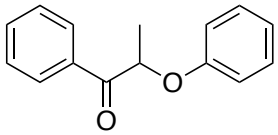

2-phenoxy-1-phenylpropan-1-one: To a stirring solution of sodium hydride (0.226 g, 5.6 mmol, 60% in mineral oil) in anhydrous THF (20 mL), 2-phenoxyacetophenone (1.0 g, 4.71 mmol) in anyhydrous THF (20 mL) was added in two portions at 0 °C, under argon. The reaction mixture was stirred for 20 min. Methyl iodide (0.32 mL, 5.6 mmol) was added dropwise at 0 °C, and the solution was warmed to room temperature. The reaction mixture was monitored by TLC. The mixture was quenched by slow addition of water (30 mL) and extracted with diethylether (2×30 mL). The combined organic extracts were washed with brine and dried over anhydrous Na_2SO_4, filtered and evaporated to give a crude oil. The oil was purified by column chromatography (pentane/DCM, 1:1) to give 2-phenoxy-1-phenyl-1-propanone as white solid (0.57 g) in 54% yield. ^{1}H NMR (500 MHz, $CDCl_3$) δ 8.14 – 8.04 (m, 2H), 7.68 – 7.55 (m, 1H), 7.48 (t, *J* = 7.8 Hz, 2H), 7.26 – 7.22 (m, 2H), 6.94 (t, *J* = 7.4, 1.0 Hz, 1H), 6.88 (d, *J* = 7.3, 1.0 Hz, 2H), 5.49 (q, *J* = 6.9 Hz, 1H), 1.72 (d, *J* = 6.9, 0.7 Hz, 3H). Spectral data are in accordance with those previously reported.[13]

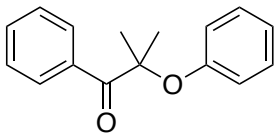

2-methyl-2-phenoxy-1-phenylpropan-1-one: This compound was prepared following a literature procedure.[9] To a stirring solution of sodium hydride (0.47 g, 11.7 mmol, 60% in mineral oil) in anhydrous THF (20 mL), 2-phenoxyacetophenone (1.0 g, 4.71 mmol) in anhydrous THF (20 mL) was added in two portions at 0 °C, under argon. The reaction mixture was stirred for 20 min. Methyl iodide (0.63 mL, 9.9 mmol) was added dropwise at 0 °C, and the solution was warmed to room temperature. The reaction mixture was monitored by TLC. The mixture was quenched by slow addition of water (30 mL) and extracted with diethyl ether (2×30 mL). The combined organic extracts were washed with brine and dried over anhydrous Na_2SO_4, filtered, and evaporated to give a crude oil. The oil

was purified by column chromatography (pentane/DCM, 4:1) to give 2-methyl-2-phenoxy-1-phenylpropan-1-one as white solid (0.5 g) in 44% yield. ^{1}H NMR (500 MHz, $CDCl_3$) δ 8.38 – 8.24 (m, 2H), 7.49 (t, *J* = 7.2, 1.3 Hz, 1H), 7.42 – 7.35 (m, 2H), 7.18 – 7.11 (m, 2H), 6.89 (t, *J* = 7.3, 1.1 Hz, 1H), 6.79 – 6.74 (m, 2H), 1.70 (s, 6H). Spectral data are in accordance with those previously reported.[9]

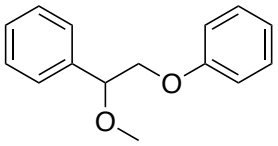

(**1-methoxy-2-phenoxyethyl)benzene:** This compound was prepared following a literature procedure.[9] To a stirring solution of sodium hydride (0.14 g, 3.5 mmol, 60% in mineral oil) in anhydrous THF (10 mL), 2-phenoxy-1-phenylethanol (0.5 g, 2.33 mmol) in anyhydrous THF (10 mL) was added in two portions at 0 °C, under argon. The resulting suspension was stirred at 0 °C for 1 h. Then iodomethane (0.174 mL, 2.80 mmol) was added dropwise. The reaction mixture was monitored by TLC. The reaction was quenched with saturated ammonium chloride solution. The aqueous layer was extracted with diethylether (2×30 mL). The combined organic extracts were washed with brine, dried over Na_2SO_4 and concentrated in vacuo. The crude product was purified by column chromatography, first with pentane to remove the mineral oil followed by (pentane/DCM 4:1) to give (1-methoxy-2-phenoxyethyl)benzene as an oil (0.39 g) in 75% yield after solvent removal. ^{1}H NMR (500 MHz, $CDCl_3$) δ 7.41 (d, *J* = 4.4 Hz, 4H), 7.38 – 7.33 (m, 1H), 7.30 – 7.24 (m, 2H), 6.97 – 6.89 (m, 3H), 4.60 (dd, *J* = 8.0, 3.6 Hz, 1H), 4.18 (dd, *J* = 10.2, 8.0 Hz, 1H), 4.01 (dd, *J* = 10.3, 3.6 Hz, 1H), 3.37 (s, 3H). Spectral data are in accordance with those previously reported.[9]

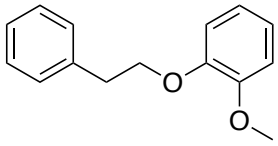

1-methoxy-2-(2-phenylethoxy)benzene: This compound was prepared following a literature procedure with modification.[9] Potassium carbonate (3.37 g, 24.4 mmol) and guaiacol (3.00 g, 24.2 mmol) were stirred in DMF (60 mL) at room temperature for 30 minutes. 2-bromo-1-phenylethane (3.00 g, 16.2 mmol) was added dropwise to the mixture and stirred overnight at room temperature. After the completion of the reaction, cold water was added into the reaction mixture. The aqueous mixture was extracted with diethylether (2×60 mL). The combined organic extracts were washed with brine, dried over Na_2SO_4 and concentrated in vacuo. The crude product was purified by column chromatography (Pentane/DCM, 4:1) to give 1-methoxy-2-(2-phenylethoxy)benzene as an oil (0.89 g) in 25% yield. ^{1}H NMR (500 MHz, $CDCl_3$) δ 7.36 – 7.29 (m, 4H), 7.26 (d, J = 9.3 Hz, 1H), 6.98 – 6.87 (m, 4H), 4.23 (dd, J = 8.1, 7.3 Hz, 2H), 3.88 (s, 3H), 3.18 (t, J = 7.7 Hz, 2H). Spectral data are in accordance with those previously reported.[14]

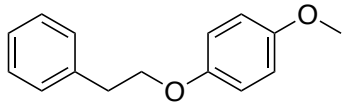

1-methoxy-4-(2-phenylethoxy)benzene: This compound was prepared following a literature procedure with modification.[9] Potassium carbonate (3.37 g, 24.4 mmol) and 4-methoxyphenol (3.00 g, 24.2 mmol) were stirred in DMF (60 mL) at room temperature for 30 minutes. 2-phenethyl bromide (3.00 g, 16.2 mmol) was added dropwise to the mixture and stirred overnight at room temperature. After the completion of the reaction, cold water was added into the reaction mixture. The aqueous mixture was extracted with diethylether (2×60 mL). The combined organic extracts were washed with brine, dried over Na_2SO_4 and concentrated in vacuo. The crude product was purified by column chromatography (Pentane/DCM, 4:1) to give 1-methoxy-4-(2-phenylethoxy)benzene as a white solid (0.94 g) in 26%

yield. ^{1}H NMR (500 MHz, $CDCl_3$) δ 7.39 – 7.20 (m, 5H), 6.87 – 6.80 (m, 4H), 4.14 (t, *J* = 7.2 Hz, 2H), 3.77 (s, 3H), 3.09 (t, *J* = 7.2 Hz, 2H). Spectral data are in accordance with those previously reported.[15]

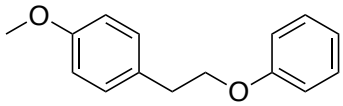

1-methoxy-4-(2-phenoxyethyl)benzene: This compound was prepared following a literature procedure with modification.[9] Potassium carbonate (0.96 g, 6.95 mmol) and phenol (0.66 g, 7.00 mmol) were stirred in DMF (30 mL) at room temperature for 30 minutes. 2-(4-methoxyphenyl)ethyl bromide (1.00 g, 4.65 mmol) was added dropwise to the mixture and stirred overnight at room temperature. After the completion of the reaction, cold water was added into the reaction mixture. The aqueous mixture was extracted with diethylether (2×30 mL). The combined organic extracts were washed with brine, dried over Na_2SO_4 and concentrated in vacuo. The crude product was purified by column chromatography (Pentane/DCM, 4:1) to give 1-methoxy-4-(2-phenoxyethyl)benzene as an oil (0.28 g) in 27% yield. ^{1}H NMR (500 MHz, $CDCl_3$) δ 7.32 – 7.27 (m, 2H), 7.24 – 7.19 (m, 2H), 6.94 (td, *J* = 7.3, 1.2 Hz, 1H), 6.91 (dd, *J* = 7.6, 1.2 Hz, 2H), 6.87 (dd, *J* = 8.6, 1.4 Hz, 2H), 4.14 (t, *J* = 7.2, 1.3 Hz, 2H), 3.81 (s, *J* = 1.4 Hz, 3H), 3.05 (t, *J* = 7.2, 1.3 Hz, 2H). Spectral data are in accordance with those previously reported.[16]

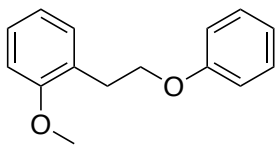

1-methoxy-2-(2-phenoxyethyl)benzene: This compound was prepared following a literature procedure with modification.[9] Potassium carbonate (0.64 g, 4.63 mmol) and phenol (0.44 g, 4.67 mmol) were stirred in DMF (30 mL) at room temperature for 30 minutes. 2-(2-methoxyphenyl)ethyl bromide (0.5 g, 2.32 mmol) was added dropwise to the mixture and stirred overnight at room temperature. After the

completion of the reaction, cold water was added into the reaction mixture. The aqueous mixture was extracted with diethylether (2×30 mL). The combined organic extracts were washed with brine, dried over Na_2SO_4 and concentrated in vacuo. The crude product was purified by column chromatography (Pentane/DCM, 4:1) to give 1-methoxy-2-(2-phenoxyethyl)benzene as an oil (0.15 g) in 28% yield. ^{1}H NMR (500 MHz, $CDCl_3$) δ 7.32 – 7.22 (m, 4H), 6.98 – 6.90 (m, 4H), 6.90 – 6.87 (m, 1H), 4.17 (t, *J* = 7.4 Hz, 2H), 3.86 (s, 3H), 3.13 (t, *J* = 7.4 Hz, 2H). Spectral data are in accordance with those previously reported.[16]

1-methyl-4-(2-phenoxyethyl)benzene: This compound was prepared following a literature procedure with modification.[9] Potassium carbonate (1.04 g, 7.53 mmol) and phenol (0.71 g, 7.54 mmol) were stirred in DMF (30 mL) at room temperature for 30 minutes. 4-methylphenethyl bromide (1.00 g, 5.02 mmol) was added dropwise to the mixture and stirred overnight at room temperature. After the completion of the reaction, cold water was added into the reaction mixture. The aqueous mixture was extracted with pentane (2×30 mL). The combined organic extracts were washed with brine, dried over Na_2SO_4 and concentrated in vacuo. The crude product was purified by column chromatography (Pentane/DCM, 4:1) to give 1- as an oil (0.41 g) in 39% yield. ^{1}H NMR (500 MHz, $CDCl_3$) δ 7.31 – 7.26 (m, 2H), 7.19 (d, *J* = 7.7 Hz, 2H), 7.14 (d, *J* = 7.6 Hz, 2H), 6.94 (tt, *J* = 7.4, 1.1 Hz, 1H), 6.92 – 6.89 (m, 2H), 4.16 (t, *J* = 7.2, 1.2 Hz, 2H), 3.08 (t, *J* = 7.2 Hz, 2H), 2.35 (s, 3H). Spectral data are in accordance with those previously reported.[17]

2-phenoxy-1-(p-tolyl)ethan-1-one: This compound was prepared according to literature procedure.[11] 2- bromo-1-(*p*-tolyl)ethan-1-one

(2.15 g, 10.1 mmol) was added to a mixture of potassium carbonate (2.07 g, 15.07 mmol) and phenol (0.95 g, 10.1 mmol) in acetone (15 mL). The mixture was stirred at room temperature overnight. The reaction was filtered; the solvent was removed by rotary evaporation and the resulting solid was re-dissolved in EtOAc/diethyl ether and washed with brine. The organic layer was dried with Na_2SO_4, rotary evaporated, and then recrystallized from 2-propanol forming a white crystal (0.59 g) in 26% yield. ^{1}H NMR (500 MHz, $CDCl_3$) δ 7.91 (d, J = 8.3 Hz, 2H), 7.32 – 7.27 (m, 4H), 7.02 – 6.96 (m, 1H), 6.95 (dt, J = 7.8, 1.0 Hz, 2H), 5.25 (s, 2H), 2.43 (s, 3H). Spectral data are in accordance with those previously reported.[18]

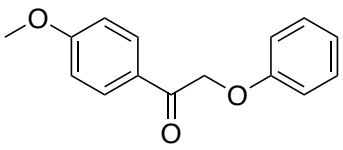

1-(4-methoxyphenyl)-2-phenoxyethan-1-one: This compound was prepared according to literature procedure.[11] Potassium carbonate (5.2 g, 37.7 mmol) and phenol (3.5 g, 37.2 mmol) were stirred in acetone (75 mL) at room temperature for 30 minutes. 2-bromo-1-(4-methoxyphenyl)ethan-1-one (7 g, 30.6 mmol) was added to the mixture and stirred overnight at room temperature. The reaction was filtered, the solvent removed by rotary evaporation, and the resulting solid dissolved in EtOAc. The EtOAc was washed with water (20 mL) and brine (20 mL), and it was then dried with Na_2SO_4. The remaining EtOAc was rotary evaporated and pumped on overnight. The solids were recrystallized from ethanol producing a white crystal (7.77 g) in 93% yield. ^{1}H NMR (500 MHz, $CDCl_3$) δ 8.02 (d, J = 8.8 Hz, 2H), 7.32 – 7.27 (m, 2H), 7.01 – 6.91 (m, 5H), 5.22 (s, 2H), 3.89 (s, 3H). Spectral data are in accordance with those previously reported.[11]

(1-methoxyethyl)benzene: This compound was prepared following a literature procedure. To a 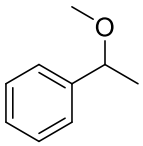 stirring solution of NaH (2 g, 49.2 mmol, 60% in mineral oil) in anhydrous THF (40 mL), 1-phenylethanol (3 g, 24.6 mmol) in anyhydrous THF (40 mL) was added under argon in two portions at 0 °C. The resulting suspension was stirred at 0 °C for 1 h. Then iodomethane (2.3 mL, 36.9 mmol) was added dropwise, and the reaction mixture was monitored by TLC. The reaction was quenched with saturated NH_4Cl solution. The aqueous layer was extracted with diethylether (2×80 mL). The combined organic extracts were washed with brine, dried over Na_2SO_4 and concentrated *in vacuo*. The crude product was purified by column chromatography (100% pentane) and dried via rotary evaporation to give (1-methoxyethyl)benzene as an oil (2.36 g) in 71% yield. ^{1}H NMR (500 MHz, $CDCl_3$) δ 7.39 – 7.35 (m, 2H), 7.34 – 7.27 (m, 3H), 4.31 (q, J = 6.5 Hz, 1H), 3.24 (s, 3H), 1.45 (d, J = 6.5 Hz, 3H). Spectral data are in accordance with those previously reported.[19]

2-(4-methoxyphenoxy)-1-phenylethan-1-one: This compound was prepared following a 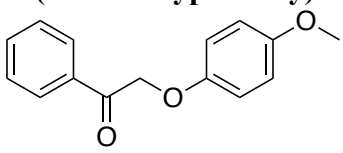 literature procedure.[11] A 250 mL round bottom flask connected with a dropping funnel was charged with 4-methoxyphenol (0.3 g, 2.25 mmol) and K_2CO_3 (0.5 g, 3.6 mmol) in acetone (20 mL) and stirred at room temperature. To this solution, 2-bromoacetophenone (0.3 g, 1.5 mmol) in acetone (20 mL) was added dropwise at room temperature. The resulting suspension was stirred at room temperature overnight; the suspension was filtered and concentrated *in vacuo*. The crude product was purified by column chromatography using 100% dichloromethane to give 2-(4-methoxyphenoxy)-1-phenylethan-1-one as a white solid (0.24 g) in 66% yield after solvent removal. ^{1}H NMR (500 MHz, $CDCl_3$) δ 8.08 – 7.92 (m, 2H),

7.66 – 7.58 (m, 1H), 7.50 (t, *J* = 7.8 Hz, 2H), 6.93 – 6.87 (m, 2H), 6.86 – 6.80 (m, 2H), 5.23 (s, 2H), 3.76 (s, 3H). Spectral data are in accordance with those previously reported.[11]

General Procedure for synthesis of substituted 2-phenylethanols. A 250 mL round bottom flask equipped with a water condenser was charged with substituted phenol (0.02 mol) in 40 mL NaOH aqueous solution (0.6 M). The mixture was allowed to stir at 65 °C for 15 mins. To this

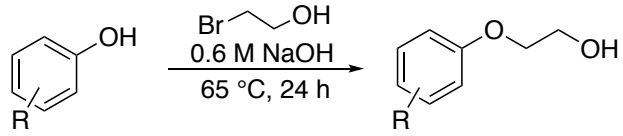

stirring mixture, 2-bromoethanol (0.01 mol) was added. The reaction mixture was stirred at 65 °C overnight. After the completion of the reaction. The aqueous reaction mixture was extracted with dichloromethane (2x40 mL) and washed with 0.6 M NaOH solution (2x40 mL). The combined organic was dried over Na_2SO_4 and concentrated *in vacuo* giving pure product. This reaction was conducted following a literature procedure.[20]

2-(4-methoxyphenoxy)ethanol: White solid (0.78 g, 47% yield). ^{1}H NMR (500 MHz, $CDCl_3$) δ

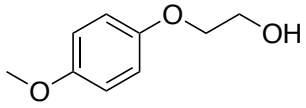

6.90 – 6.81 (m, 4H), 4.04 (dd, *J* = 5.2, 3.8 Hz, 2H), 3.98 – 3.91 (m, 2H), 3.77 (s, 3H), 2.03 (t, *J* = 6.3 Hz, 1H). Spectral data are in accordance with those previously reported.[20]

2-(2-methoxyphenoxy)ethanol: Colorless oil (0.51 g, 30% yield). ^{1}H NMR (500 MHz, $CDCl_3$) δ

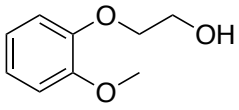

7.04 – 6.81 (m, 4H), 4.17 – 4.08 (m, 2H), 3.96 – 3.90 (m, 2H), 3.87 (s, 3H). Spectral data are in accordance with those previously reported.[20]

2-(3-methoxyphenoxy)ethanol: Colorless oil (0.83 g, 50% yield). ^{1}H NMR (500 MHz, $CDCl_3$) δ 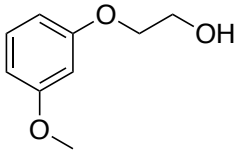

7.19 (t, *J* = 8.2 Hz, 1H), 6.55 – 6.51 (m, 2H), 6.49 (t, *J* = 2.3 Hz, 1H), 4.14 – 4.03 (m, 2H), 3.99 – 3.90 (m, 2H), 3.79 (s, 3H). Spectral data are in accordance with those previously reported.[20]

1-methyl-2-(2-phenoxyethyl)benzene: This compound was prepared following a literature procedure with modification.[9] Potassium carbonate (2.08 g, 15.06 mmol) and phenol (0.995 g, 10.54 mmol) were stirred in DMF (30 mL) at room temperature for 30 minutes. 2-methylphenethyl bromide (2.00 g, 10.04 mmol) was added dropwise to the mixture and stirred overnight at room temperature. After the completion of the reaction, cold water was added into the reaction mixture. The aqueous mixture was extracted with pentane (2×30 mL). The combined organic extracts were washed with brine, dried over Na_2SO_4 and concentrated in vacuo. The crude product was purified by column chromatography (Pentane/DCM, 4:1) to give 1-methyl-2-(2-phenoxyethyl)benzene as an oil (0.36 g) in 17% yield. ^{1}H NMR (500 MHz, $CDCl_3$) δ 7.29 (dd, *J* = 8.6, 7.2 Hz, 2H), 7.26 – 7.23 (m, 1H), 7.18 (t, *J* = 4.7, 2.6 Hz, 3H), 6.96 (t, *J* = 7.4, 1.0 Hz, 1H), 6.94 – 6.90 (m, 2H), 4.16 (t, *J* = 7.4 Hz, 2H), 3.13 (t, *J* = 7.4 Hz, 2H), 2.39 (s, 3H). ^{13}C NMR (126 MHz, Chloroform-*d*) δ 158.77, 136.53, 136.26, 130.34, 129.54, 129.48, 126.69, 126.12, 120.72, 114.48, 67.60, 33.07, 19.52.

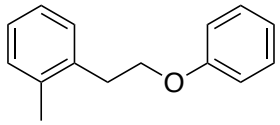

(2-phenoxypropyl)benzene: This compound was prepared following a literature procedure with modification.[21] A 100 mL round bottom flask equipped with a water condenser was charged with cesium carbonate (9.6 g, 29.4 mmol),

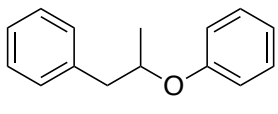

iodobenzene (3 g, 14.7 mmol), 1,10-phenanthroline (0.53 g, 2.94 mmol, 20 mol%), copper(I) iodide (0.28 g, 1.47 mmol, 10 mol%), 1-phenylpropan-2-ol (2.01 g, 14.7 mmol) and 40 mL of toluene. The reaction mixture was reflux under N_2 for 48 hours. The aqueous mixture was extracted with pentane (2×50 mL). The combined organic extracts were washed with brine, dried over Na_2SO_4 and concentrated in vacuo. The crude product was purified by column chromatography (Pentane/DCM, 4:1) to give (2-phenoxypropyl)benzene as an oil (1.06 g) in 34% yield. ^{1}H NMR (500 MHz, $CDCl_3$) δ 7.36 – 7.18 (m, 7H), 6.97 – 6.87 (m, 3H), 4.59 (h, J = 6.2 Hz, 1H), 3.12 (dd, J = 13.6, 5.8 Hz, 1H), 2.83 (dd, J = 13.6, 6.8 Hz, 1H), 1.31 (dd, J = 6.1, 0.7 Hz, 3H). Spectral data are in accordance with those previously reported.[22]

2.3.11 General Synthesis Procedure of Electron-Donating Diphenyl Ethers

The ether dimers were prepared following a literature procedure with modification.[23] A 250 mL round bottom flask equipped with water condenser was charged with mixture of 9.8 mmol of iodobenzene, 12.7 mmol of aryl alcohol (1.3 equiv), 0.98 mmol of N,N-dimethylglycine (10 mol%), 0.98 mmol of CuI (10 mol%), 21.5 mmol of Cs_2CO_3 (2.2 equiv) and 100 mL of 1,4-dioxane. The reaction mixture was held at the reflux temperature of 1,4-dioxane for 24 hours under nitrogen atmosphere. Upon completion, the cooled reaction mixtures were filtered to remove the inorganic salt, the filtrate was then poured into 100 mL of DI water and extracted with 2x100 mL of dichloromethane. The combined organic layers were extracted with 2x50 mL of 0.6 M NaOH solution to wash out the excess aryl alcohol, then washed with brine, dried using Na_2SO_4 and concentrated under vacuum. The crude product was purified by column chromatography using DCM/Hexanes (4:1) to give the pure product.

4-phenoxytoluene (Yield 63%): ^{1}H NMR (500 MHz, $CDCl_3$) δ 7.35 – 7.28 (m, 2H), 7.14 (d, *J* = 8.1 Hz, 2H), 7.07 (tt, *J* = 7.4, 1.1 Hz, 1H), 7.02 – 6.96 (m, 2H), 6.96 – 6.88 (m, 2H), 2.34 (s, 3H). Spectral data are in accordance with those previously reported.[23]

3-phenoxytoluene (Yield 35%): ^{1}H NMR (500 MHz, $CDCl_3$) δ 7.38 – 7.32 (m, 2H), 7.23 (t, *J* = 7.8 Hz, 1H), 7.11 (tt, *J* = 7.4, 1.2 Hz, 1H), 7.05 – 7.00 (m, 2H), 6.93 (ddt, *J* = 7.5, 1.6, 0.8 Hz, 1H), 6.87 – 6.80 (m, 2H), 2.34 (d, *J* = 0.7 Hz, 3H). Spectral data are in accordance with those previously reported.[23]

2-phenoxytoluene (Yield 43%): ^{1}H NMR (500 MHz, $CDCl_3$) δ 7.34 – 7.28 (m, 2H), 7.18 (t, *J* = 7.7 Hz, 1H), 7.11 – 7.01 (m, 2H), 6.97 – 6.86 (m, 3H), 2.26 (s, 3H). Spectral data are in accordance with those previously reported.[24]

4-phenoxyanisole (Yield 69%): ^{1}H NMR (500 MHz, $CDCl_3$) δ 7.34 – 7.28 (m, 2H), 7.08 – 7.02 (m, 1H), 7.02 – 6.97 (m, 2H), 6.97 – 6.93 (m, 2H), 6.93 – 6.86 (m, 2H), 3.82 (s, 3H). Spectral data are in accordance with those previously reported.[23]

2-phenoxyanisole (Yield 53%): ^{1}H NMR (500 MHz, $CDCl_3$) δ 7.34 – 7.28 (m, 2H), 7.14 (ddd, *J* = 8.1, 7.3, 1.7 Hz, 1H), 7.06 (tt, *J* = 7.4, 1.1 Hz, 1H), 7.02 (dd, *J* = 8.2, 1.5 Hz, 1H), 7.00 – 6.91 (m, 4H), 3.85 (s, 3H). Spectral data are in accordance with those previously reported.[23]

3-phenoxyanisole (Yield 57%): ^{1}H NMR (500 MHz, $CDCl_3$) δ 7.39 – 7.32 (m, 2H), 7.26 – 7.21 (m, 1H), 7.15 – 7.09 (m, 1H), 7.07 – 7.01 (m, 2H), 6.70 – 6.65 (m, 1H), 6.63 – 6.57 (m, 2H), 3.79 (s, 3H). Spectral data are in accordance with those previously reported.[25]

1-fluoro-4-phenoxybenzene (Yield 63%): ^{1}H NMR (500 MHz, $CDCl_3$) δ 7.37 – 7.29 (m, 2H), 7.09 (tt, *J* = 7.6, 1.1 Hz, 1H), 7.06 – 6.94 (m, 6H). Spectral data are in accordance with those previously reported.[26]

1-ethyl-4-phenoxybenzene (Yield 35%): ^{1}H NMR (500 MHz, $CDCl_3$) δ 7.38 – 7.29 (m, 2H), 7.21 – 7.14 (m, 2H), 7.13 – 7.05 (m, 1H), 7.00 (dd, *J* = 8.7, 1.1 Hz, 2H), 6.95 (d, *J* = 8.5 Hz, 2H), 2.65 (q, *J* = 7.6 Hz, 2H), 1.25 (t, *J* = 7.6 Hz, 3H). Spectral data are in accordance with those previously reported.[27]

2.3.12 General Synthesis Procedure of Electron-Withdrawing Diphenyl Ethers

The ether dimers were prepared following a literature procedure with modification.[23] A 250 mL round bottom flask equipped with water condenser was charged with mixture of 9.8 mmol of aryl bromide, 12.7 mmol of phenol (1.3 equiv), 0.98 mmol of N,N-dimethylglycine (10 mol%), 0.98 mmol of CuI (10 mol%), 21.5 mmol of Cs_2CO_3 (2.2 equiv) and 100 mL of 1,4-dioxane. The reaction mixture was held at the reflux temperature of 1,4-dioxane for 24 hours under nitrogen atmosphere. Upon completion, the cooled reaction mixtures were filtered to remove the inorganic salt, the filtrate was then poured into 100 mL of DI water and extracted with 2x100 mL of dichloromethane. The combined organic layers were extracted with 2x50 mL of 0.6 M NaOH

solution to wash out the excess phenol, then washed with brine, dried using Na_2SO_4 and concentrated under vacuum. The crude product was purified by column chromatography using DCM/Hexanes (4:1) to give the pure product.

4-phenoxybenzonitrile (Yield 55%): ^{1}H NMR (500 MHz, $CDCl_3$) δ 7.64 – 7.56 (m, 2H), 7.45 – 7.37 (m, 2H), 7.25 – 7.20 (m, 1H), 7.11 – 7.04 (m, 2H), 7.04 – 6.96 (m, 2H). Spectral data are in accordance with those previously reported.[26]

1-phenoxy-4-(trifluoromethyl)benzene (Yield 67%): ^{1}H NMR (500 MHz, $CDCl_3$) δ 7.61 – 7.53 (m, 2H), 7.43 – 7.36 (m, 2H), 7.19 (ddd, *J* = 8.5, 6.8, 1.1 Hz, 1H), 7.11 – 6.99 (m, 4H). Spectral data are in accordance with those previously reported.[28]

4-phenoxybenzaldehyde (Yield 38%): ^{1}H NMR (500 MHz, $CDCl_3$) δ 9.92 (s, 1H), 7.88 – 7.79 (m, 2H), 7.45 – 7.37 (m, 2H), 7.23 (ddt, *J* = 8.6, 7.4, 1.2 Hz, 1H), 7.12 – 7.03 (m, 4H). Spectral data are in accordance with those previously reported.[29]

1-(4-phenoxyphenyl)ethan-1-one (Yield 68%): ^{1}H NMR (500 MHz, $CDCl_3$) δ 7.94 (d, *J* = 8.8 Hz, 2H), 7.43 – 7.36 (m, 2H), 7.22 – 7.18 (m, 1H), 7.07 (dt, *J* = 7.8, 1.1 Hz, 2H), 7.00 (d, *J* = 8.8 Hz, 2H), 2.58 (s, 3H). Spectral data are in accordance with those previously reported.[26]

1-(4-phenoxyphenyl)ethan-1-ol: This compound was prepared following a literature procedure. 1-(4-phenpxyphenyl)ethan-1-one (1.02 g, 4.8 mmol) was added to 30 mL MeOH. The mixture was hold at 0 °C in ice bath, $NaBH_4$ (0.18 g, 4.8 mmol) was added in small portions within 1 hour. The

reaction was then stirred overnight at room temperature. After the completion of the reaction, saturated NH_4Cl (50 mL) solution was added to the mixture and was extracted with 2x50 mL dichloromethane. The combined organic layers were dried over anhydrous Na_2SO_4 and concentrated under vacuum, giving 68% yield of the pure product. ^{1}H NMR (500 MHz, $CDCl_3$) δ 7.39 – 7.30 (m, 4H), 7.10 (tt, *J* = 7.5, 1.1 Hz, 1H), 7.04 – 6.96 (m, 4H), 4.90 (qd, *J* = 6.4, 3.2 Hz, 1H), 1.77 (d, *J* = 3.5 Hz, 1H), 1.51 (d, *J* = 6.5 Hz, 3H). Spectral data are in accordance with those previously reported.[30]

2-phenoxyphenol: This compound was prepared following a literature procedure with modification.[31] A 250 mL round bottom flask equipped with water condenser was charged with 1.44 g of 1-methoxy-2-phenoxybenzene, 24 mL of HBr (48%) solution and 48 mL of glacial acetic acid. The solution mixture was stirred at reflux temperature for 24 hours and allowed to cool to room temperature. The reaction mixture was extracted with 2x60 mL of dichloromethane, and the combined organic layer was washed with DI water (2x50 mL), then dried over anhydrous Na_2SO_4, and concentrated under vacuum. Both thin layer chromatography and ^{1}H NMR indicated no further purification was needed, which given 1.07 g of 2-phenoxyphenol (82% yield). ^{1}H NMR (500 MHz, $CDCl_3$) δ 7.40 – 7.32 (m, 2H), 7.14 (tt, *J* = 7.5, 1.2 Hz, 1H), 7.09 – 7.01 (m, 4H), 6.92 – 6.81 (m, 2H), 5.58 (s, 1H). Spectral data are in accordance with those previously reported.[32]

4,4'-oxybis(methoxybenzene):This compound was prepared following a literature procedure with modification.[23] A 250 mL round bottom flask equipped with water condenser was charged with mixture of 12.8 mmol of 4-bromoanisole, 17.9 mmol of 4-methoxyphenol (1.5 equiv), 0.97 mmol of N,N-dimethylglycine (8 mol%), 2.1 mmol of CuI (16 mol%), 27.5 mmol of Cs_2CO_3 (2.15 equiv)

and 100 mL of 1,4-dioxane. The reaction mixture was held at the reflux temperature of 1,4-dioxane for 24 hours under a nitrogen atmosphere. Upon completion, the cooled reaction mixtures were filtered to remove the inorganic salt, the filtrate was then poured into 100 mL of DI water and extracted with 2x100 mL of dichloromethane. The combined organic layers were extracted with 2x50 mL of 0.6 M NaOH solution to wash out the excess 4-methoxyphenol, then washed with brine, dried using Na_2SO_4 and concentrated under vacuum. The crude product was purified by column chromatography using DCM/Hexanes (4:1 to 100% DCM) to give 1.26 g of 4,4'-oxybis(methoxybenzene) in 43% yield. ^{1}H NMR (500 MHz, $CDCl_3$) δ 6.92 (d, J = 9.1 Hz, 4H), 6.85 (d, J = 9.1 Hz, 4H), 3.79 (s, 6H). Spectral data are in accordance with those previously reported.[33]

2.4 Conclusion

This new electrocatalytic method is of potential value for reductive fragmentation of both lignin linkages and various persistent organic pollutants (POPs). Importantly, such electrocatalytic strategies are "green" as they enable the coupling of renewable energy (electricity from non-fossil sources) to the processing of sustainable carbon sources (biomass) and the mitigation of pollutants. Having demonstrated effective cleavage of the sp^3 C-O bonds of beta-O-4 linkage models, and the generally unreactive sp^2 C-O bonds of diaryl ether systems, as well as the activation of C-F bonds, future work will extend these mild, "green" ECH methods to applications in real lignin upgrading and in the remediation of emerging contaminants, while further exploring the scope and functional group tolerance of these processes.

Most aryl ethers used in these mechanistic analyses have reported syntheses in the literature. Synthetic procedures in making the aryl ether models generally followed reported methodologies. However, Ullmann Coupling was selected for all diaryl ether syntheses based its the feasibility and low cost, since most of the more advanced methodologies required expensive or commercially available ligands. The selected methodology[23] of the Ullmann reaction does not include every diaryl ether that was needed for the substituent studies in the mechanistic analysis, thus, the syntheses of these diaryl ethers in this chapter were beyond the scope of the original reported methodology.

2.5 Spectra

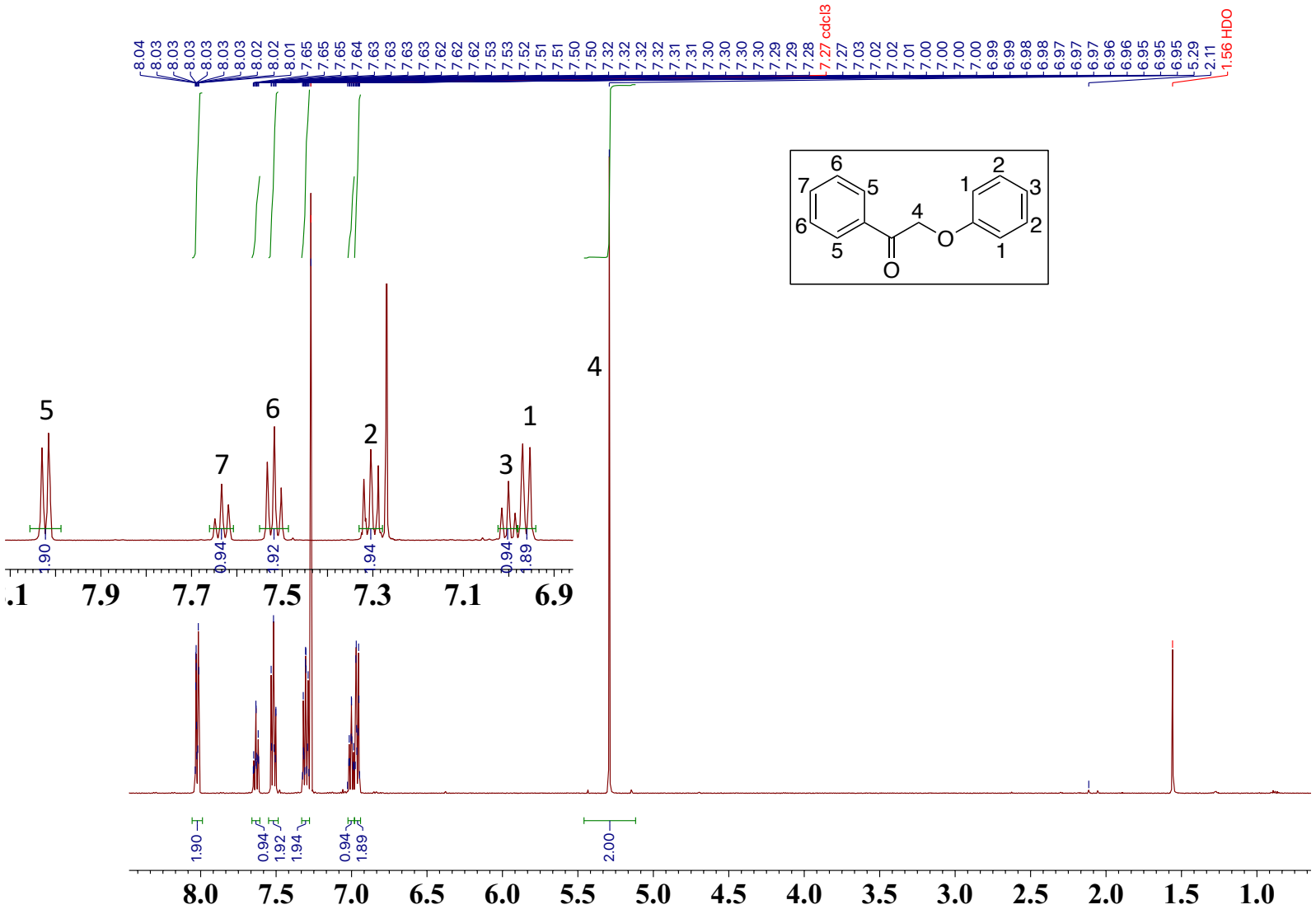

Figure 2.15 ^{1}H NMR of **2-phenoxyacetophenone**

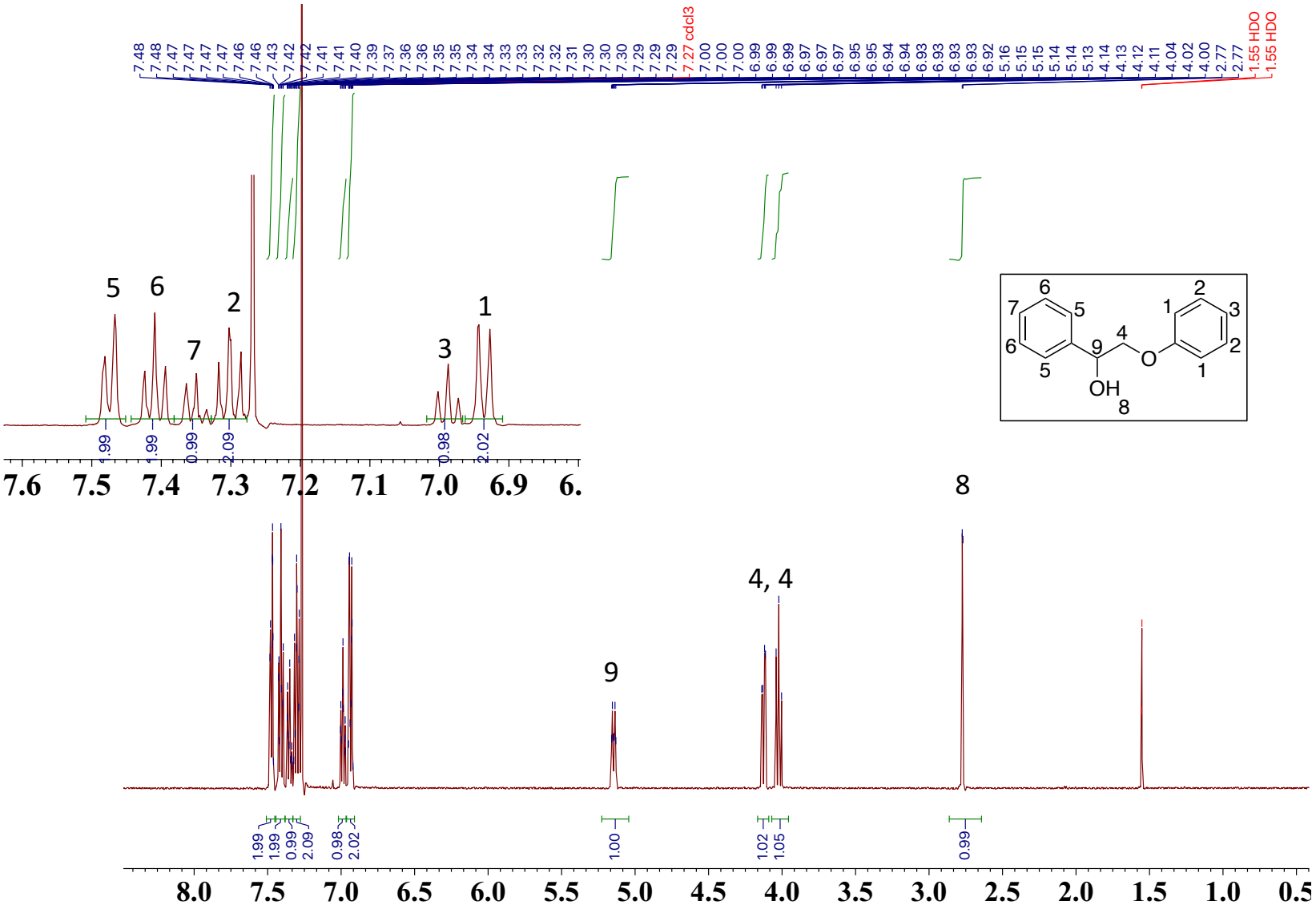

Figure 2.16 ^{1}H NMR of **2-phenoxy-1-phenylethan-1-ol**

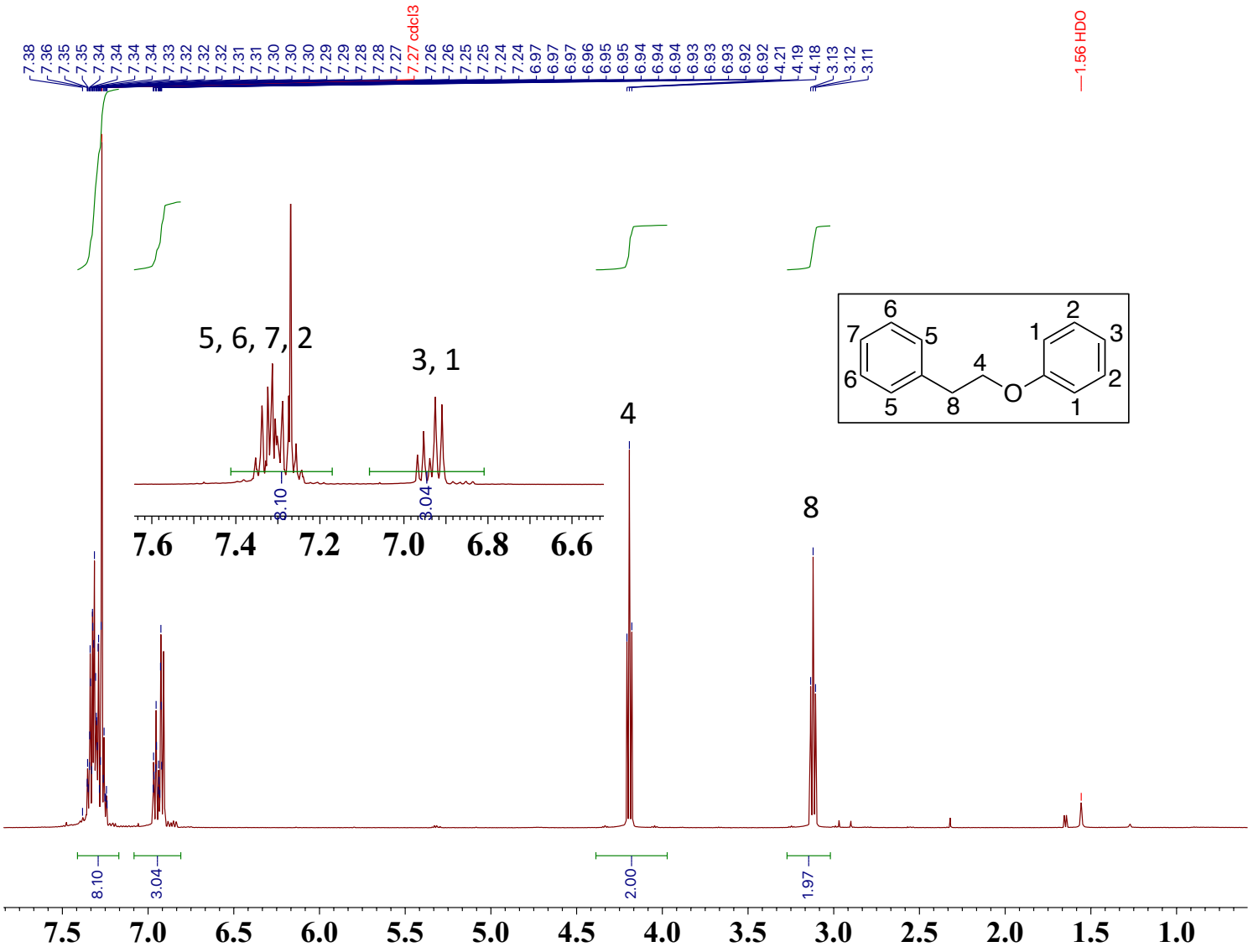

Figure 2.17 ^{1}H NMR of **2-phenoxy-1-phenylethane**

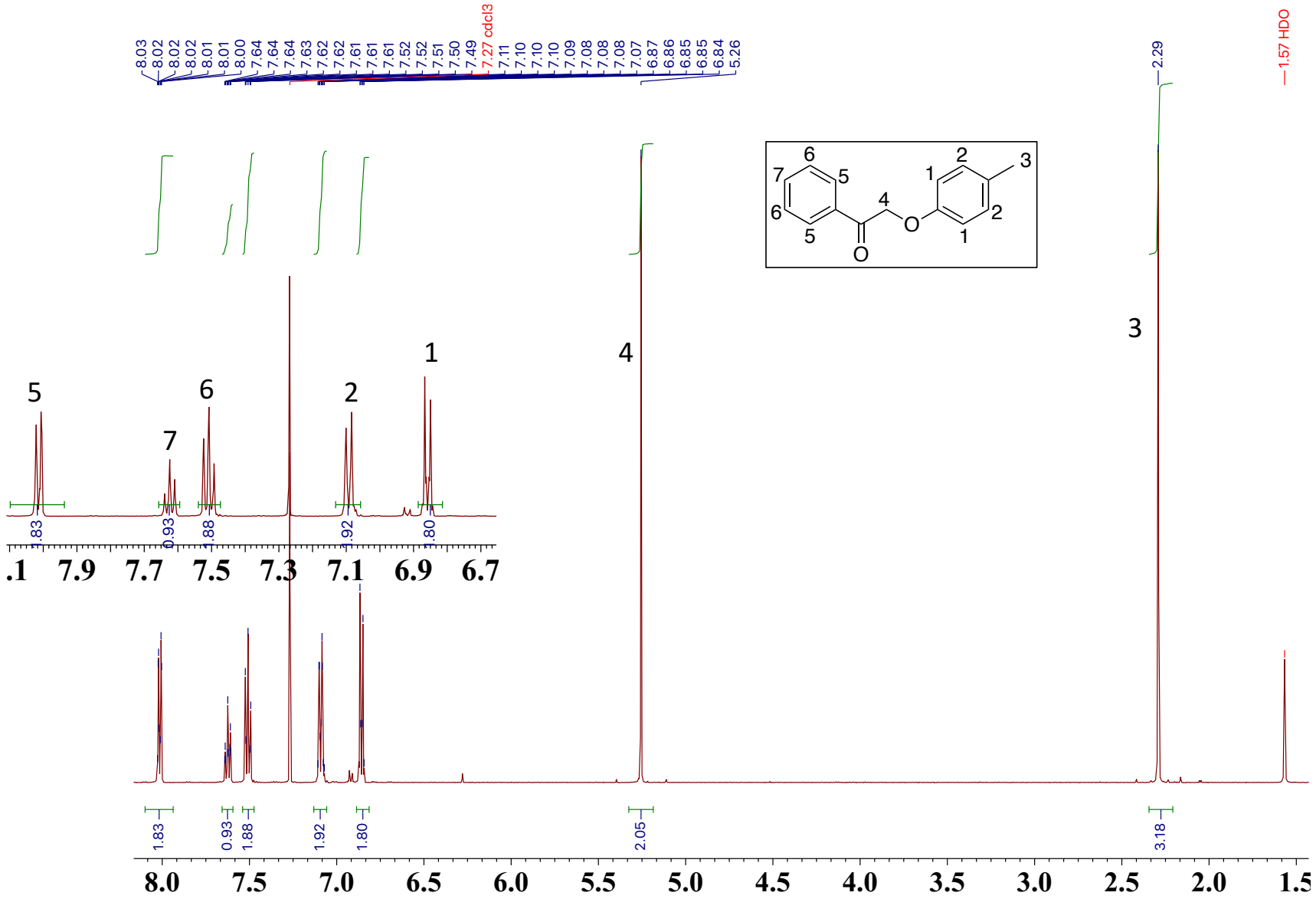

Figure 2.18 ^{1}H NMR of **1-phenyl-2-(p-tolyloxy)ethan-1-one**

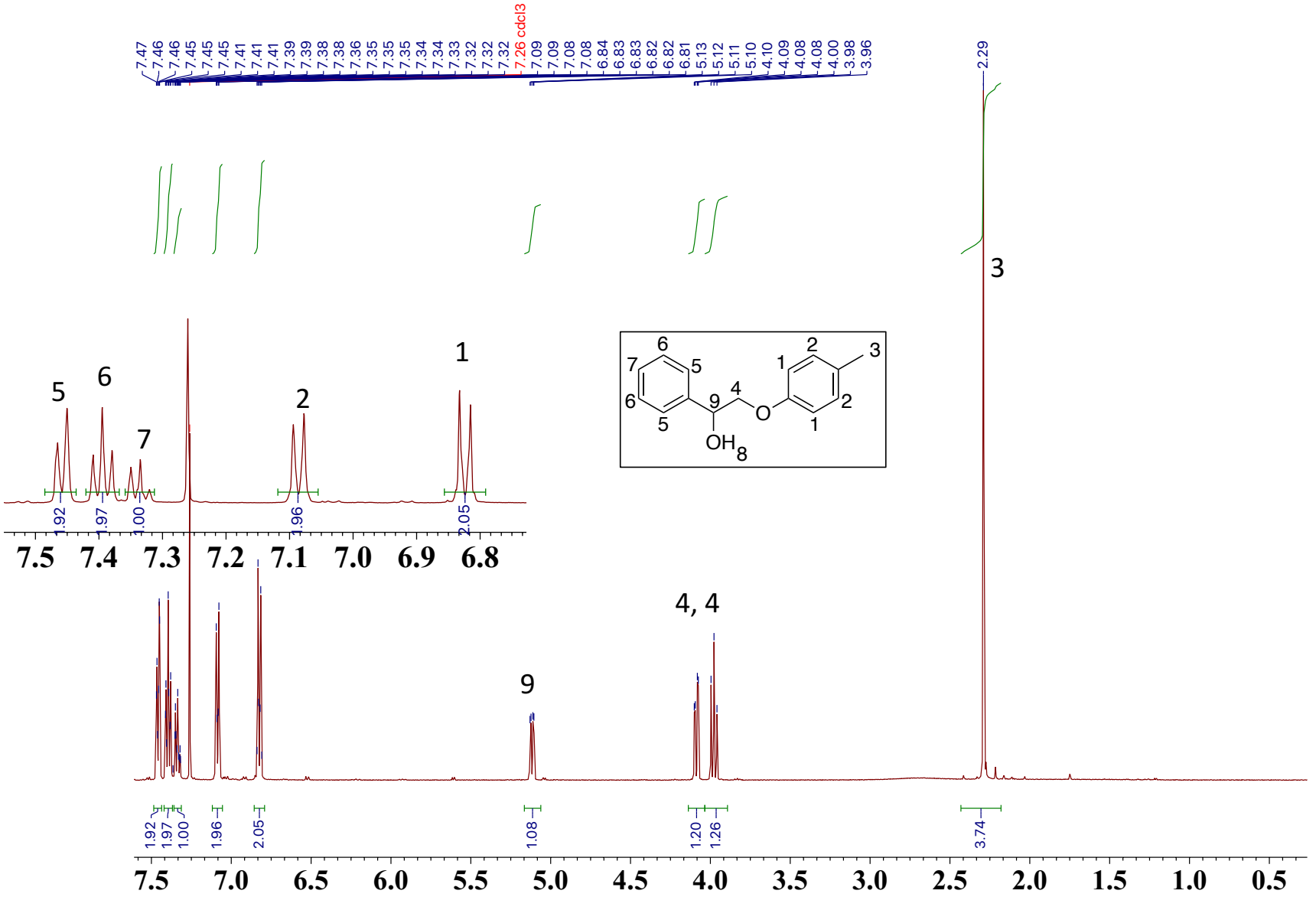

Figure 2.19 ^{1}H NMR of **1-phenyl-2-(p-tolyloxy)ethanol**

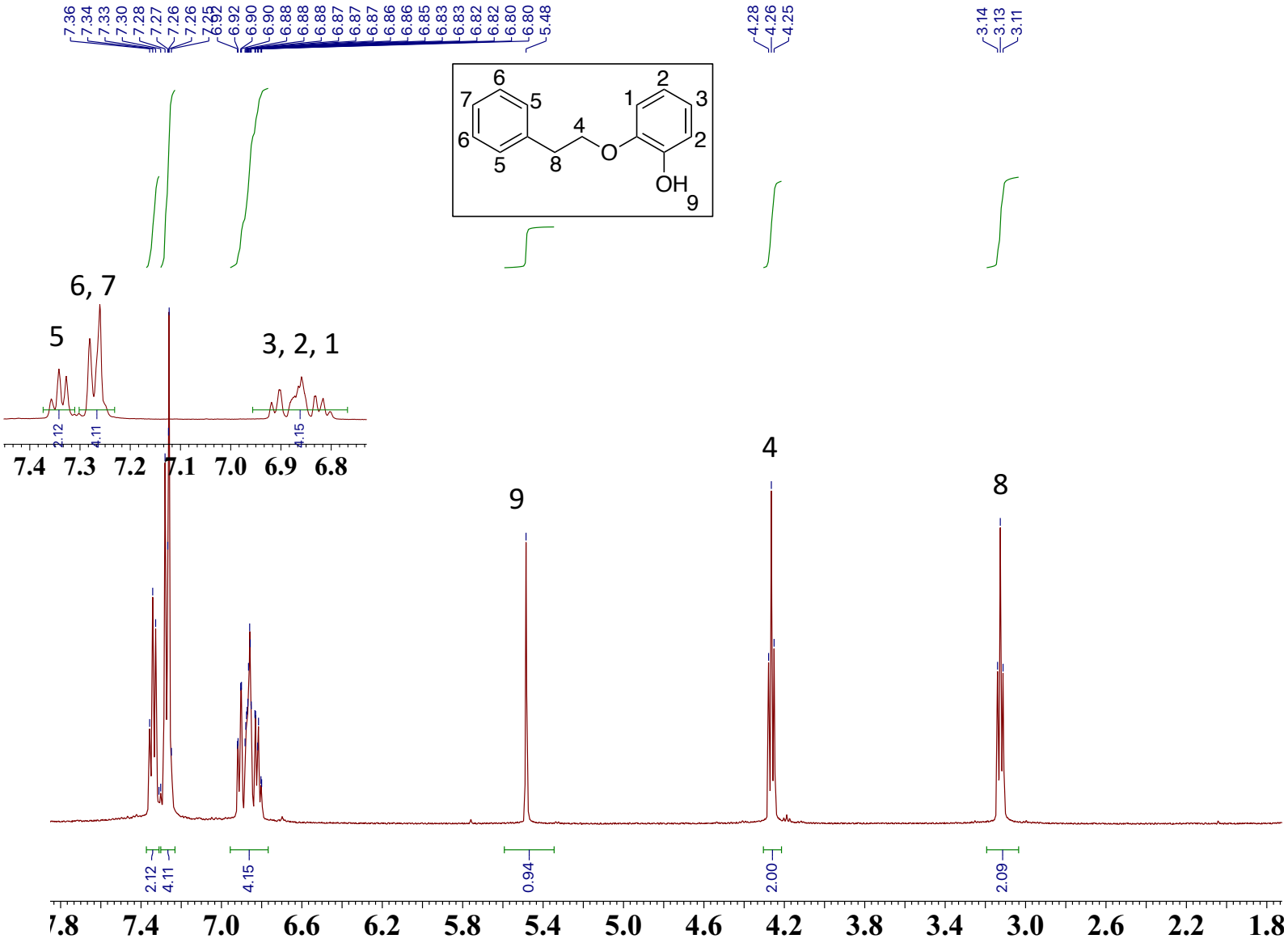

Figure 2.20 ^{1}H NMR of **2-(2-phenylethoxy)phenol**

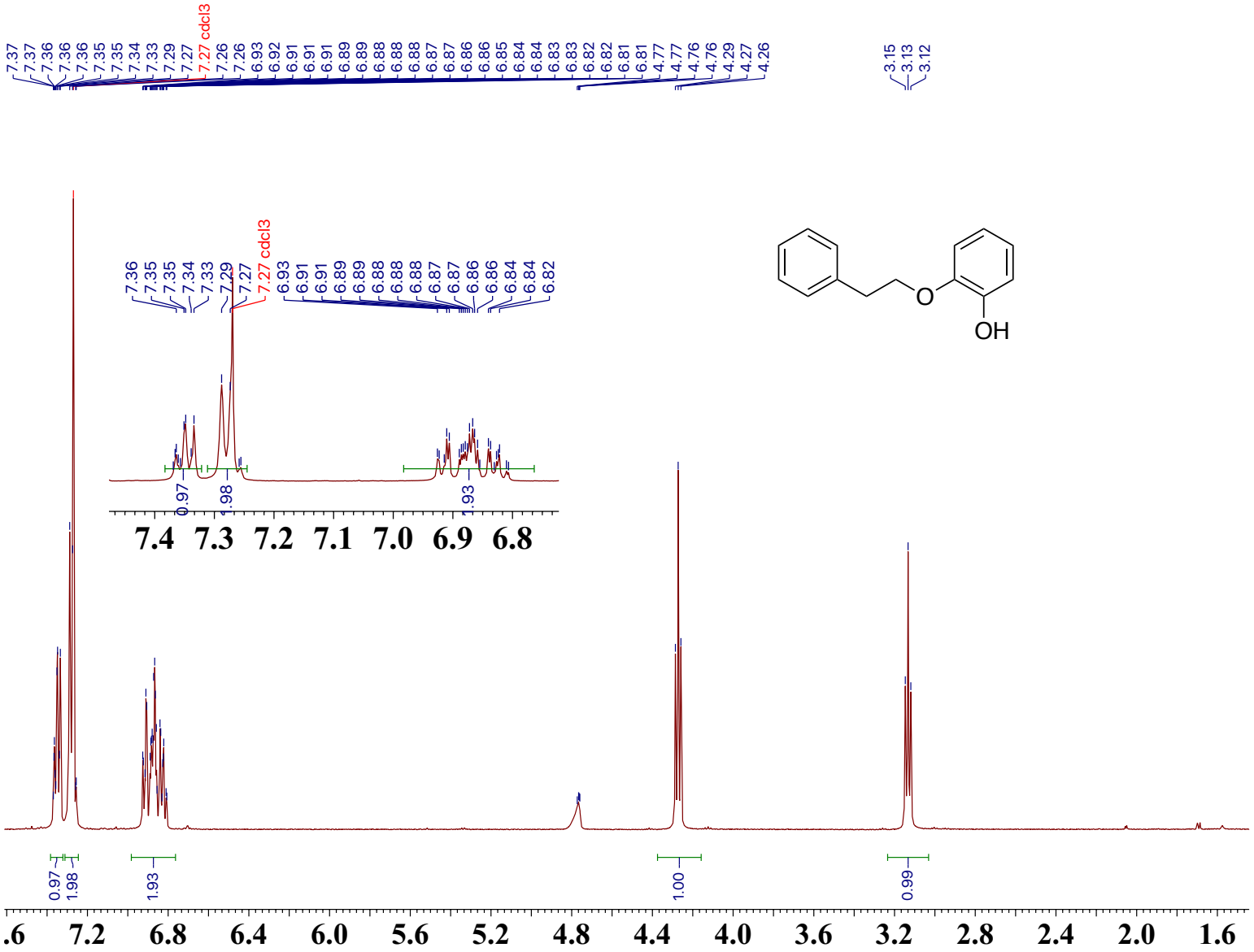

Figure 2.21 ^{1}H NMR of **2-(2-phenylethoxy)phenol** D_2O shaken

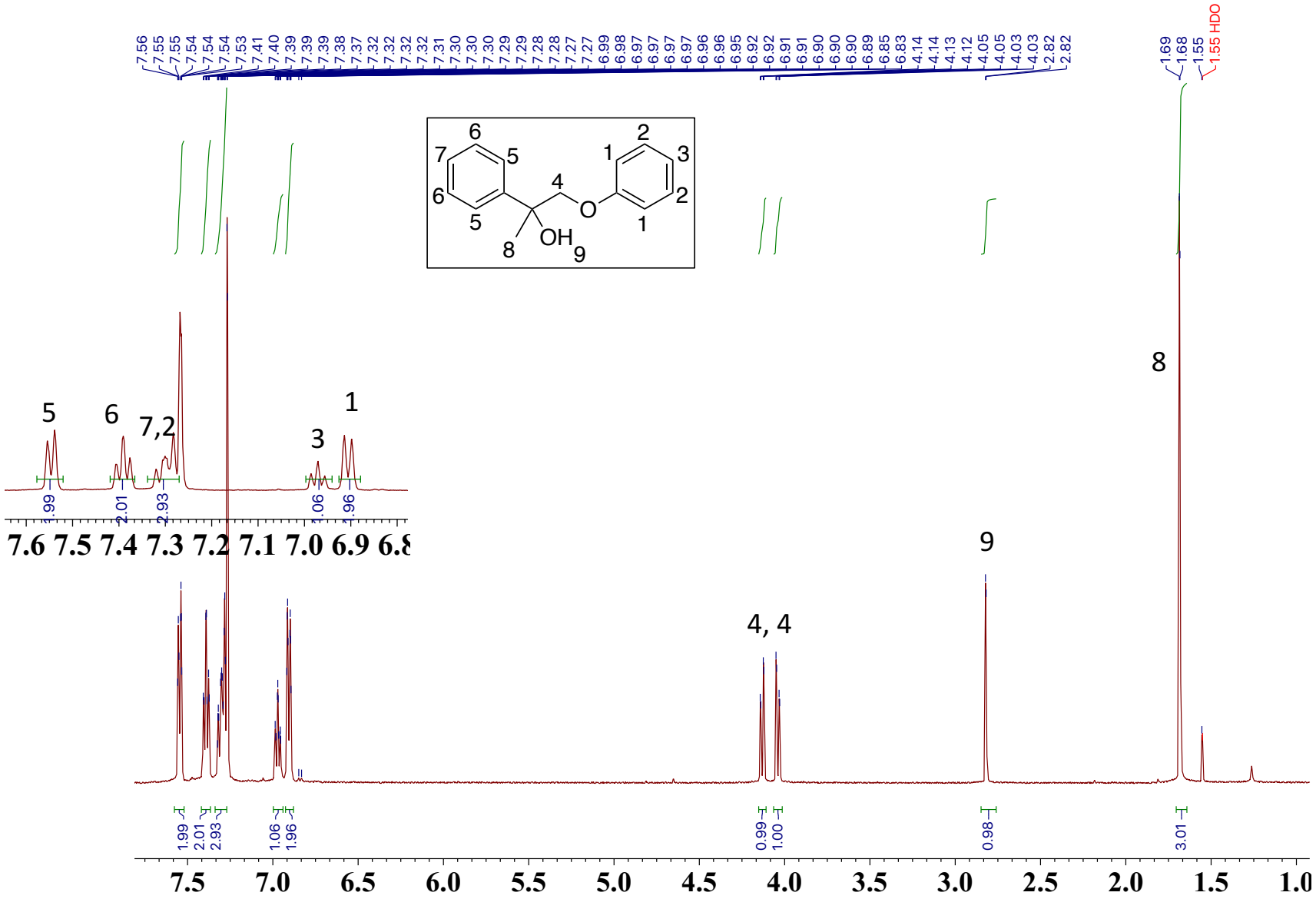

Figure 2.22 ^{1}H NMR of **1-phenoxy-2-phenyl-2-propanol**

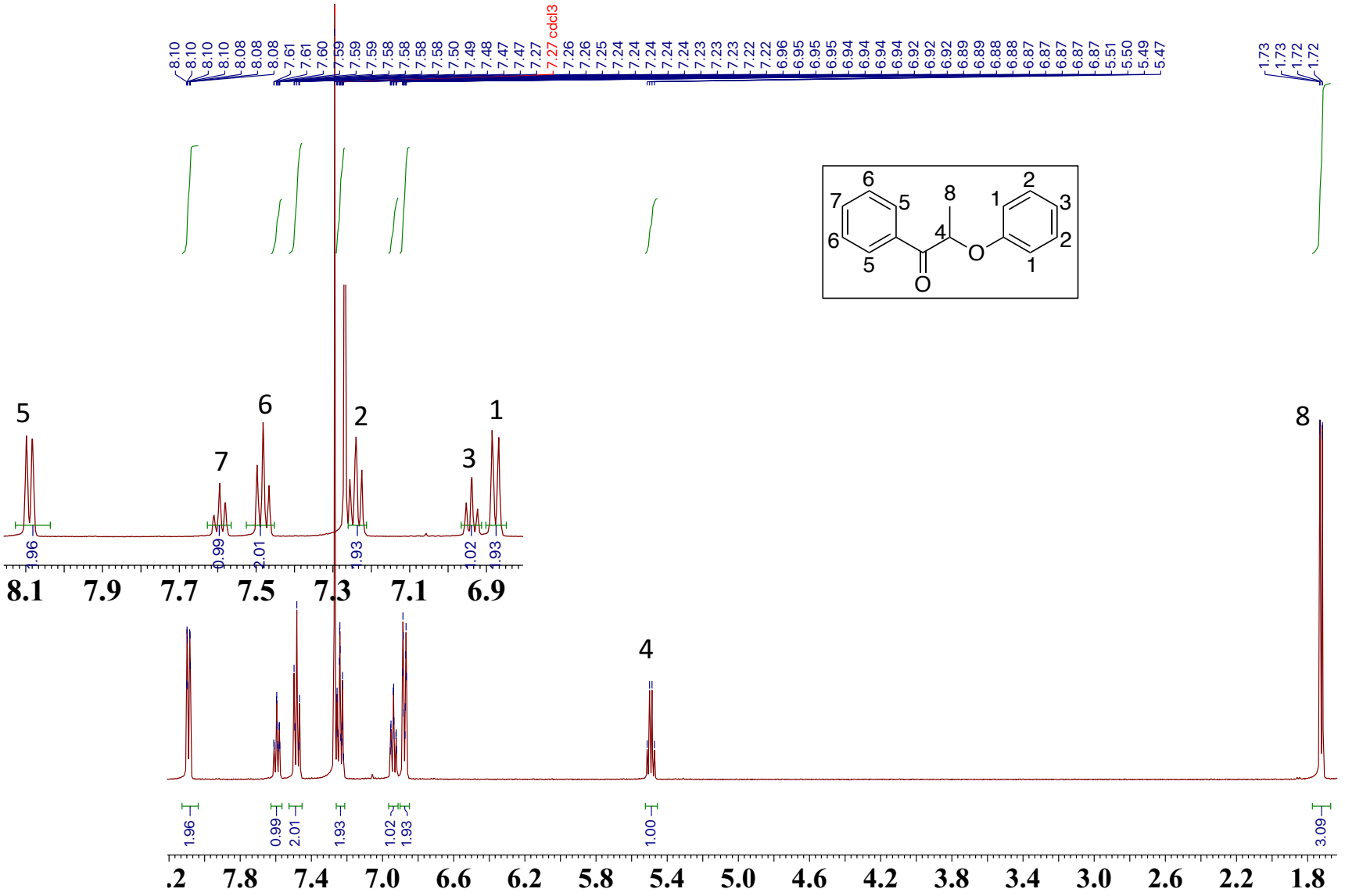

Figure 2.23 ^{1}H NMR of **2-phenoxy-1-phenylpropan-1-one**

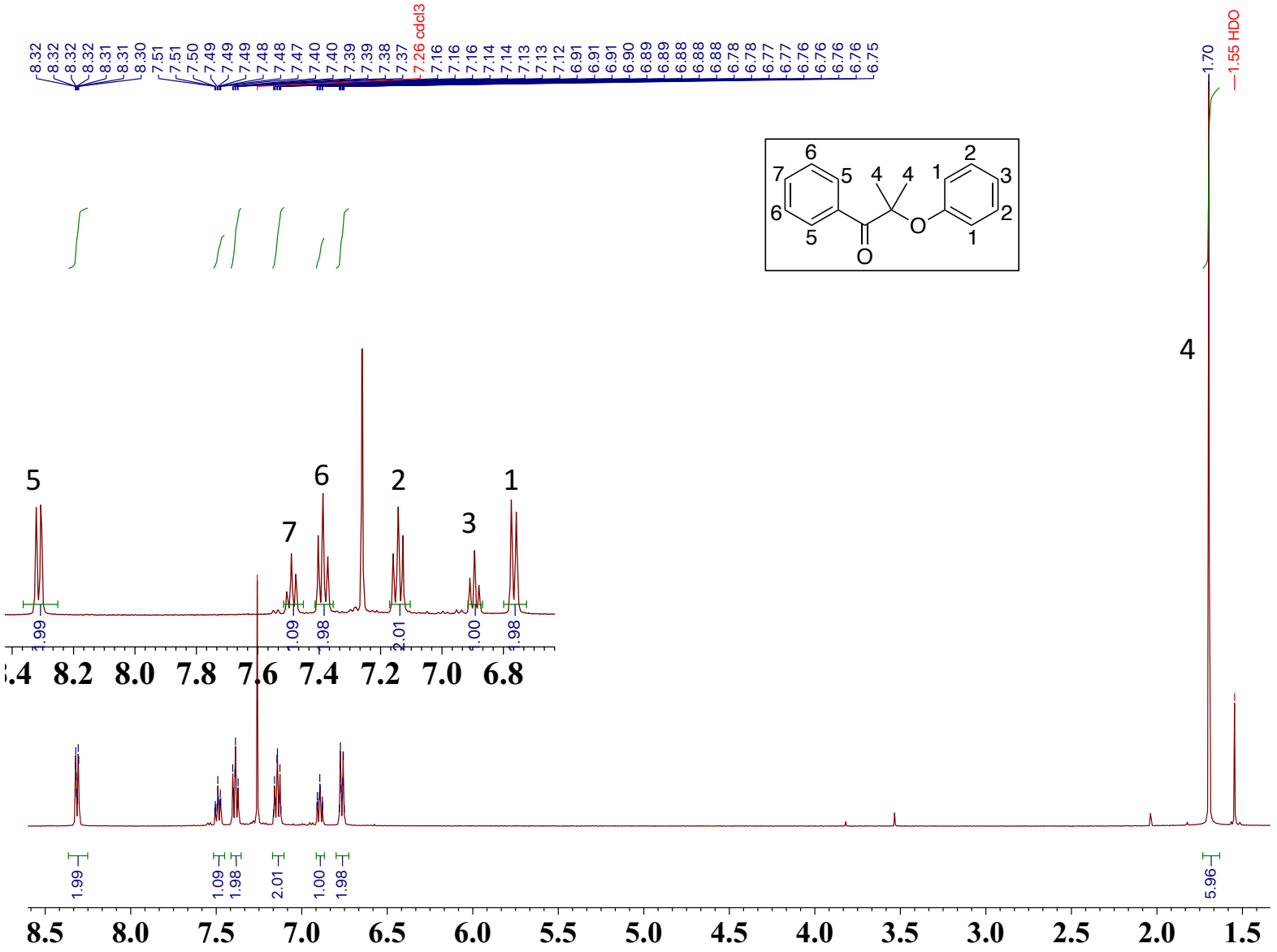

Figure 2.24 ^{1}H NMR of **2-methyl-2-phenoxy-1-phenylpropan-1-one**

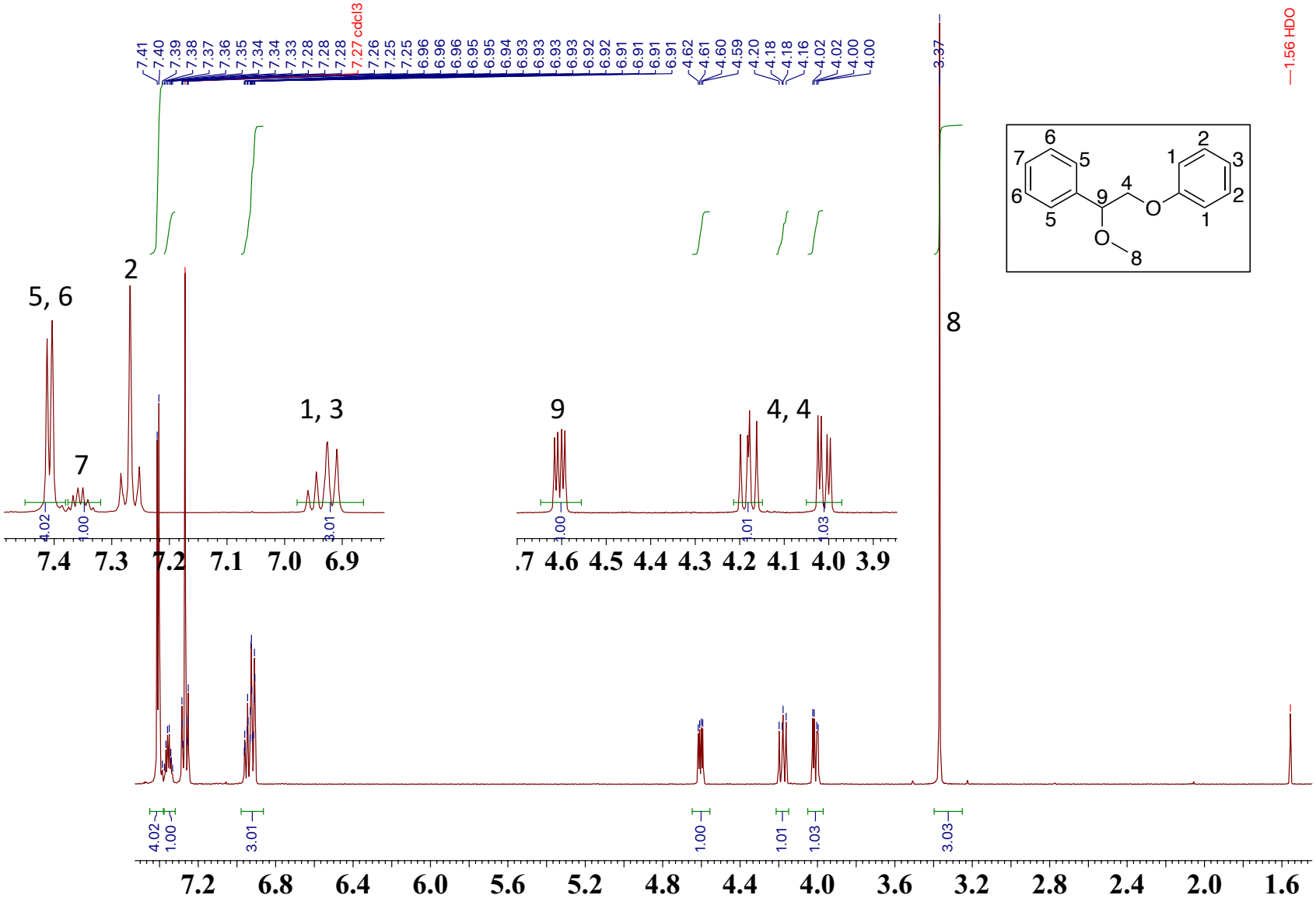

Figure 2.25 ^{1}H NMR of (**1-methoxy-2-phenoxyethyl)benzene**

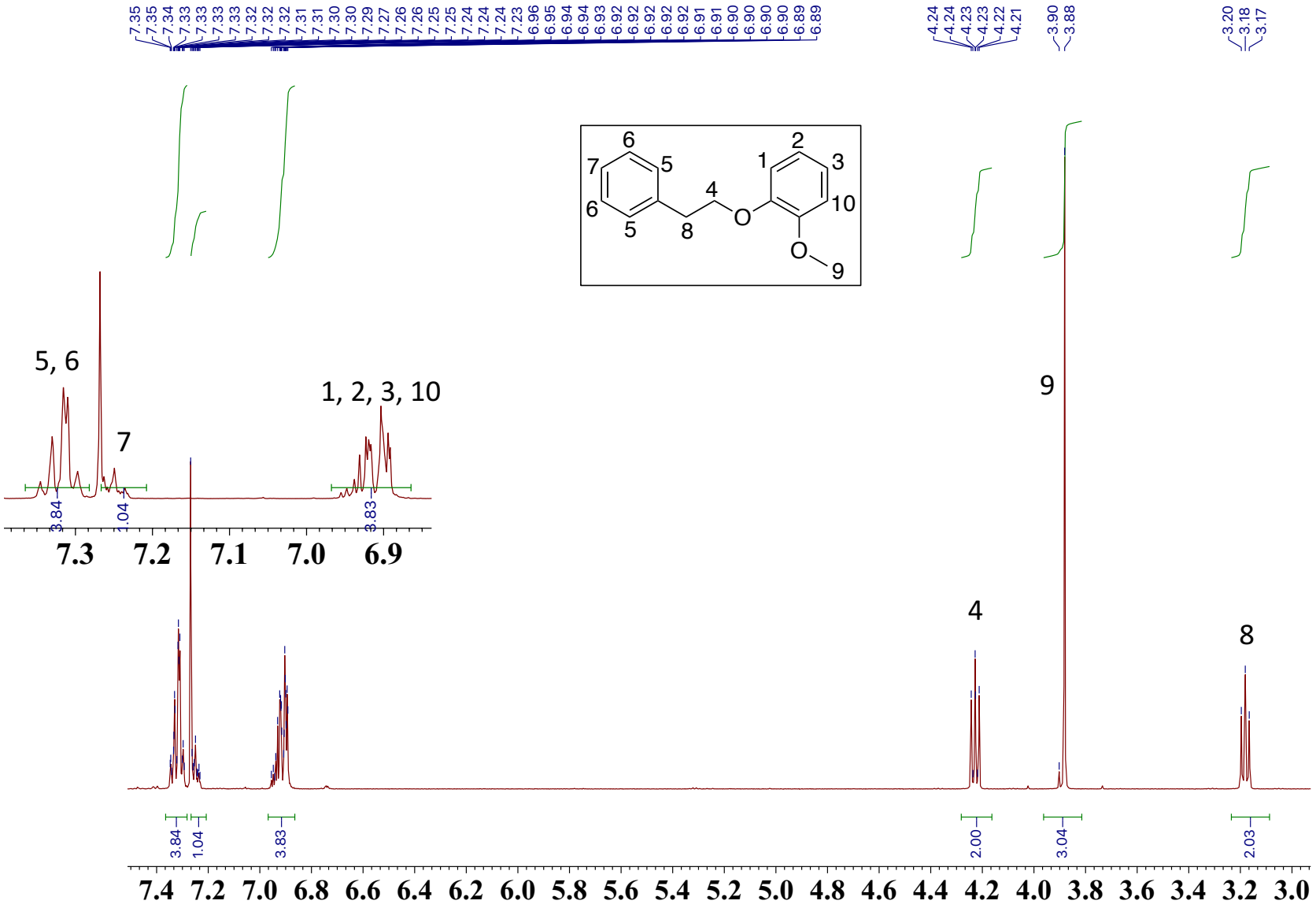

Figure 2.26 ^{1}H NMR of **1-methoxy-2-(2-phenylethoxy)benzene**

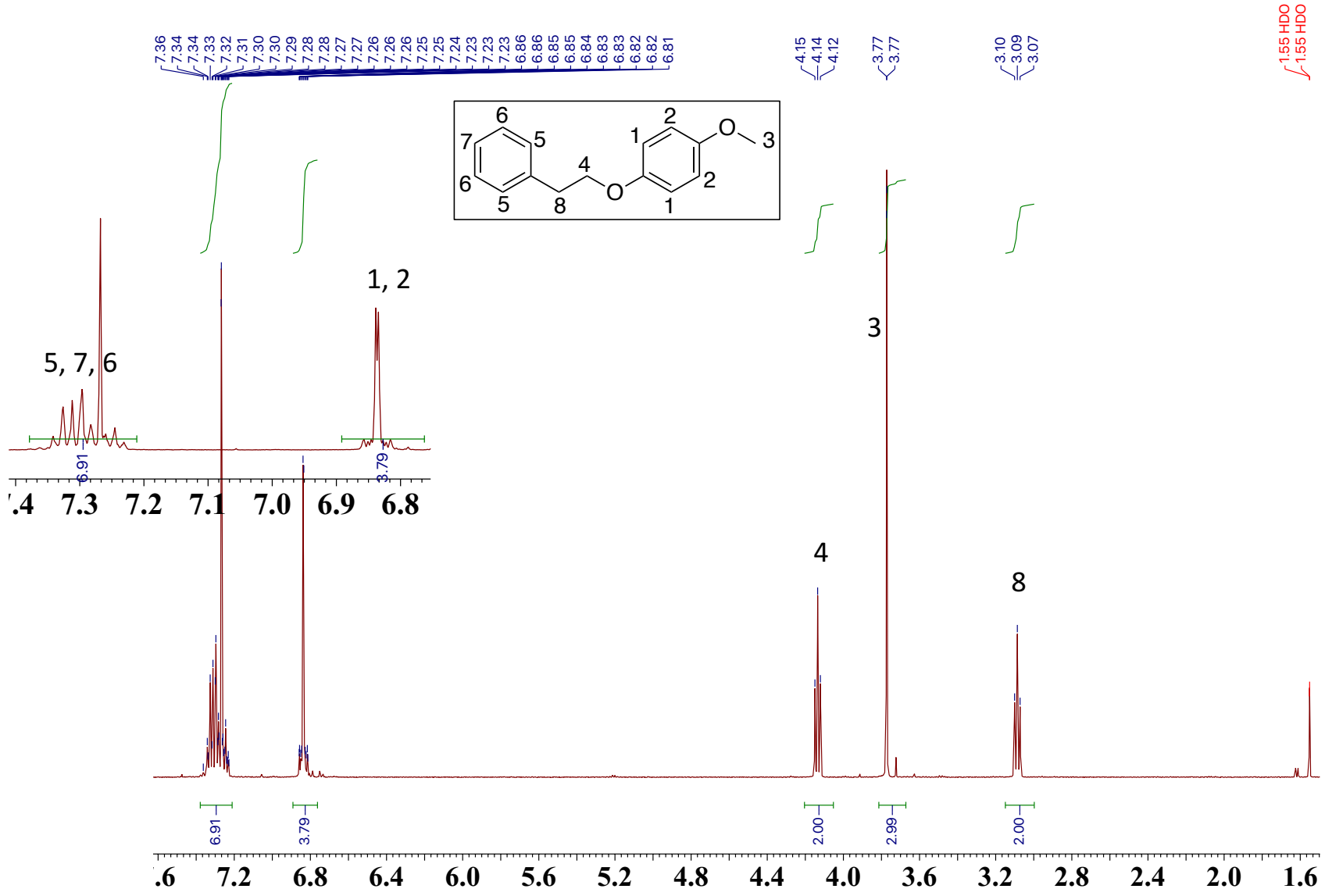

Figure 2.27 ^{1}H NMR of **1-methoxy-4-(2-phenylethoxy)benzene**

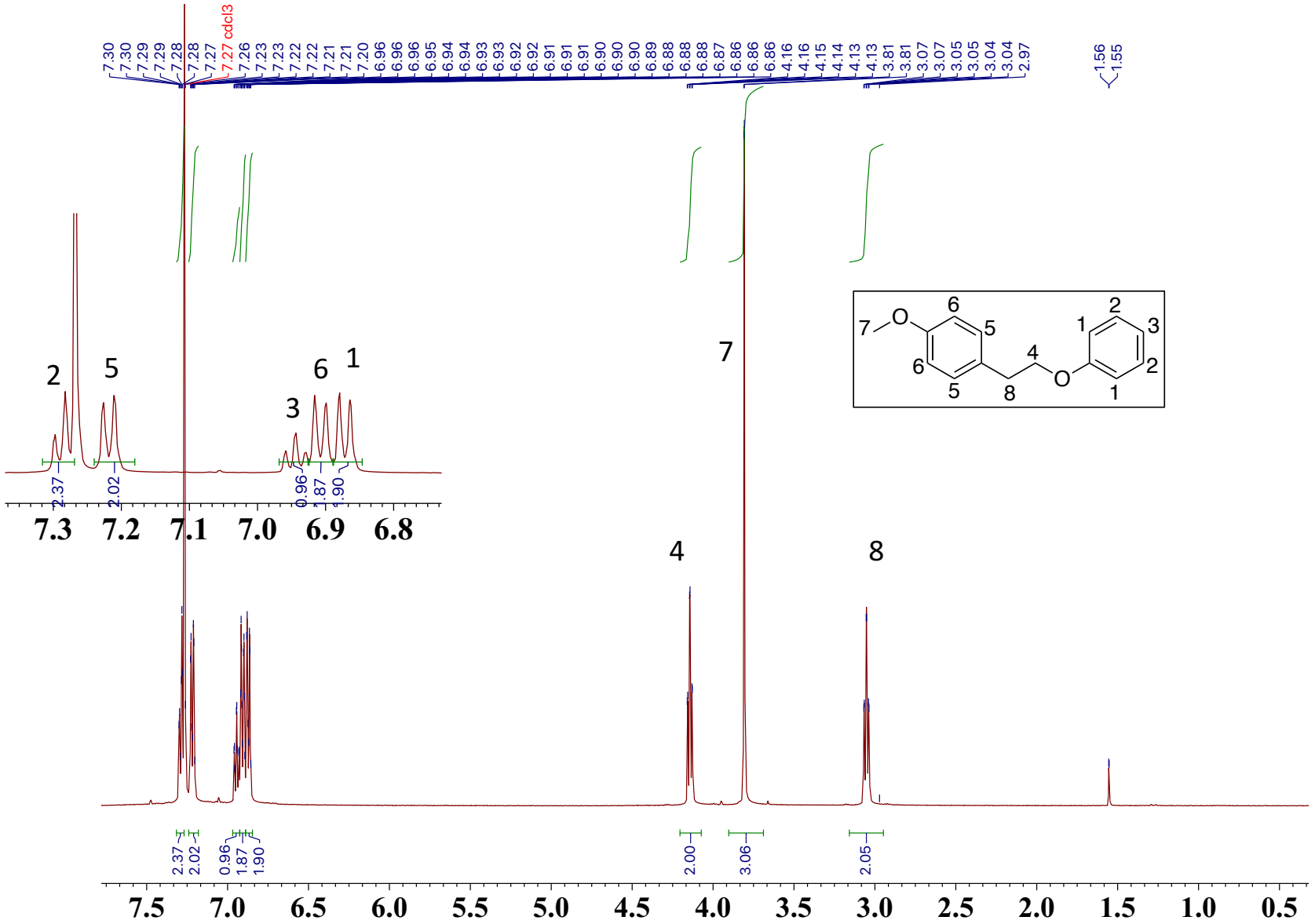

Figure 2.28 ^{1}H NMR of **1-methoxy-4-(2-phenoxyethyl)benzene**

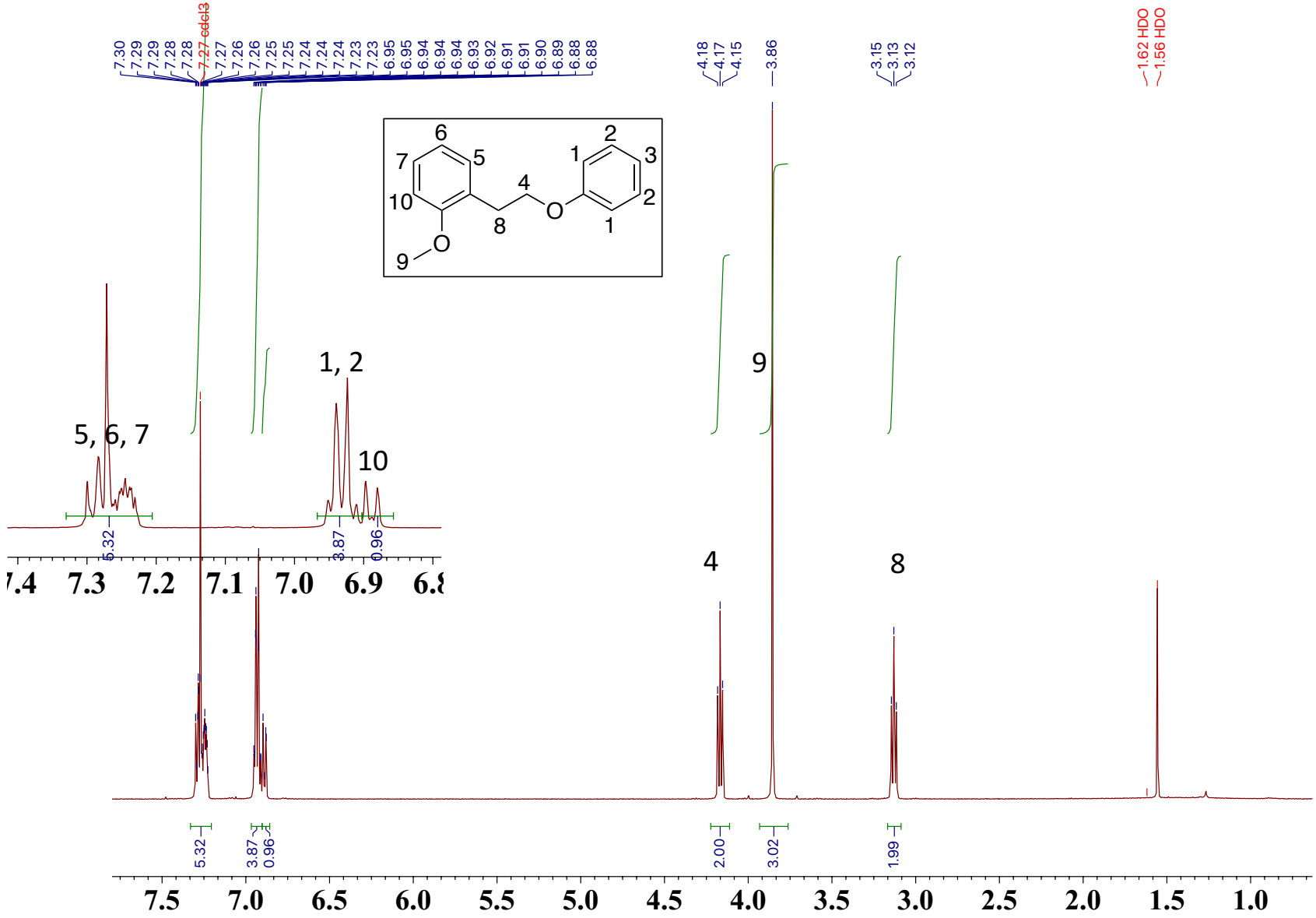

Figure 2.29 ^{1}H NMR of **1-methoxy-2-(2-phenoxyethyl)benzene**

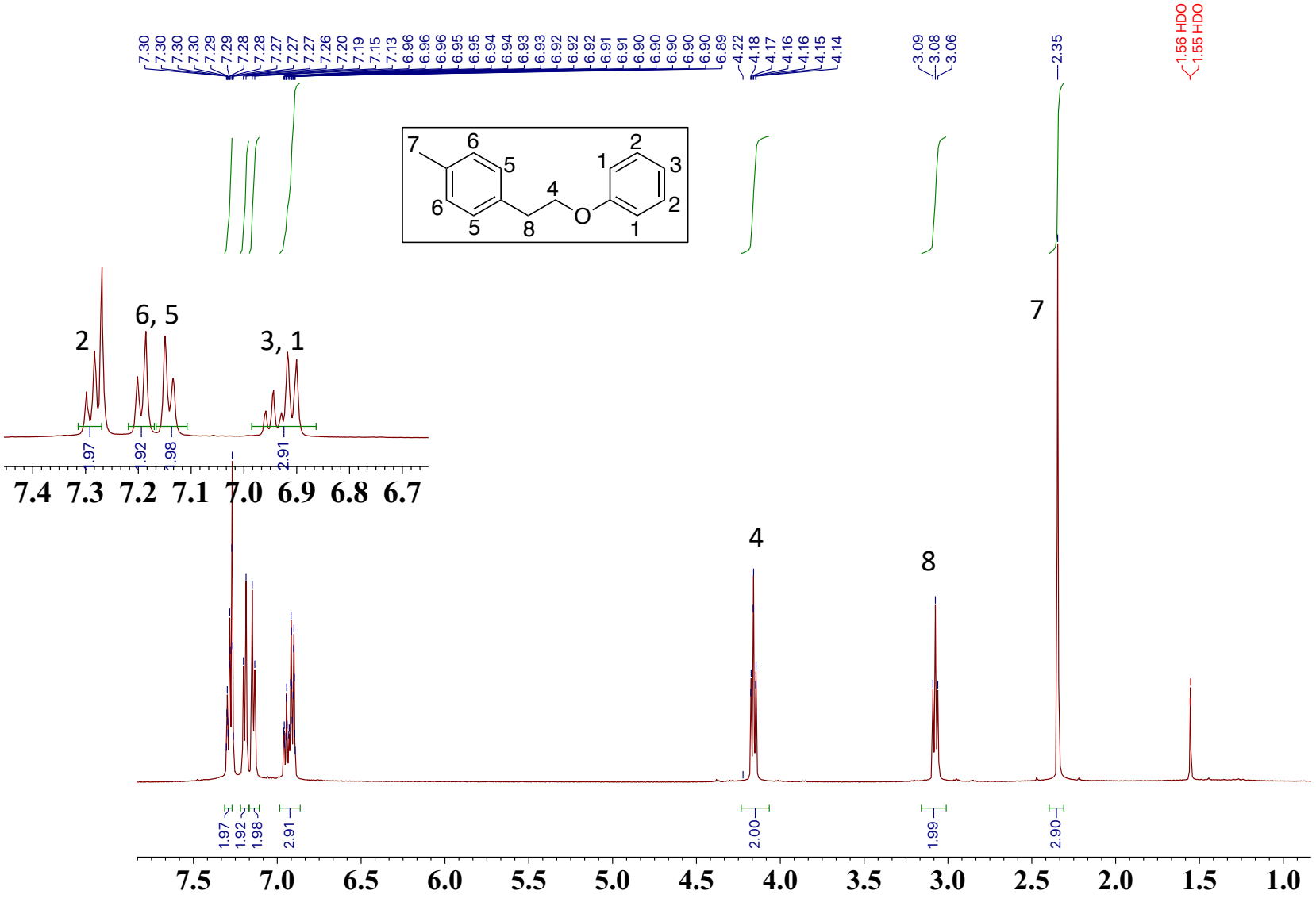

Figure 2.30 ^{1}H NMR of **1-methyl-4-(2-phenoxyethyl)benzene**

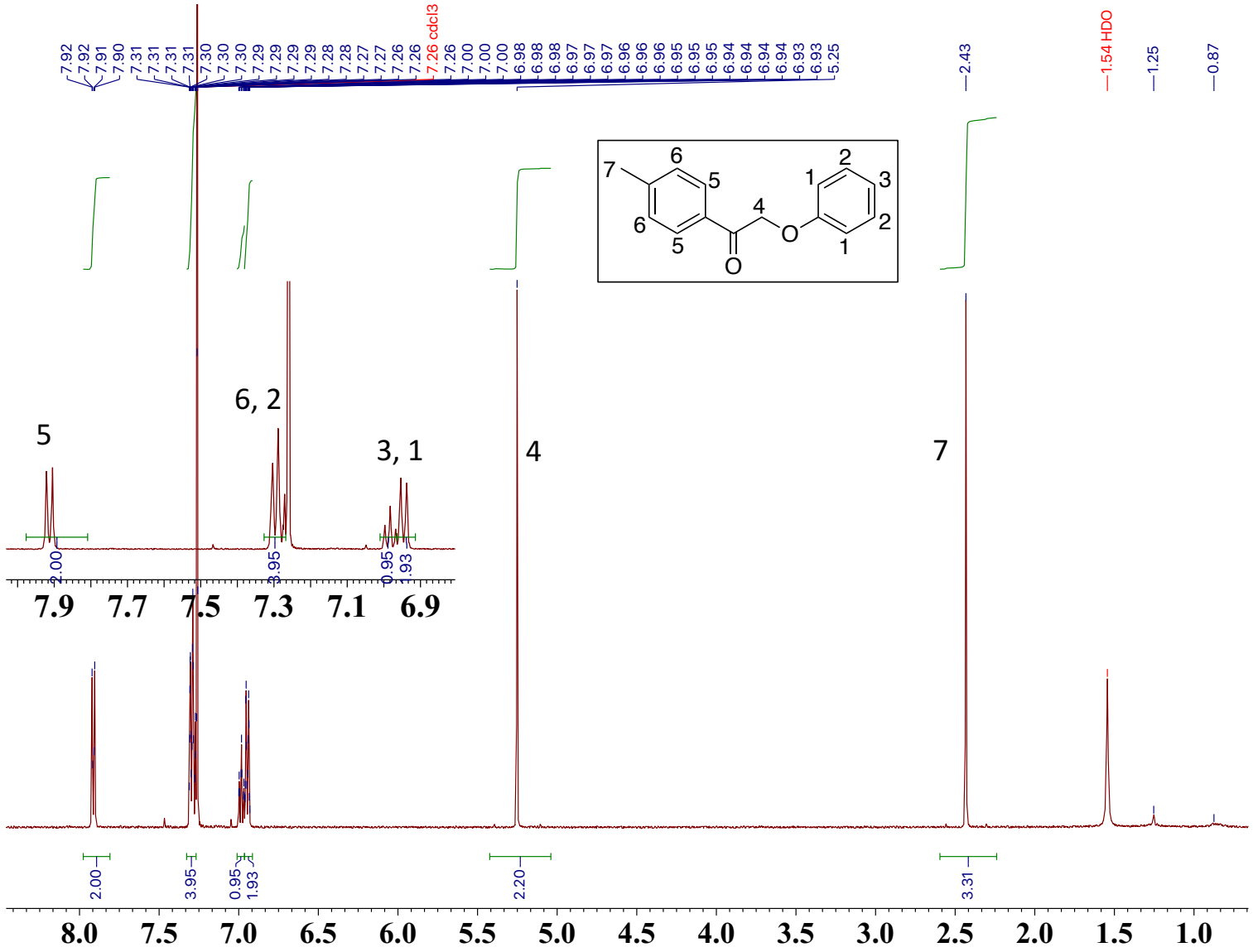

Figure 2.31 ^{1}H NMR of **2-phenoxy-1-(p-tolyl)ethan-1-one**

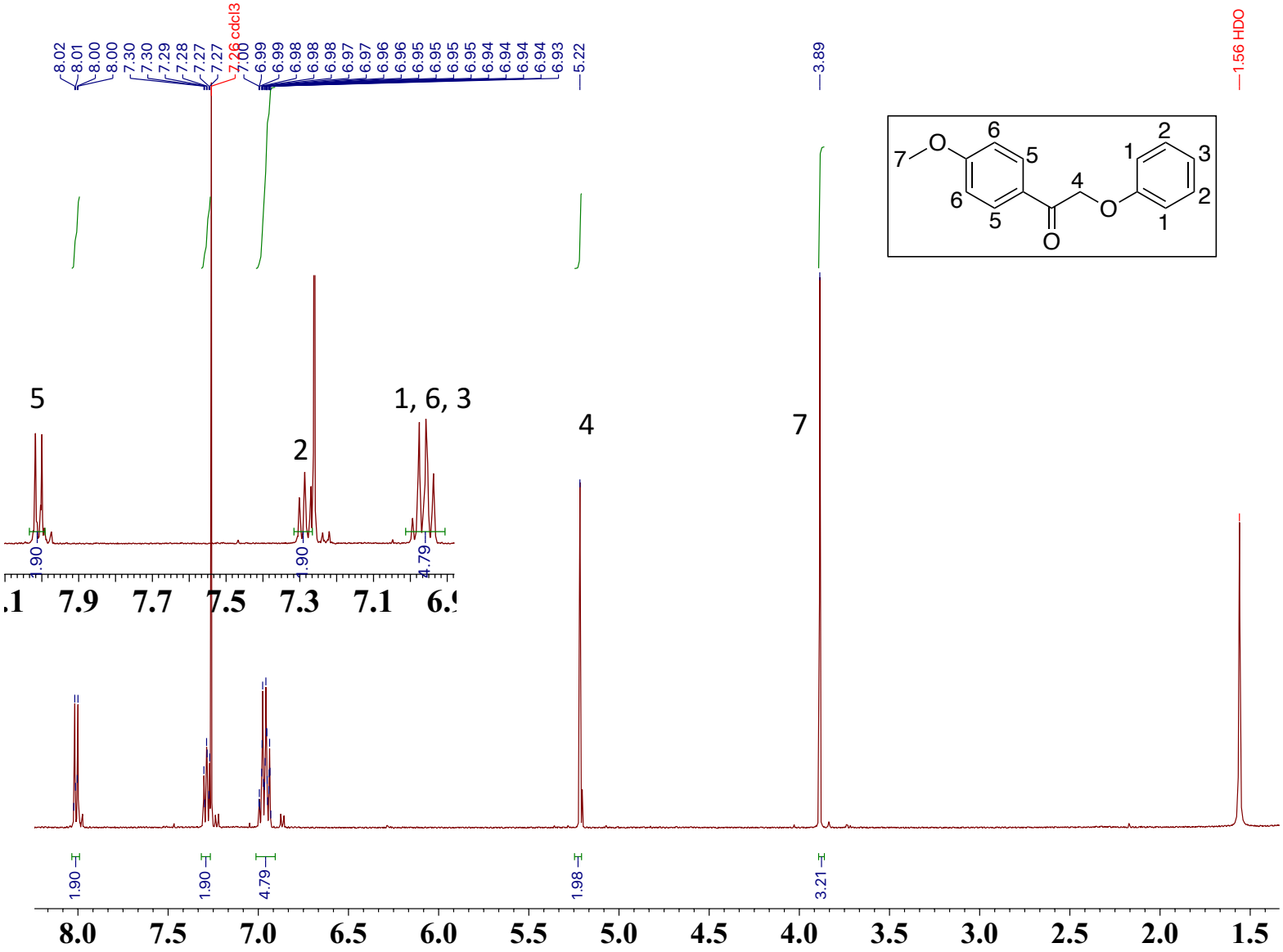

Figure 2.32 ^{1}H NMR of **1-(4-methoxyphenyl)-2-phenoxyethan-1-one**

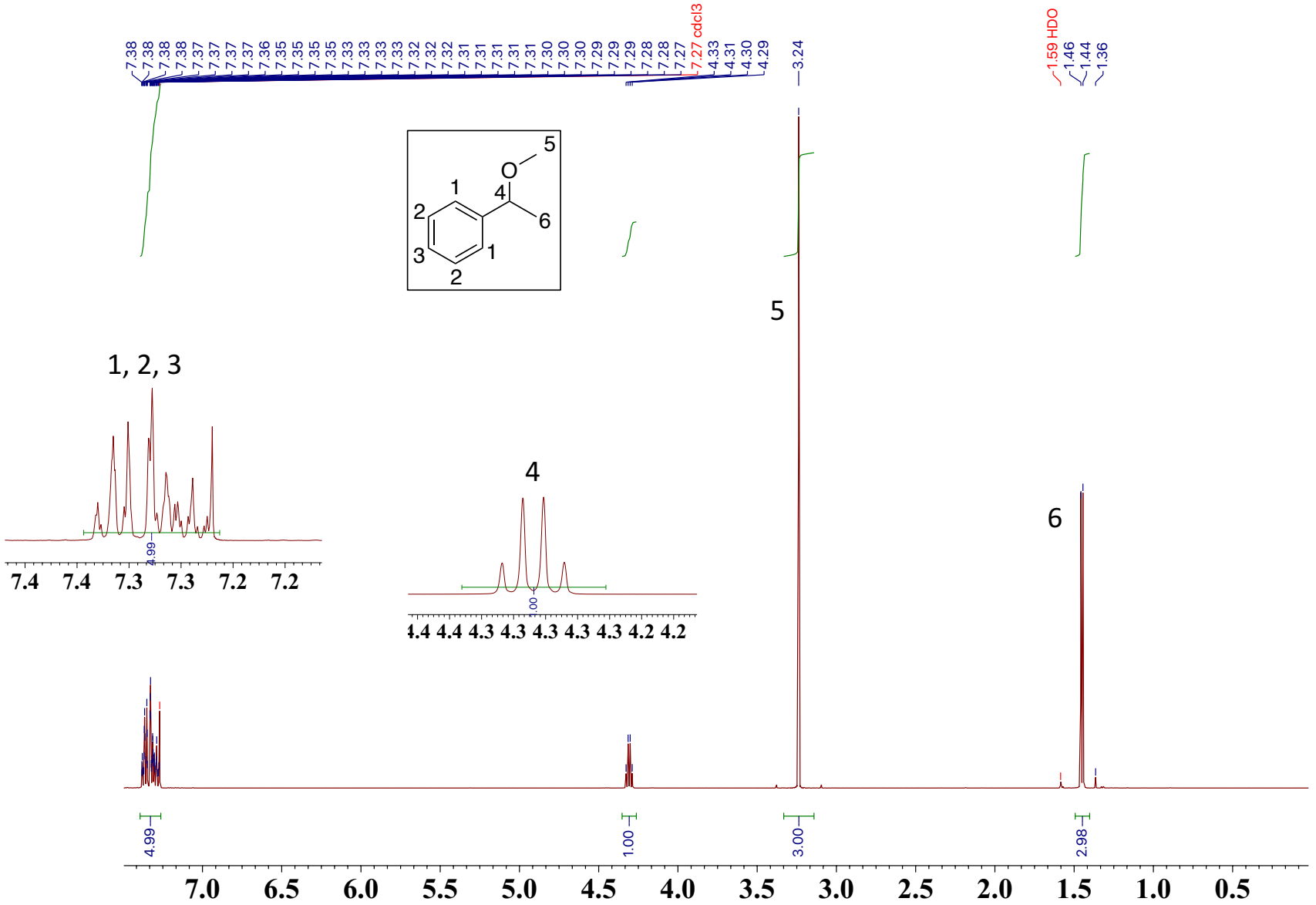

Figure 2.33 ^{1}H NMR of **1-methoxyethyl)benzene**

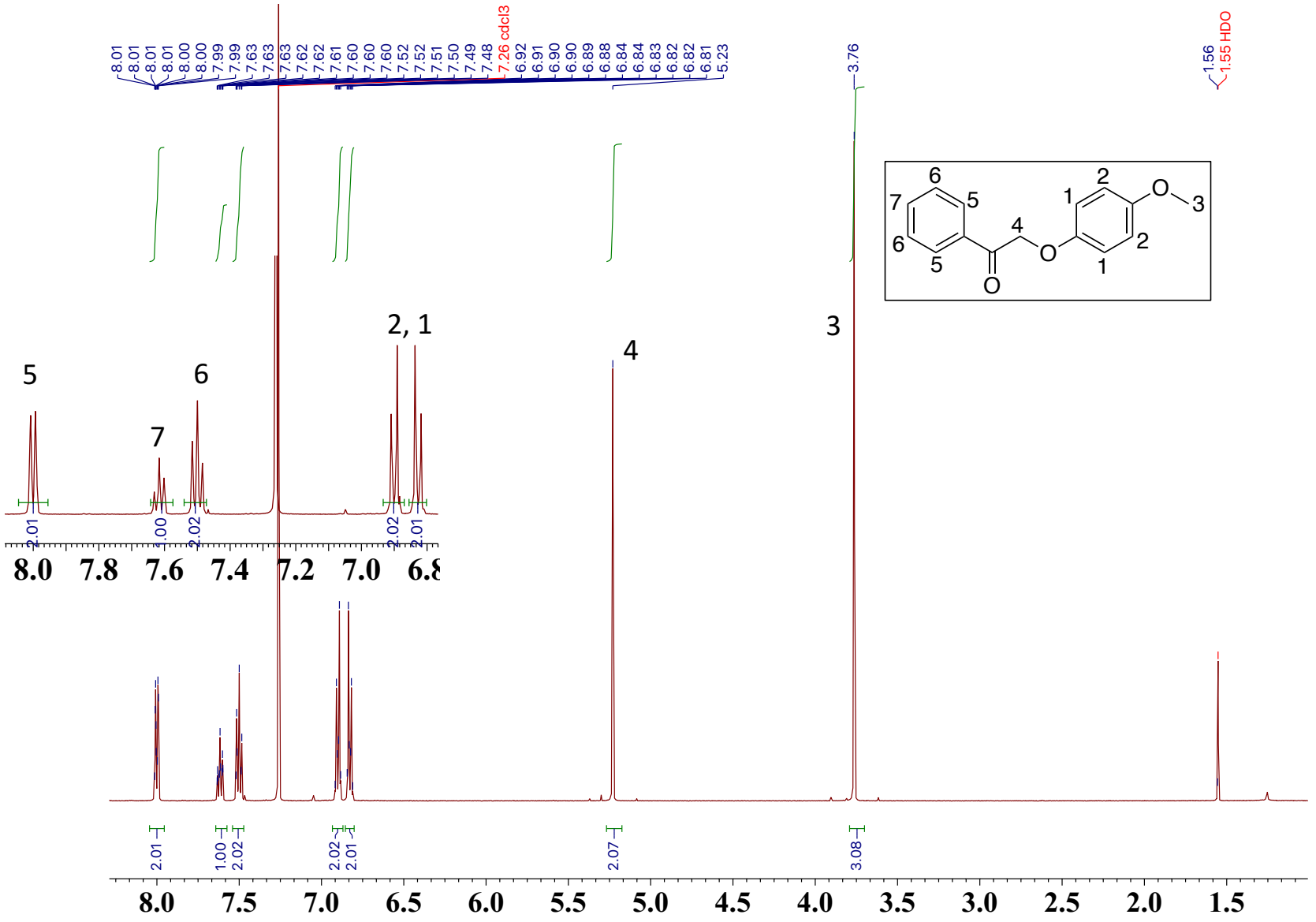

Figure 2.34 ^{1}H NMR of **2-(4-methoxyphenoxy)-1-phenylethan-1-one**

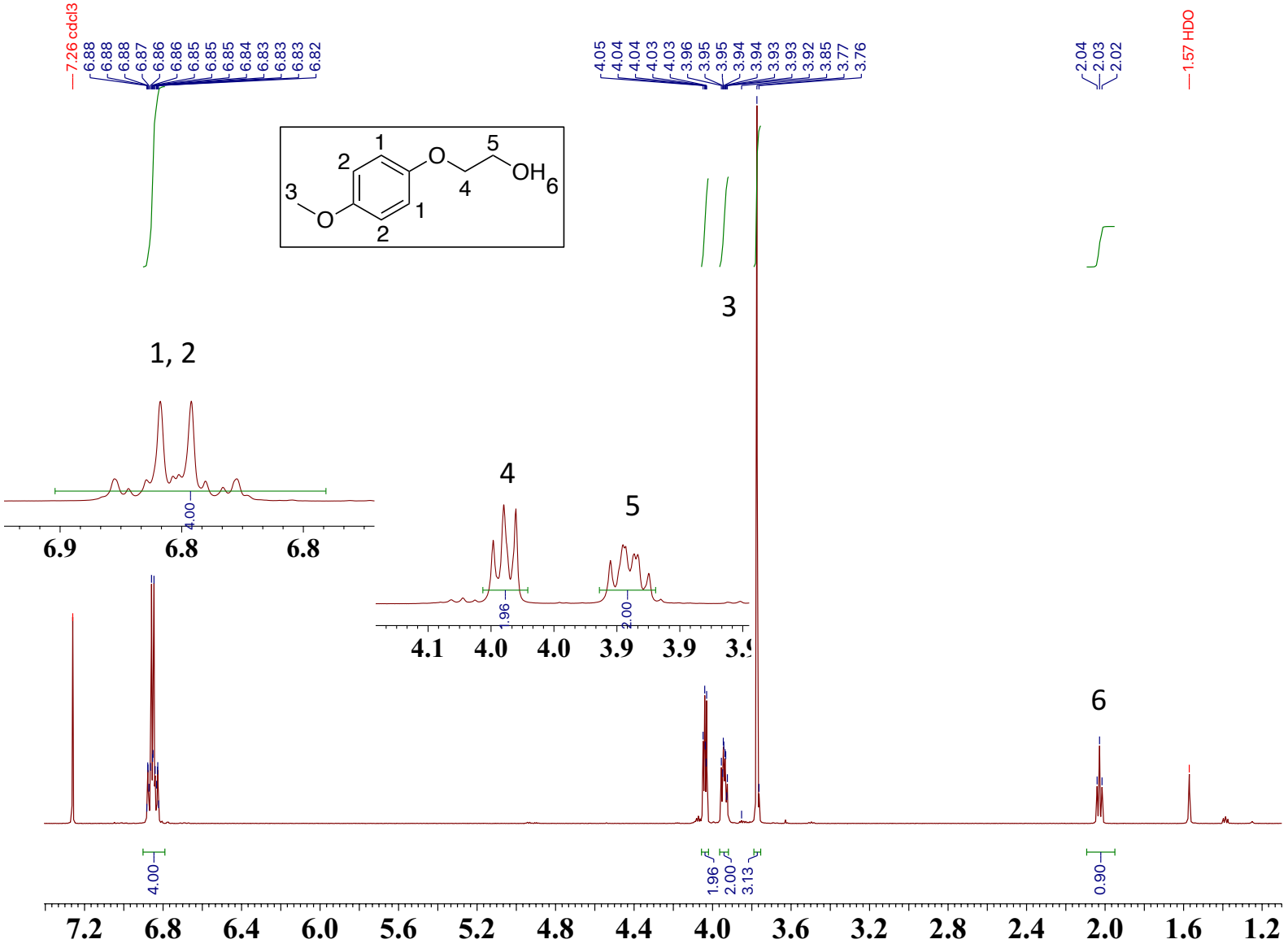

Figure 2.35 ^{1}H NMR of **2-(4-methoxyphenoxy)ethanol**

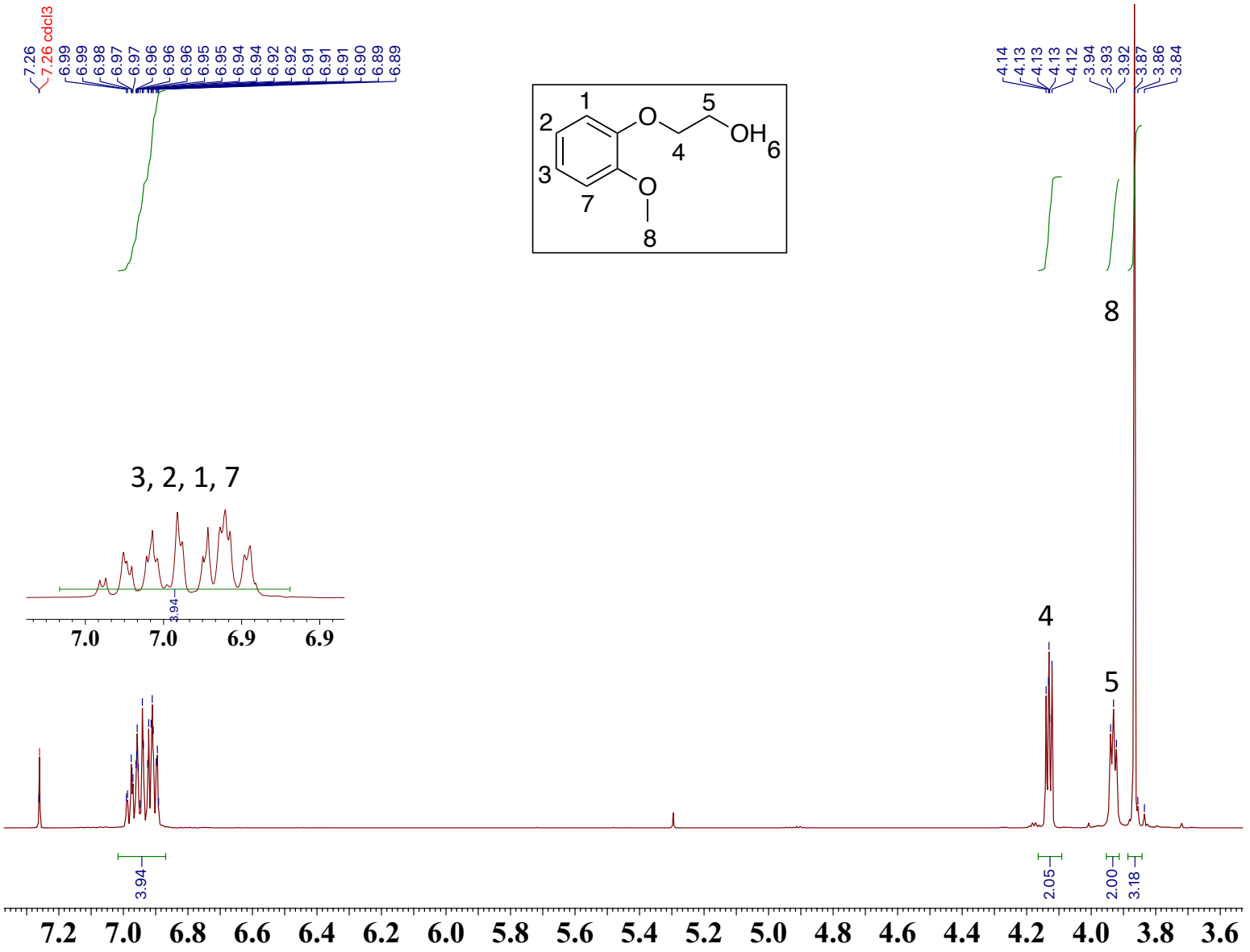

Figure 2.36 ^{1}H NMR of **2-(2-methoxyphenoxy)ethanol**

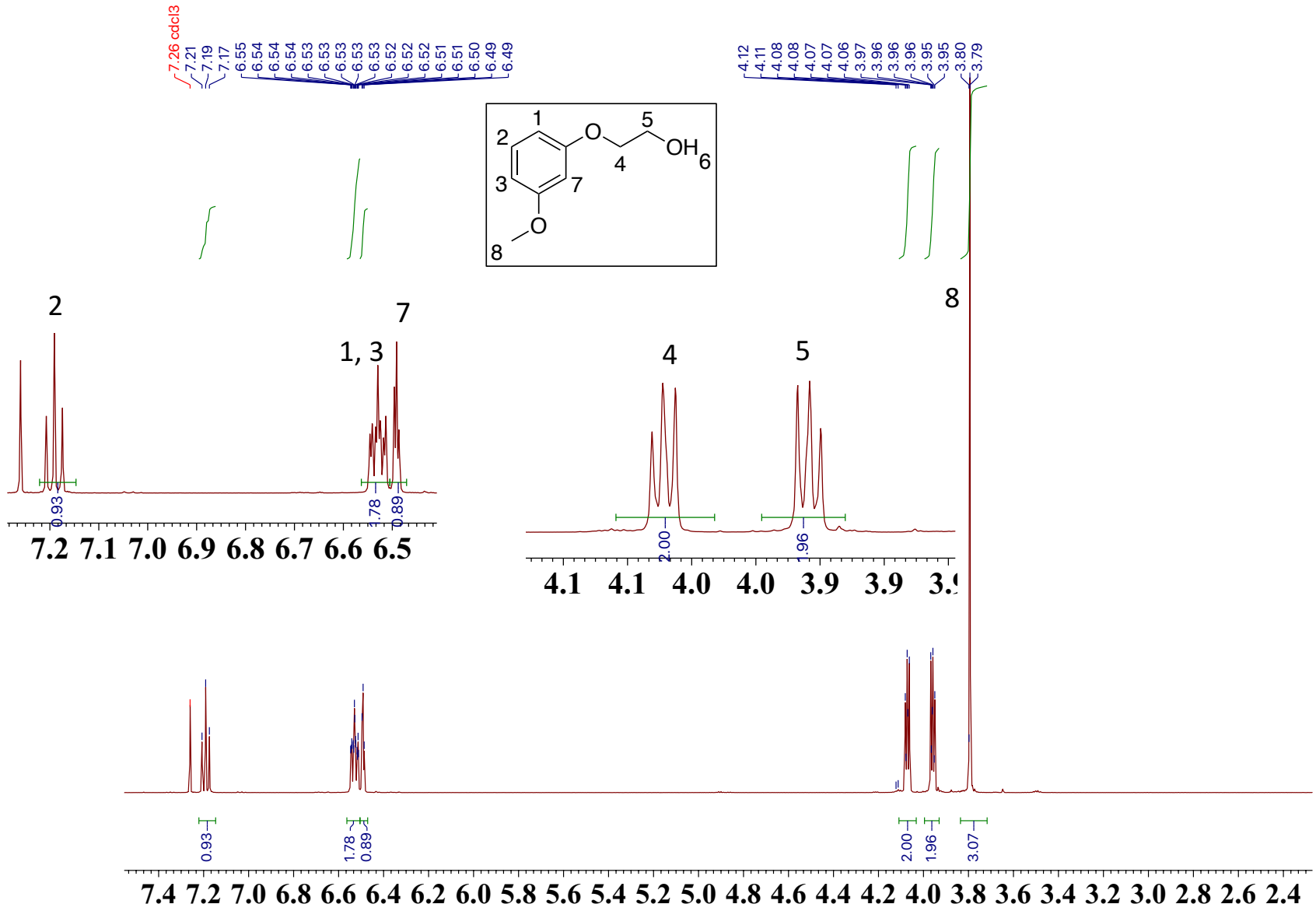

Figure 2.37 ^{1}H NMR of **2-(3-methoxyphenoxy)ethanol**

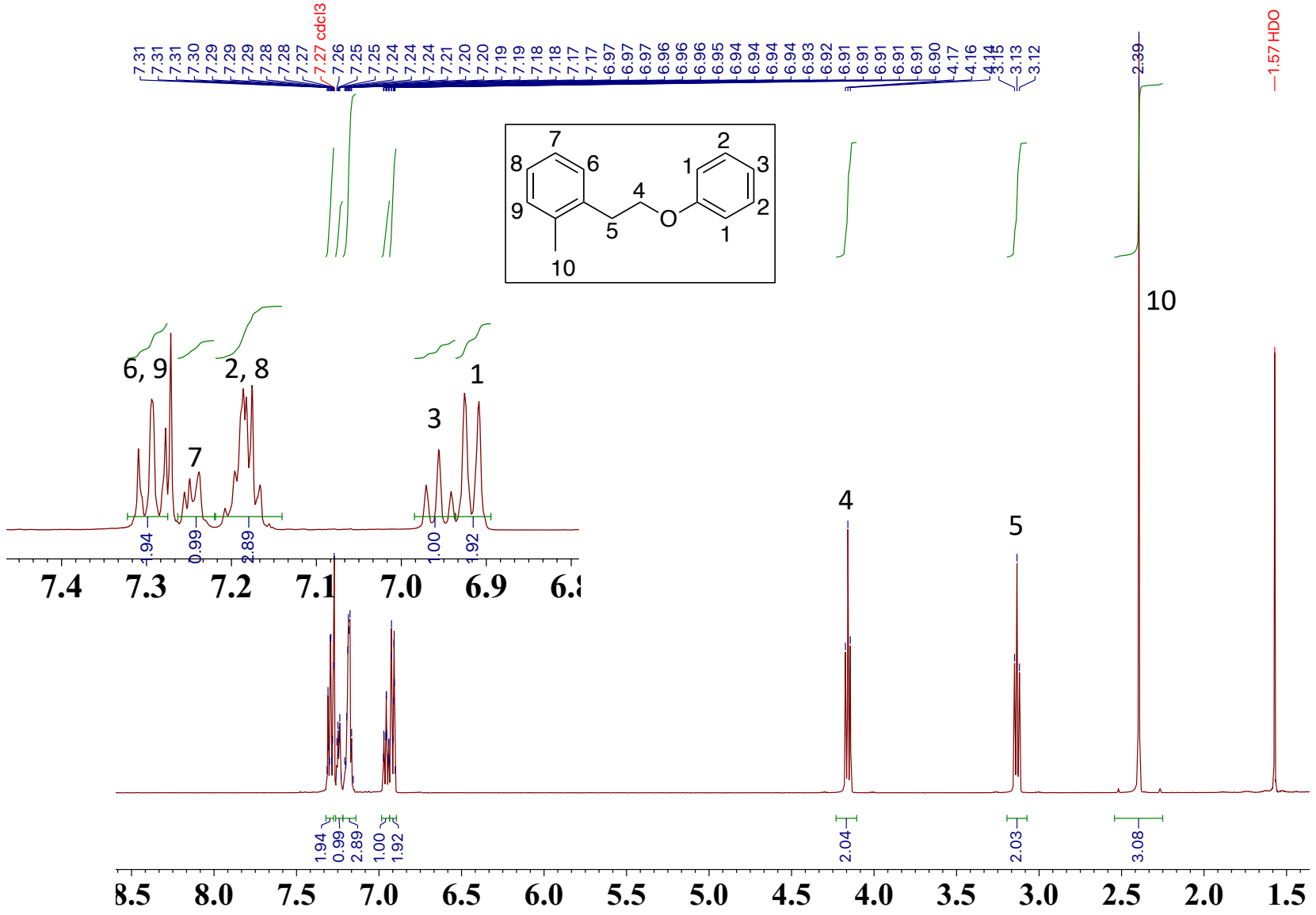

Figure 2.38 ^{1}H NMR of **1-methyl-2-(2-phenoxyethyl)benzene**

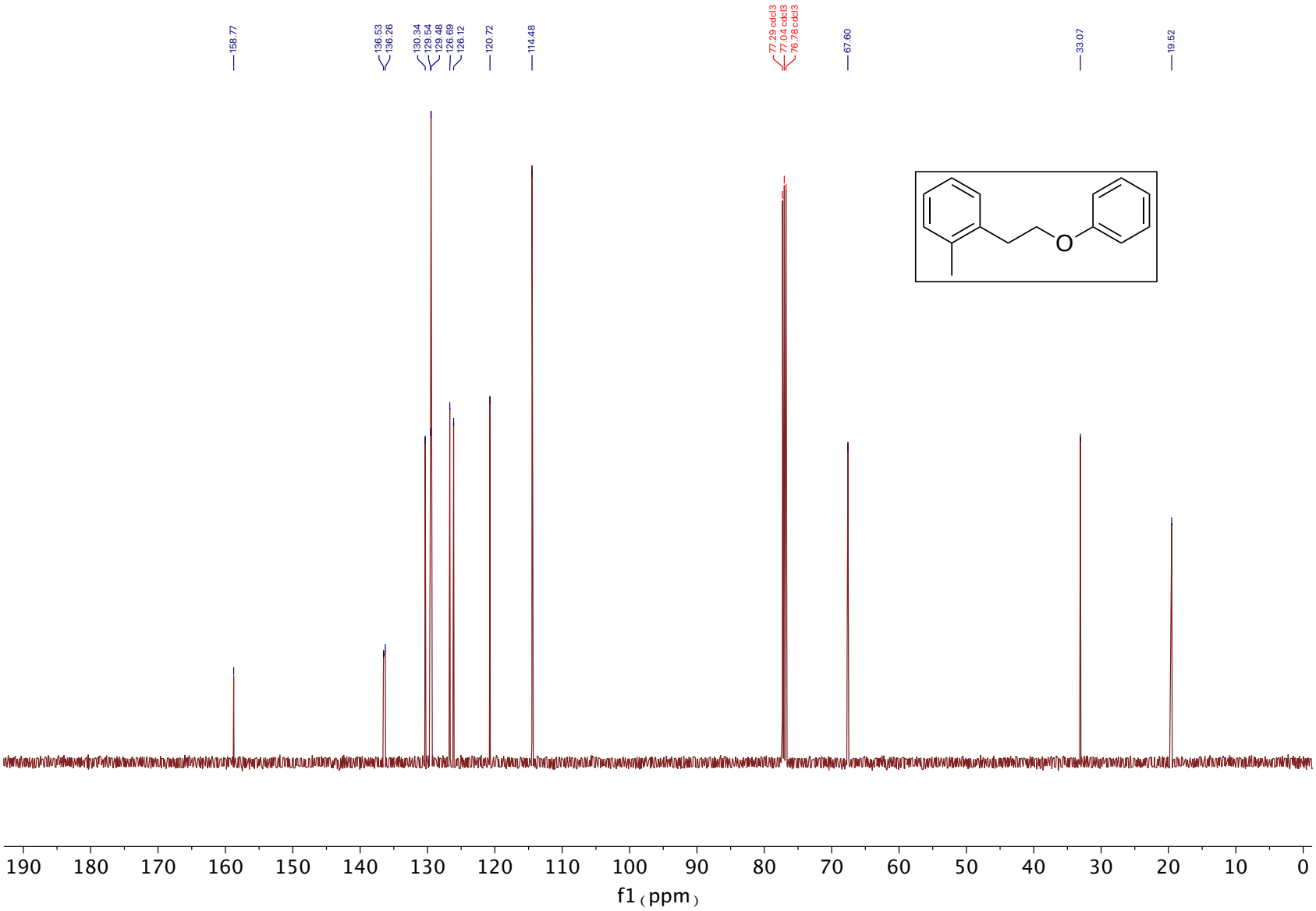

Figure 2.39 ^{13}C NMR of **1-methyl-2-(2-phenoxyethyl)benzene**

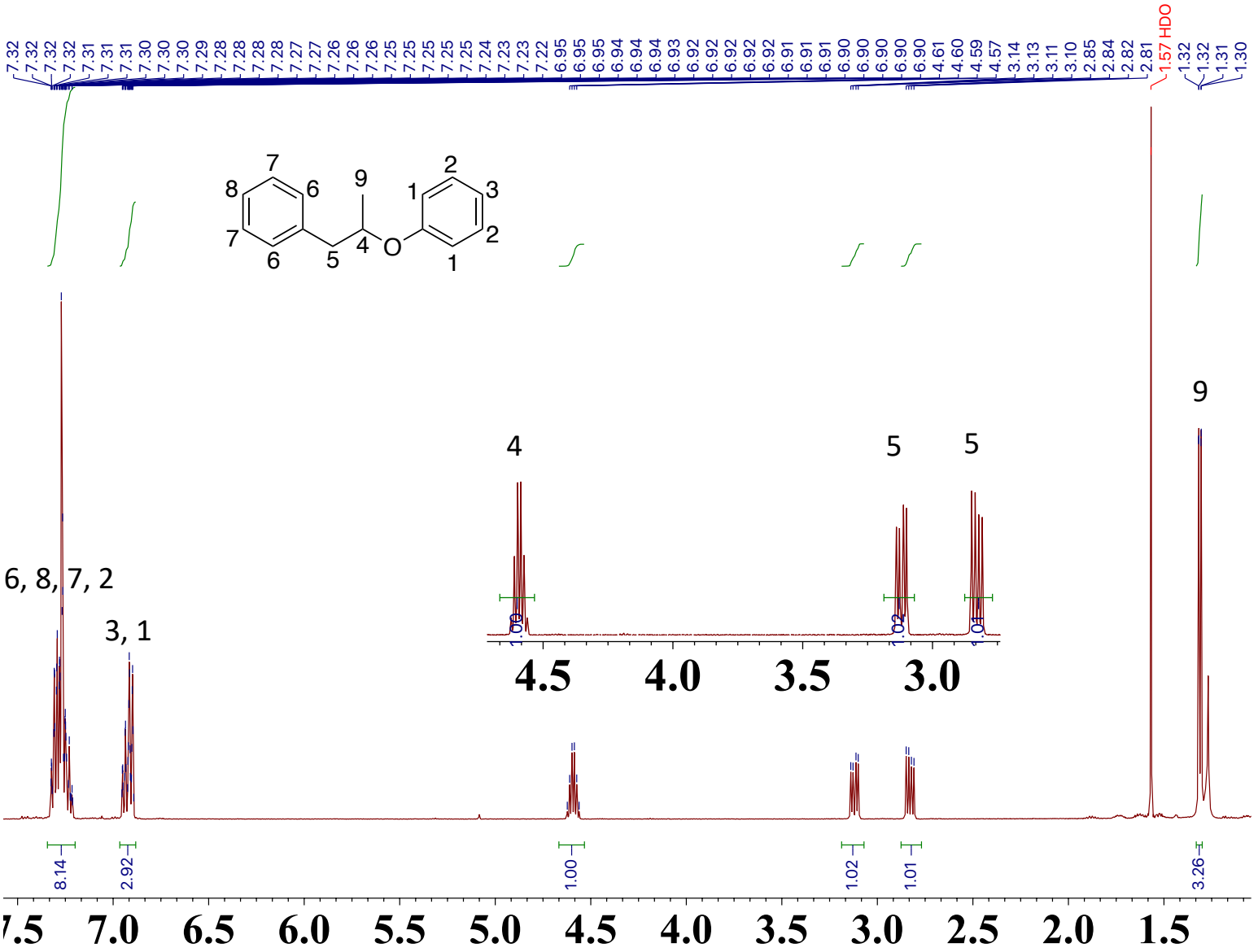

Figure 2.40 ^{1}H NMR of **(2-phenoxypropyl)benzene**

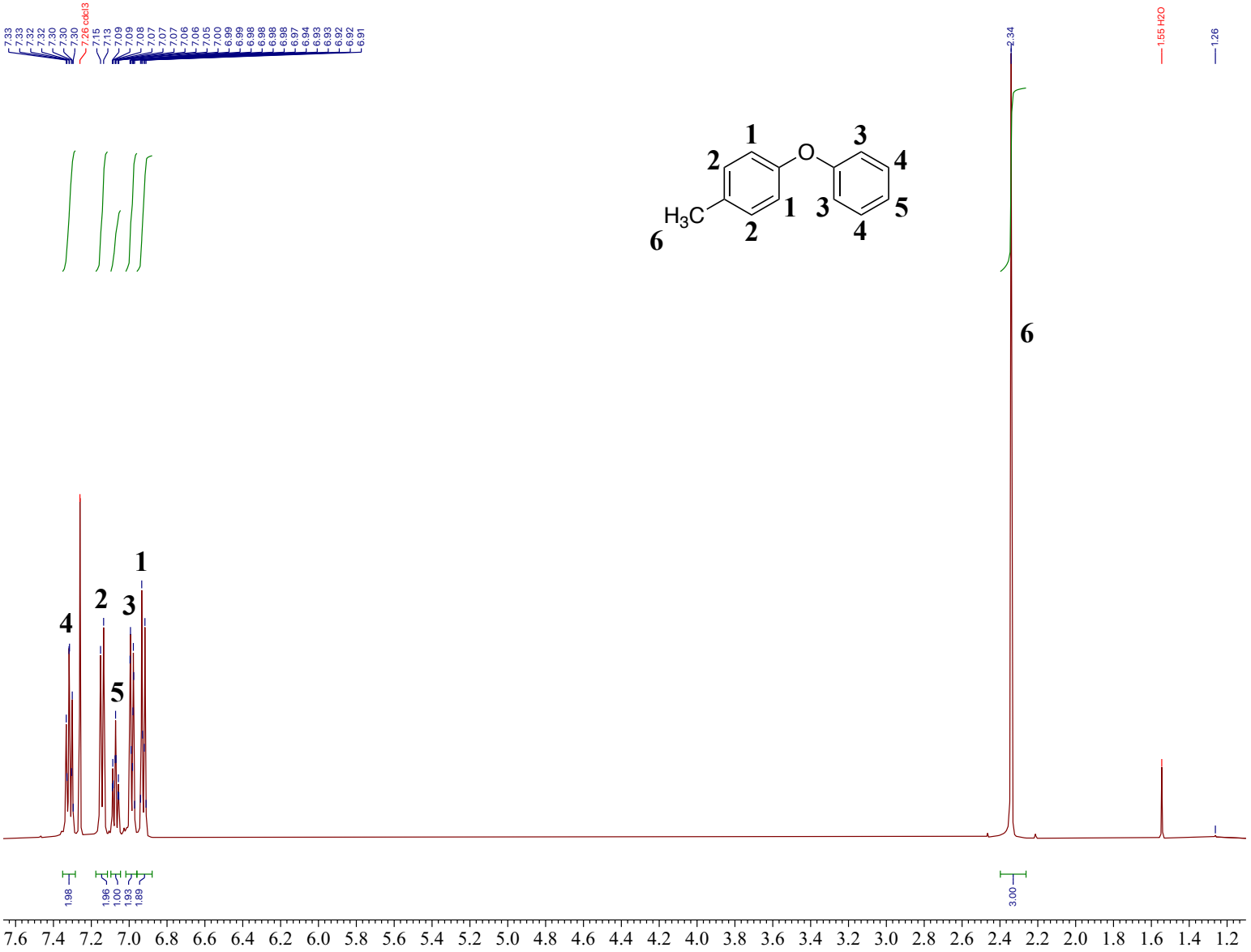

Figure 2.41 ^{1}H NMR of **4-phenoxytoluene**

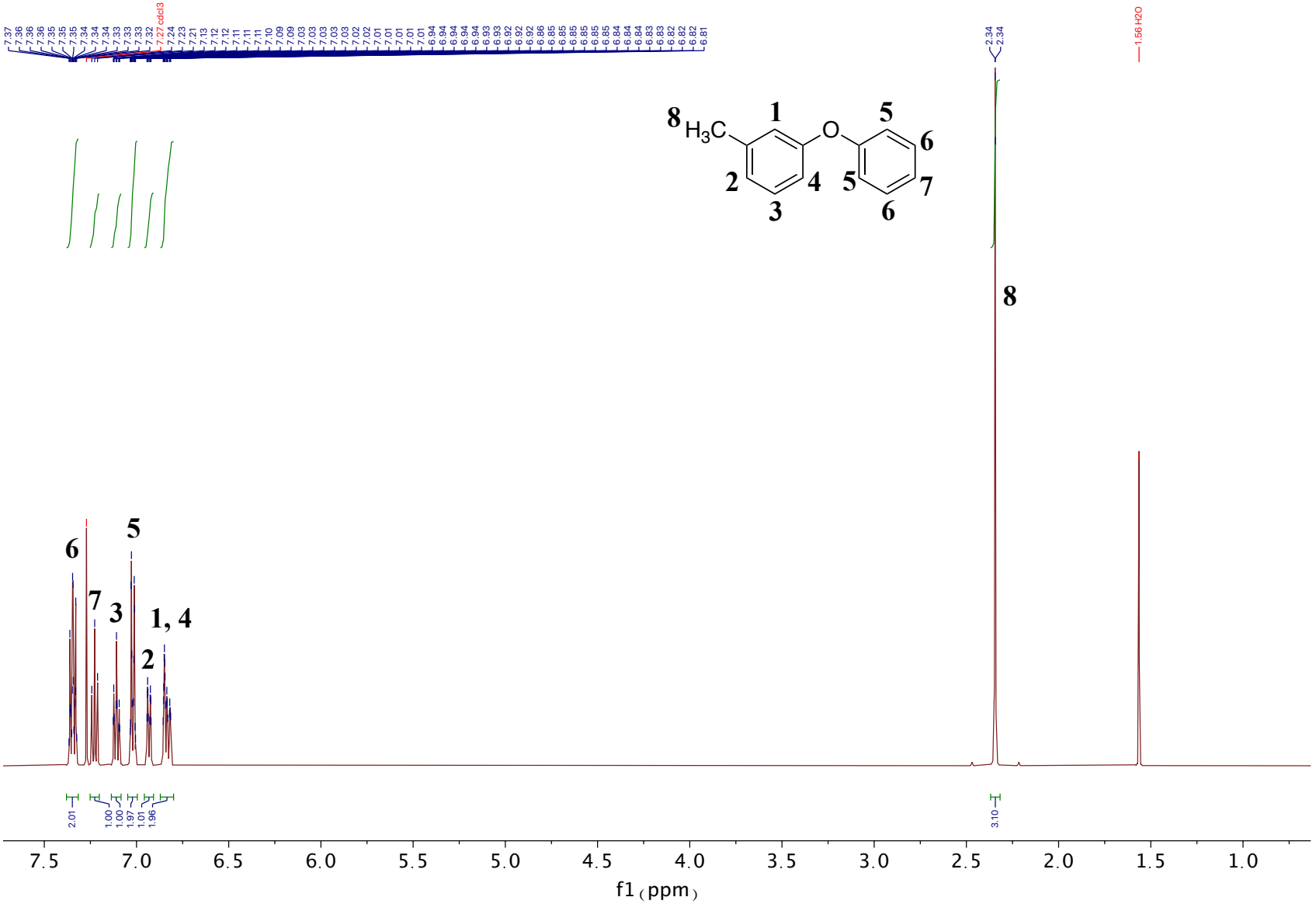

Figure 2.42 ^{1}H NMR of **3-phenoxytoluene**

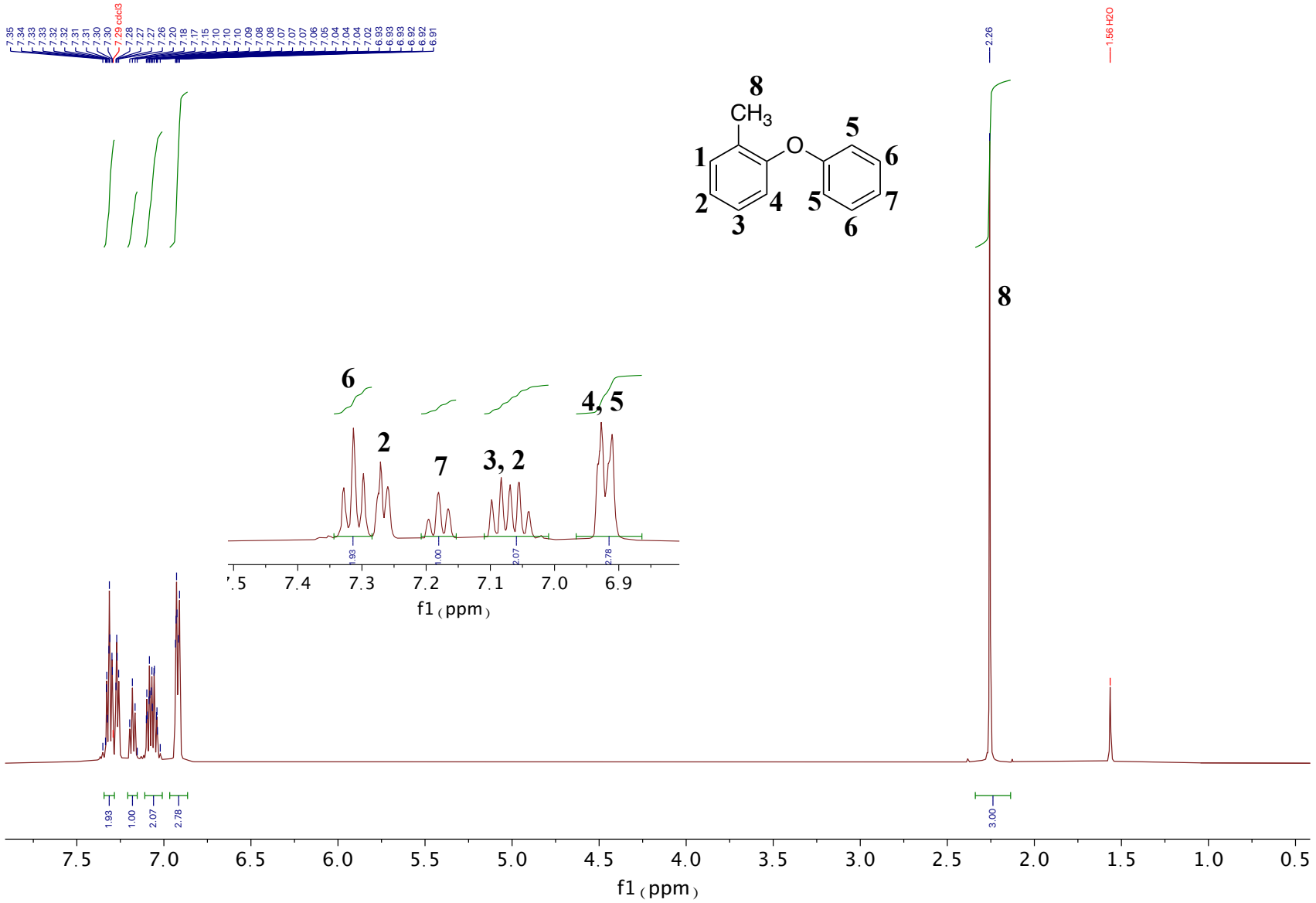

Figure 2.43 ^{1}H NMR of **2-phenoxytoluene**

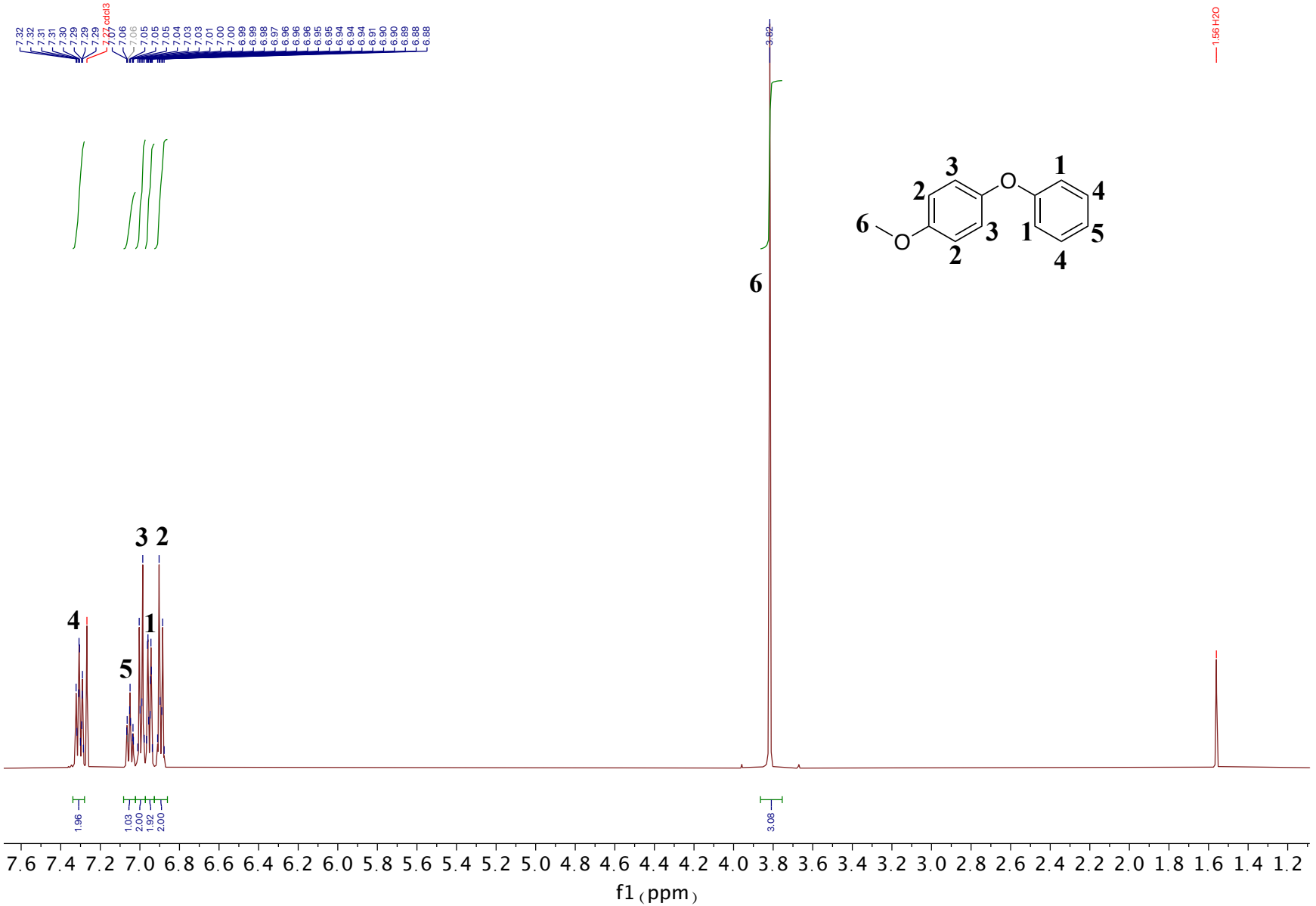

Figure 2.44 ^{1}H NMR of **4-phenoxyanisole**

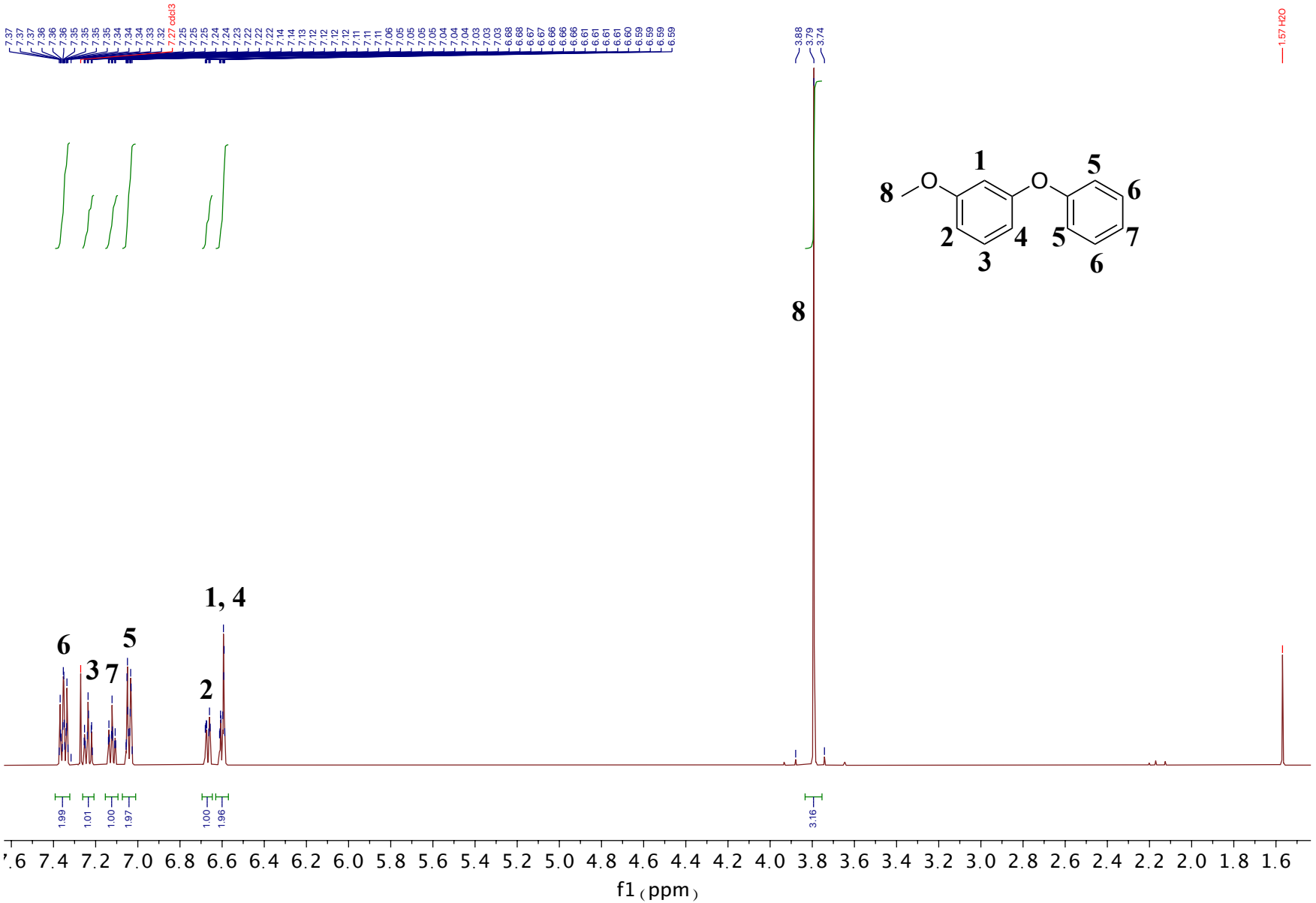

Figure 2.45 ^{1}H NMR of **3-phenoxyanisole**

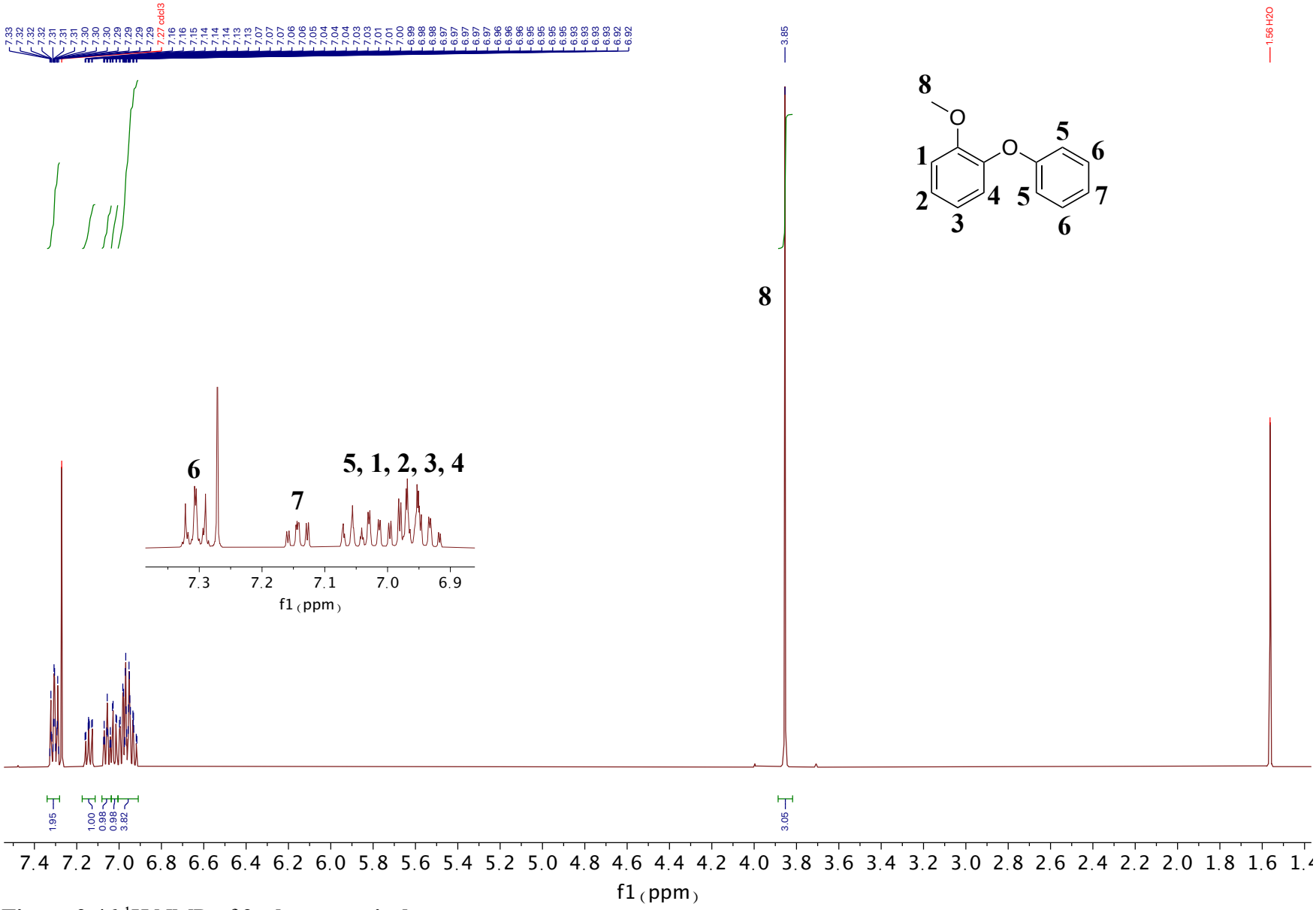

Figure 2.46 ^{1}H NMR of **2-phenoxyanisole**

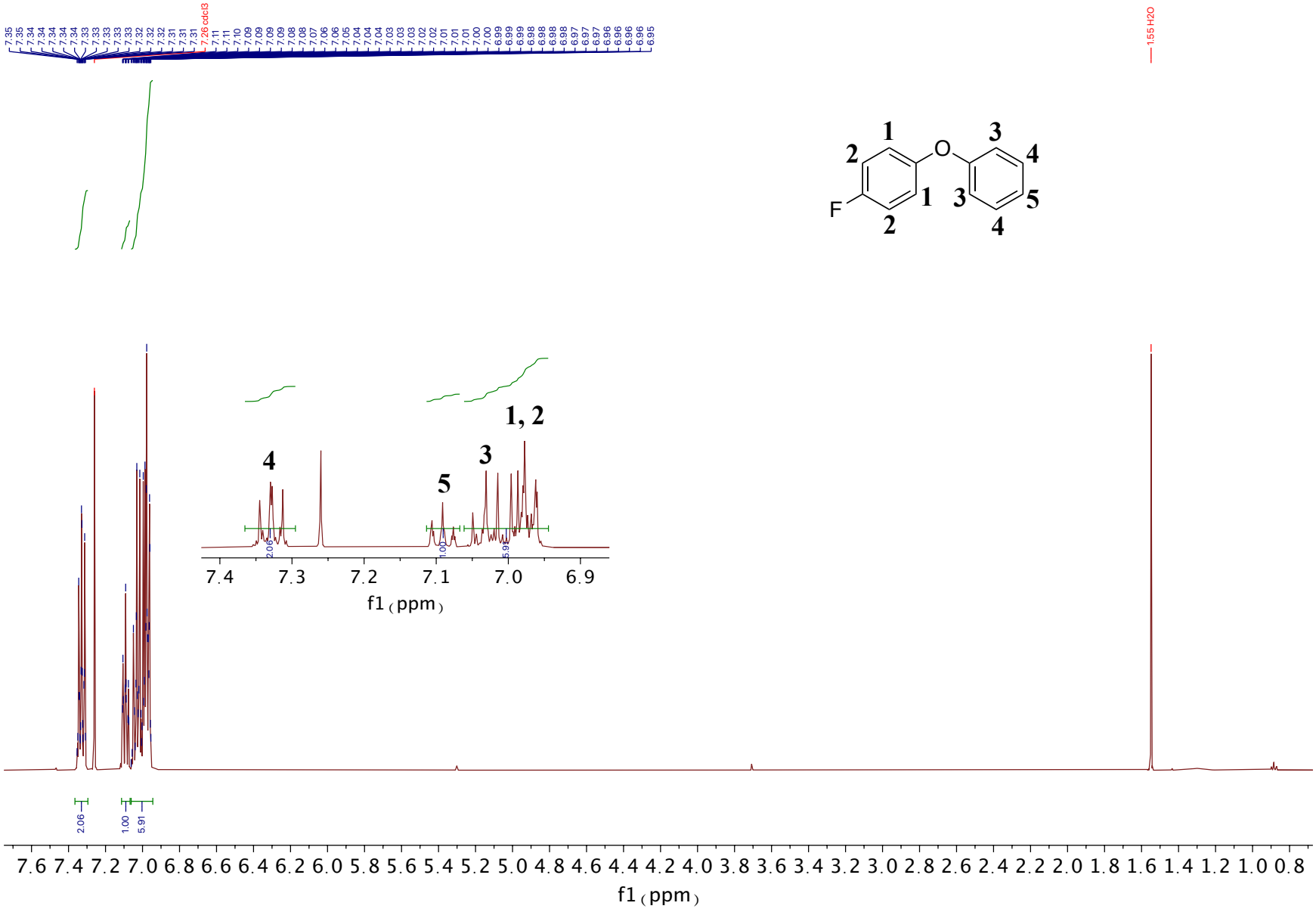

Figure 2.47 ^{1}H NMR of **1-fluoro-4-phenoxybenzene**

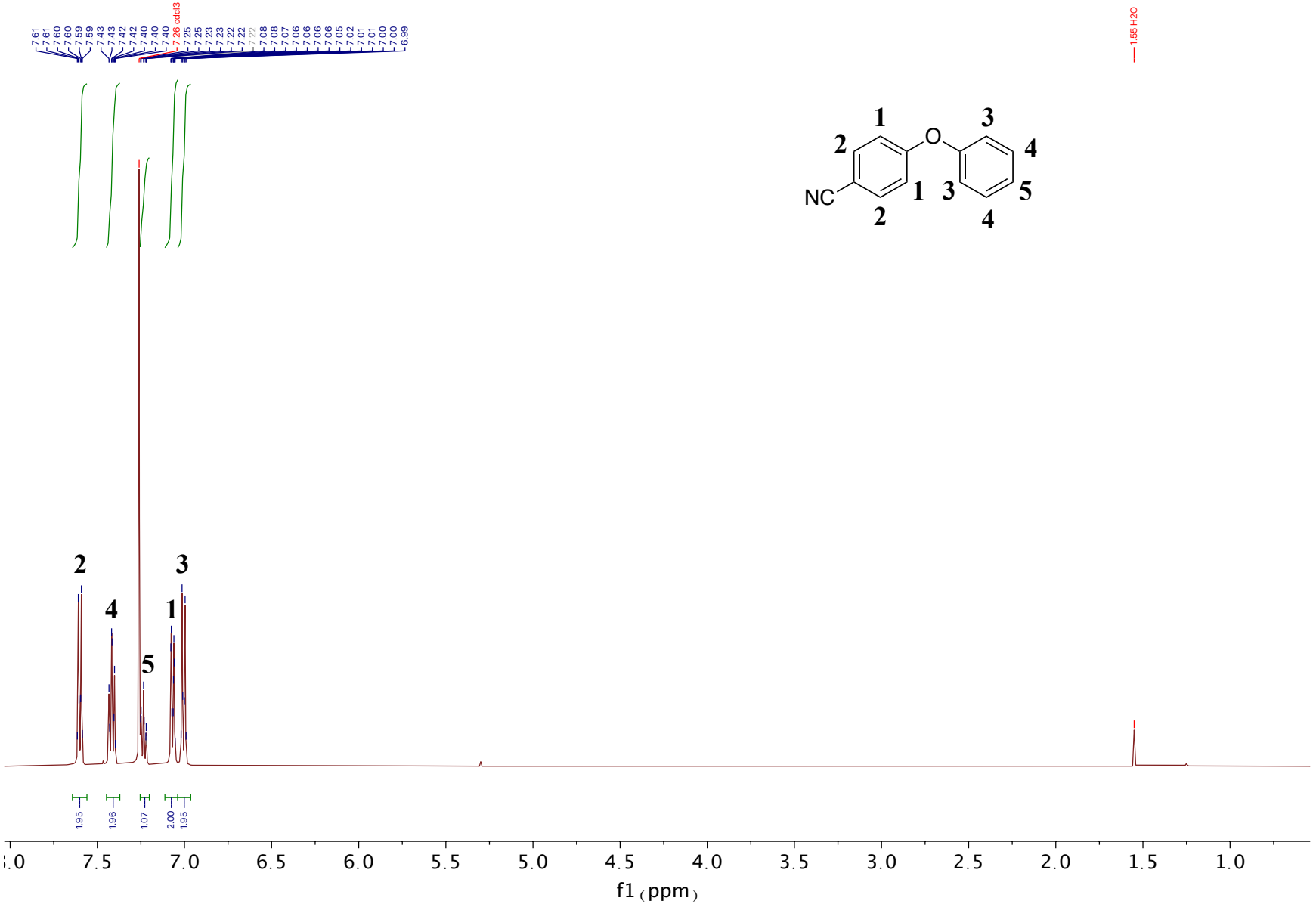

Figure 2.48 ^{1}H NMR of **4-phenoxybenzonitrile**

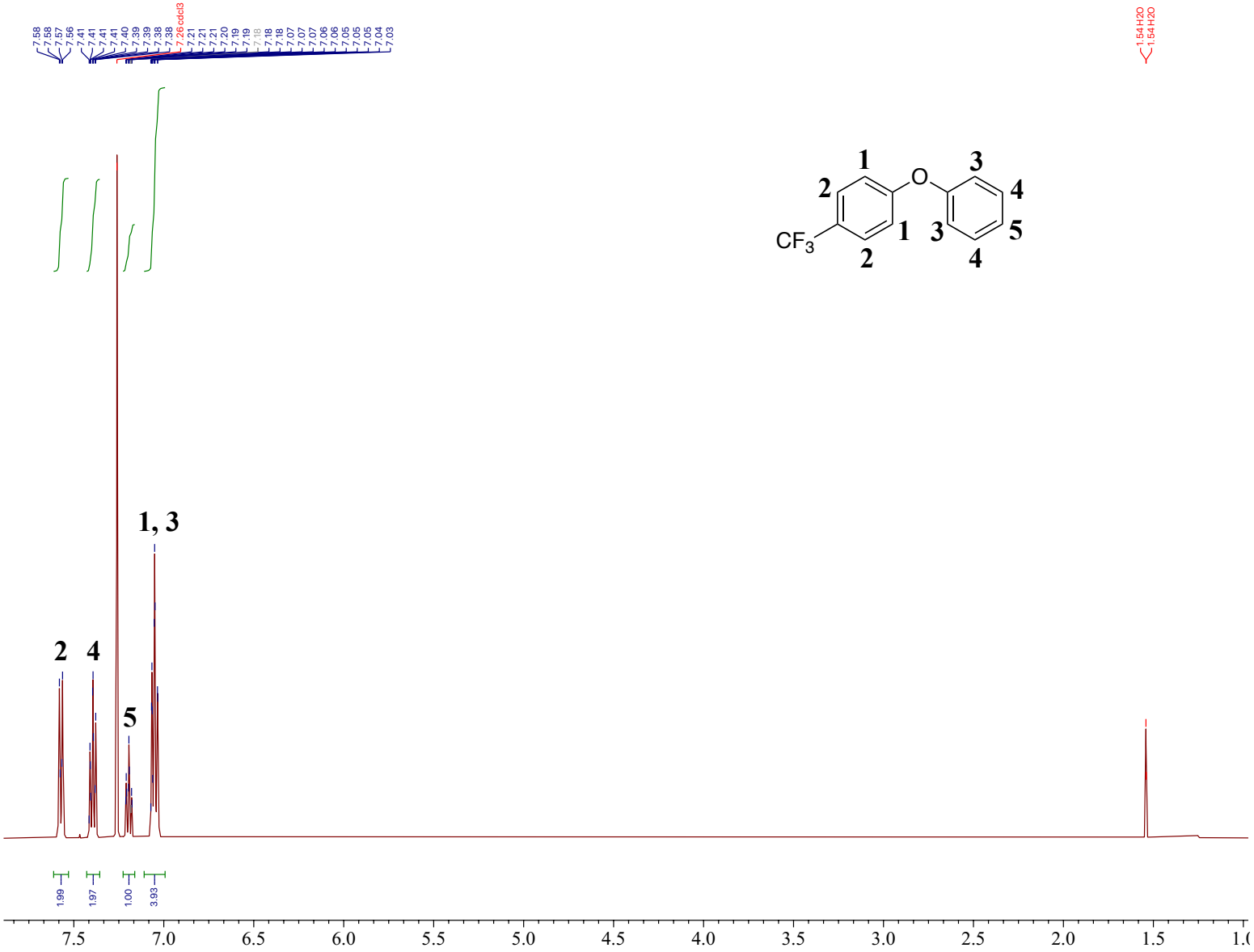

Figure 2.49 ^{1}H NMR of **1-phenoxy-4-(trifluoromethyl)benzene**

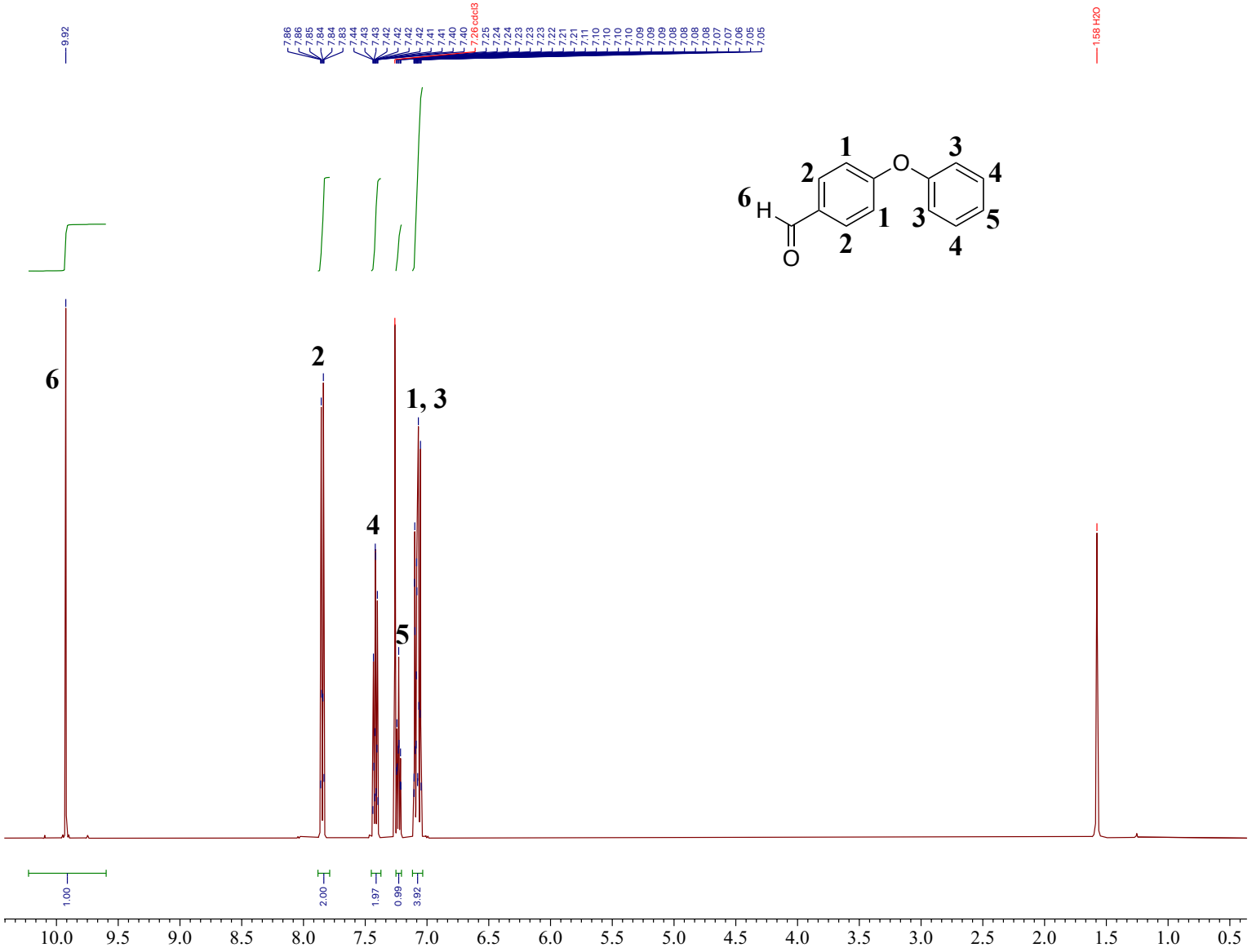

Figure 2.50 ^{1}H NMR of **4-phenoxybenzaldehyde**

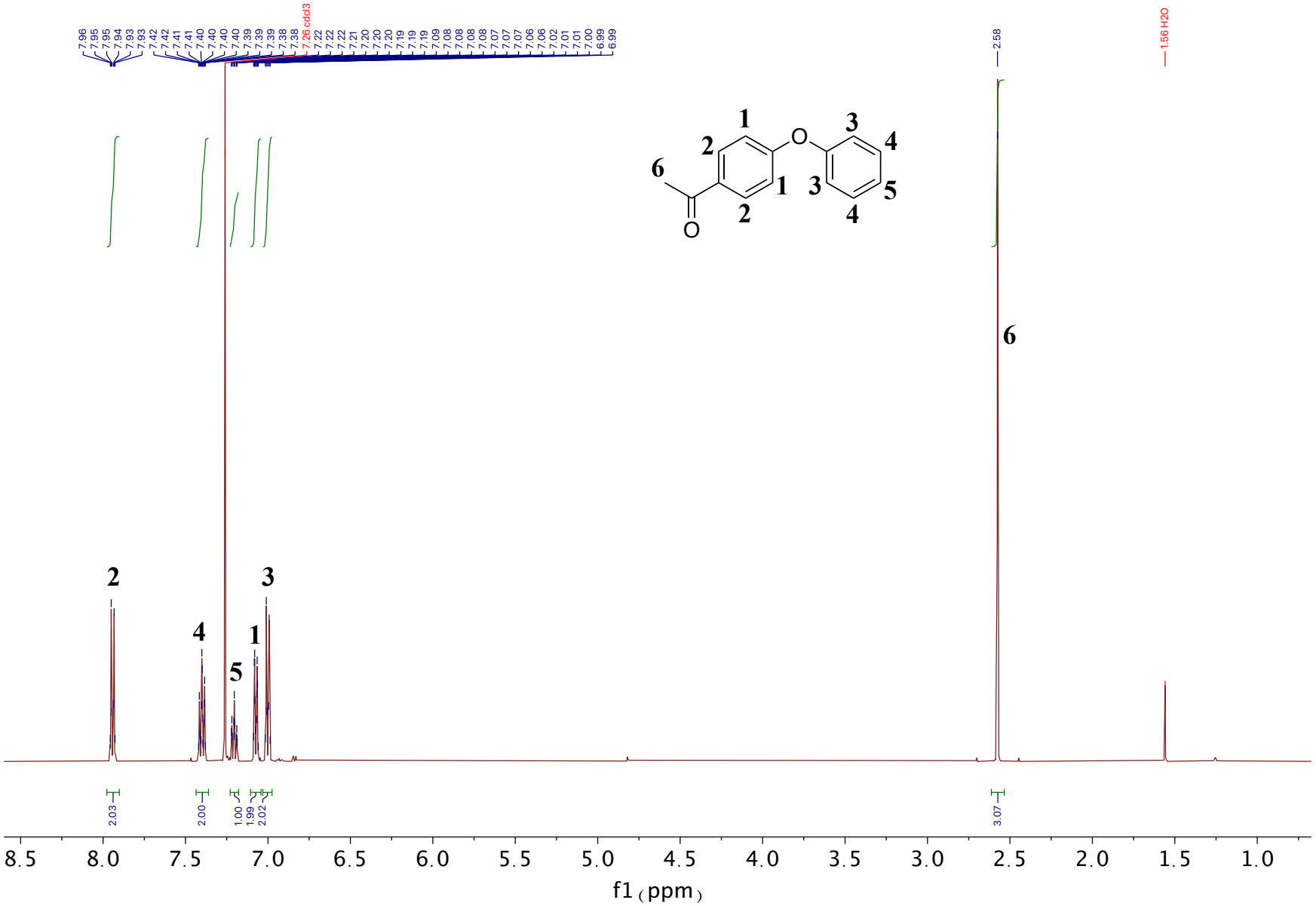

Figure 2.51 ^{1}H NMR of **1-(4-phenoxyphenyl)ethan-1-ones**

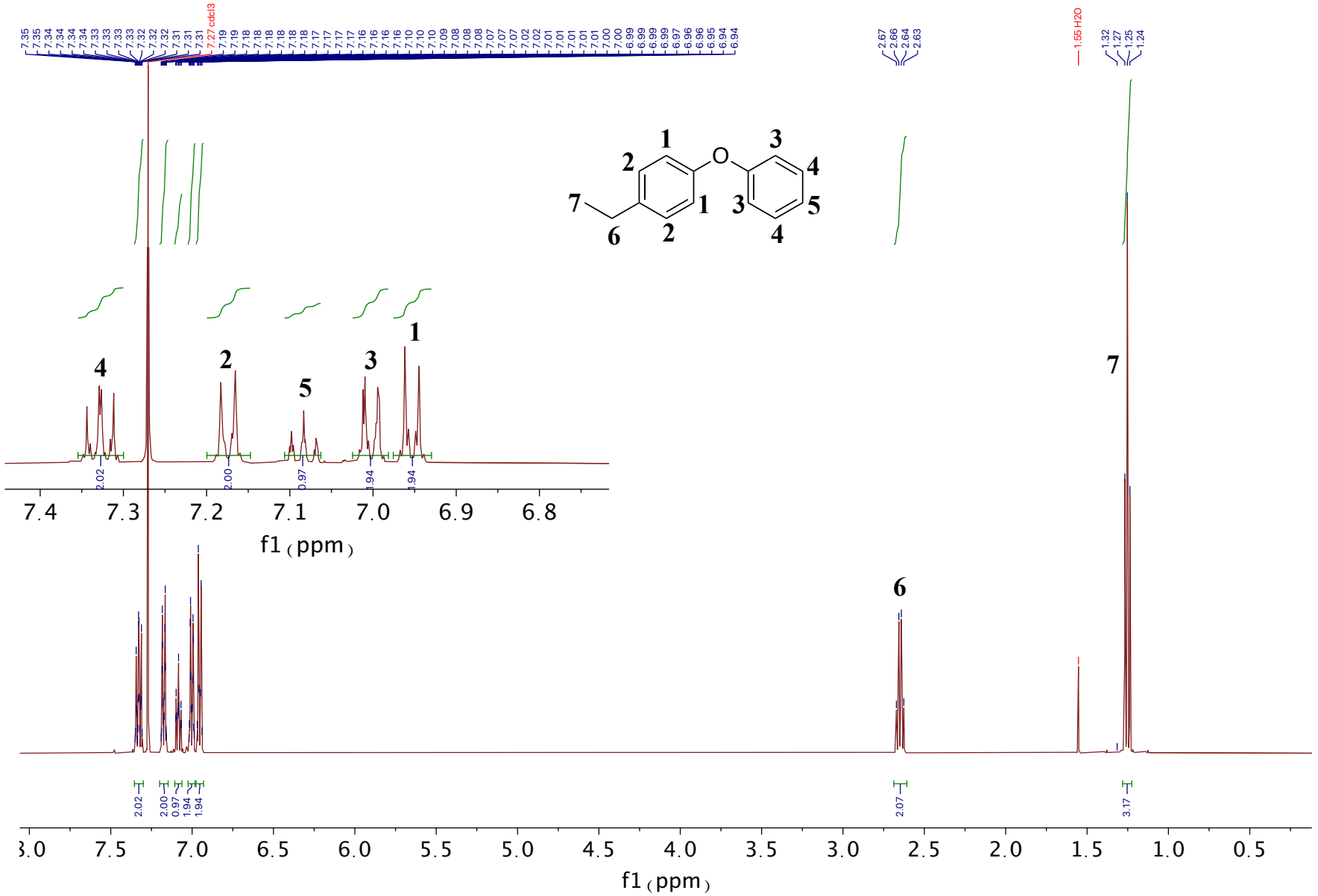

Figure 2.52 ^{1}H NMR of **1-ethyl-4-phenoxybenzene**

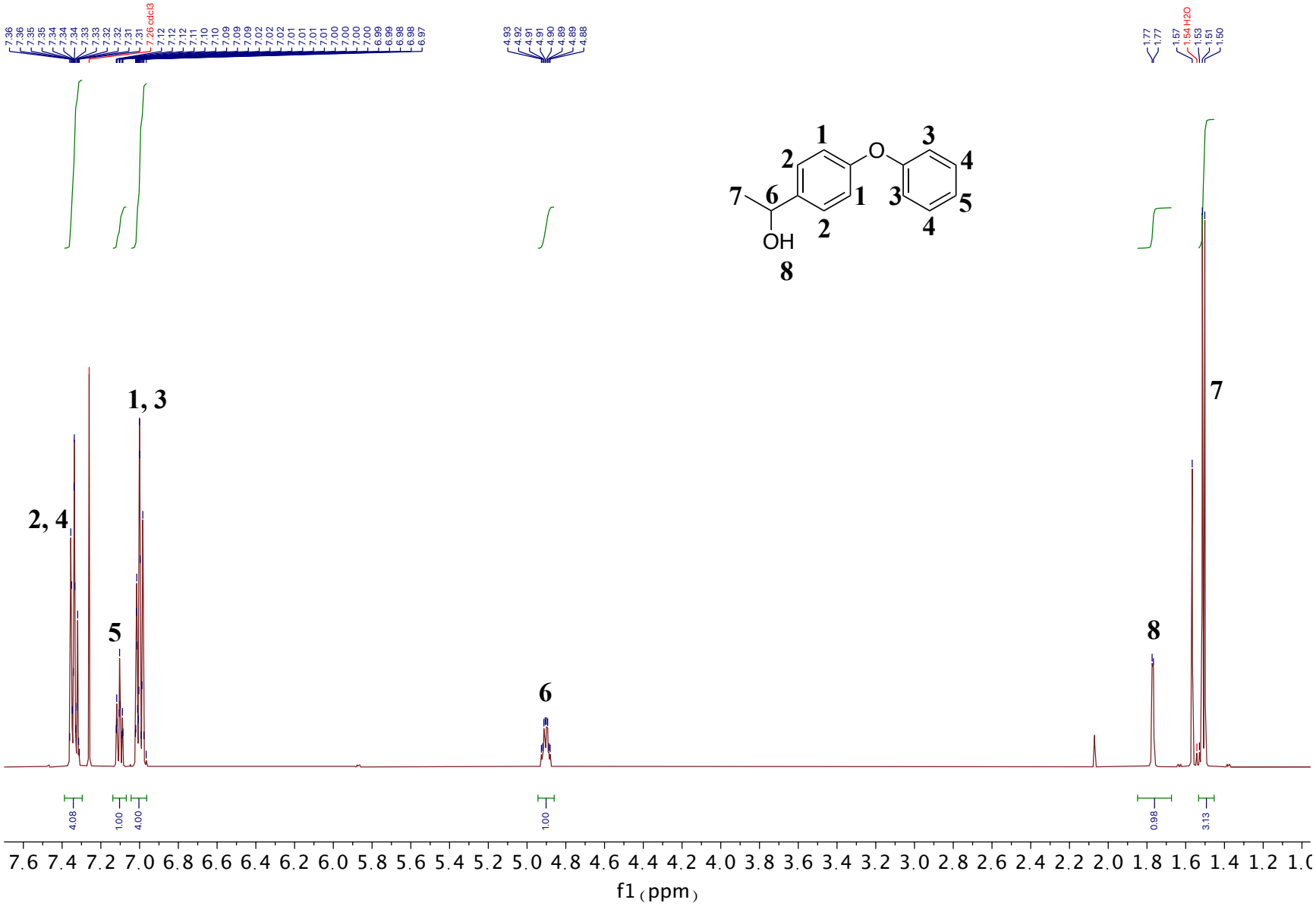

Figure 2.53 ^{1}H NMR of **1-(4-phenoxyphenyl)ethan-1-ol**

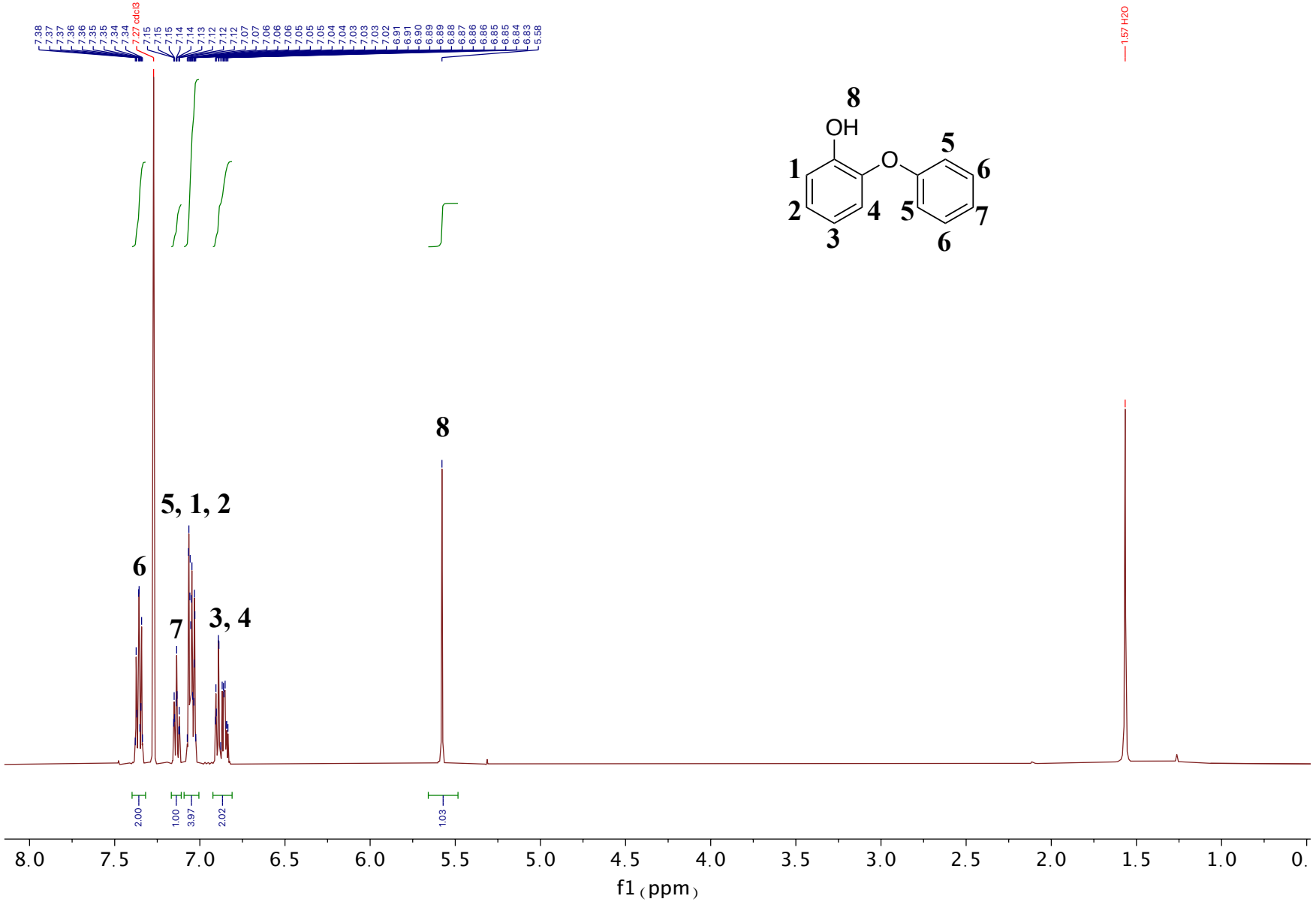

Figure 2.54 ^{1}H NMR of **2-phenoxyphenol**

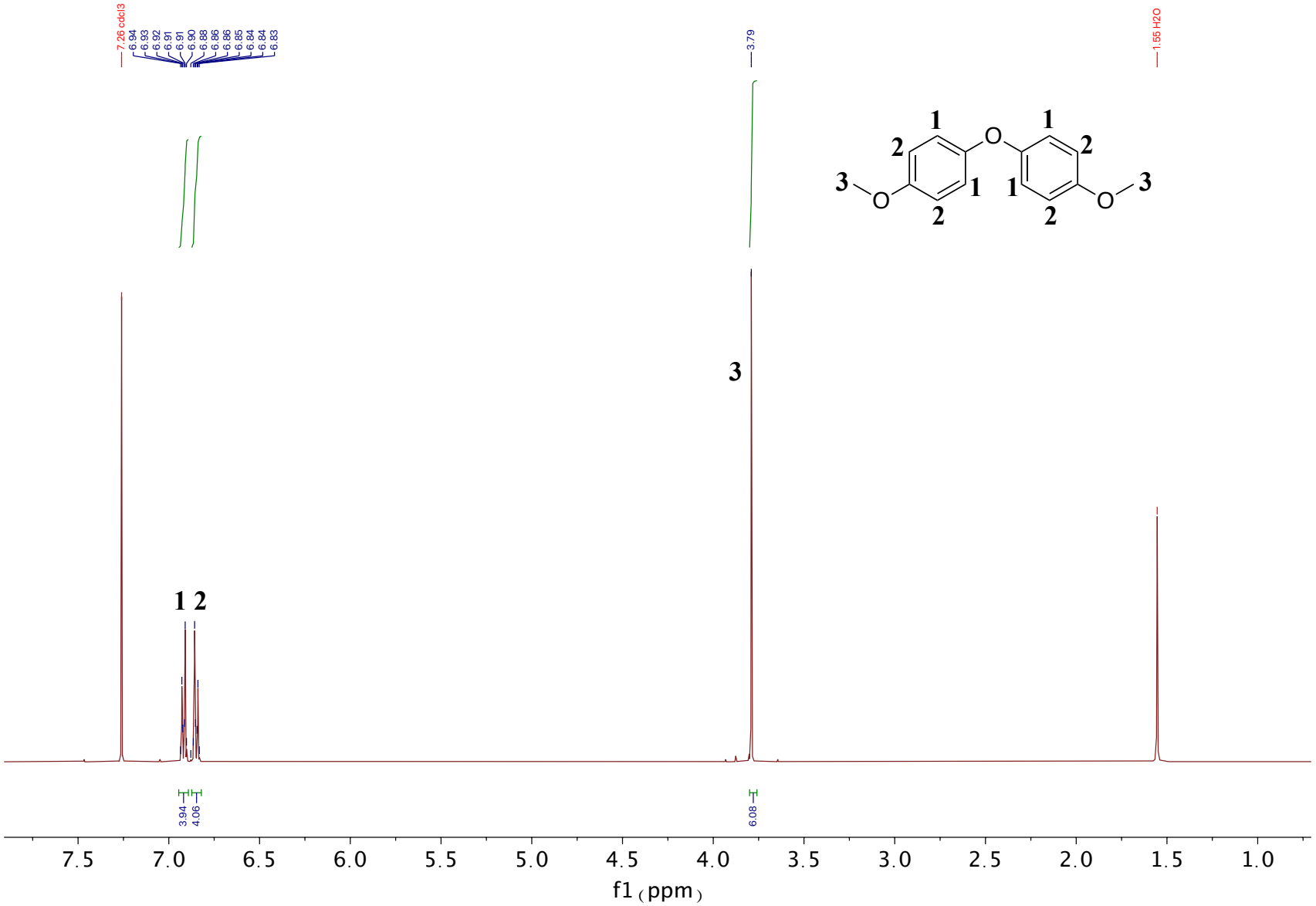

Figure 2.55 ^{1}H NMR of **4,4'-oxybis(methoxybenzene)**

REFERENCES

REFERENCES

1. Hao, P., Electrocatalytic Hydrogenation of Monomeric, Dimeric, and Polymeric Lignin Model Compounds with Raney Nickel: Chemistry, Mechanistic, and Product Toxicity Studies . Michigan State University, East Lansing, MI, 2018.

2. de Castro, I. B. D.; Graca, I.; Rodriguez-Garcia, L.; Kennema, M.; Rinaldi, R.; Meemken, F., Elucidating the reactivity of methoxyphenol positional isomers towards hydrogen-transfer reactions by ATR-IR spectroscopy of the liquid-solid interface of RANEY (R) Ni. *Catalysis Science & Technology* **2018,** *8* (12), 3107-3114.

3. Mauriello, F.; Paone, E.; Pietropaolo, R.; Balu, A. M.; Luque, R., Catalytic Transfer Hydrogenolysis of Lignin-Derived Aromatic Ethers Promoted by Bimetallic Pd/Ni Systems. *ACS Sustainable Chemistry & Engineering* **2018,** *6* (7), 9269-9276.

4. Belot, G.; Desjardins, S.; Lessard, J., Electrocatalytic hydrogenation of organic-compounds on Devarda copper and Raney-nickel electrodes in basic-media. *Tetrahedron Letters* **1984,** *25* (47), 5347-5350.

5. Ma, X. X.; Liu, S. J.; Liu, Y.; Gu, G. D.; Xia, C. H., Comparative study on catalytic hydrodehalogenation of halogenated aromatic compounds over Pd/C and Raney Ni catalysts. *Scientific Reports* **2016,** *6*, 11.

6. Lam, C. H.; Lowe, C. B.; Li, Z. L.; Longe, K. N.; Rayburn, J. T.; Caldwell, M. A.; Houdek, C. E.; Maguire, J. B.; Saffron, C. M.; Miller, D. J.; Jackson, J. E., Electrocatalytic upgrading of model lignin monomers with earth abundant metal electrodes. *Green Chemistry* **2015,** *17* (1), 601-609.

7. Zhou, Y. T.; Klinger, G. E.; Hegg, E. L.; Saffron, C. M.; Jackson, J. E., Multiple Mechanisms Mapped in Aryl Alkyl Ether Cleavage via Aqueous Electrocatalytic Hydrogenation over Skeletal Nickel. *Journal of the American Chemical Society* **2020,** *142* (8), 4037-4050.

8. Kanan, M. W.; Nocera, D. G., In situ formation of an oxygen-evolving catalyst in neutral water containing phosphate and Co2+. *Science* **2008,** *321* (5892), 1072-1075.

9. Galkin, M. V.; Dahlstrand, C.; Samec, J. S. M., Mild and Robust Redox-Neutral Pd/C-Catalyzed Lignol -O-4 Bond Cleavage Through a Low-Energy-Barrier Pathway. *ChemSusChem* **2015,** *8* (13), 2187-2192.

10. Chen, J. Z.; Liu, D. L.; Butt, N.; Li, C.; Fan, D. Y.; Liu, Y. G.; Zhang, W. B., Palladium-Catalyzed Asymmetric Hydrogenation of alpha-Acyloxy-1-arylethanones. *Angewandte Chemie-International Edition* **2013,** *52* (44), 11632-11636.

11. Cao, Y.; Wang, N.; He, X.; Li, H. R.; He, L. N., Photocatalytic Oxidation and Subsequent Hydrogenolysis of Lignin beta-O-4 Models to Aromatics Promoted by In Situ Carbonic Acid. *ACS Sustainable Chemistry & Engineering* **2018,** *6* (11), 15032-15039.

12. Sang, D. Y.; Tian, J.; Tu, X. D.; He, Z. J.; Yao, M., Cleavage of Catechol Monoalkyl Ethers by Aluminum Triiodide-Dimethyl Sulfoxide. *Synthesis-Stuttgart* **2019,** *51* (3), 704-712.

13. Fabbri, C.; Bietti, M.; Lanzalunga, O., Generation and reactivity of ketyl radicals with lignin related structures. On the importance of the ketyl pathway in the photoyellowing of lignin containing pulps and papers. *Journal of Organic Chemistry* **2005,** *70* (7), 2720-2728.

14. Sawatzky, R. S.; Hargreaves, B. K. V.; Stradiotto, M., A Comparative Ancillary Ligand Survey in Palladium-Catalyzed C-O Cross-Coupling of Primary and Secondary Aliphatic Alcohols. *European Journal of Organic Chemistry* **2016,** (14), 2444-2449.

15. Vaxelaire, C.; Souquet, F.; Lannou, M. I.; Ardisson, J.; Royer, J., Anodic Oxidation: An Attractive Alternative to CAN-Mediated Cleavage of para-Methoxyphenyl Ethers. *European Journal of Organic Chemistry* **2009,** (19), 3138-3140.

16. Fleury-Bregeot, N.; Presset, M.; Beaumard, F.; Colornbel, V.; Oehlrich, D.; Rombouts, F.; Molander, G. A., Suzuki-Miyaura Cross-Coupling of Potassium Alkoxyethyltrifluoroborates: Access to Aryl/Heteroarylethyloxy Motifs. *Journal of Organic Chemistry* **2012,** *77* (22), 10399-10408.

17. Vechorkin, O.; Proust, V.; Hu, X. L., Functional Group Tolerant Kumada-Corriu-Tamao Coupling of Nonactivated Alkyl Halides with Aryl and Heteroaryl Nucleophiles: Catalysis by a Nickel Pincer Complex Permits the Coupling of Functionalized Grignard Reagents. *Journal of the American Chemical Society* **2009,** *131* (28), 9756-9766.

18. Enthaler, S.; Spilker, B.; Erre, G.; Junge, K.; Tse, M. K.; Beller, M., Biomimetic transfer hydrogenation of 2-alkoxy- and 2-aryloxyketones with iron-porphyrin catalysts. *Tetrahedron* **2008,** *64* (17), 3867-3876.

19. Shah, S. T. A.; Singh, S.; Guiry, P. J., A Novel, Chemoselective and Efficient Microwave-Assisted Deprotection of Silyl Ethers with Selectfluor. *Journal of Organic Chemistry* **2009,** *74* (5), 2179-2182.

20. Hu, Z. P.; Zhang, S. S.; Zhou, W. C.; Ma, X.; Xiang, G. Y., Synthesis and antibacterial activity of 3-benzylamide derivatives as FtsZ inhibitors. *Bioorganic & Medicinal Chemistry Letters* **2017,** *27* (8), 1854-1858.

21. Wolter, M.; Nordmann, G.; Job, G. E.; Buchwald, S. L., Copper-catalyzed coupling of aryl iodides with aliphatic alcohols. *Organic Letters* **2002,** *4* (6), 973-976.

22. Simon, M. O.; Girard, S. A.; Li, C. J., Catalytic Aerobic Synthesis of Aromatic Ethers from Non-Aromatic Precursors. *Angewandte Chemie-International Edition* **2012,** *51* (30), 7537-7540.

23. Ma, D. W.; Cai, Q., N,N-Dimethyl glycine-promoted Ullmann coupling reaction of phenols and aryl halides. *Organic Letters* **2003,** *5* (21), 3799-3802.
24. Hu, T. J.; Chen, X. R.; Wang, J.; Huang, J., CuO Nanoparticles on Ionic Polymer for Coupling Reactions of Aryl Bromides and Chlorides with Phenols. *ChemCatChem* **2011,** *3* (4), 661-665.

25. Burgos, C. H.; Barder, T. E.; Huang, X. H.; Buchwald, S. L., Significantly improved method for the Pd-catalyzed coupling of phenols with aryl halides: Understanding ligand effects. *Angewandte Chemie-International Edition* **2006,** *45* (26), 4321-4326.

26. Phan, N. T. S.; Nguyen, T. T.; Nguyen, V. T.; Nguyen, K. D., Ligand-Free Copper-Catalyzed Coupling of Phenols with Nitroarenes by using a Metal-Organic Framework as a Robust and Recoverable Catalyst. *ChemCatChem* **2013,** *5* (8), 2374-2381.

27. Zhang, R. Z.; Liu, J. M.; Wang, S. F.; Niu, J. Z.; Xia, C. G.; Sun, W., Magnetic CuFe2O4 Nanoparticles as an Efficient Catalyst for C-O Cross-Coupling of Phenols with Aryl Halides. *ChemCatChem* **2011,** *3* (1), 146-149.

28. Zhang, S. L.; Bie, W. F., Isolation and characterization of copper(III) trifluoromethyl complexes and reactivity studies of aerobic trifluoromethylation of arylboronic acids. *RSC Advances* **2016,** *6* (75), 70902-70906.

29. Zhang, J. L.; Chen, J. X.; Liu, M. C.; Zheng, X. W.; Ding, J. C.; Wu, H. Y., Ligand-free copper-catalyzed coupling of nitroarenes with arylboronic acids. *Green Chemistry* **2012,** *14* (4), 912-916.

30. Furuta, A.; Nishiyama, H., Highly efficient catalytic system for hydrosilylation of ketones with iron(II) acetate-thiophenecarboxylate. *Tetrahedron Letters* **2008,** *49* (1), 110-113.

31. Dingemans, T. J.; Mendes, E.; Hinkley, J. J.; Weiser, E. S.; StClair, T. L., Poly(ether imide)s from diamines with para-, meta-, and ortho-arylene substitutions: Synthesis, characterization, and liquid crystalline properties. *Macromolecules* **2008,** *41* (7), 2474-2483.

32. Gogoi, P.; Bezboruah, P.; Gogoi, J.; Boruah, R. C., ipso-Hydroxylation of Arylboronic Acids and Boronate Esters by Using Sodium Chlorite as an Oxidant in Water. *European Journal of Organic Chemistry* **2013,** *2013* (32), 7291-7294.

33. Ramezani, L.; Yahyazadeh, A.; Sheykhan, M., The First C-Cl Activation in Ullmann C-O Coupling by MOFs. *ChemCatChem* **2018,** *10* (20), 4636-4651.

Chapter 3. Mechanistic Investigation of Aryl Alkyl Ether Cleavage via Aqueous Electrocatalytic Hydrogenation (ECH) over Skeletal Nickel*

This chapter presents a mechanistic analysis of electrocatalytic hydrogenolysis (ECH) of lignin-relevant aryl ethers over Raney® nickel electrodes in water at 60 °C. Direct analysis of such heterogeneous catalyzed systems is challenging due to the multiphase reaction environment, non-uniform metal surfaces, and roles of medium and electrochemical variables. Nonetheless, guiding principles are needed to understand, control, and ultimately design practical catalytic processes for biomass cleavage and upgrading. This work's insights come from product, rate, competition, and isotopic labeling studies of a broad range of aryl alkyl ether substrates undergoing electrocatalytic hydrogenation/hydrogenolysis (ECH).

3.1 Introduction

Due to the limited supply of renewable carbon; to address climate change and the need for sustainable liquid fuels, efficient carbon utilization is key (Figure 3.1).[1] Lignin, at 60-65 wt%, the most carbon rich biomass fraction, accounts for 15-30 wt% of total biomass.[2, 3] Despite its high carbon and energy content, this resource is underutilized due to its complexity and reactivity. On the other hand, lignin's varied methoxyphenolic subunits and crosslinking modes make it a natural source of small building blocks for chemicals and fuels.[4-9]

In recent decades, various strategies for lignin depolymerization have been explored. Classical lignin removal from biomass (usually to isolate cellulose for paper-making) entails treatment with strong bases, acids, and/or oxidants, harsh conditions that create new crosslinking.

*This chapter is adapted from Zhou, Y. T.; Klinger, G. E.; Hegg, E. L.; Saffron, C. M.; Jackson, J. E., Multiple Mechanisms Mapped in Aryl Alkyl Ether Cleavage via Aqueous Electrocatalytic Hydrogenation (ECH) over Skeletal Nickel. *J. Am. Chem. Soc.* **2020,** *142*, 4037-4050.

Newer efforts have targeted protecting schemes[10-12] and milder oxidative and reductive cleavage strategies[13-18] to avoid such condensation. A particular focus has been cleavage of the so-called β-O-4 alkyl aryl ether (orange in Figure 3.1), the most common of the various linkages in the lignin polymer. Studies of model lignin linkages have uncovered mild β-O-4 ether cleavage processes using reactive homogeneous metal complexes in organic solvents.[19-21] However, such molecular catalysts can be sensitive to air and water, components unavoidable in biomass processing.

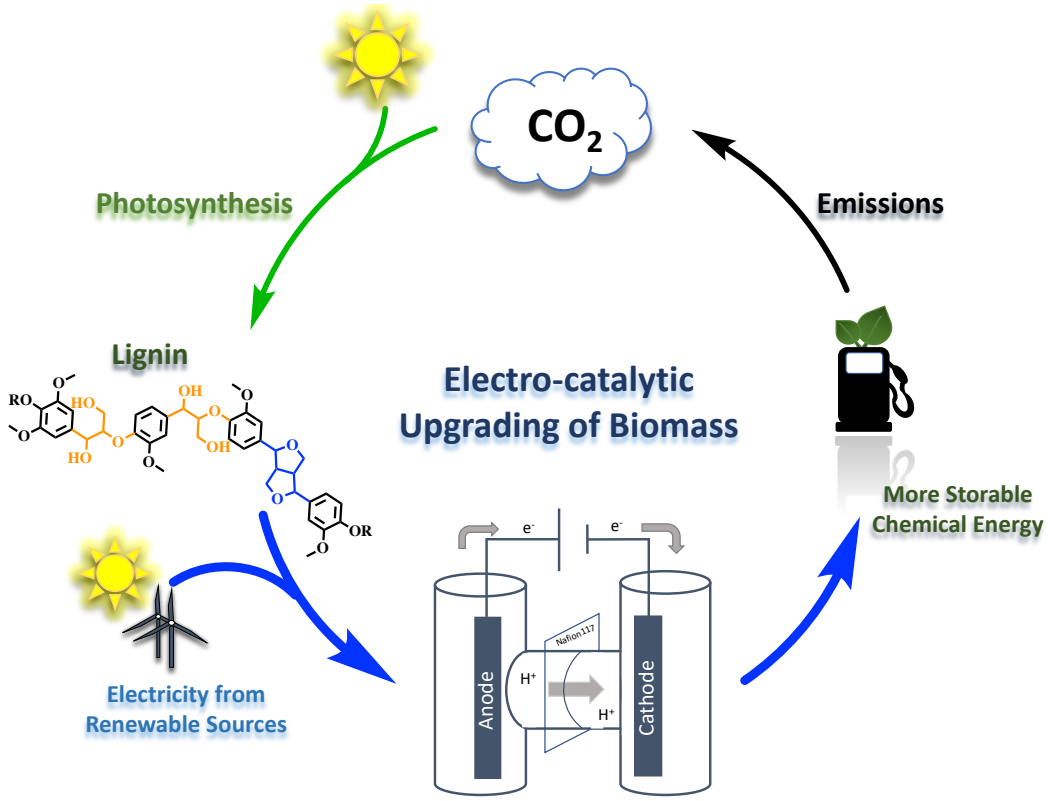

Figure 3.1 Cycle of carbon and energy

Heterogeneous catalytic methods have also been developed to depolymerize models and even real lignin under aqueous conditions. Most of these "green" reactions require hydrogen gas, itself a fossil-derived resource in today's economy. For instance, Lercher and co-workers reported

mild (120 °C) aqueous phase hydrogenolysis of model aryl ethers over a SiO_2 supported nickel catalyst, but 6 bar of H_2 was required to provide H atoms on the catalyst surface.[22] Dyson's group then found that bimetallic Ni and noble metal nanoparticles enabled such cleavages under milder aqueous conditions (95 °C, 1 atm H_2).[23] These valuable studies offered some mechanistic insights, highlighting Ni as the key C-O ether cleavage catalyst, with the noble metals effecting aryl ring saturation.

Building on our own previous studies explored the effects of methoxy substituent position[24] and para-alkyl chain length[37] on guaiacyl type ether C-O cleavage via ECH (Figure 3.2a). Both studies probed the effects of substituent steric bulk on alkyl aryl ether bond hydrogenolysis over skeletal Ni cathodes. The term "skeletal Ni" (or Raney® Ni) reflects the surface topology of the reactive Ni formed by etching the aluminum out of NiAl alloy with strong base. Figure 3.2b shows an electron micrograph of a skeletal Ni electrode, revealing both its roughness and its polycrystalline character.

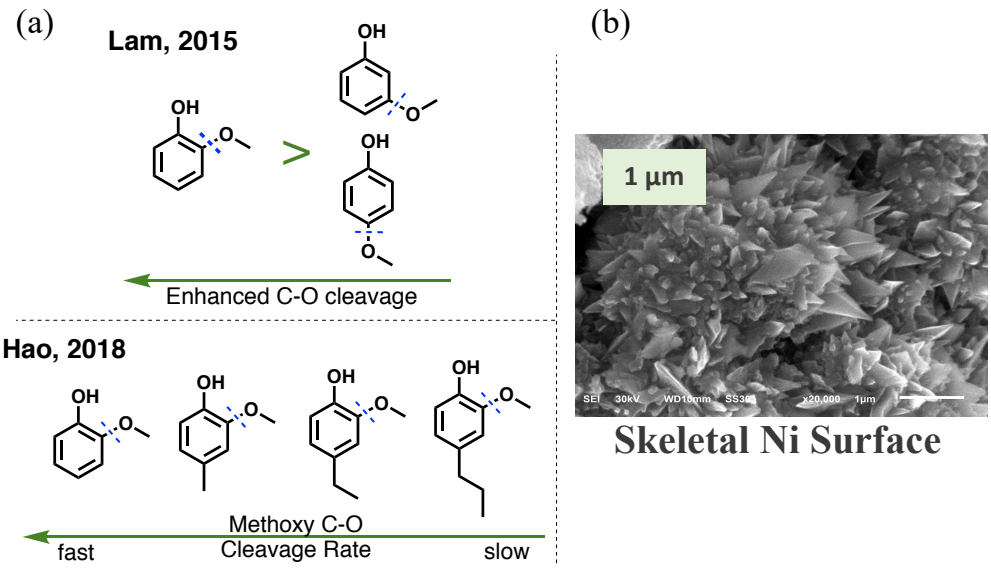

Figure 3.2 (a) Methoxy position and para-alkyl length effects on guaiacyl ether cleavage. (b) SEM image of skeletal Ni.

Beyond the above monomer studies, our skeletal Ni electrodes have shown promise in ECH of actual lignin. As assessed by 2D HSQC NMR and GPC analyses, ECH had little effect on unmodified Cu-AHP[38] lignin (Figure 3.3a), but after DDQ treatment, which oxidized the lignin polymer's benzylic alcohol sites to ketones, ECH cleavage significantly increased (Figure 3.3b).[25] Other groups have also noted that the presence of the α ketone accelerates the breakdown of the β-O-4 ether linkage,[13-15] and the model studies (Figure 3.3c) described herein find similar reactivity patterns, which we rationalize below.

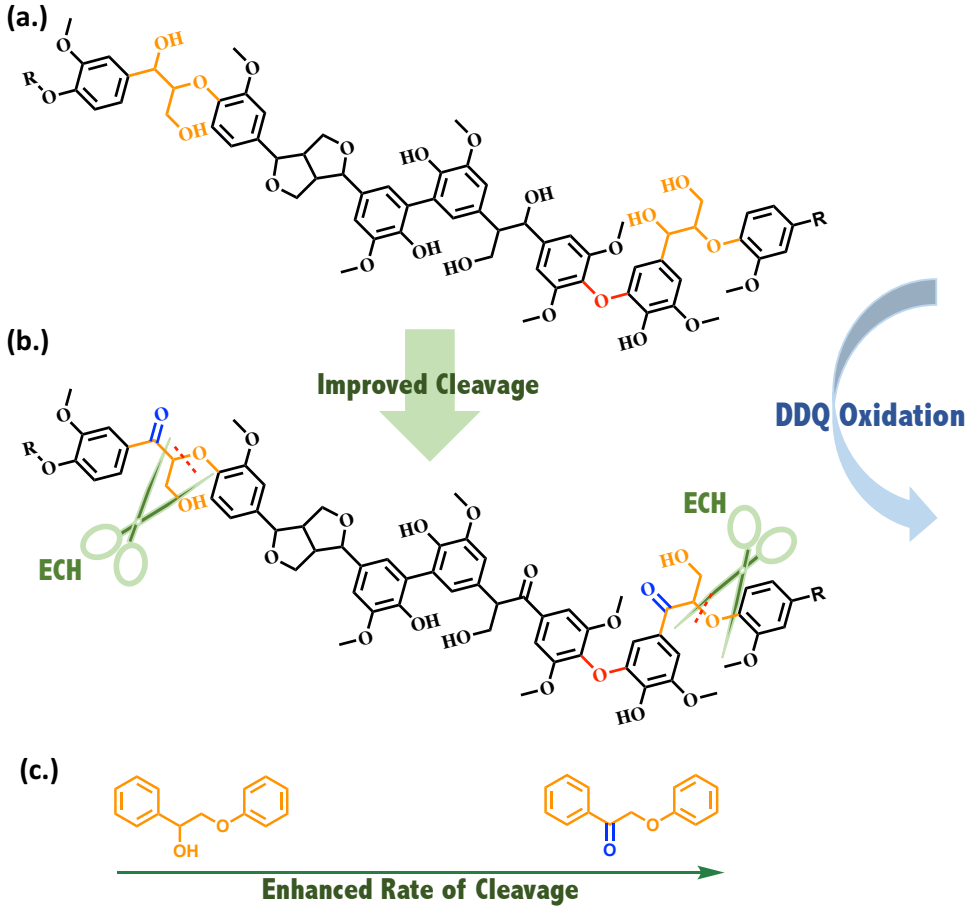

Figure 3.3 (a) Structure of a hypothetical lignin fragment, with β-O-4 linkages highlighted in orange; (b) structure of the DDQ oxidized analogue of the species in (a), which undergoes faster and more complete depolymerization via ECH; (c) small molecule models of the above β-O-4 linkages.

Again, heterogeneous metal catalysis in biomass upgrading has been criticized for its lack of control in product selectivity.[13, 17, 19] High selectivity can be directly connected to the efficiency and sustainability of chemical production. The low temperature electro-catalyzed hydrogenation (ECH) method discussed in this work efficiently breaks down both sp^3 C-O and sp^2 C-O bonds of a wide range of aryl alkyl ethers under ambient pressure at 60 °C in aqueous media. Detailed kinetic and competition analyses, augmented by deuterium labeling studies, have revealed a hierarchy of C-O cleavage rates of different functionalized aryl ethers by the solid Ni cathode. Importantly, a fast mechanism, distinct from that for the unoxidized β-O-4 ether linkage, has emerged for cleavage of α ketone ethers. Such molecular understanding offers rational guidance for the design of selective heterogeneous catalytic processes.

3.2 Cleavage Pathway of 2-Phenoxyacetophenone (Ketone Linkage)

*3.2.1 Two Possible C-O Cleavage Paths of Ketone **1***

Upon ECH treatment, 2-phenoxyacetophenone **1** was cleaved at the sp^3 hybridized β C-O ether bond. Two potential pathways (Figure 3.4) were considered for this process: (a) direct C-O cleavage of **1** to release phenol and acetophenone; or (b) initial reduction of the ketone to alcohol **2** which is then cleaved into 1-phenylethanol and phenol. Further reduction leads to the hydrogenation and deoxygenation products cyclohexanol, 1-cyclohexylethanol, and ethylbenzene as end products.

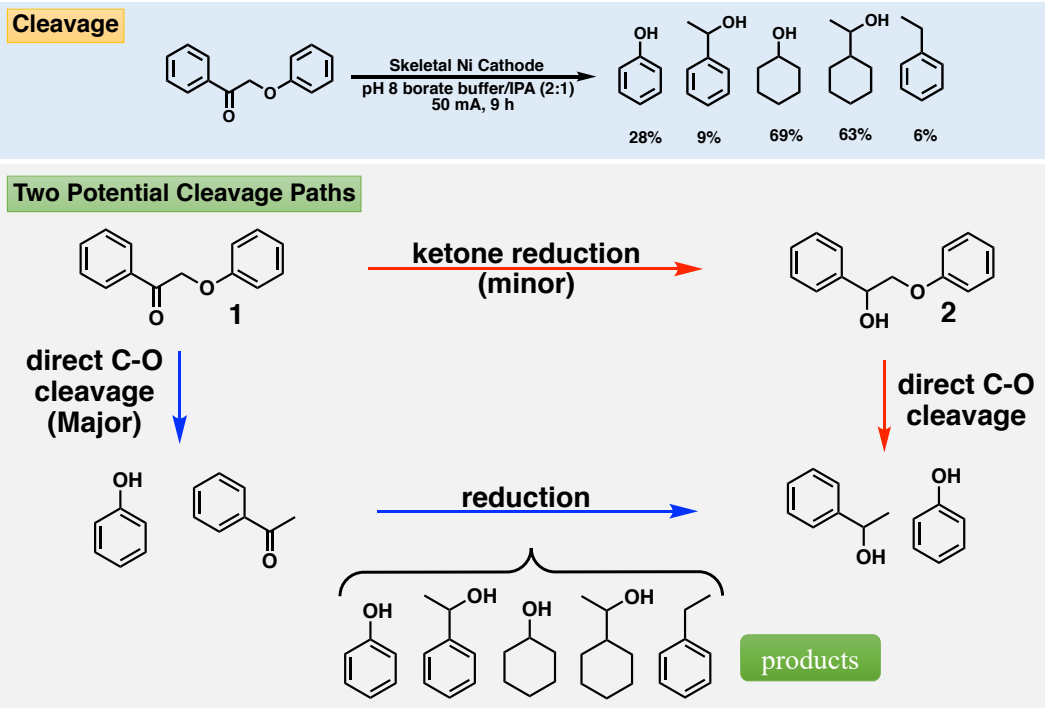

Figure 3.4 Major and minor cleavage paths of ketone **1**

*3.2.2 Direct C-O Cleavage of Ketone **1** Without Interconversion to **2** is the Major Pathway*

ECH of the ketone dimer **1** at 50 mA (Figure 3.5a), yielded acetophenone, the key intermediate that differentiates the two paths, but only in a small amount. However, no alcohol dimer **2** was seen in this fast cleavage condition. Slower reduction, run at 5 mA (Figure 3.5c) with discharged catalyst, showed substantial acetophenone buildup, pointing to direct cleavage (blue path in Figure 3.4). Discharged catalyst was used to enable the observation of reaction solely due to passage of charge (for details, see chapter 2 catalytic methodology). The small amounts of alcohol **2** formed (red path) did not break down until most of ketone **1** was cleaved and acetophenone was reduced (Figure 3.5c). This behavior is consistent with the finding (Figures 3.5

b and d) that the β-O-4 alcohol **2** is cleaved roughly half as fast as the ketone **1**, and the two do not significantly interconvert.

Kinetic Rate Comparisons between Ketone 1 and Alcohol 2

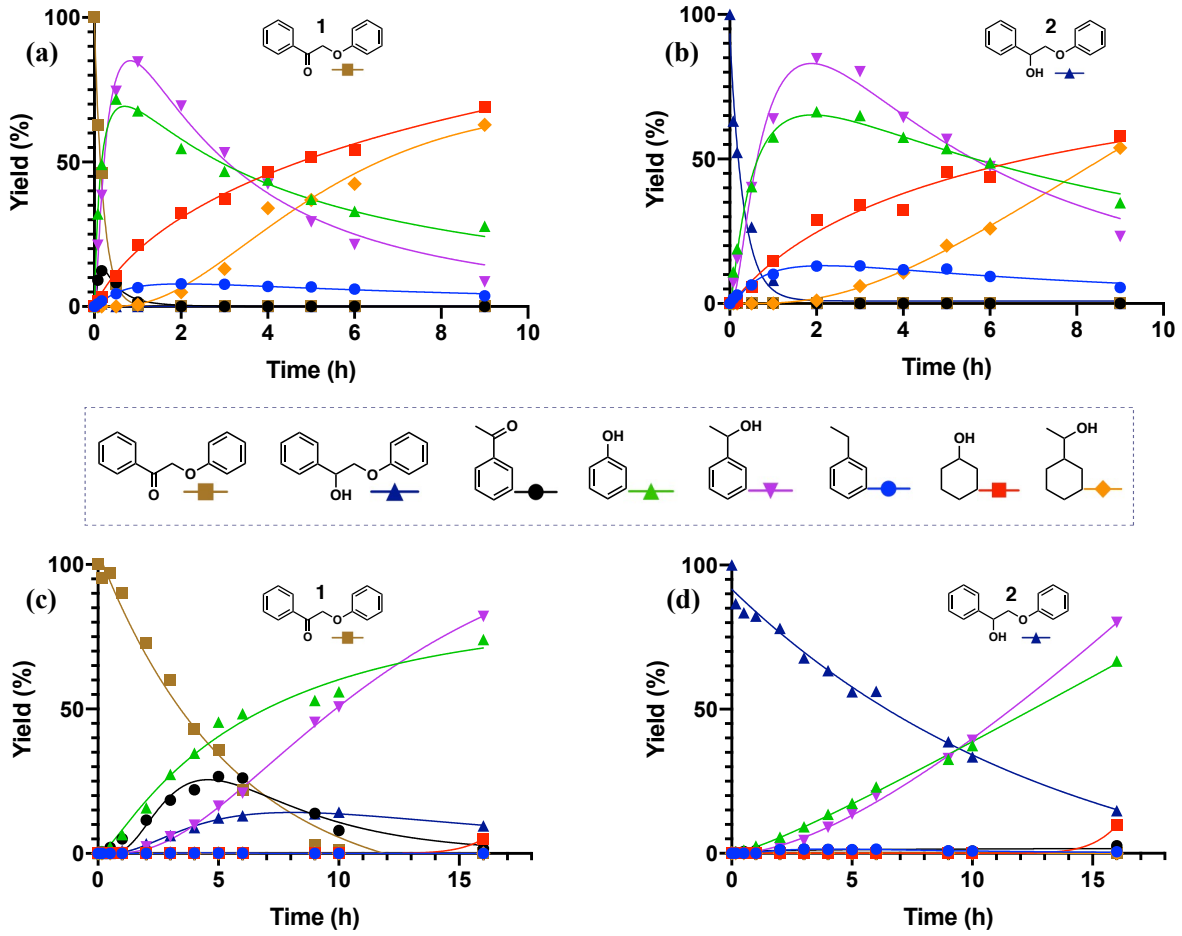

Figure 3.5 ECH of ketone **1**: (a) with active catalyst (IPA treated electrode) at 50 mA (8 mA/cm^2); (c) discharged catalyst (acetone treated electrode) at 5 mA (0.8 mA/cm^2). ECH of alcohol **2**: (b) active catalyst at 50 mA; (d) discharged catalyst at 5 mA (for details, see chapter 2 of ECH methodology). All end points were analyzed in triplicate with resulting uncertainties of < ±5%.

Direct cleavage and the ketone's accelerating effect were further confirmed by competition studies in 1:1 mixtures of ketone and alcohol β-O-4 models, with the phenolic leaving groups differentiated by methylation (Figures 3.6 a and b). Both pairings of methyl-labeled/unlabeled

phenol fragments in alcohol/ketone substrates were examined (i.e., **1**/**4** and **2**/**3**), as alkyl groups on the para positions of guaiacols are known to substantially inhibit aryl methyl ether cleavage (Figure 3.2a). In both competitions, the ketone cleavage products were released faster than those from the alcohol. In these studies, the methyl labels had little effect on the phenols' leaving group abilities. However, the liberated *p*-cresol products did undergo ring saturation more slowly than the unsubstituted phenol, as highlighted in Figure 3.6.

Direct Competitions between Ketone 1 and Alcohol 2

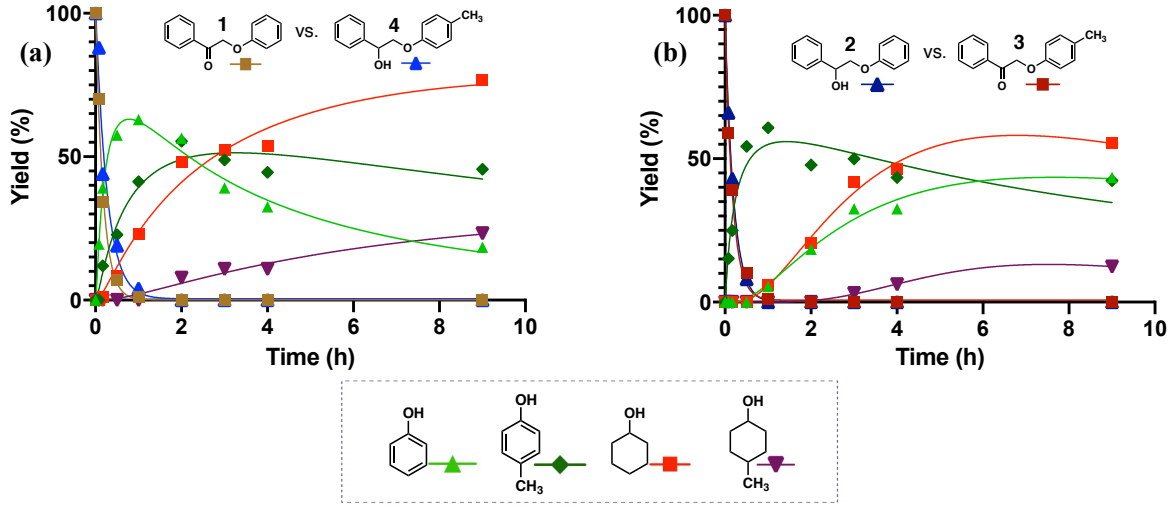

Figure 3.6 Direct competitions of ketone and alcohol models: (a) methyl labeled alcohol **4** vs. ketone **1** at 50 mA (b) alcohol **2** vs. methyl labeled ketone **3** at 50 mA. All end points were analyzed in triplicate with resulting uncertainties of < ±5%.

The findings that ketone **1** and alcohol **2** undergo direct ether cleavage without interconversion (Figure 3.4), and that the ketone is much faster, explain the faster depolymerization seen in DDQ oxidized Cu-AHP lignin, which is activated by the presence of the α carbonyl. The above results make two further mechanistically significant points: (a) The selectivity of ECH for ether cleavage in the ketone is a surprising contrast to the behavior of more conventional reducing agents such as $NaBH_4$, which quickly reduce ketones, including **1**, leaving

ethers untouched; and (b) though para alkyl group substitution strongly perturbs phenol saturation to the corresponding cyclohexanols, this apparent steric influence is barely felt in the phenoxide leaving group in the above ether cleavages, suggesting that their interactions with the surface are qualitatively different from those involved in aromatic monomer hydrogenations.[37, 26]

The above contrasts highlight the mechanistic diversity of aryl alkyl ether cleavages, with rates and site selectivities strongly affected by seemingly simple variations in functionality. Here, we step back and review what is already known about substituent effects on skeletal Ni electrode-catalyzed aryl ether breakdown.

3.3 Mapping the Cleavage Mechanism of Functionalized Alkyl Aryl Ethers

3.3.1 Cleavage Paradox of Constitutionally Similar Aryl Ethers.

Our previously reported ECH studies of guaiacyl type aryl ethers found more efficient methoxy group cleavage from ortho-hydroxyanisole **5** (guaiacol) than from its meta and para isomers. The easier ether cleavage in guaiacol was tentatively attributed to the intramolecular H-bonding between the hydroxyl and the neighboring methoxy group.[24]

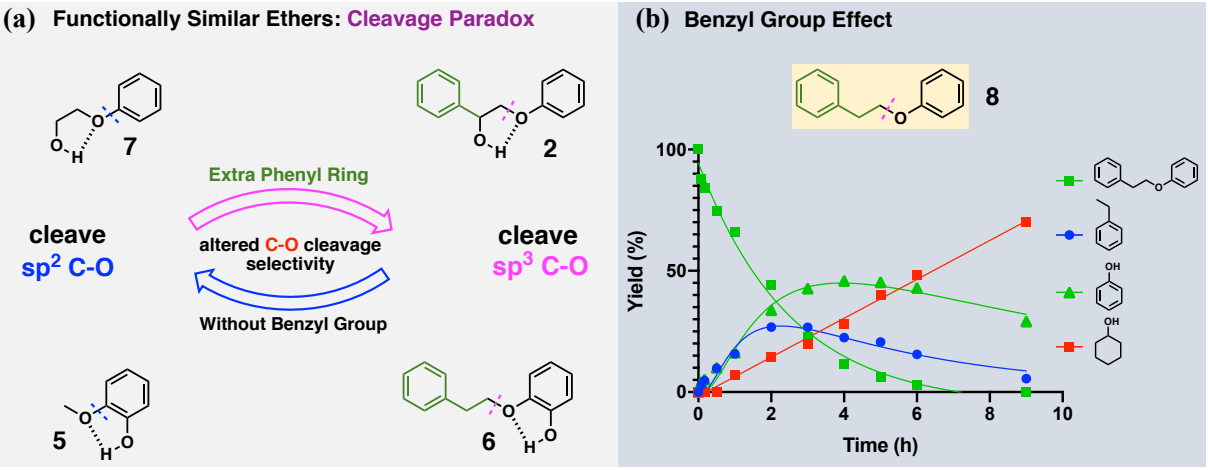

Figure 3.7 (a) Constitutionally similar aryl ethers give opposite (sp^2 vs. sp^3) C-O cleavage (b) predicted cleavage result of **8**

As in guaiacol **5**, the ether bond in alcohol **2** is also capable of intramolecular H-bonding; surprisingly, however, it breaks at the sp^3 C-O bond instead of the aryl C-O bond (Figure 3.5). Considering that the H-bonding from the vicinal hydroxyl is not exactly the same as from a phenolic hydroxyl, we synthesized and tested the 2-(2-phenylethoxy)phenol **6**, an aryl ether with the hydroxyl group ortho to the ether bond (for full kinetics, see Figure 3.42). As shown in Figure 3.7a, this guaiacol-like aryl ether, with intramolecular H-bonding like that in **5**, still underwent the opposite C-O bond cleavage; **5** was cleaved at the sp^2 C-O bond, but **6** was cleaved at the sp^3 C-O bond. Similarly, contrasting behaviors were seen between aryl ethers **2** and **7** in Figure 3.7a, which differ by only one phenyl ring. Again, the C-O cleavage selectivity was completely switched (for kinetics, see Figure 3.41). Evidently, the sp^3 C-O bond cleavage is activated by the extra benzene ring on the benzyl side. These results call for a study of the simplest model: 2-phenoxy-1-phenylethane **8** (Figure 3.7b); if benzylic activation controls the outcome, sp^3 C-O cleavage is predicted.

Impact on Cleavage Rate of Different Functionality on the α Site

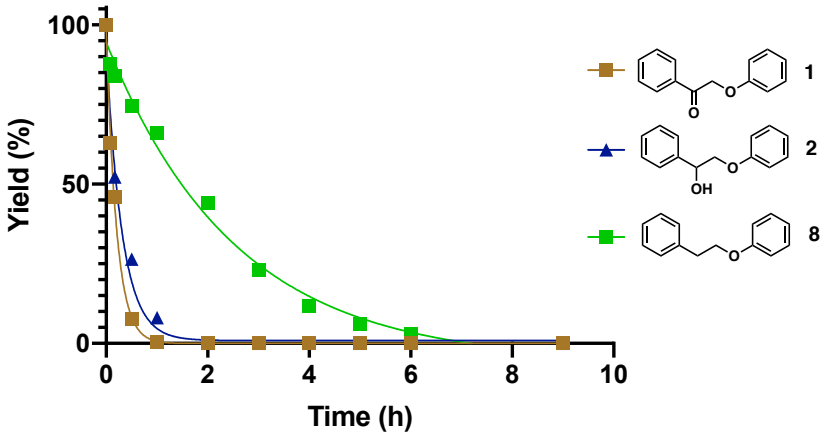

Figure 3.8 Kinetic ECH at 60 °C and 50 mA for α functionalized β-O-4 model compounds.

ECH of **8** was conducted as shown in Figure 3.7b, it was cleaved at the sp^3 C-O bond completely in 6 hours, generating ethylbenzene and phenol. Thus, the sp^3 C-O (beta C-O) bond cleavage is activated by the phenyl ring of 2-phenoxy-1-phenylethane ethers, independent of other functionalities on the ethyl moiety. This result is striking. Notably, neither anisole (methoxybenzene) nor ethoxybenzene undergo any significant cleavage under these conditions. In considering the cleavage of **8**, it is tempting to envision the phenoxy ring interacting more strongly with the catalytic surface, as it is directly attached to the bond being cleaved. Previous reports have interpreted cleavage results this way.[22] However, as shown in Figure 3.8, this β sp^3 C-O bond cleavage selectivity is mainly activated by the less electron rich benzylic ring, with the rate somewhat influenced by α substituents.

3.3.2 H/D Exchange of Different β-O-4 Models over Skeletal Nickel

To understand not only the above activation of β C-O cleavage by the benzylic ring, but also its rate modulation by α substituents, we probed interactions between these β-O-4 aryl ethers and the skeletal nickel surface via isotope exchange experiments with D_2O in the ECH cells. Since the input of electricity speeds up the breakdown of the ether dimers, H/D exchange experiments were conducted without current, to slow the cleavage of the dimers and reveal initial catalyst interactions. These results are summarized in Figure 3.9.

As shown in Figure 3.9a, H/D exchanges occurred at the α C-H of the unsubstituted β-O-4 model **8** (for spectra analyses, see Figures 3.34-3.37), supporting the hypothesis that the presence of the benzyl moiety activates the β C-O cleavage (Figure 3.7). The mono- and dideuterated substrates grew in at similar rates rather than sequentially, suggesting that once the aryl ether substrate was adsorbed onto the catalytic active site, incorporation of one or both deuteriums occurs rapidly before release. Substrate adsorption and release are likely rate limiting since, at 60°

C, only ~20% of **8** had undergone exchange in 9 hours. Alcohol **2** (Figure 3.9b) showed results similar to those of **8** (for spectra analyses, see Figures 3.27-3.32), with ~55% isotope exchange occurring at the benzylic α C-H over 9 hours. Notably, no β C-H exchange was seen in either case, confirming that alcohol **2** does not interconvert with ketone **1**.

H/D Isotope Exchange of Different β-O-4 Dimer Models over Skeletal Nickel Surface

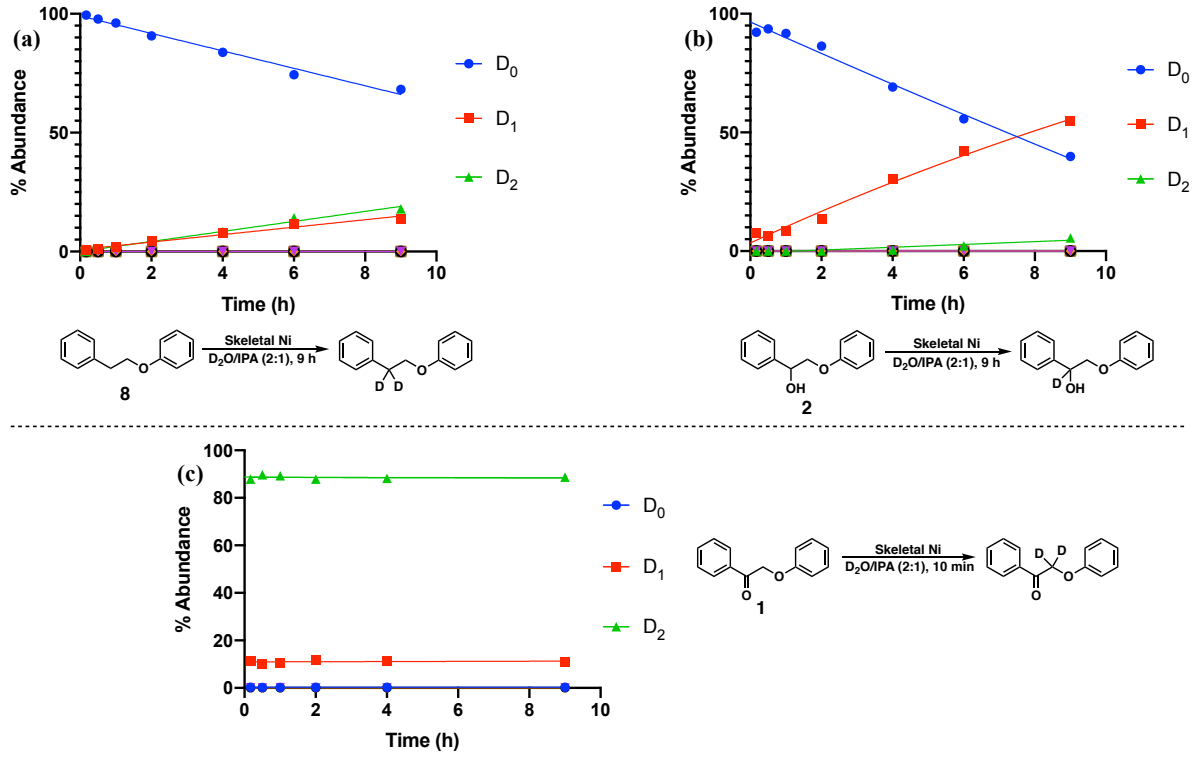

Figure 3.9 H/D isotope exchange on skeletal nickel electrode surface at 60 °C of three substrates: (a) 2-phenoxy-1-phenylethane **8**; (b) 2-phenoxy-1-phenylethanol **2** (workup included a H_2O wash to ensure that only carbon-labeled sites were counted: for the unwashed figure see Figure 3.26); (c) 2-phenoxyacetophenone **1**. D_n (n = 0~2) represent numbers of deuterium atoms incorporated.

*3.3.3 Proposed C-O Cleavage Mechanisms of the Different β-O-4 Linkages in **2** and **8***

The above labeling results suggest that the C-O cleavages of 2-phenoxy-1-phenylethane **8** and 2-phenoxy-1-phenylethanol **2** occur via similar α C-H activation mechanisms. Two paths may be envisioned, as shown in Figure 3.10 a-b. In path A, Ni coordinates at the aromatic ring of the benzyl side and then inserts into a benzylic (α) C-H bond, giving a Ni benzyl complex. Notably, the α site's H/D exchange is faster in alcohol **2** than in **8**, perhaps due to stabilization of the benzyl Ni complex by the benzylic hydroxyl. After activation of the α C-H sites, depending on the conditions, either α H/D exchange or β C-O cleavage may occur (Figure 3.10a). Without current input and in D_2O, return of a Ni surface deuterium to the benzylic position re-aromatizes the ring, weakening its adsorption and enabling release of the deuterated species **2** or **8**. With current applied, the Ni surface donates electrons to effect β elimination of the phenoxide leaving group, giving the corresponding phenol. The styrenic elimination products then undergo rapid saturation of the sidechain to form ethylbenzene and the ring saturated end product cyclohexylethanol.

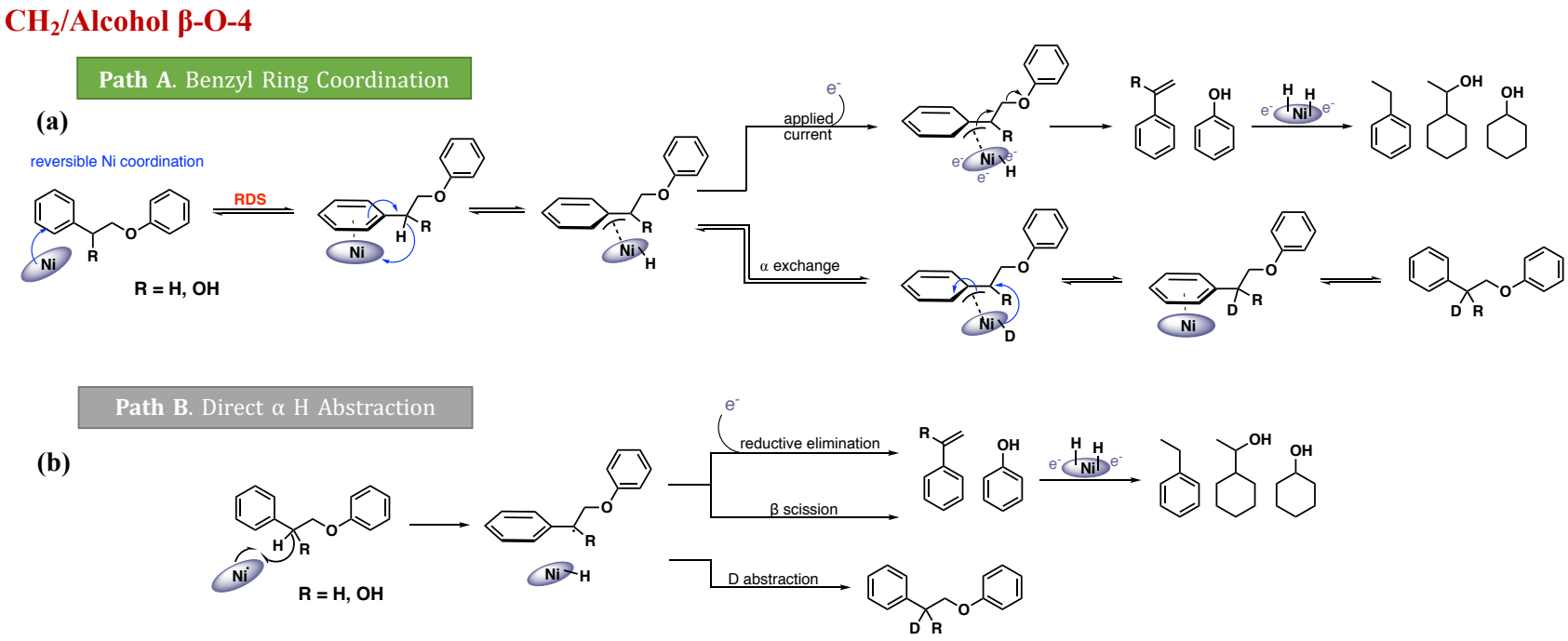

Figure 3.10 Proposed C-O cleavage mechanisms of the parent and alcohol β-O-4 ethers (a) C-H activation via phenyl ring coordination (b) direct H abstraction via Ni radical.

A possible alternative α C-H activation mechanism, is shown as path B (Figure 3.10 b). Here, the benzylic site is activated by direct α H abstraction without coordination to the phenyl benzene ring. The benzylic radical from **2** or **8** can then either be electrochemically reduced to an anion which readily eliminates the leaving group, or can undergo β radical scission to release the aromatic monomers directly. The corresponding H/D exchange mechanisms are also shown in Figure 3.10 b. Different from path A, the direct H abstraction in path B is likely irreversible. Importantly, path B is incompatible with the essentially equal rates of mono- and di-deuteration of **8**. Radical abstraction of diffusible species would be expected to form di-deuterated forms via sequential rather parallel processes. As will be seen below, substituent studies further support path A over the radical abstraction path B.

*3.3.4 C-O Cleavage in Ketone Dimer **1**: A New Fast Mechanism*

To our surprise, the H/D exchange results for the ketone β-O-4 model **1** were completely different from those for **2** and **8**, as shown in Figure 3.9 c. Within 10 minutes both of the β C-H hydrogens on the ketone were exchanged, a rate roughly 100x faster than the benzylic H/D exchange seen in alcohol **2**. The catalyst is essential; H/D exchange via simple base-catalyzed keto-enol tautomerization is at least two orders of magnitude slower at the same pH but without the catalyst (for spectra analyses, see Figures 3.22-3.25). This remarkable acceleration of the isotope exchange is reminiscent of the high ether cleavage reactivity of ketone **1** as seen in the ECH cleavage kinetics (Figure 3.5). The surface-bound ketone is completely different from the H/D exchange intermediate in alcohol **2**, which shows no hydrogen exchange at the β-position, as noted above.

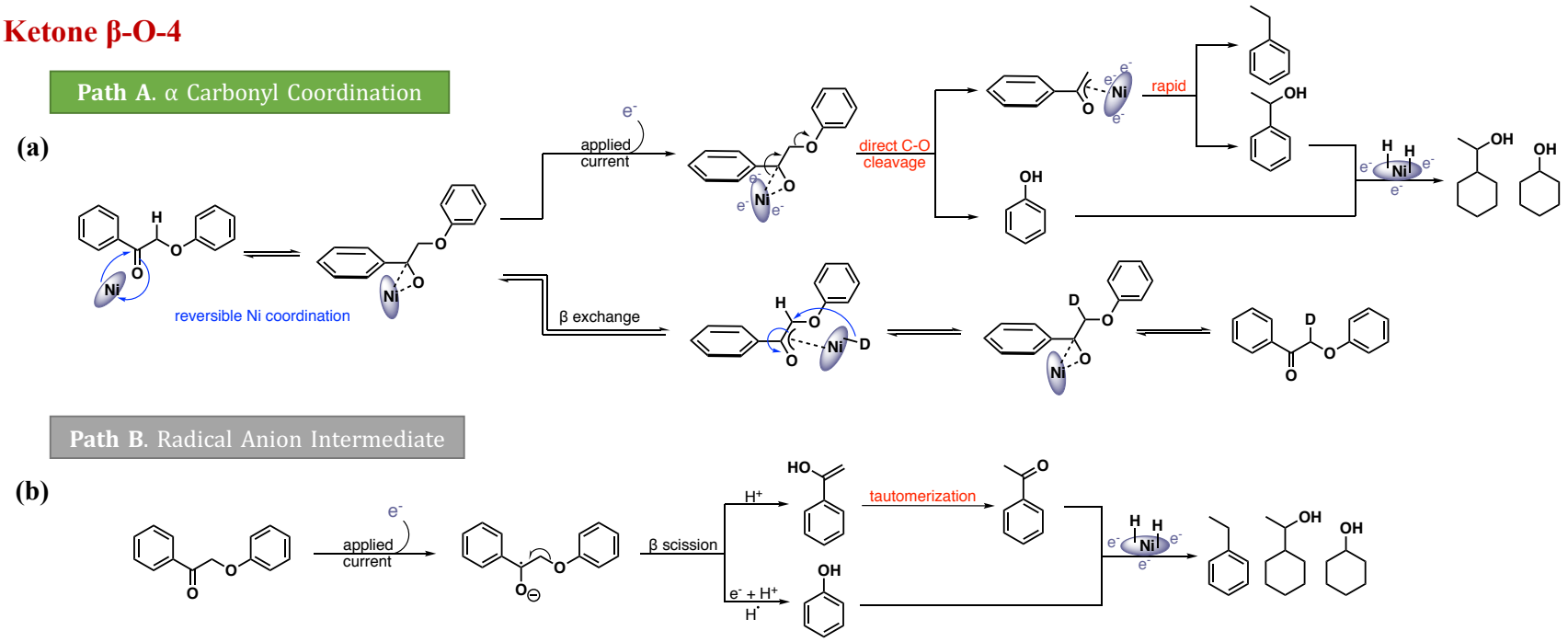

Figure 3.11 Proposed C-O cleavage mechanisms of ketone β-O-4 ether (a) carbonyl coordination (b) electron transfer fragmentation.

Two potential C-O cleavage mechanisms of **1** were also proposed (paths A and B) in Figures 3.11 c-d. Ketone **1** may activate the ether C-O bond directly via Ni coordination to the α carbonyl (Figure 3.11 c). When current is flowing, this carbonyl coordination is followed by phenoxide elimination to give an enol- or enolate-Ni complex and phenol. Consistent with the rapid H/D exchange, the surface bound enol-Ni complex is likely favorable. It could either be immediately reduced to the downstream products or desorb and tautomerize to acetophenone, as seen in the ECH plots in Figures 3.5.

A second possible mechanism (path B) is electron transfer to the ketone to form the radical anion. Such processes are well known in the electrochemical literature, based on electrodes made of non-catalytic materials such as mercury, lead, or carbon.[27, 28] Here, ketone **1** would first gain an electron from the electrode to become a radical anion (Figure 3.11b), and then undergo β scission to the aryl enol anion and phenoxy radical. The enol would tautomerize into acetophenone, and the phenoxy radical would receive another electron and a proton from the solvent, or couple with a surface hydrogen atom to become phenol. Both arenes would then be further reduced to the end products (Figure 3.11b). Based on the direct involvement of catalyst in the rapid H/D exchange (without applied current), and as will be further developed in the substituent and noncatalytic electrode studies below, the carbonyl coordination mechanism Path A (Figure 3.11a) is identified as the more plausible cleavage mechanism for the breakdown of the ketone β-O-4 linkage.

3.4 Testing the Cleavage Hypotheses with Modified β-O-4 Models

3.4.1 β-O-4 Models with Blocked α and β C-H Sites

To test the proposed mechanisms of the CH_2/alcohol β-O-4 ether cleavage, first the role of the α C-H was examined. Paths A and B both begin with α C-H activation (Figure 3.10a-b), leading to β C-O cleavage. Thus, a β-O-4 ether **9** without α C-H sites should not undergo cleavage (Figure 3.12). On the other hand, the proposed cleavage mechanisms (Figure 3.11a-b) of the ketone **1** do not involve activation of β C-H sites. Thus, β-O-4 ether **10** without β hydrogens should still undergo cleavage. Both special β-O-4 models (**9** and **10**) were synthesized and tested under standard ECH conditions (Figure 3.13).

Figure 3.12 β-O-4 models without α and β C-H

As predicted, once the α site is no longer accessible, the cleavage of the β C-O is completely inhibited (Figure 3.13a). Even at high current (50 mA), only ~2% of the cleavage product was detected after 9 hours. We can conclude that α C-H activation is required for 2-phenoxy-1-phenylethane type ether C-O cleavage in species **2** and **8**. In contrast, the β-O-4 ketone **10**, which lacks β C-H sites (Figure 3.13b), was cleaved completely at the β C-O bond within 4 hours. These results support the mechanism in Figures 3.10-3.11, where the electron rich Ni cathode must coordinate at the α carbon to achieve the β C-O breakdown.

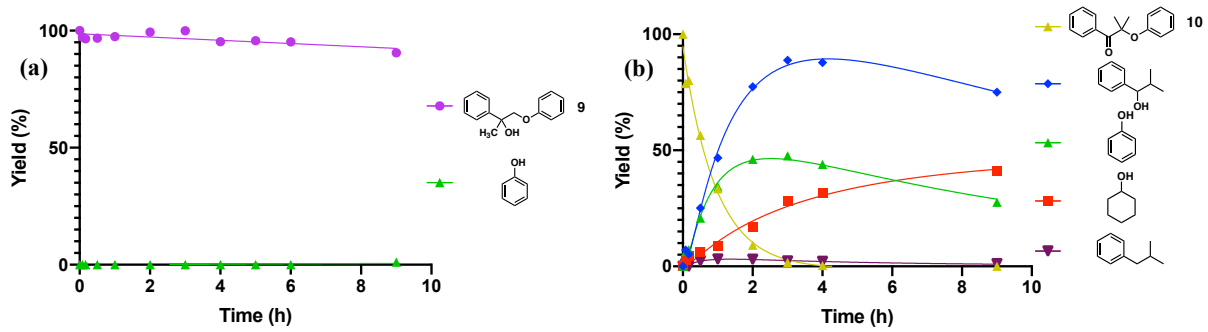

Figure 3.13 Kinetic ECH at 60 °C, and 50 mA for (a) a model without α C-H sites and (b) a model without β C-H sites. For the latter, a trace amount of 1-cyclohexyl-2-methylpropanone was also detected.

3.5 Substituent Effects

3.5.1 Confirmation of Cleavage Path A for CH_2/Alcohol β-O-4 Models

To gain further insight into the C-H_α activation mechanism (A or B) for the CH_2/alcohol β-O-4 ethers **8** and **2**, substituent studies were conducted. Path A (Figure 3.10a) suggested rate limiting Ni coordination to the benzyl moiety's phenyl ring prior to benzylic C-H insertion; therefore, varying substituents on this ring should severely impede binding and therefore slow the cleavage rate (Figure 3.14). On the other hand, formation of the radical intermediate in path B (Figure 3.10b) would not be strongly affected by substituents on the phenyl ring, whether sterically demanding (methyl) or electron donating (methoxy). If anything, these substituents should

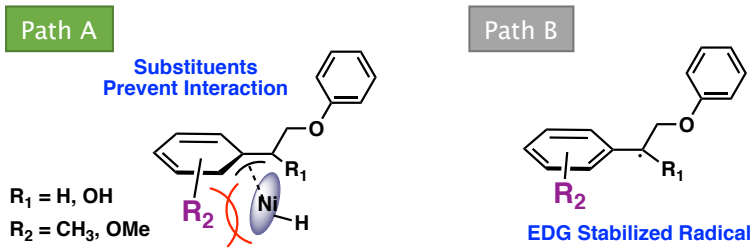

Figure 3.14 Cleavage intermediates of paths A and B for CH_2/alcohol models

stabilize the radical, enhancing the cleavage rate (Figure 3.14). For either path, substituents on the leaving phenol ring are not expected to significantly affect cleavage rates.

As shown in Figure 3.15b, all substituents on the benzylic phenyl ring slow or even stop the ether's C-O cleavage. Somewhat surprisingly, even in the para position, the sterically small methyl group significantly impedes the C-O cleavage of the aryl ether as shown by **11**. The methyl in the ortho position in **12**, directly adjacent to the α carbon undergoing activation, interferes even more effectively. Importantly, in **13** and **14** the sterically smaller but more potent electron donating methoxy substituents in these two positions inhibit even more strongly, essentially stopping the reaction altogether. This enormous slowdown rules out Path B, where, as noted above, the

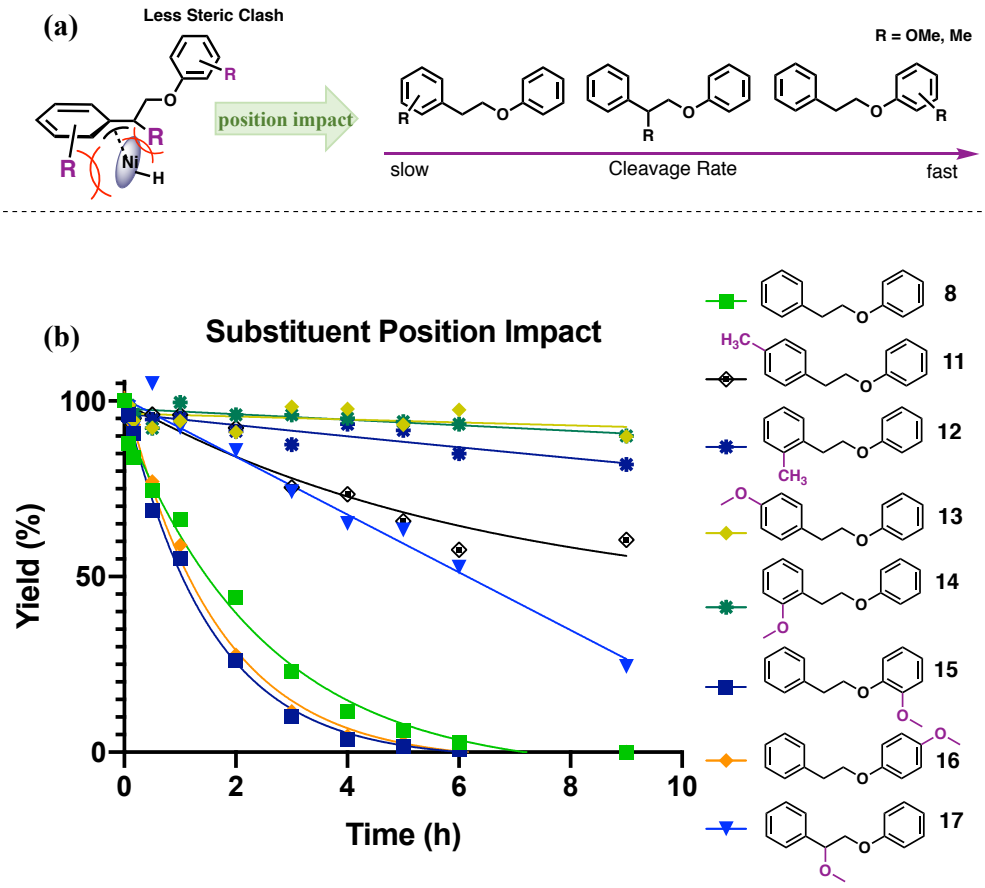

Figure 3.15 (a) Impact of Steric/EDG in different positions. (b) rates of ether cleavage for different methoxy/methyl substituted 2-phenoxy-1-phenylethanes under standard ECH condition.

substituents would be expected to decrease the barrier. Instead, we interpret these effects as inhibition of the catalyst surface adsorption invoked in Path A which activates the benzyl ring prior to the Ni insertion on the α C-H. Meanwhile, as expected for Path A, the phenolic ring substituted compounds **15** and **16** do not inhibit cleavage at all.

We attribute the slow reaction in **17** to the steric effect of the methoxy in the α position; the disubstituted side chain apparently prefers a rotamer that inhibits both binding and C-H conjugation with the benzylic ring's π system. The wide rate variations among the various methoxylated and methylated β-O-4 models are summarized in Figure 3.15a. The closer substituents are to the phenyl ring where the rate limiting benzyl group activation occurs the stronger the perturbation.

The substituent perturbations presented by methoxy and methyl groups (Figure 3.15) agree with the surface isotope exchange results in supporting the path A mechanism (Figure 3.10a). The inhibition from methoxy substituents was not only seen in the β-O-4 type diaryl ether system. Our previous work also found that methoxy group position significantly modulated aryl ether cleavage and aromatic reduction in the methoxyphenols.[24] And neither anisole nor methoxylated 2-phenoxyethanol were cleaved even under 50 mA current. On the basis of the results from the previous monomers and here the dimers, we infer that methoxy groups function as electron donating bulky substituents, inhibiting aromatic ring interaction with the electron rich Ni cathode surface, which clearly prefers electrophilic moieties such as carbonyl.

3.5.2 Confirmation of Cleavage Path A for Ketone β-O-4 Models

To differentiate the mechanisms A or B proposed for the cleavage of ketone **1** and its congeners, substituent studies were conducted that probed structural effects on the reaction. The direct Ni coordination to the carbonyl in path A suggests that substitution on the neighboring aryl ring should have relatively little effect on the ketone's reactivity (Figure 3.16). The alternative path B mechanism has the cathode functioning more as an electron source, which donates an electron to the benzylic ketone, enabling the fragmentation of the C-O ether bond.

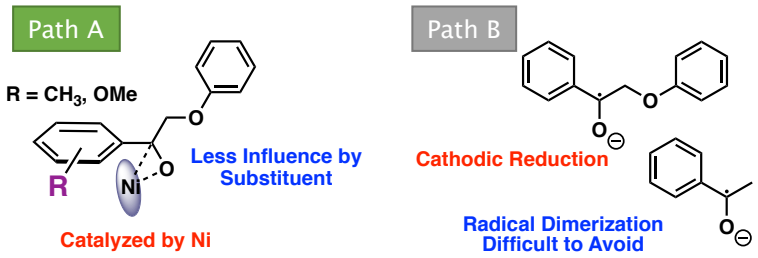

Figure 3.16 Cleavage intermediates of paths A and B for ketone models

Figure 3.17 summarizes the substituent effects on the ketone dimer models, and compares them with the corresponding substituted analogues of compound **8**. As shown in Figure 3.17a, sterically demanding groups in the β position slow C-O cleavage in both series. Ketone **1** is an order of magnitude faster than **8**, a ratio that is retained in comparing **19** to **18**. Most importantly, activation by the ketone moiety is so much stronger than the steric perturbations that even the sterically crowded **10** remains more than twice as fast as sterically unhindered **8**. These results provide further evidence for the high affinity of the Ni catalyst towards the carbonyl moiety.

It is been suggested that the greater reactivity of **1** vs **2** is simply a reflection of the relative homolytic bond strengths of the respective C-O bonds.[13] Addition of methyl groups along the series **1**, **19**, and **10** would be expected to weaken the ether C-O bond, and therefore accelerate cleavage; this expectation is supported by quantum chemical modeling.[41] However, as seen in Figure 3.17a, each methylation instead slows cleavage by a factor of approximately 2. Compounds **8** and **18** present a similar comparison.

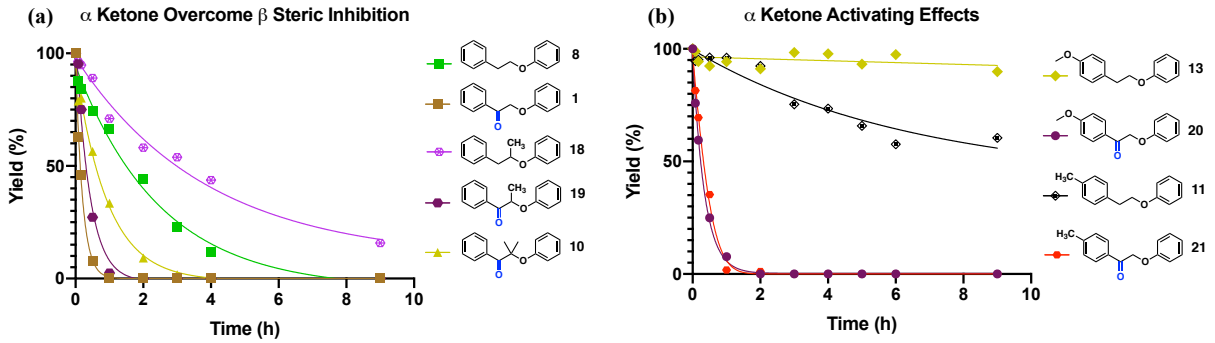

Figure 3.17 Rates of ether cleavage for different substituted 2-phenoxy-1-phenylethanes under standard ECH conditions. (a) Ketone moiety activates more than β methylation hinders; (b) α ketone reactivates C-O cleavage of inactive aryl ethers.

3.5.3 Reactivation of C-O Cleavage by the Carbonyl Moiety

Introduction of a carbonyl in the α position effectively recovers the reactivity of the unreactive β-O-4 ethers. For the strongly inhibited para methoxy 2-phenoxy-1-phenyl ethane **13** and para methyl 2-phenoxy-1-phenyl ethane **11**, addition of a carbonyl at the α position (**20** and **21**) accelerates the cleavage (Figure 3.17b) to rates even faster than the unsubstituted **8** (Figure 3.17a). Adding the carbonyl activates C-O cleavage to nearly, but not quite, the same rate as for **1**, largely mitigating the effects of the electron-donating methyl and methoxy substituents. These donor groups slightly weaken the carbonyl's electrophilicity, but the large acceleration relative to

13 and **11** supports the path A mechanism (Figure 3.11a) in which the Ni directly coordinates to the α carbonyl, largely decoupling the reaction from variations on the benzene ring.

3.6 C-O Cleavage Does Not Proceed via Electron Transfer Mechanism

3.6.1 Cathodic Electrolysis Using Reticulated Vitreous Carbon (RVC) Electrode

The nickel cathode may participate via direct adsorption and catalytic conversion in the C-O cleavage as in Path A or may enable cathodic reduction in the electron-transfer fragmentation of Path B. To probe this question, electrolyses with a reticulated vitreous carbon (RVC) carbon electrode were performed. Electron transfer is expected with this non-catalytic material, which would be unable to perform the path A type of cleavage mechanism.

Table 3.1 RVC[a] Cathodic Electrolysis and Skeletal Ni Catalyzed Cleavage of β-O-4 Aryl Ethers

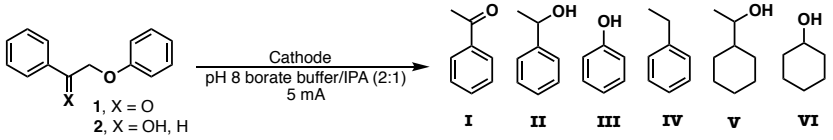

En	*Subst.*	*Electrode*	*Curr. (mA)*	*Time (h)*	*Conv. (%)*	*Yields of products (%)*					
						I	**II**	**III**	**IV**	**V**	**VI**
1[b]	ketone **1**	RVC	50	9	>99	<1	21	91	0	0	0
2	ketone **1**	RaNi	50	9	>99	0	9	28	6	63	69
3	ketone **1**	RVC	5	16	89	72	0	57	0	0	0
4	ketone **1**	RaNi	5	16	>99	2	82	74	0	0	5
5	alcohol **2**	RVC	50	9	0	no rxn					
6	alcohol **2**	RaNi	50	9	>99	0	23	35	6	54	58
7	alcohol **2**	RVC	5	16	0	no rxn					
8	alcohol **2**	RaNi	5	16	85	0	80	67	<1	0	10

[a]Reticulated vitreous carbon (RVC) cathode was used in the non-metal catalyzed cathodic cleavage of **1** and **2** under the standard reaction condition (60 °C, pH 8 borate buffer/IPA (2:1)) as experiments catalyzed by skeletal Ni electrode. [b]Radical dimerization product 2,3-diphenylbutane-2,3-diol was formed (NMR see Figure 3.39).

As shown in Table 3.1, with the RVC cathode under the same reaction condition as for the skeletal Ni cathode, the products of the reductions were significantly different. In 9-hour cathodic reductions, at 50 and 5 mA, both Ni (Entries 2, 4) and RVC (Entries 1, 3) electrodes cleaved ketone **1** into the aromatic products phenol and acetophenone. However, the RVC produced none of the downstream ring saturation products even in the high current case (Entry 1).

Both electrodes achieved fairly rapid C-O cleavage at high current. At low current (5 mA, Entries 3, 4), cleavage by the RVC was clearly slower, despite the fact that only C-O fragmentation products were observed. However, in the case of the Ni electrode, substantial conversion to downstream hydrogenation products were seen. Thus, the C-O ether cleavage on the skeletal Ni electrode surface is qualitatively different from the electron transfer process. Meanwhile, as reported by Yamamoto and co-workers, carbon electrodes are capable of electron transfer to the benzylic ketone of acetophenone, leading to pinacol coupling of two ketyl radicals to generate 2,3-diphenylbutane-2,3-diol as the stereoisomers.[29]

With the RVC at high current, the amount of acetophenone dropped quickly within 1 hour of cathodic treatment (see Figure 3.38a). After 9 hours of reduction, only about 21% of 1-phenylethanol was observed (Table 3.1, Entry 1). Instead, the diol product from dimerization of the radical anions was detected (see Figure 3.39); such dimerization is hard to avoid in electron transfer reductions of ketones.[27, 29] Importantly, no such dimerization products were found in the skeletal Ni catalyzed processes.

Notably, the products of reduction over the skeletal Ni electrodes were also similar to classic hydrogenation results based on heterogeneous Ni catalysts.[22, 23] As mentioned in the introduction, Ni catalyzes aryl ether bond cleavage in classic, high-temperature hydrogenation/hydrogenolysis processes either using hydrogen gas or hydrogen transfer solvents.

Such processes do not involve cathodic electron transfer, but lead to the same products as this skeletal Ni catalyzed ECH process.

Attempted reduction of the alcohol **2** using the RVC electrode was also explored. As expected, for an electron transfer process, no reaction was observed (Table 3.1, Entries 5,7). To enable cleavage of alcohol **2**, the Ni metal catalyst was required (Entries 6, 8).

3.7 Cleavage Summary of β-O-4 Type Alkyl Aryl Ethers

3.7.1 Proposed Distinct Cleavage Mechanisms of β-O-4 Alkyl Aryl Ethers

On the basis of the above H/D isotopic exchange studies, reaction competitions, rate analyses as a function of substituents, and reduction experiments with non-catalytic electrodes, we have uncovered distinct ether cleavage mechanisms for the alcohol and oxidized (ketone) β-O-4 linkage models. Both involve adsorption on the catalytic Ni surface, but the modes of adsorption differ. As shown in Figure 3.18a, alcohol **2** and its congeners adsorb via phenyl ring coordination followed by benzylic C-H activation. In contrast, the ketone models derived from **1** adsorb to the

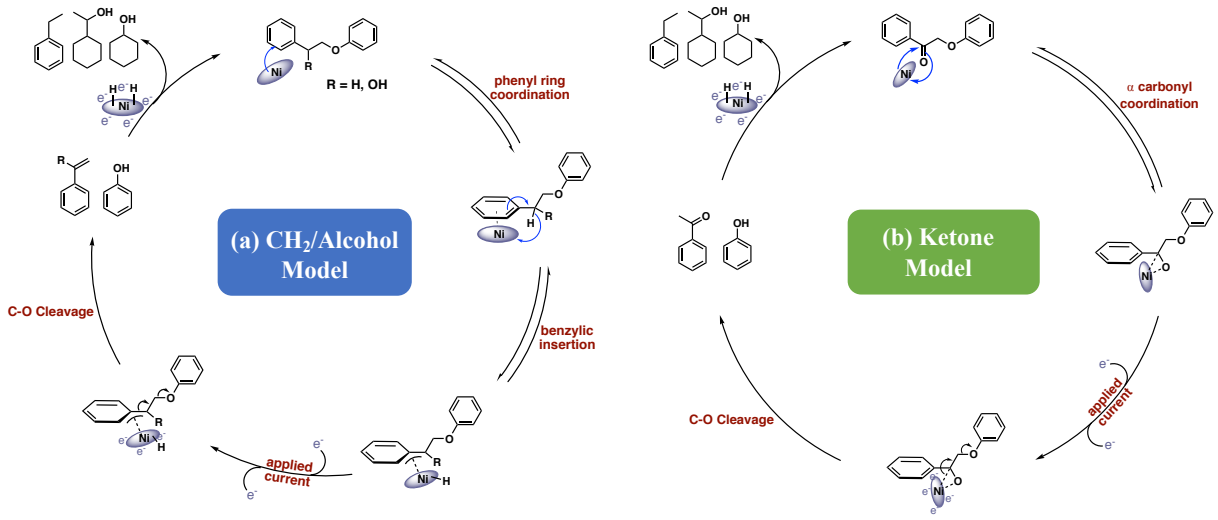

Figure 3.18 Proposed mechanism for skeletal Ni electrode catalyzed hydrogenation of β-O-4 aryl ethers.

Ni surface via the carbonyl moiety (Figure 3.18b). Both of these intermediates establish Ni-C interactions vicinal to the ether C-O bond. With applied current, the Ni surface then donates charge to effect β elimination of the phenoxide leaving group.

3.7.2 Hierarchy of C-O Cleavage Rates of 2-phenoxy-1-phenylethane with Different Functionality

Kinetic studies of the ketone and alcohol models and their substituted analogues show a wide range of rates. Here we propose a hierarchy (Figure 3.19) of C-O cleavage rates of β-O-4 related aryl ethers that contain different functionalities as quantified by their ECH half-lives (Table 3.2). The oxidized β-O-4 ketone displays the highest cleavage rate on the scale, due to the high affinity of Ni towards carbonyl groups. This effect is also seen in the acetone co-solvent study (chapter 2, Figures 2.3-2.4). The methyl and methoxy group position mapping show large reactivity variations across the structure of the β-O-4 aryl ethers, with stronger effects when closer to the benzyl ring. Thus, in the cleavage rate hierarchy, the closer the R group is to the binding site, the slower the rate of C-O ether cleavage. When there is no α C-H, cleavage is completely prohibited, since activation of the α position is required for sp^3 C-O ether bond cleavage of 2-phenoxy-1-phenylethane (β-O-4) type aryl ethers.

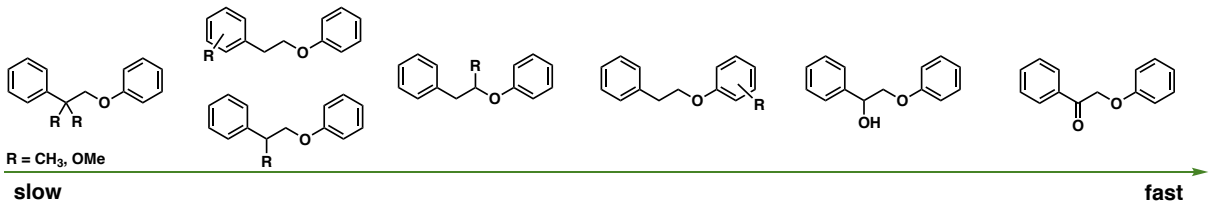

Figure 3.19 Cleavage rate hierarchy of different β-O-4 relative aryl ethers

Table 3.2 Substituents Varied Aryl Ethers Cleavage Half-life

β Steric Effect	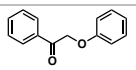 $t_{1/2}$ (8.2 ± 0.9 min)[a]	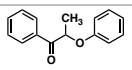 $t_{1/2}$ (17.0 mins)	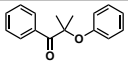 $t_{1/2}$ (39.1 mins)
α Functionality	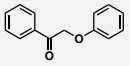 $t_{1/2}$ (8.2 ± 0.9 min)[a]	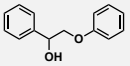 $t_{1/2}$ (13.6 ± 1.5 mins)[a]	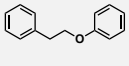 $t_{1/2}$ (93.0 ± 8.1 mins)[a]
Substituent Position	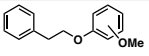 $t_{1/2}$ (para: 69.2 min) $t_{1/2}$ (ortho: 57.7 ± 7.6 min)[a]	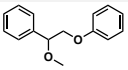 $t_{1/2}$ (363 mins)	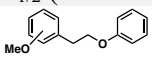 ortho & para (no reaction)[a]

[a]Not all rate experiments were replicated, but our reaction and analytical procedures proved quite reproducible, as illustrated by the uncertainties shown in these cases. Typical uncertainties fall in a range of 5-10%.

3.8 Conclusions

3.8.1 Mechanism of C-O Cleavage in β-O-4 Type Aryl Ethers over Skeletal Ni

Motivated initially by the cleavage rate acceleration seen in oxidized Cu-AHP lignin depolymerization via ECH, we have subjected a series of substrates that model the β-O-4 type aryl ether linkage to ECH to map the sequence of reaction steps. Kinetic measurements and the identification of key reduction intermediates from ketone and alcohol models show that the C-O ether bond undergoes direct cleavage without ketone-alcohol interconversion to release the corresponding arenes. Isotope exchange experiments indicate that β C-O cleavage in the alcohol and simple ether models (**2** and **8**) begins with C-H activation at the benzylic α site. For the ketone model, the nucleophilic Ni electrode directly coordinates with the polarized carbonyl π system without breaking the aromaticity of the neighboring phenyl ring, leading to rapid cleavage. For both cleavages, radical processes have been ruled out by the combination of isotope studies, substituent effects, non-catalytic electrode reductions, and quantum chemical modeling. The high

affinity of the charged Ni cathode surface towards carbonyl systems was further exploited in the use of acetone co-solvent and current control to allow fine tuning of the reduction selectivity.

This work has unambiguously demonstrated two distinct mechanisms for Ni-catalyzed cleavage of simple β-O-4 models linked via alcohol or ketone-bearing carbon chains. Though several previous studies had empirically noted that such ether cleavages occur, relatively little mechanistic analysis was available. The new insights explain the substantial acceleration of lignin depolymerization by preliminary oxidation, and they demonstrate that the enhanced depolymerization is not simply due to bond dissociation energy differences between ketone and alcohol-type linkages.

3.8.2 Substituent Effects on the β-O-4 Type Aryl Ether Cleavage

Methoxy and methyl substituents significantly modulate reactivity as a function of their placement. Such electron rich bulky groups can significantly impact the ether cleavage rate by hindering Ni binding/C-H insertion at the α position in substrates like 2-phenoxy-1-phenylethane **8**. Attached to the benzylic arene ring, they may inhibit adsorption on the electron rich nickel surface both sterically and by adding electron density to the aromatic system, decreasing its electrophilicity. Oxidation to the α-ketone form as in **1** largely neutralizes those inhibitory effects on the cleavage as the nickel coordination is now centered on the carbonyl. These findings are of substantial practical importance because most of the arene moieties in real lignin bear methoxy groups. Overall, the mechanistic insights gained from this wide-ranging study of ECH activated ether cleavage reactions over skeletal Ni have mapped out a C-O ether bond cleavage hierarchy that offers guidance in selection of reaction conditions to predict and control product selectivities.

3.9 Supplemental Experimental Details

3.9.1 General Experimental Procedure of H/D Isotope Exchange of β-O-4 Aryl Ethers

The H/D isotope exchange experiments of all aryl ether substrates followed a similar procedure. A cylinder shaped one compartment cell was equipped with a small stir bar and a rubber stopper with a stainless-steel metal clip. The acetone treated skeletal Ni catalyst (same size and preparation as the electrode) was hung on the metal clip and placed inside the one compartment cell, positioned high enough to avoid contact with the stirrer. 20 mL of D_2O with the addition of 8 mL 2-propanol (non-deuterated) was charged inside the cell. As with the ECH studies, another 2 ml of 2-propanol was used to dissolve the weighed aryl ether substrate (0.25 mmol) in a 4-mL glass vial, before it was added to the D_2O solution. The entire set up was placed in a water bath where the temperature was maintained at 60 °C. The skeletal Ni catalyst was allowed to react with the D_2O/2-propanol mixture for 1 hour, and then the vial with 2 mL of 2-propanol with the aryl ether substrate was added into the D_2O solution and allowed to exchange for 9 hours at 60 °C under ambient pressure. No current was applied in the exchange experiments to avoid conversion to downstream reduced products.

Quantitative Analysis Preparation:

At each desired time point 0.25 mL of D_2O solution was syringed into a 1.7 mL conical vial and analyzed by GC-MS as described earlier.

Note, an extra step was needed to accurately assess the amount of deuterium that was incorporated in the alcohol β-O-4 aryl ether, because the H/D exchange on –OH functional groups happens instantaneously. The H/D exchange measurement of alcohol 2-phenoxy-1-phenylethanol was sampled twice at each time point, and two different extractions were conducted at each time

point. One is normally extracted with 1 mL of dichloromethane and then inject into the GC-MS for quantification. The other one is first extracted with 1 mL of dichloromethane, then the dichloromethane extract was washed with 1 mL of deionized non-deuterated water to make sure there was no D on the –OH functional group, followed by injection on GC-MS. Both non-washed and washed exchange kinetics were analyzed.

3.9.2 MS Fitting Method of H/D Isotope Labeling Experiment

The total ion abundance of different mass fragments after H/D exchange was provided by GC-MS. However, GC-MS only gives the total ion mass chromatogram of each measurement. The total ion mass chromatogram represents a mixture of D_n dimer isotopmers. The intensity of each measured ion fragment is also a combination of the intensities of the same mass fragment from different D_n incorporated aryl ether dimer. Therefore, to determine the % abundance of D_n in the exchange results, the proportion of D_n in each mixture is defined as fraction coefficient X_n (n = 0,1,2,3...n). The sum of the products of fraction coefficient X_n times peak fragment intensity I_n should be the total intensity of the corresponding peak in the total ion chromatogram. Meanwhile, the relative fragmentation pattern of different D labeled aryl ethers should not change, only the peak value will shift by one for each H that was replaced by D incorporated inside the compound (Figure 3.20).

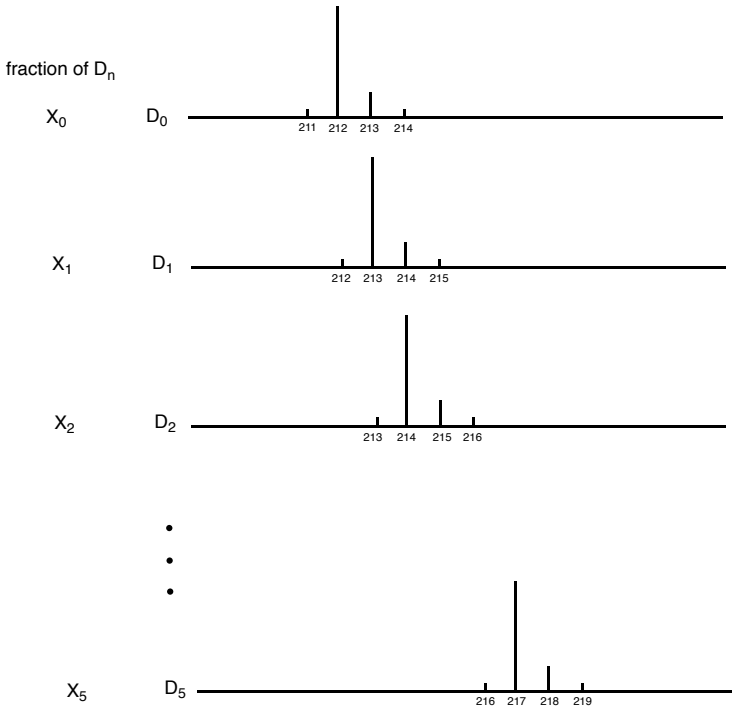

Figure 3.20 As the numbers of D labels in the compound increase, the mass fragmentation pattern and intensity remains the same; only the peak's m/z value will shift. Fractional coefficients X_n were used as the proportions of D_n in the total ion mixture.

Excel solver was used to fit the corresponding fraction X_n of D_n in the total ion mixture. Below is an example of the solver fitting method of 2-phenoxyacetophenone H/D exchange at 10 min.

As presented in Table 3.3, column 2 is the intensity distribution of unlabeled 2-phenoxyacetophenone fragments (parent). Column 3 is the intensity distribution of the D labeled mixture (labeled). The fitted intensity of each ion was calculated by the below **equation 3** and tabulated in column 4-9, where fraction coefficient X_n is tabulated in column 2 (row 11-17). The values of the fractional coefficients X_n were found through excel solver as presented in **equation 5** in giving the minimum value of the sum of the square errors. The square error is calculated by

equation 4 and tabulated in column 10, where the smaller the deviation, the closer the fitted intensity to the actual labeled intensity. Based on solved X_n, the percent abundance of D_n is plotted.

$$\%Ion\ Intensity_{fitted} = X_n * \%Ion\ Intensity_{parent} \quad [3]$$

$$Square\ Error = (\sum_{0}^{5} \%Ion\ Intensity_{fitted} - \%Ion\ Intensity_{labeled})^2 \quad [4]$$

$$Solver: \left[minimize \sum_{0}^{5} Square\ error = by\ Varying\ X_n \right] \quad [5]$$

$$\%Abundance\ (D_n) = \frac{X_n}{\sum_0^5 X_n} * 100 \quad [6]$$

Table 3.3 Ketone Model 2-Phenoxyacetophenone H/D Exchange MS Fitting at 10 min

mass frag. (m/z)	MS Intensity (parent)	MS Intensity (labeled)	Fitted Int. X_0*Parent	Fitted Int. X_1*Parent	Fitted Int. X_2*Parent	Fitted Int. X_3*Parent	Fitted Int. X_4*Parent	Fit. I. X_5*P	Square Error
210.079	0.01	0	3.79E-05						1.44063E-09
210.983	0.03	0	0.000113867	0.001354892					2.15725E-06
212.094	25.2	0.11	0.095648138	0.004064677	0.010285769				2.00621E-12
213.1	3.9	3.46	0.014802688	3.414328793	0.030857306	1.12217E-05			7.09511E-17
214.1	0.37	26.45	0.001404358	0.528408027	25.92013672	3.36652E-05	1.22961E-05		2.43227E-11
215.1	0.03	4.09	0.000113867	0.050131018	4.011449731	0.028278796	3.68883E-05	0	1.06079E-10
216.1	0	0.42	0	0.004064677	0.380573436	0.00437648	0.03098620	0	6.31821E-13
217.053	0	0.03	0	0	0.030857306	0.000415205	0.00479548	0	3.68205E-05
Deuterium number (D_n)	Fraction Coefficient X_n	% Abundance							Sum of Square Errors
D0	0.00379556	0.32435148							2.15883E-06
D1	0.13548923	11.5782975							
D2	1.02857685	87.8975264							
D3	0.00112217	0.09589595							
D4	0.00122961	0.10507701							
D5	0	0							

Analogous analyses applied to the fragments with NMR evidence (below) confirm the assigned locations of the D labels.

3.9.3 Fitted Result and Spectra of D_n in the Kinetic H/D Exchange Experiments of Alkyl Aryl Ethers

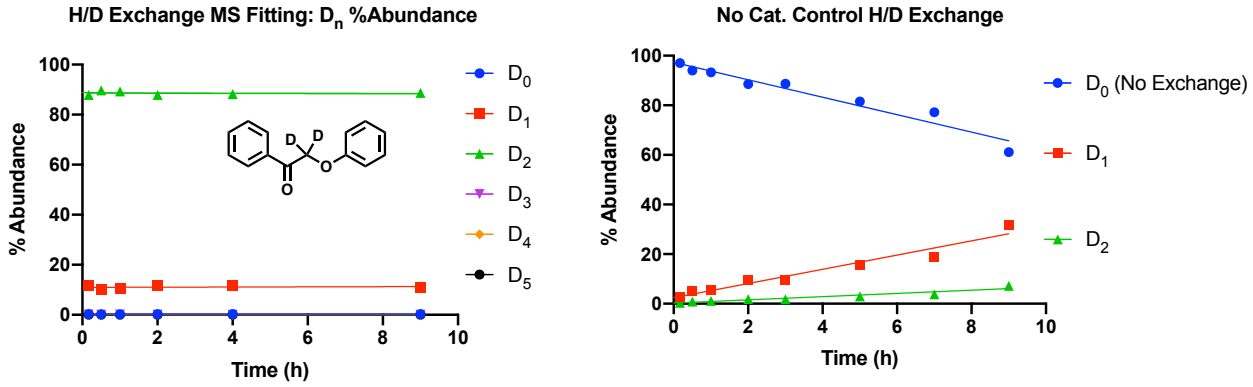

Figure 3.21 Plotted %Abundance of D_n of 2-phenoxyacetophenone in 2:1 D_2O/IPA with exchange catalyzed by acetone treated skeletal nickel.

Quantitation of the H/D exchange was determined by GC-MS. The location of the exchange is determined by mass fragmentation and NMR evidence in the section below. Control experiment shows results with catalyst omitted.

H/D Exchange Mass Spectra and NMR Spectra of 2-phenoxyacetophenone (Ketone β-O-4)

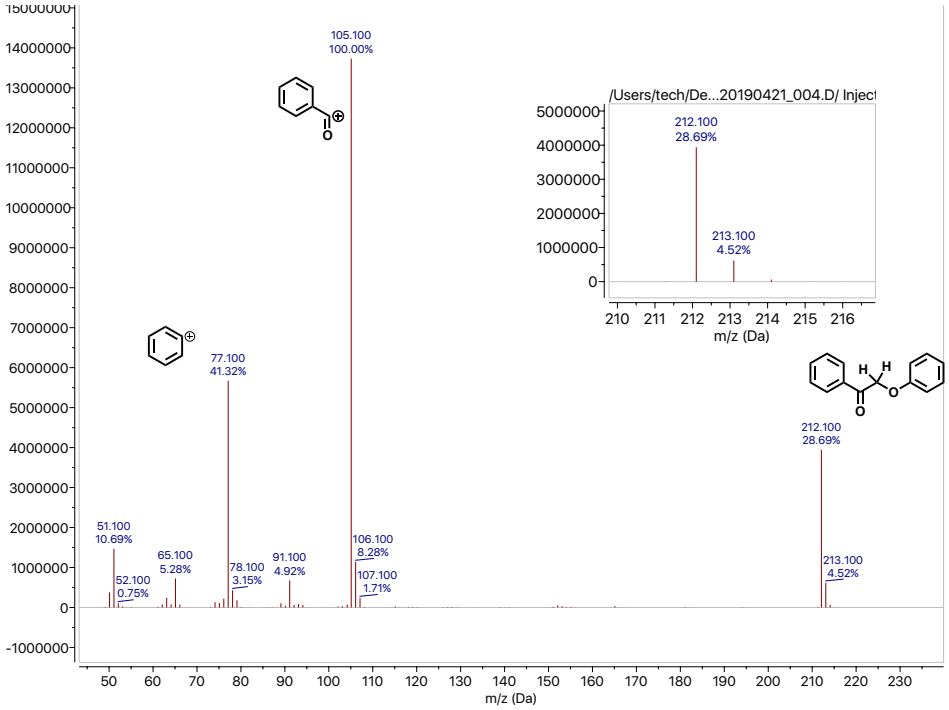

Figure 3.22 Mass Spectra of unlabeled 2-phenoxyacetophenone without exchange.

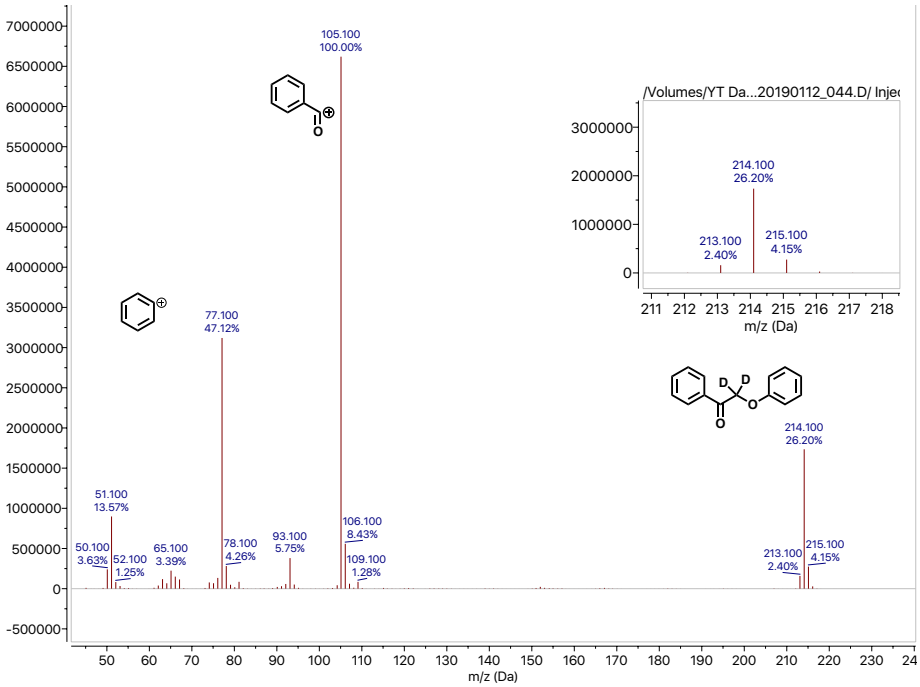

Figure 3.23 Mass Spectra of labeled 2-phenoxyacetophenone after 10 mins exchange. Notice, compared with the unlabeled parent mass, the major fragment 105 ($PhCO^+$) was remained the same, which indicated the exchange happened on the lost fragment. The exchange location is further confirmed by NMR.

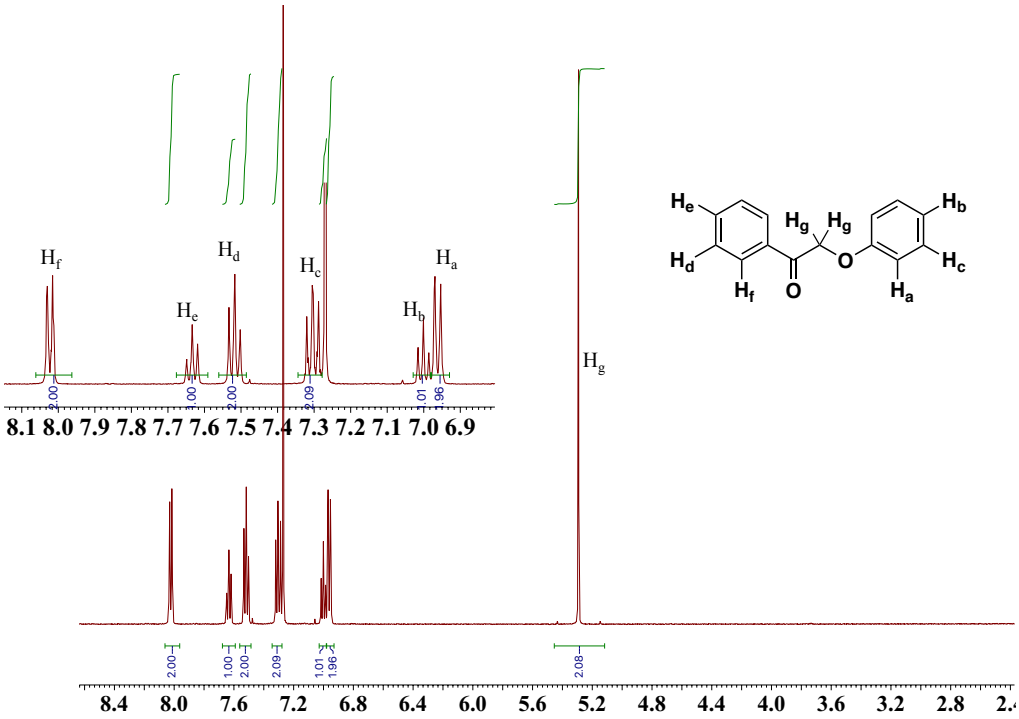

Figure 3.24 NMR Spectra of unlabeled 2-phenoxyacetophenone without exchange.

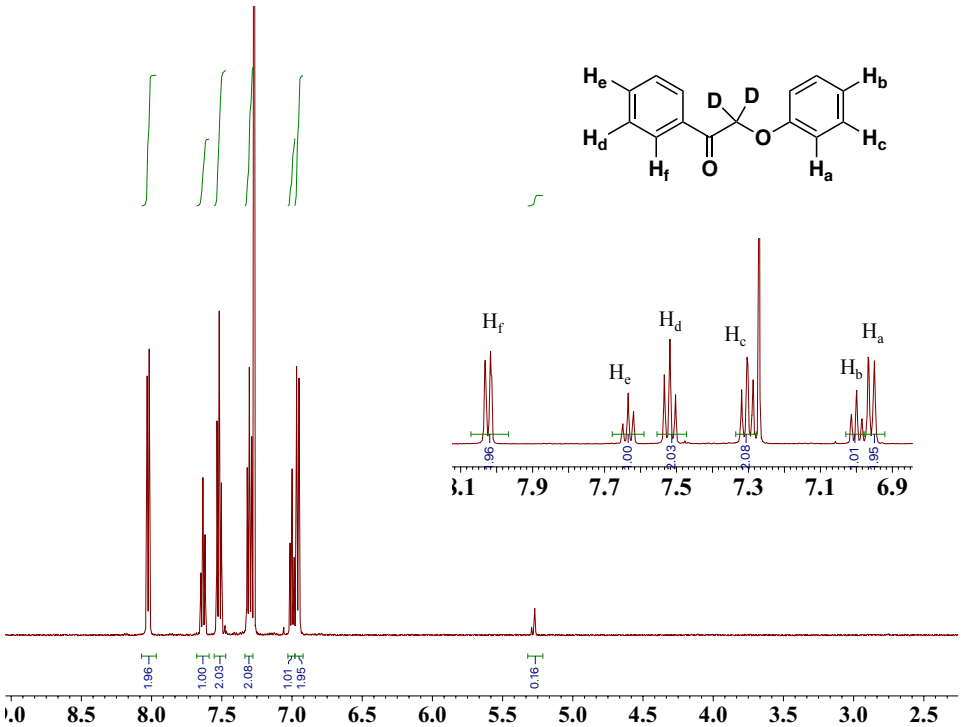

Figure 3.25 NMR Spectra of labeled 2-phenoxyacetophenone after exchange for 10 mins. As indicated in the spectra, only beta C-H were exchange, which matched up with the fitted MS % abundance where D_2 is the major numbers of the D incorporation.

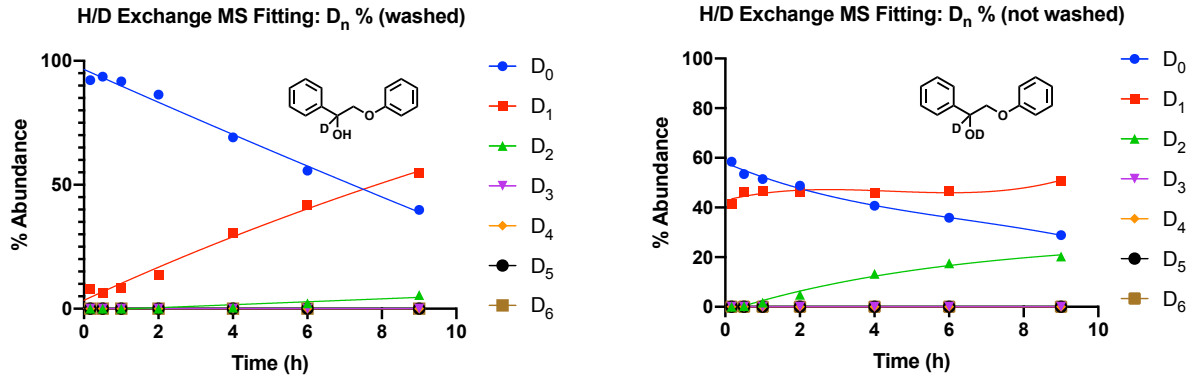

Figure 3.26 Plotted %Abundance of D_n of 2-phenoxy-1-phenylethanol both washed and non-washed trials.

The D incorporated on the alcohol functional group is easy to lose in the analytical sample preparation process. To proper counting the number of D incorporated on the aryl ether, washed trials were performed to remove the D on -OH. The quantitative exchange result was determined by GC-MS. The location of the exchange is determined by mass fragmentation and NMR evidence in the section below.

H/D Exchange Mass Spectra and NMR Spectra of 2-phenoxy-1-phenylethanol (alcohol β-O-4)

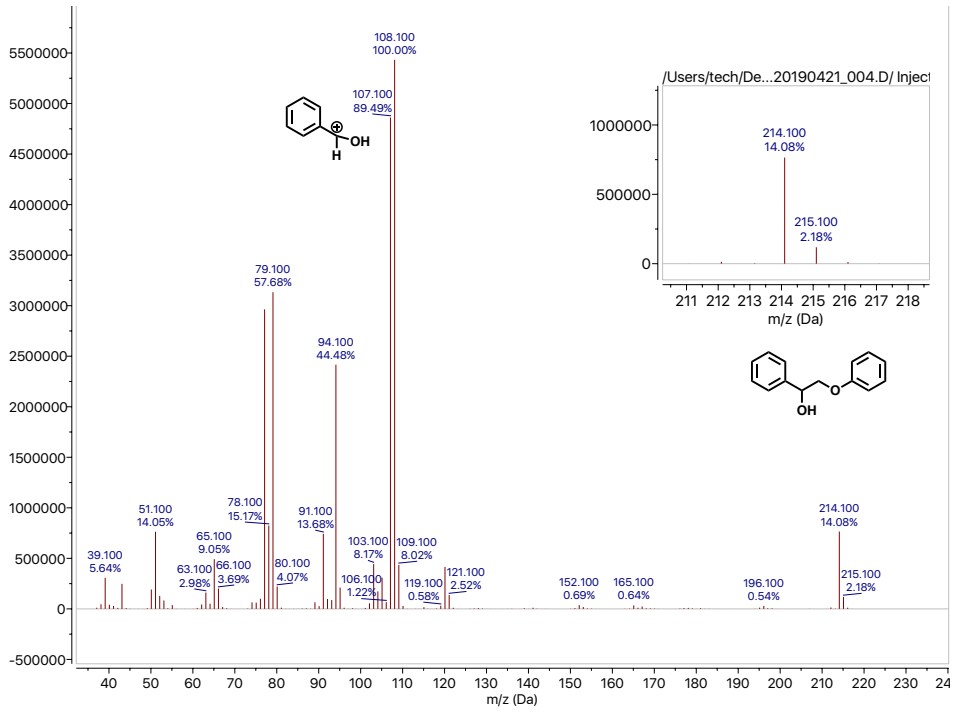

Figure 3.27 Mass Spectra of unlabeled 2-phenoxy-1-phenylethanol without exchange.

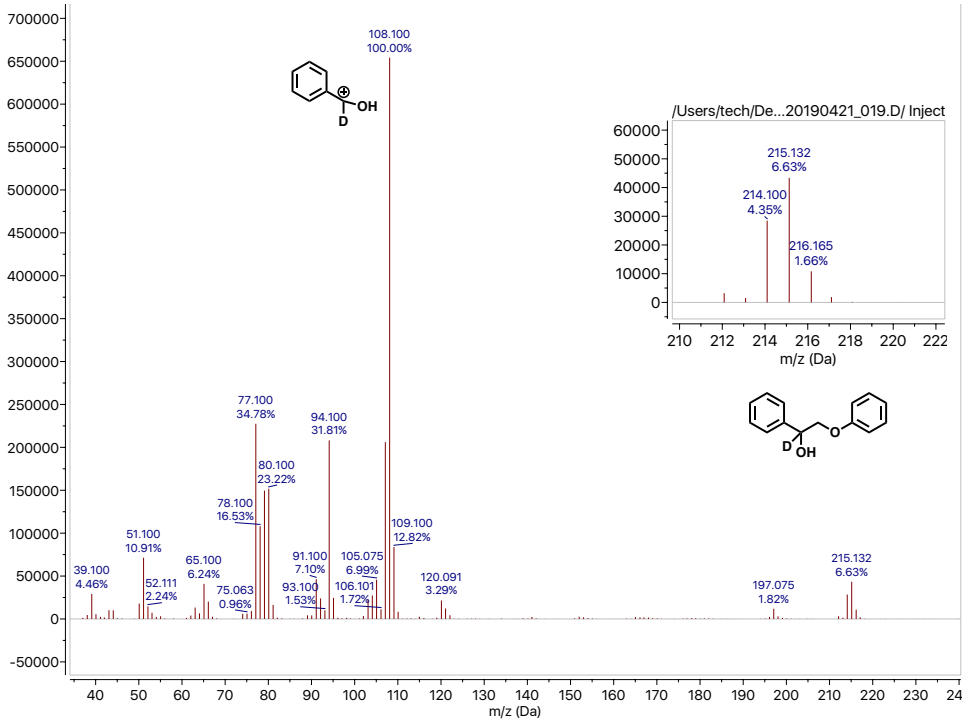

Figure 3.28 Mass Spectra of 2-phenoxy-1-phenylethanol after 9-hour H/D isotope exchange. Analytical sample washed with DI water to remove the D on alcohol -OH functional group. The exchange location is further confirmed by NMR.

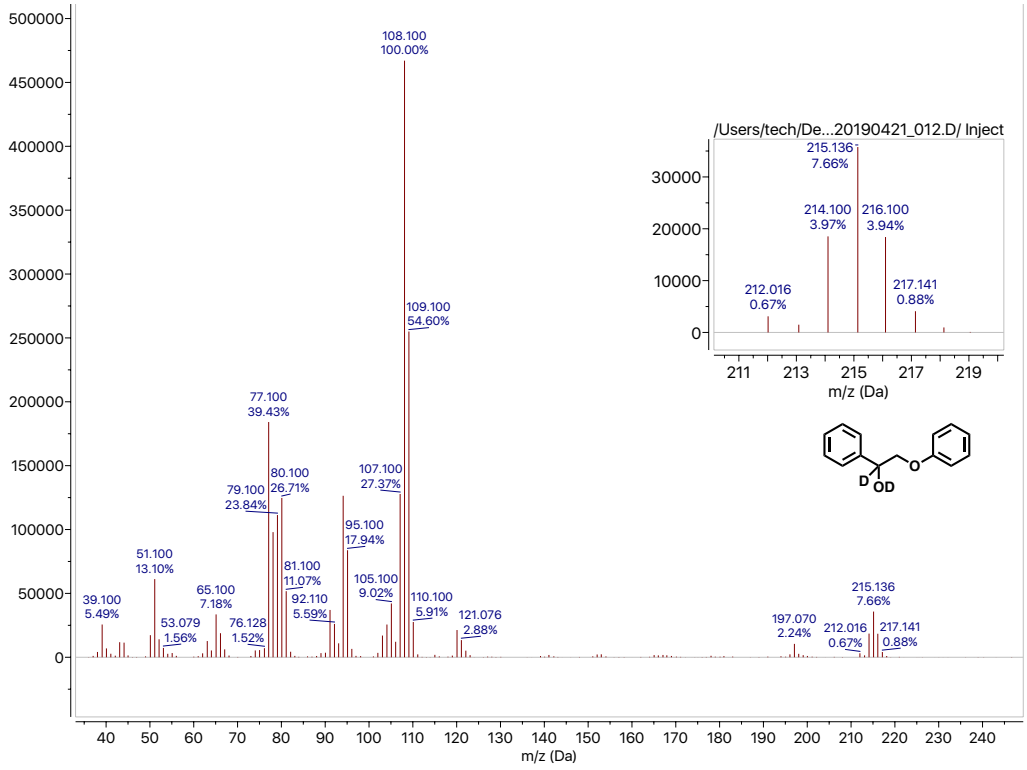

Figure 3.29 Mass Spectra of 2-phenoxy-1-phenylethanol after 9-hour H/D isotope exchange. Analytical sample not washed. The exchange location is further confirmed by NMR.

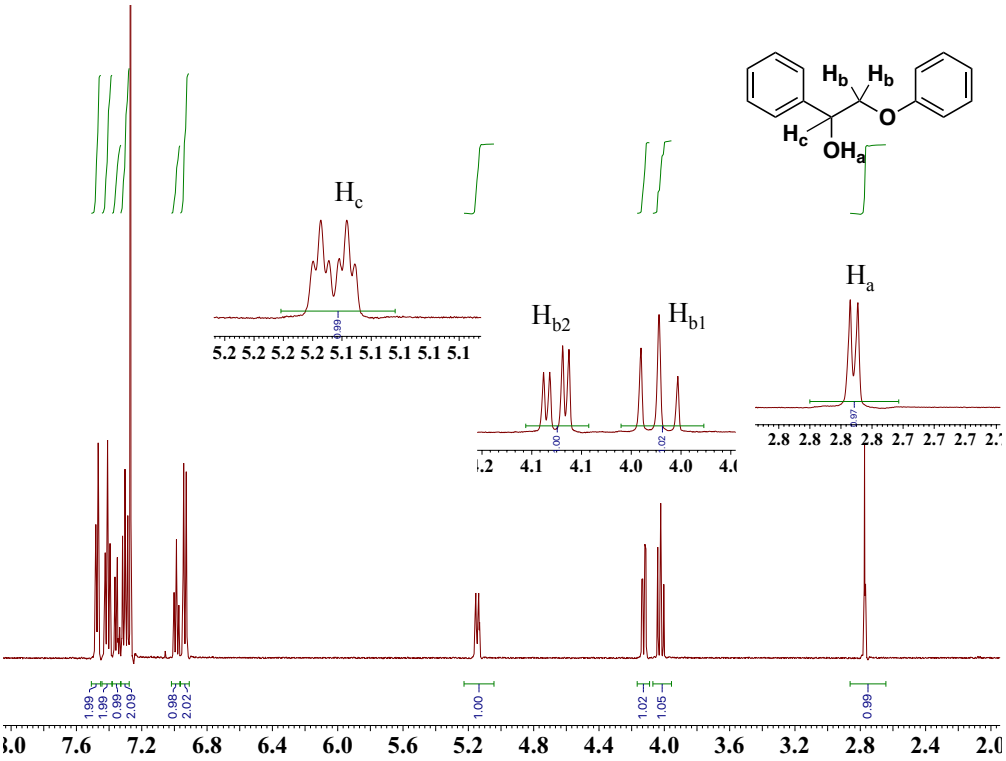

Figure 3.30 NMR Spectra of unlabeled 2-phenoxy-1-phenylethanol **without** exchange.

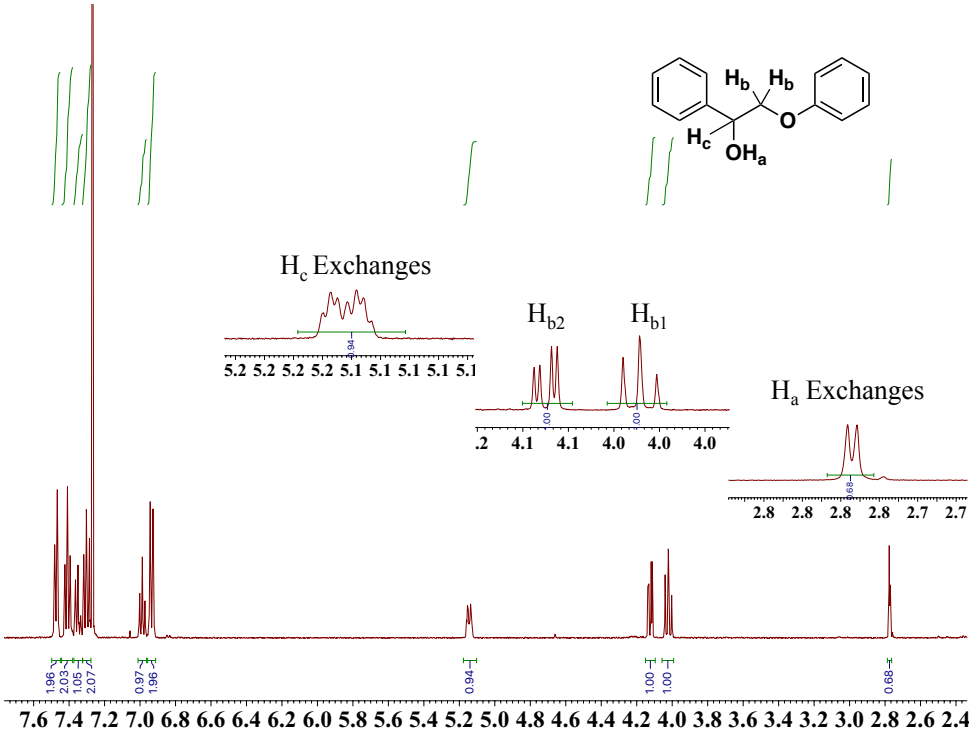

Figure 3.31 NMR Spectra of 2-phenoxy-1-phenyl ethanol after H/D isotope **exchange** for 30 mins at 60 °C, the -OD exchange (H_a) varies during the NMR sample preparation. The -OH and α C-H start to exchange.

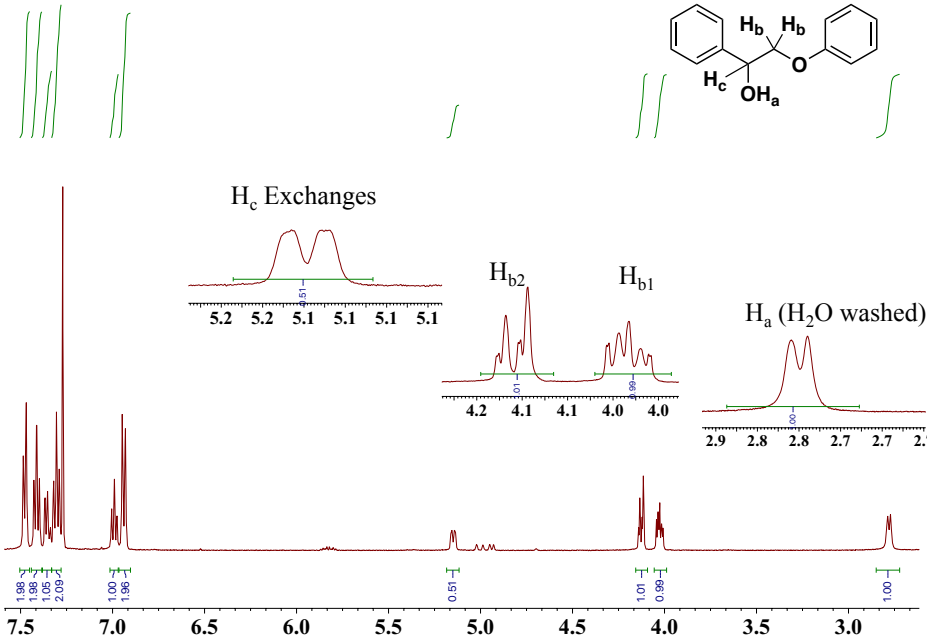

Figure 3.32 NMR Spectra of 2-phenoxy-1-phenyl ethanol after H/D isotope **exchange** for 9 hours at 60 °C (sample was extracted and washed with H_2O), the -OD exchange (H_a) was removed. Approximately half of the α (H_c) were exchanged, which matched up with the fitted MS % abundance.

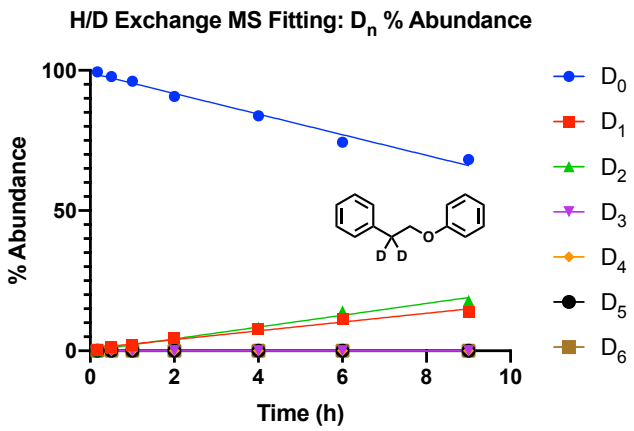

Figure 3.33 Plotted %Abundance of D_n of 2-phenoxy-1-phenylethane.

The quantitative exchange result was determined by GC-MS. The location of the exchange is determined by mass fragmentation and NMR evidence in the below section.

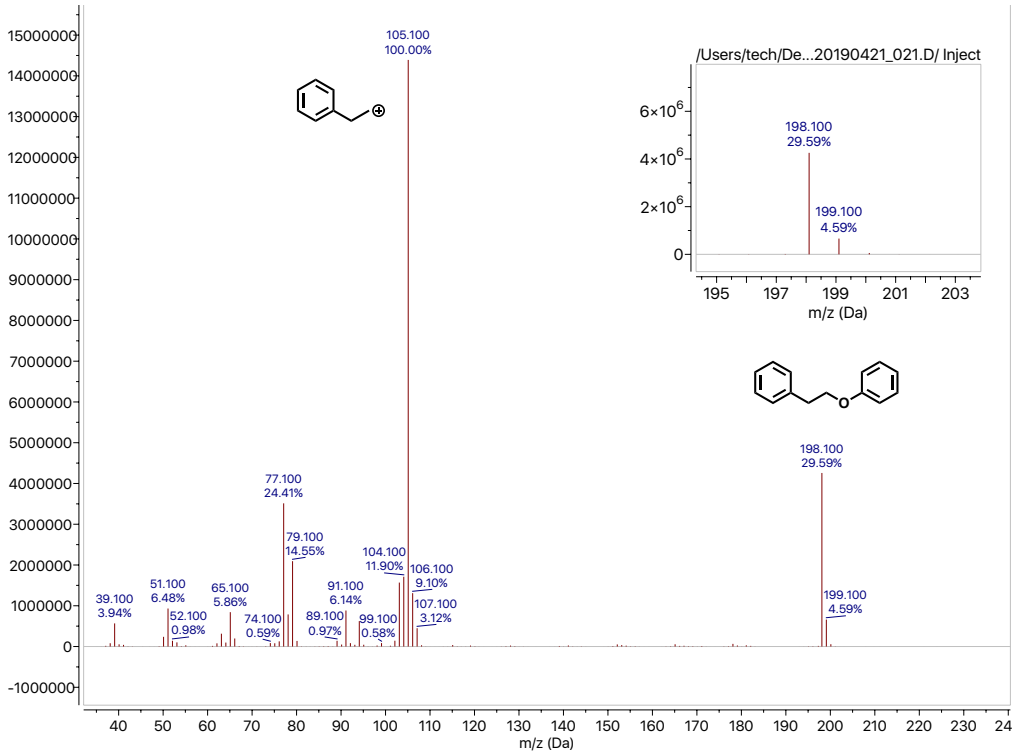

Figure 3.34 Mass Spectra of unlabeled 2-phenoxy-1-phenyl ethane without exchange.

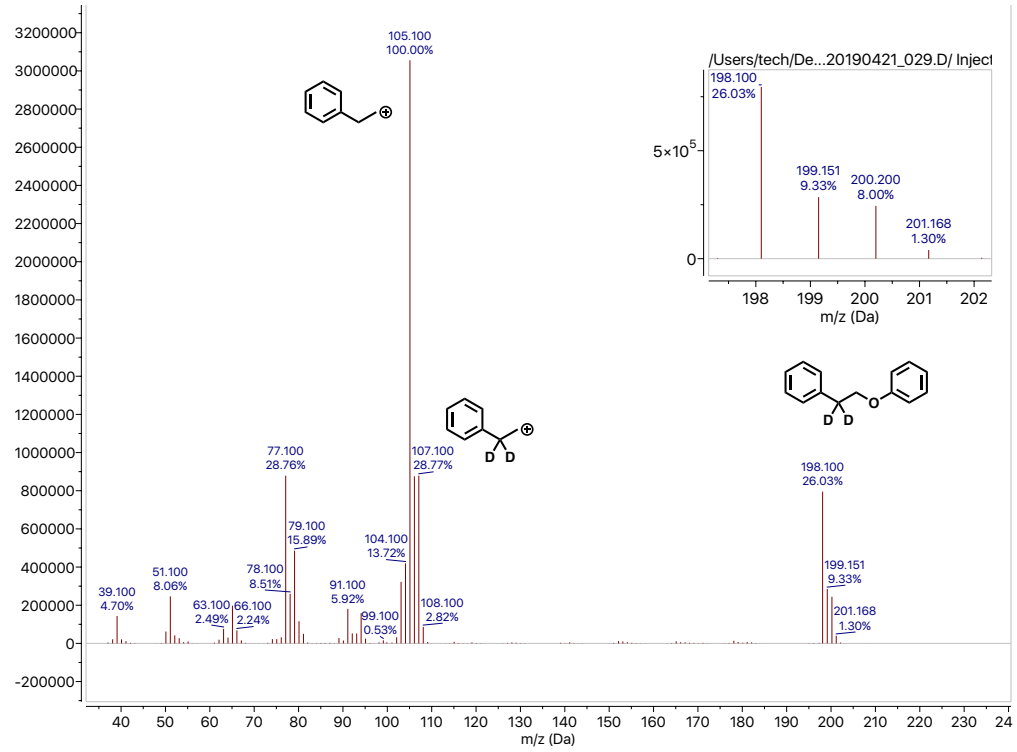

Figure 3.35 Mass Spectra of labeled 2-phenoxy-1-phenylethane after 9-hour exchange. Increases in m/z 199 and 200 are seen, with both ions showing similar intensities. The exchange location is further confirmed by NMR.

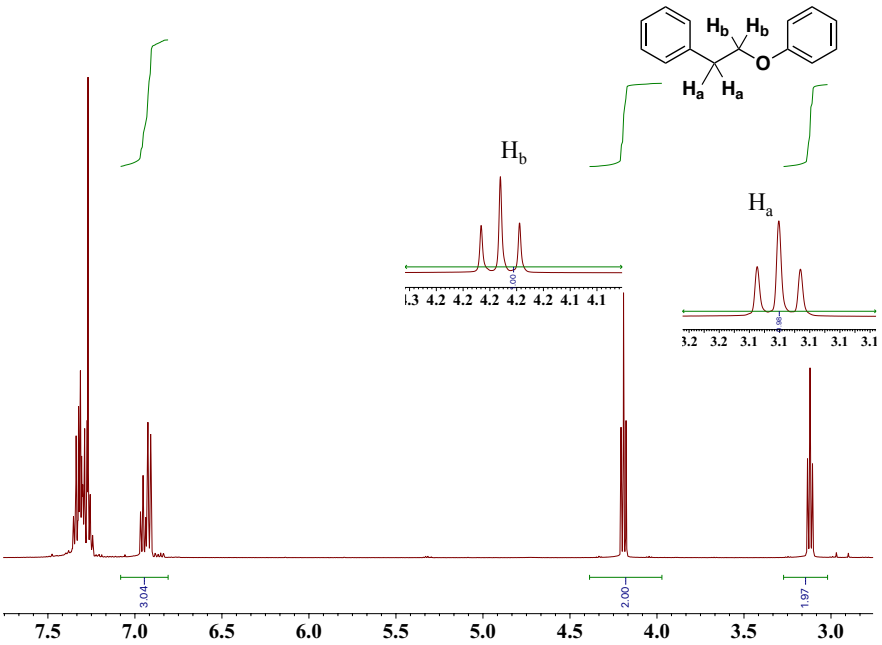

Figure 3.36 NMR Spectra of unlabeled 2-phenoxy-1-phenylethane without exchange.

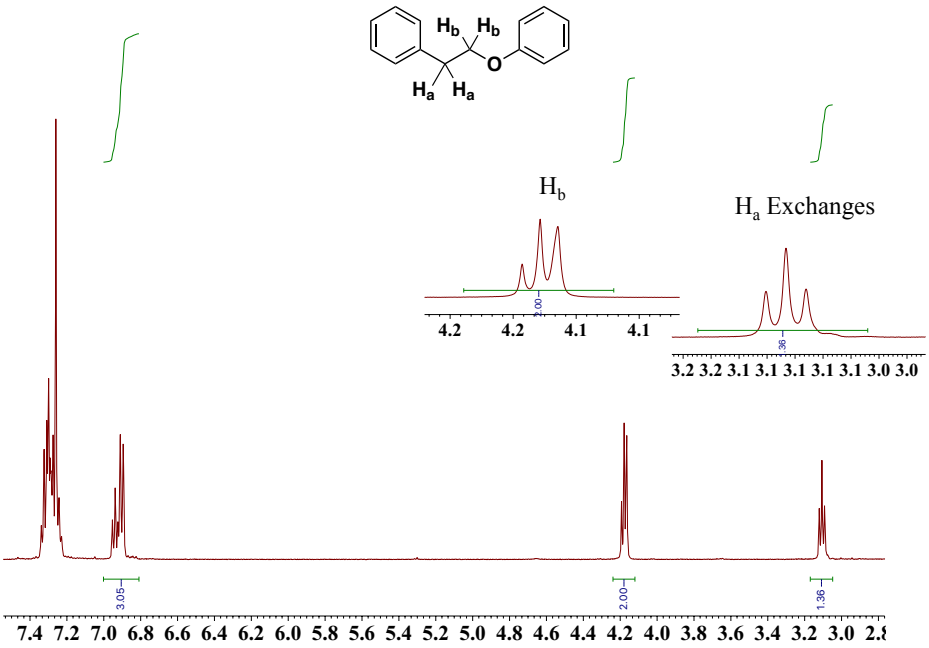

Figure 3.37 NMR Spectra of labeled 2-phenoxy-1-phenylethane after 9-hour H/D exchange. As indicated in the spectra, only α C-H were exchanged, which matched up with the fitted MS % abundance where D_2 is the maximum number of the D incorporated in 2-phenoxy-1-phenylethane.

Cathodic Reduction 2-phenoxyacetophenone Ketone 1 via RVC Electrode @ (5 and 50 mA)

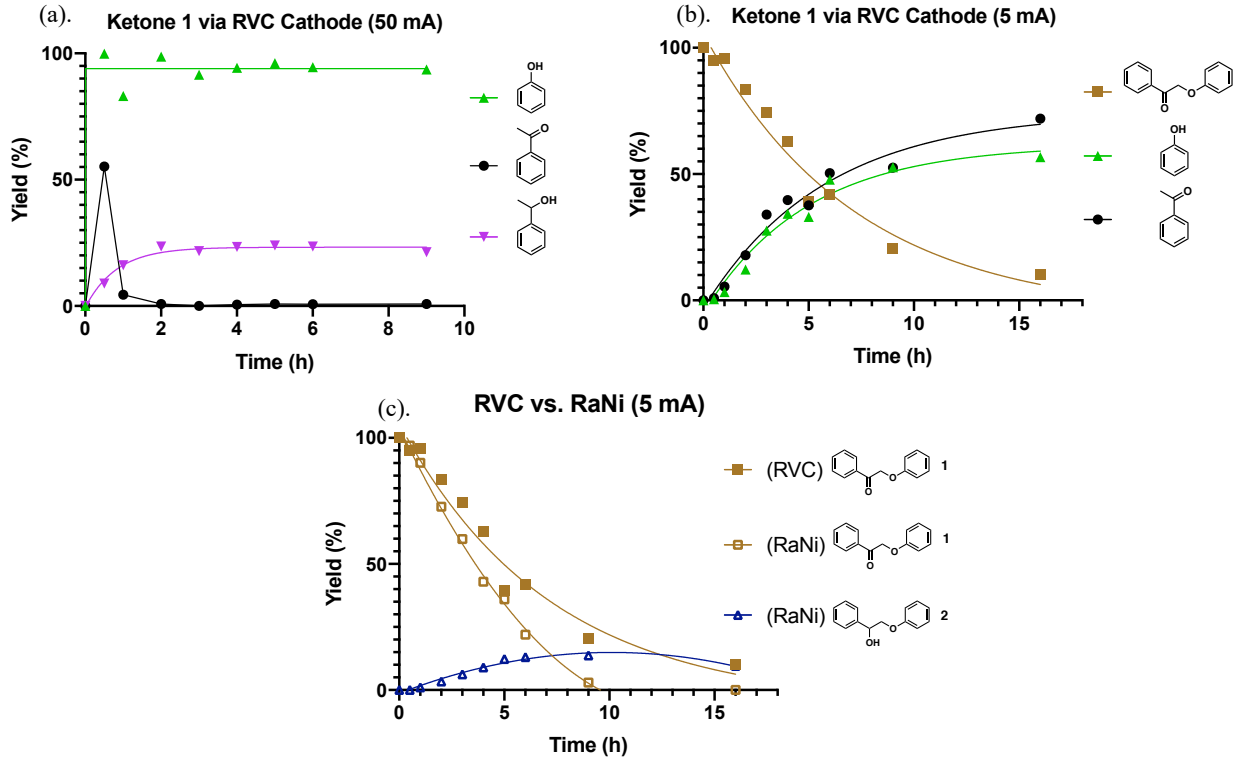

Figure 3.38 (a) Full kinetic measurement of cathodic reduction of ketone **1** using RVC electrode at 50 mA (Table 1, Entry 1). (b) Full kinetic measurement of cathodic reduction of ketone **1** using RVC electrode at 5 mA (Table 1, Entry 3). (c) Ketone **1** cleavage rate comparison between RVC electrode and Ni electrode at 5 mA (for full kinetic data of Ni electrode @ 5 mA, see Figure 3c). Cathodic reductions were performed at the same standard conditions as the Ni ECH experiments: 50 or 5 mA, 60 °C with 33% v/v IPA.

2,3-diphenylbutane-2,3-diol from Cathodic Reduction Experiment Using RVC Cathode (Table 1, Entry 1)

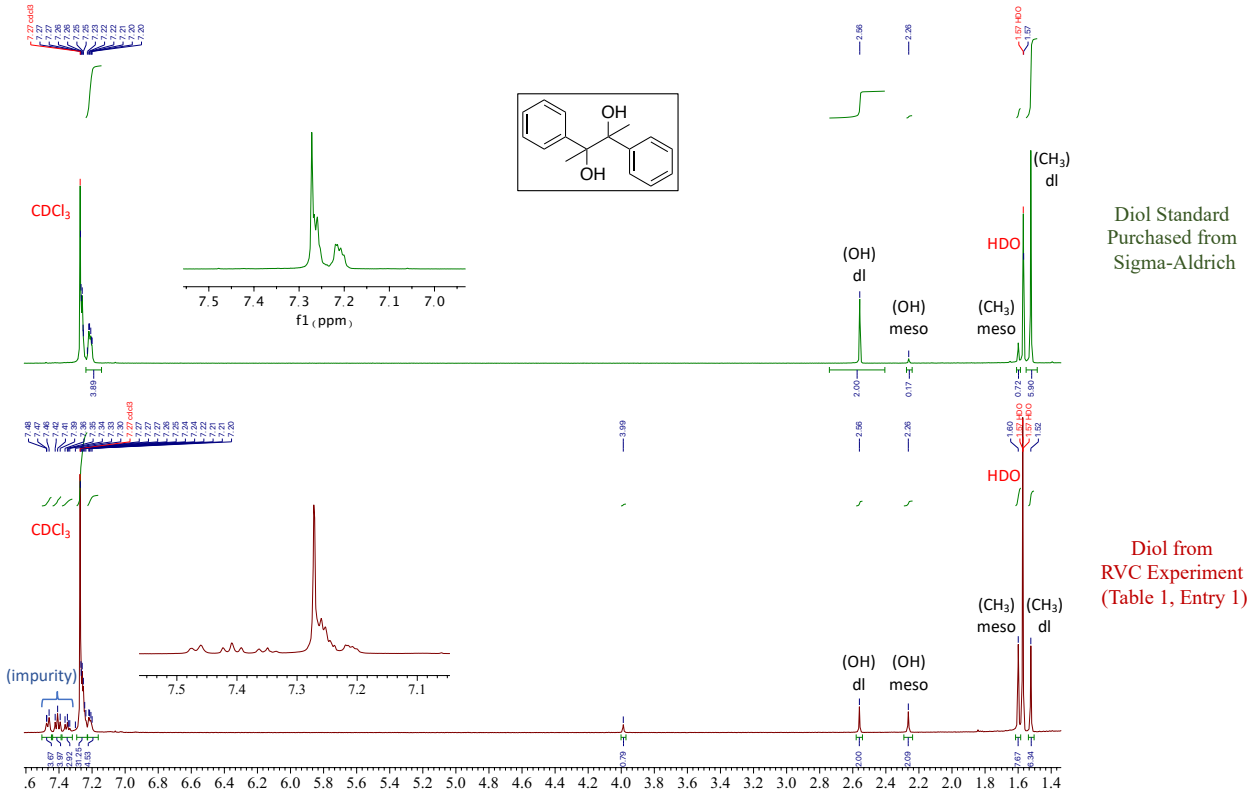

Figure 3.39 NMR Spectra of 2,3-diphenylbutane-2,3-diol; standard spectra of diol purchased from Sigma-Aldrich with mixtures of meso and dl diastereomers as labeled (Green Spectrum). 2,3-diphenylbutane-2,3-diol from cathodic reduction at 50 mA using RVC electrode (Red Spectra), both meso and dl were formed in the radical dimerization process with approximately 1:1 ratio.

Spectral data are also in accordance with those previously reported.[31] A small amount of unknown aromatic impurity accompanied the material isolated by column chromatography. Beside the cleavage product phenol, compounds in the red spectra are the largest spot in the thin-layer chromatography (Hexane/EtOAc 4:1).

3.9.4 Full ECH Kinetic Measurements for Alkyl Aryl Ethers

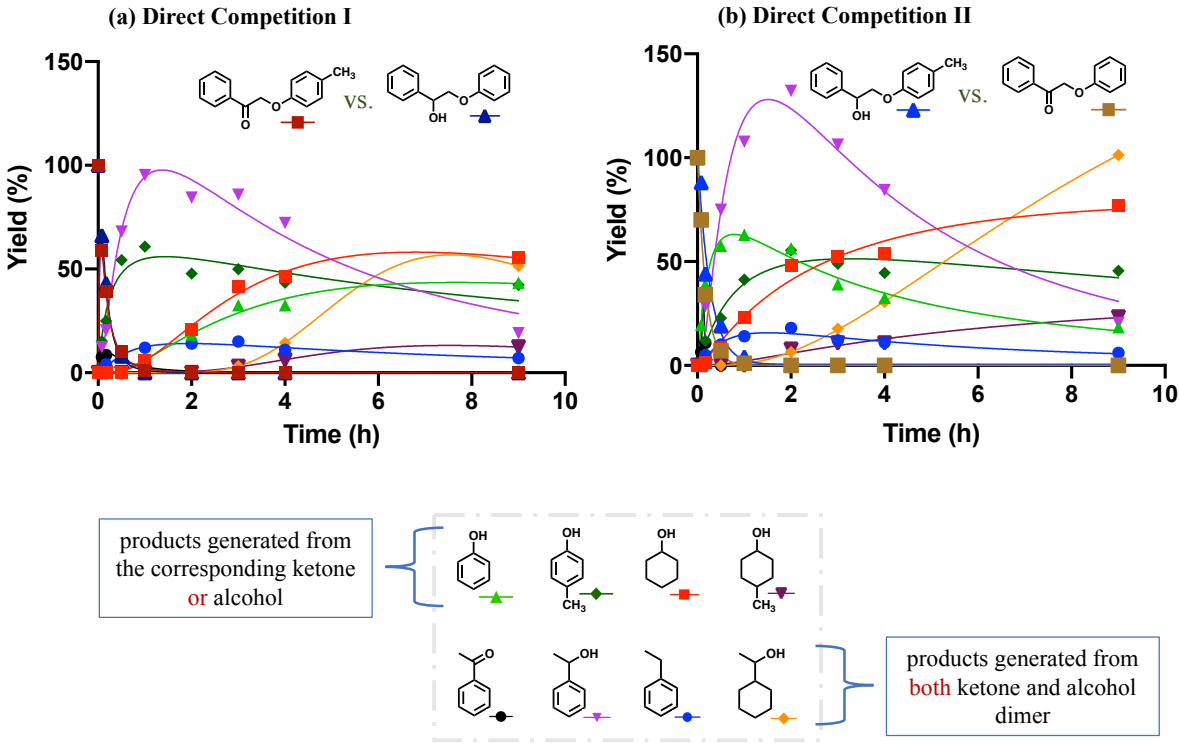

Figure 3.40 (a) Full kinetic measurement of direct competition of methyl labeled ketone model and unlabeled alcohol model. (b) Full kinetic measurement of direct competition of unlabeled ketone model and methyl labeled alcohol model. ECH performed at standard condition, 50 mA, 60 °C and IPA treated electrode with 33% v/v IPA.

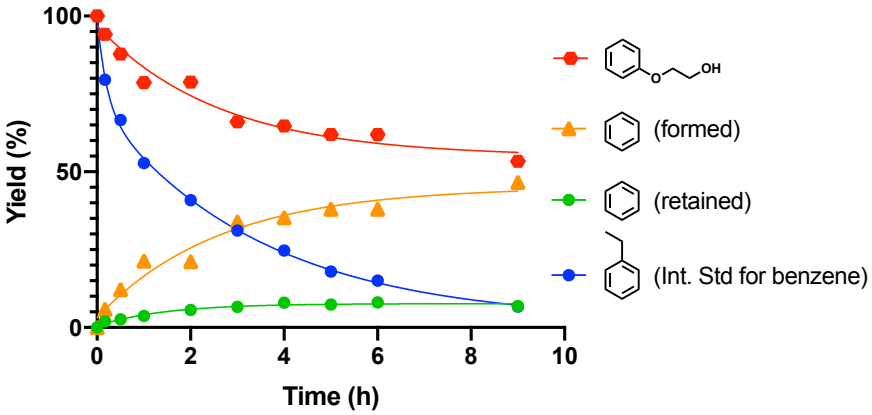

Figure 3.41 ECH measurement of 2-phenylethanol at standard condition, 50 mA, 60 °C and IPA treated electrode with 33% v/v IPA.

Note, ethylbenzene is used as the internal evaporation correction of benzene, but the evaporation rate of ethylbenzene is faster than the formation rate of benzene, thus cannot applied the correction. The amount of benzene that was detected and quantified by GC-MS was near 8% (green circles). The benzene that was formed (orange triangles) is from the subtraction of the remaining starting material 2-phenylethanol (red hexagons), no other product was observed. Though the ethylene glycol by product was expected, its high water solubility prevents its effective analysis in the organic extracts from these reactions.

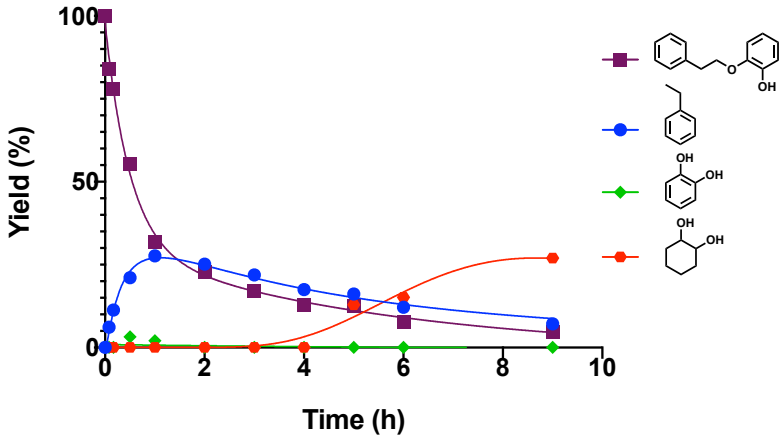

Figure 3.42 ECH measurement of 2-(2-phenylethoxy)phenol at standard condition, 50 mA, 60 °C and IPA treated electrode with 33% v/v IPA. 1,2-dihydroxycyclohexane yield was corrected by extraction losses.

No yield corrections were applied for the dimer 2-(2-phenylethoxy)phenol, ethylbenzene and catechol. The formed amount of catechol and ethylbenzene were higher than the reported numbers. Note, two different extraction solvents (dichloromethane and ethyl acetate) were used, 2-(2-phenylethoxy)phenol, ethylbenzene and 1,2-dihydroxycyclohexane were quantified from the dichloromethane extraction. Due to the high solubility of catechol in the aqueous buffer mixture, ethyl acetate extraction only captured trace amounts of catechol. Both extractions were performed according to the standard procedure described in the analyzation section.

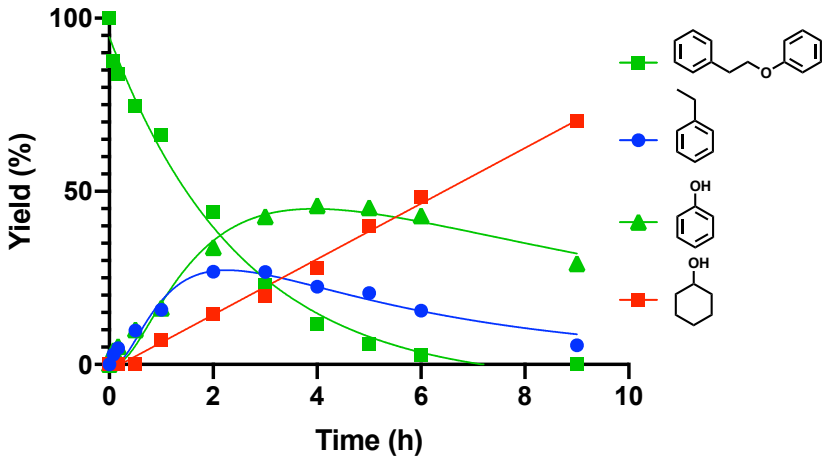

Figure 3.43 ECH measurement of 1-phenyl-2-phenoxyethane at standard condition, 50 mA, 60 °C and IPA treated electrode with 33% v/v IPA.

The yield of phenol was corrected for extraction losses. The yield of cyclohexanol was corrected for evaporation. No yield corrections were applied on 2-phenoxy-1-phenyl ethane and ethylbenzene.

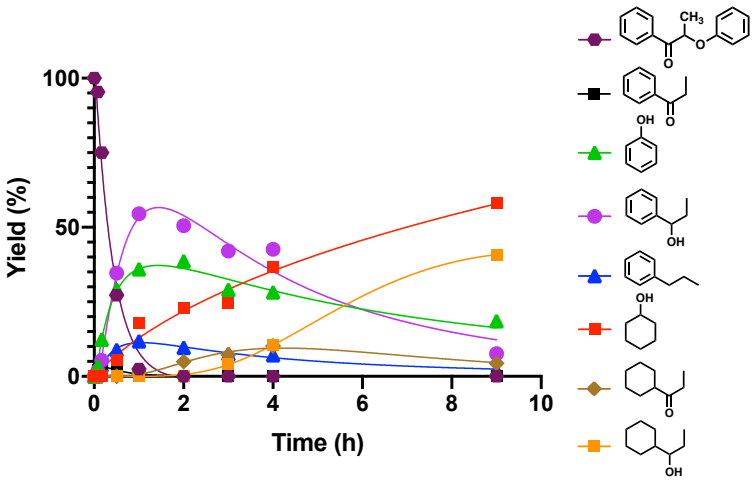

Figure 3.44 ECH measurement of 2-phenoxy-1-phenylpropanone at standard condition, 50 mA, 60 °C and IPA treated electrode with 33% v/v IPA.

The yield of phenol was corrected for extraction losses. The yield of cyclohexanol was corrected for evaporation. The yield of 1-phenylpropanone was corrected using the extraction efficiency of acetophenone. The yield of 1-phenylpropanol was corrected using the extraction efficiency of 1-phenylethanol. The yield of 1-cyclohexylpropanol was corrected using the evaporation curve of 1-cyclohexylethanol. No yield correction was applied on 2-phenoxy-1-phenylpropanone and propylbenzene.

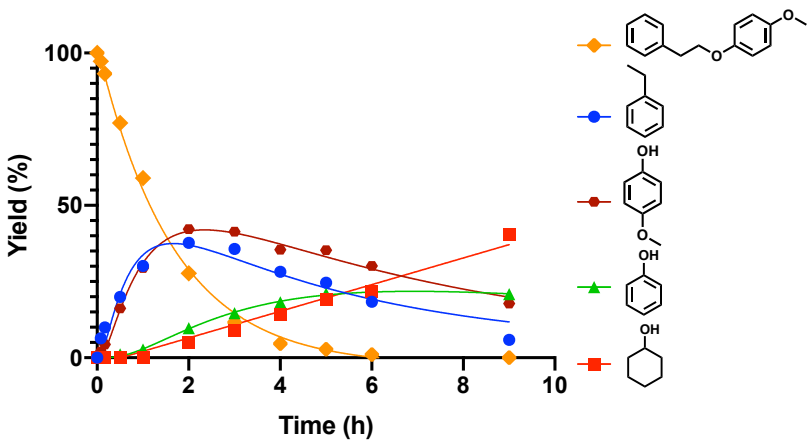

Figure 3.45 ECH measurement of 1-methoxy-4-(2-phenylethoxy)benzene at standard condition, 50 mA, 60 °C and IPA treated electrode with 33% v/v IPA.

The yield of phenol was corrected for extraction losses. The yield of cyclohexanol was corrected for evaporation. The yield of 4-methoxyphenol was corrected for the extraction losses. No yield correction was applied on 1-methoxy-4-(2-phenylethoxy)benzene and ethylbenzene.

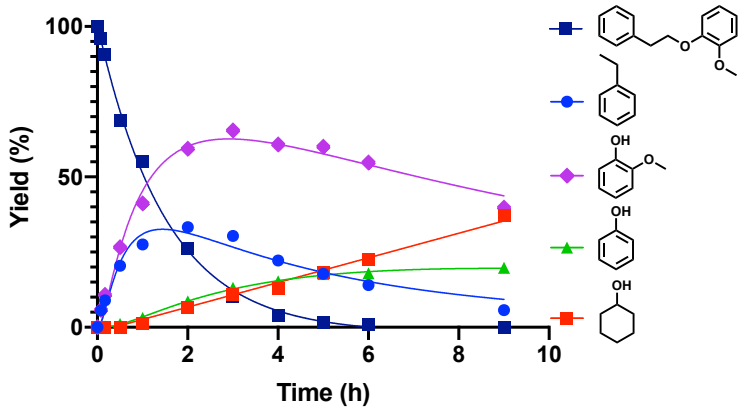

Figure 3.46 ECH measurement of 1-methoxy-2-(2-phenylethoxy)benzene at standard conditions, 50 mA, 60 °C and IPA treated electrode with 33% v/v IPA.

The yield of phenol was corrected for extraction losses. The yield of cyclohexanol was corrected for evaporation. The yield of 2-methoxyphenol was corrected for the extraction losses. No yield correction was applied on 1-methoxy-2-(2-phenylethoxy)benzene and ethylbenzene.

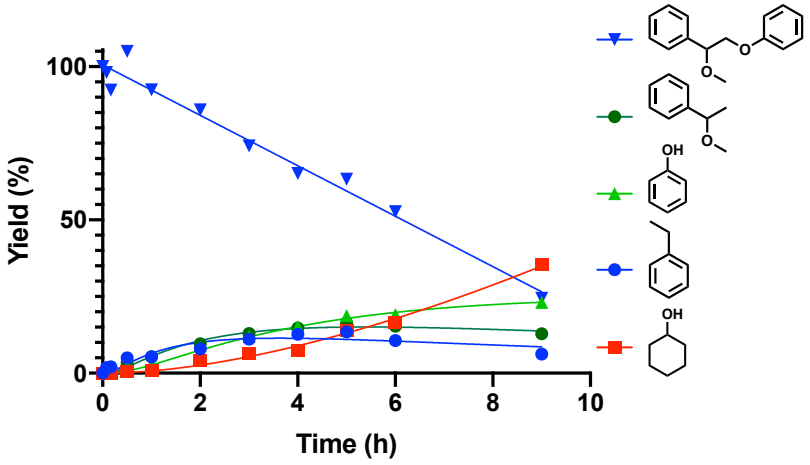

Figure 3.47 ECH measurement of 2-methoxy-1-phenoxy-2-phenylethane at standard conditions, 50 mA, 60 °C and IPA treated electrode with 33% v/v IPA.

The yield of phenol was corrected for extraction losses. The yield of cyclohexanol was corrected for evaporation losses. No yield corrections were applied on 2-methoxy-1-phenoxy-2-phenylethane, 1-methoxyphenylethane and ethylbenzene.

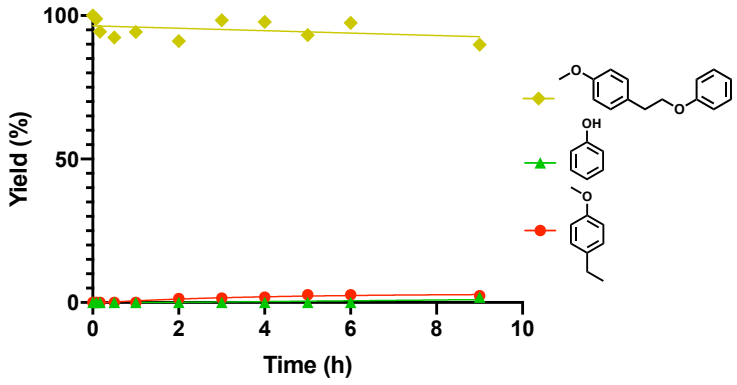

Figure 3.48 ECH measurement of 1-methoxy-4-(2-phenoxyethyl)benzene at standard condition, 50 mA, 60 °C and IPA treated electrode with 33% v/v IPA. Less than 3% cleavage product was observed.

No yield corrections were applied in the substrate and products.

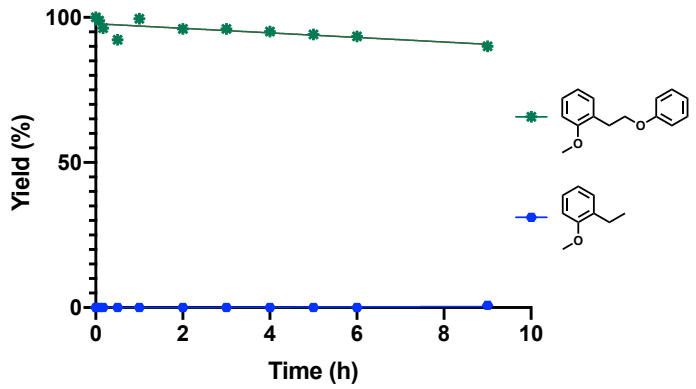

Figure 3.49 ECH measurement of 1-methoxy-2-(2-phenoxyethyl)benzene at standard condition, 50 mA, 60 °C and IPA treated electrode with 33% v/v IPA. Less than 2% cleavage product was observed.

No yield corrections were applied in the substrate and products.

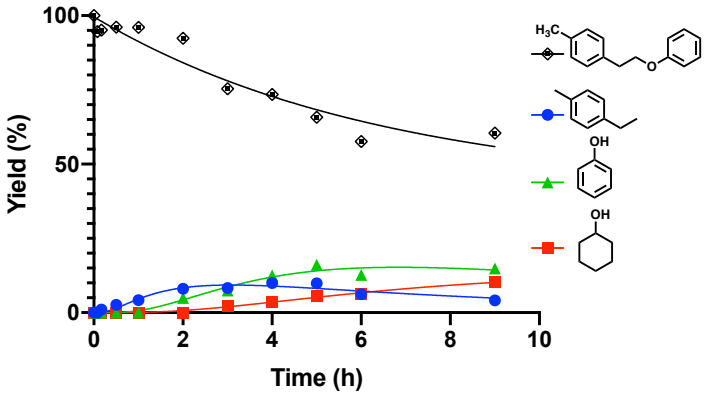

Figure 3.50 ECH measurement of 1-methyl-4-(2-phenoxyethyl)benzene at standard conditions, 50 mA, 60 °C and IPA treated electrode with 33% v/v IPA.

The yield of phenol was corrected for extraction losses. The yield of cyclohexanol was corrected for evaporation losses. No yield corrections were applied on 4-ethyltoluene and substrate.

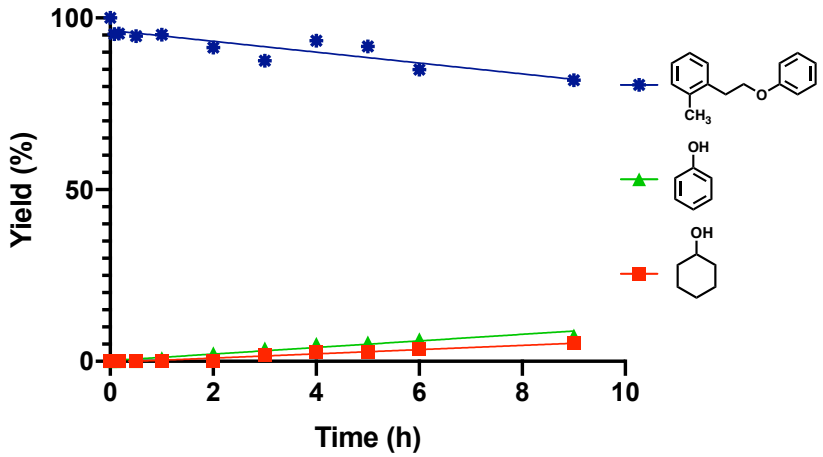

Figure 3.51 ECH measurement of 1-methyl-2-(2-phenoxyethyl)benzene at standard conditions, 50 mA, 60 °C and IPA treated electrode with 33% v/v IPA.

The yield of phenol was corrected for extraction losses. The yield of cyclohexanol was corrected for evaporation losses. No yield correction was applied on substrate.

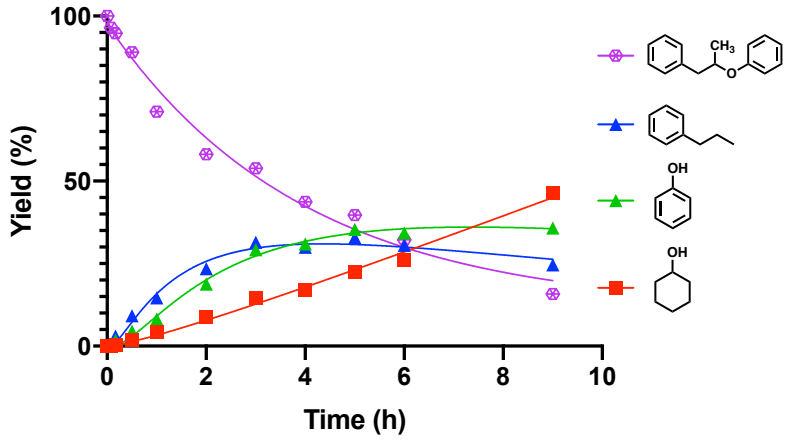

Figure 3.52 ECH measurement of 2-(phenoxypropyl)benzene at standard conditions, 50 mA, 60 °C and IPA treated electrode with 33% v/v IPA.

The yield of phenol was corrected for extraction losses. The yield of cyclohexanol was corrected for evaporation losses. No yield corrections were applied on propylbenzene and substrate.

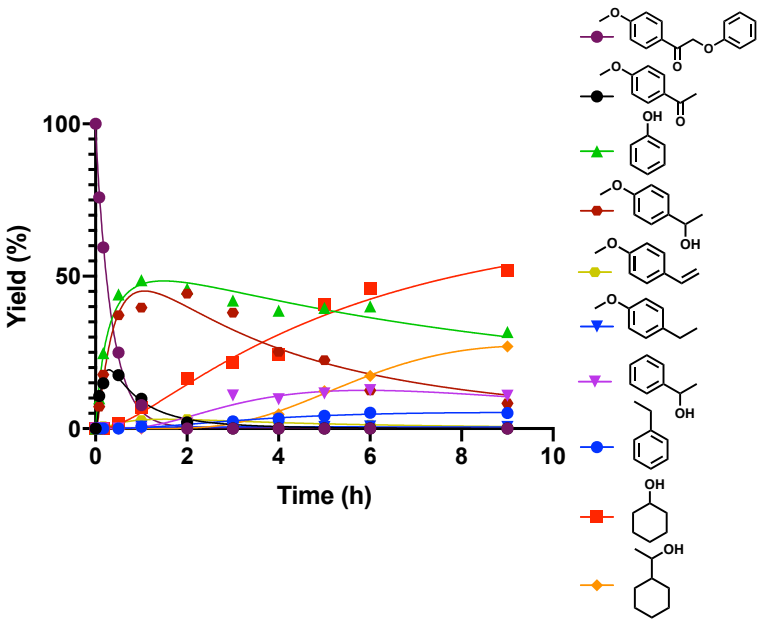

Figure 3.53 ECH measurement of 1-(4-methoxyphenyl)-2-phenoxyethanone at standard condition, 50 mA, 60 °C and IPA treated electrode with 33% v/v IPA.

The yield of phenol and 1-phenylethanol were corrected for extraction losses. The yield of cyclohexanol and 1-cyclohexylethanol were corrected for evaporation losses. The yield of 4-methoxyacetophenone was corrected using the extraction efficiency of acetophenone. The yield of 4-methoxyphenylethanol was corrected using the extraction efficiency of 1-phenylethanol. No yield correction was applied on 1-(4-methoxyphenyl)-2-phenoxyethanone, ethylbenzene, 4-methoxystyrene and 4-ethylanisole.

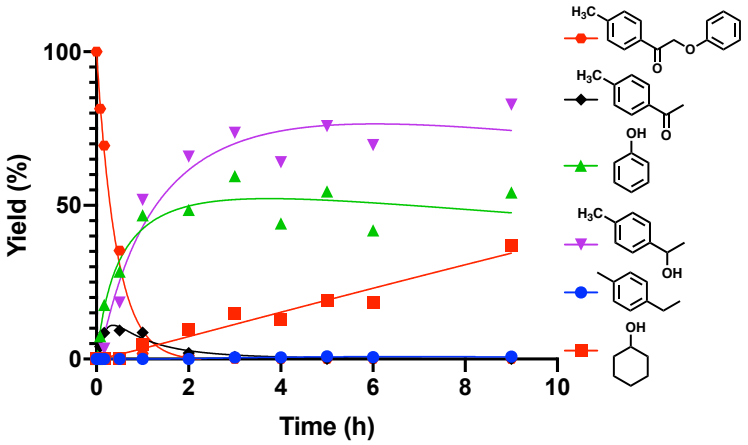

Figure 3.54 ECH measurement of 1-(4-methylphenyl)-2-phenoxyethanone at standard condition, 50 mA, 60 °C and IPA treated electrode with 33% v/v IPA.

The yield of phenol was corrected for extraction losses. The yield of cyclohexanol was corrected for evaporation losses. The yield of 4-methylacetophenone was corrected using the extraction efficiency of acetophenone. The yield of 4-methylphenylethanol was corrected using the extraction efficiency of 1-phenylethanol. No yield correction was applied on 1-(4-methylphenyl)-2-phenoxyethanone and 4-ethyltoluene.

REFERENCES

REFERENCES

1. Lam, C. H.; Das, S.; Erickson, N. C.; Hyzer, C. D.; Garedew, M.; Anderson, J. E.; Wallington, T. J.; Tamor, M. A.; Jackson, J. E.; Saffron, C. M., Towards sustainable hydrocarbon fuels with biomass fast pyrolysis oil and electrocatalytic upgrading. *Sustainable Energy & Fuels* **2017,** *1* (2), 258-266.

2. Cox, P. M.; Betts, R. A.; Jones, C. D.; Spall, S. A.; Totterdell, I. J., Acceleration of global warming due to carbon-cycle feedbacks in a coupled climate model. *Nature* **2000,** *408* (6809), 184-187.

3. Boerjan, W.; Ralph, J.; Baucher, M., Lignin biosynthesis. *Annual Review of Plant Biology* **2003,** *54*, 519-546.

4. Crestini, C.; Melone, F.; Sette, M.; Saladino, R., Milled Wood Lignin: A Linear Oligomer. *Biomacromolecules* **2011,** *12* (11), 3928-3935.

5. Isikgor, F. H.; Becer, C. R., Lignocellulosic biomass: a sustainable platform for the production of bio-based chemicals and polymers. *Polymer Chemistry* **2015,** *6* (25), 4497-4559.

6. Karkas, M. D.; Matsuura, B. S.; Monos, T. M.; Magallanes, G.; Stephenson, C. R. J., Transition-metal catalyzed valorization of lignin: the key to a sustainable carbon-neutral future. *Organic & Biomolecular Chemistry* **2016,** *14* (6), 1853-1914.

7. Schutyser, W.; Renders, T.; Van den Bosch, S.; Koelewijn, S. F.; Beckham, G. T.; Sels, B. F., Chemicals from lignin: an interplay of lignocellulose fractionation, depolymerisation, and upgrading. *Chemical Society Reviews* **2018,** *47* (3), 852-908.

8. Xu, C. P.; Arancon, R. A. D.; Labidi, J.; Luque, R., Lignin depolymerisation strategies: towards valuable chemicals and fuels. *Chemical Society Reviews* **2014,** *43* (22), 7485-7500.

9. Zakzeski, J.; Bruijnincx, P. C. A.; Jongerius, A. L.; Weckhuysen, B. M., The Catalytic Valorization of Lignin for the Production of Renewable Chemicals. *Chemical Reviews* **2010,** *110* (6), 3552-3599.

10. Amiri, M. T.; Dick, G. R.; Questell-Santiago, Y. M.; Luterbacher, J. S., Fractionation of lignocellulosic biomass to produce uncondensed aldehyde-stabilized lignin. *Nature Protocols* **2019,** *14* (3), 921-954.

11. Shuai, L.; Amiri, M. T.; Questell-Santiago, Y. M.; Heroguel, F.; Li, Y. D.; Kim, H.; Meilan, R.; Chapple, C.; Ralph, J.; Luterbacher, J. S., Formaldehyde stabilization facilitates lignin monomer production during biomass depolymerization. *Science* **2016,** *354* (6310), 329-333.

12. Deuss, P. J.; Scott, M.; Tran, F.; Westwood, N. J.; de Vries, J. G.; Barta, K., Aromatic Monomers by in Situ Conversion of Reactive Intermediates in the Acid-Catalyzed

Depolymerization of Lignin. *Journal of the American Chemical Society* **2015,** *137* (23), 7456-7467.

13. Wang, M.; Zhang, X. C.; Li, H. J.; Lu, J. M.; Liu, M. J.; Wang, F., Carbon Modification of Nickel Catalyst for Depolymerization of Oxidized Lignin to Aromatics. *ACS Catalysis* **2018,** *8* (2), 1614-1620.

14. Zhang, C. F.; Li, H. J.; Lu, J. M.; Zhang, X. C.; MacArthur, K. E.; Heggen, M.; Wang, F., Promoting Lignin Depolymerization and Restraining the Condensation via an Oxidation-Hydrogenation Strategy. *ACS Catalysis* **2017,** *7* (5), 3419-3429.

15. Rahimi, A.; Ulbrich, A.; Coon, J. J.; Stahl, S. S., Formic-acid-induced depolymerization of oxidized lignin to aromatics. *Nature* **2014,** *515* (7526), 249-252.

16. Garedew, M.; Young-Farhat, D.; Jackson, J. E.; Saffron, C. M., Electrocatalytic Upgrading of Phenolic Compounds Observed after Lignin Pyrolysis. *ACS Sustainable Chemistry & Engineering* **2019,** *7* (9), 8375-8386.

17. Sergeev, A. G.; Webb, J. D.; Hartwig, J. F., A Heterogeneous Nickel Catalyst for the Hydrogenolysis of Aryl Ethers without Arene Hydrogenation. *Journal of the American Chemical Society* **2012,** *134* (50), 20226-20229.

18. Klinger, G. E. *et al.* Biomimetic Reductive Cleavage of Keto Aryl Ether Bonds by Small-Molecule Thiols. *ChemSusChem*, **12**, 4775-4779 (2019).

19. Sergeev, A. G.; Hartwig, J. F., Selective, Nickel-Catalyzed Hydrogenolysis of Aryl Ethers. *Science* **2011,** *332* (6028), 439-443.

20. Chan, J. M. W.; Bauer, S.; Sorek, H.; Sreekumar, S.; Wang, K.; Toste, F. D., Studies on the Vanadium-Catalyzed Nonoxidative Depolymerization of Miscanthus giganteus-Derived Lignin. *ACS Catalysis* **2013,** *3* (6), 1369-1377.

21. Nichols, J. M.; Bishop, L. M.; Bergman, R. G.; Ellman, J. A., Catalytic C-O Bond Cleavage of 2-Aryloxy-1-arylethanols and Its Application to the Depolymerization of Lignin-Related Polymers. *Journal of the American Chemical Society* **2010,** *132* (36), 12554-12555.

22. He, J. Y.; Zhao, C.; Lercher, J. A., Ni-Catalyzed Cleavage of Aryl Ethers in the Aqueous Phase. *Journal of the American Chemical Society* **2012,** *134* (51), 20768-20775.

23. Bulut, S.; Siankevich, S.; van Muyden, A. P.; Alexander, D. T. L.; Savoglidis, G.; Zhang, J. G.; Hatzimanikatis, V.; Yan, N.; Dyson, P. J., Efficient cleavage of aryl ether C-O linkages by Rh-Ni and Ru-Ni nanoscale catalysts operating in water. *Chemical Science* **2018,** *9* (25), 5530-5535.

24. Lam, C. H.; Lowe, C. B.; Li, Z. L.; Longe, K. N.; Rayburn, J. T.; Caldwell, M. A.; Houdek, C. E.; Maguire, J. B.; Saffron, C. M.; Miller, D. J.; Jackson, J. E., Electrocatalytic upgrading of

model lignin monomers with earth abundant metal electrodes. *Green Chemistry* **2015,** *17* (1), 601-609.

25. Hao, P., Electrocatalytic Hydrogenation of Monomeric, Dimeric, and Polymeric Lignin Model Compounds with Raney Nickel: Chemistry, Mechanistic, and Product Toxicity Studies. Michigan State University, East Lansing, MI, 2018.

26. Mahdavi, B.; Lafrance, A.; Martel, A.; Lessard, J.; Menard, H.; Brossard, L., Electrocatalytic hydrogenolysis of lignin model dimers at Raney nickel electrodes. *Journal of Applied Electrochemistry* **1997,** *27* (5), 605-611.

27. Andersen, M. L.; Mathivanan, N.; Wayner, D. D. M., Electrochemistry of electron-transfer probes. The role of the leaving group in the cleavage of radical anions of alpha-aryloxyacetophenones. *Journal of the American Chemical Society* **1996,** *118* (20), 4871-4879.

28. Barba, F.; Velasco, M. D.; Guirado, A., Cathodic reduction of phenacyl bromide. *Electrochimica Acta* **1983,** *28* (2), 259-260.

29. Nakahara, K.; Naba, K.; Saitoh, T.; Sugai, T.; Obata, R.; Nishiyama, S.; Einaga, Y.; Yamamoto, T., Electrochemical Pinacol Coupling of Acetophenone Using Boron-Doped Diamond Electrode. *ChemElectroChem* **2019,** *6* (16), 4153-4157.

30. Galkin, M. V.; Dahlstrand, C.; Samec, J. S. M., Mild and Robust Redox-Neutral Pd/C-Catalyzed Lignol -O-4 Bond Cleavage Through a Low-Energy-Barrier Pathway. *ChemSusChem* **2015,** *8* (13), 2187-2192.

31. Steiner, A.; Williams, J. D.; Rincon, J. A.; de Frutos, O.; Mateos, C.; Kappe, C. O., Implementing Hydrogen Atom Transfer (HAT) Catalysis for Rapid and Selective Reductive Photoredox Transformations in Continuous Flow. *European Journal of Organic Chemistry* **2019,** *2019* (33), 5807-5811.

Chapter 4. Mechanistic Investigation of Diaryl Ether Cleavage via Aqueous Electrocatalytic Hydrogenation (ECH) over Skeletal Nickel*

In this chapter, experimental mechanistic studies of diaryl ethers undergoing electrocatalytic hydrogenolysis (ECH) over skeletal Ni cathodes were reported. Initial studies of the parent DPE revealed that ether cleavage occurs prior to phenyl ring hydrogenation. Comparisons were then pursued among four functionalized DAEs—diphenyl ether, 4-phenoxyanisole, 4-phenoxytoluene and 4-phenoxyphenol—together with their reaction products. Based on the combined results of rate comparisons, substituent electronic and positional studies, isotope labeling experiments, and regioselectivity investigations, two distinct mechanisms for C-O cleavage were established for the four representative functionalized substrates. Extension to ortho- and meta- substituted analogues, and analysis of the effects of a suite of additional substituents revealed their impacts on the rates and selectivities of aryl C-O bond cleavage, and also uncovered the activation of various functional groups (CH_3, CF_3) commonly seen as unreactive. The mechanistic insights obtained also uncovered conditions in which the strong sp^2 C-O ether bond could be cleaved without over reduction of the monomeric phenolic products.

4.1 Introduction

General, low-cost methods and well-defined mechanisms for diaryl ether (DAE) cleavage remain an outstanding challenge with importance both in biomass utilization and in pollution mitigation. Tools to break down plant matter, with its diaryl ether-rich lignin, are needed to supply renewable replacements for fossil carbon building blocks. Meanwhile, the rapid growth and

*This chapter is adapted from Zhou, Y. T.; Klinger, G. E.; Hegg, E. L.; Saffron, C. M.; Jackson, J. E., Electrocatalytic Hydrogenolysis (ECH) of Diaryl Ethers Over Skeletal Ni: C-O Cleavage Occurs by Direct Elimination via Benzyne Intermediates. Submitted to *Nature Commun.* **2021**.

expanding usage of agrochemicals that include DAE moieties is drawing attention to their persistence and impacts as emerging contaminants.[1-3]

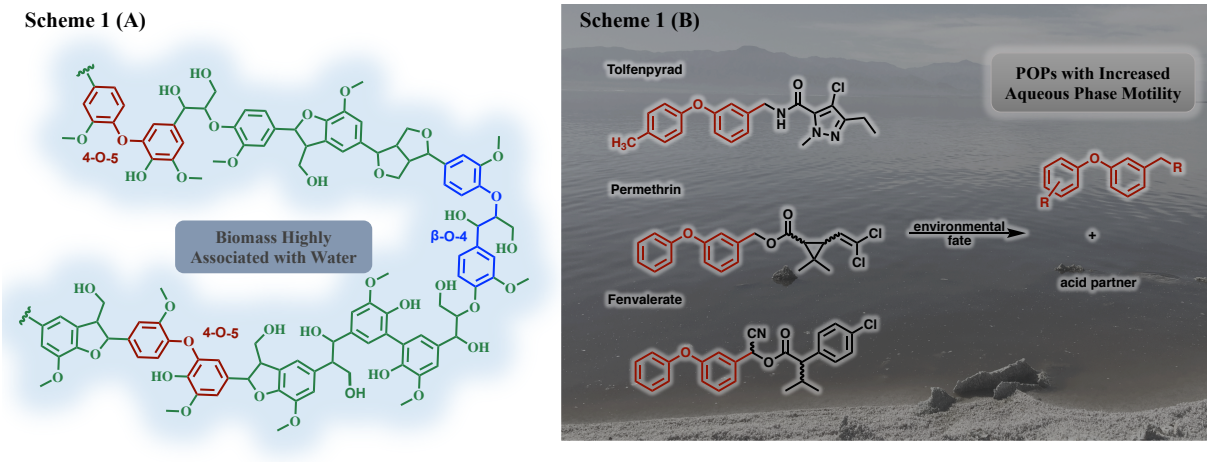

Figure 4.1 (A) Lignin structure, highlighting diphenyl ether linkage (4-O-5) (B) POPs with increased mobility from environmental degradation of widely used agrochemicals.

To cleave lignin's most common linkage, the sp^3 C-O bond of the β-O-4 aryl alkyl ether (Figure 4.1a, highlighted in blue), various strategies have been devised, such as oxidatively activated reductive cleavage,[4-8] protection reduction schemes,[9-11] and photochemical degradation.[12, 13] But the second most common linkage, the 4-O-5 ether (Figure 4.1 a, highlighted in red) has received less attention, perhaps because its diaryl ether C-O bonds are among the strongest in the lignin polymer (c.f. the 86 kcal/mol bond C-O dissociation energy of diphenyl ether).[14]

Diaryl ether substructures are also important in recently developed agrochemicals,[15] endowing them with outstanding hydrophobicity, lipophilicity, cell wall penetration, and resistance to degradation.[15, 16] However, unlike their hydrophilic sidechains, the DAE headgroups in these products resist environmental breakdown (Figure 4.1b),[17] accumulating as persistent organic pollutants (POPs) in surface and ground waters.[3, 18-20] For example, of the reported

environmental fates of tolfenpyrad, recently approved for usage in the US, none successfully breaks down the DAE moiety.[20, 21,22]

Some homogeneous catalytic DAE hydrogenolysis reactions show good selectivity and reduction control. However, those so far reported also require inert organic solvents, not readily compatible with the non-inert natural environments of the above described DAE substrates.[23-27] On the other hand, their molecular, homogeneous conditions typically allow detailed mechanistic studies.

Heterogeneous catalysis offers potentially greater compatibility with the complexity of biomass, especially the associated water. However, to cleave the strong sp^2 C-O bonds in DAEs, classic hydrogenation methods commonly run at high pressure (40-65 bar) and temperature (200-300 °C) reaction conditions.[28-30] Some milder hydrogenolyses have been developed, mostly requiring precious metals (Pd[31], Rh[32], Ru[31, 32], Pt[33]), but improved conditions (120-150 °C; 6-12 bar H_2) with Ni nanoparticles have recently been reported.[34, 35] Nonetheless, two issues remain: (a) these robust but severe heterogeneous catalytic DAE cleavage reactions show low selectivity, with ring saturation of the phenolic products hard to avoid; and (b) most reports have focused on diphenyl ether (DPE) alone, whereas the DAE scaffolds noted above carry various functionalities.[15]

The surprisingly large effects of substituents on both reactivity and C-O bond cleavage selectivity in DAE cleavage are explored here, building on our own background in the development of electrocatalytic organic reductions over skeletal nickel catalysts.[36-39] In the present work, aqueous phase electrocatalytic hydrogenolyses (ECH) with earth abundant skeletal Ni cathodes at 60 °C and ambient pressure are applied to a diverse slate of DAE substrates. By forming the active hydrogen species by proton reduction on the catalyst surface (reflected by

bubbles evolving from the cathode), ECH avoids the hazards of handling H_2 gas, the limitations of H_2 solubility and transport in aqueous solvent, and the kinetic barrier to H_2 dissociation. However, the structural complexity of the skeletal metal and the three-phase (solid, liquid, gas) nature of phenomena there prevent the use of surface spectroscopies or credible quantum chemical simulations[39, 40] to probe substrate-catalyst interactions. Consequently, our mechanistic investigations center on substituent effects beyond the parent DPE case,[34, 41] reaction rates, selectivities, isotopic labeling, and solvent and inhibition studies to understand the aryl ether C-O reductive electrocatalytic hydrogenolysis processes.

4.2 Mapping the cleavage mechanism of diphenyl ether

4.2.1 The C-O Bond in Diphenyl Ether is Directly Cleaved Without Ring Hydrogenation

Electrocatalytic hydrogenolysis (ECH) of DPE produced benzene and cyclohexanol (Figure 4.2). Two potential routes to these products can be envisioned for the cleavage process. In Route A, DPE is directly cleaved to benzene and phenol. Phenol then undergoes fast ring saturation

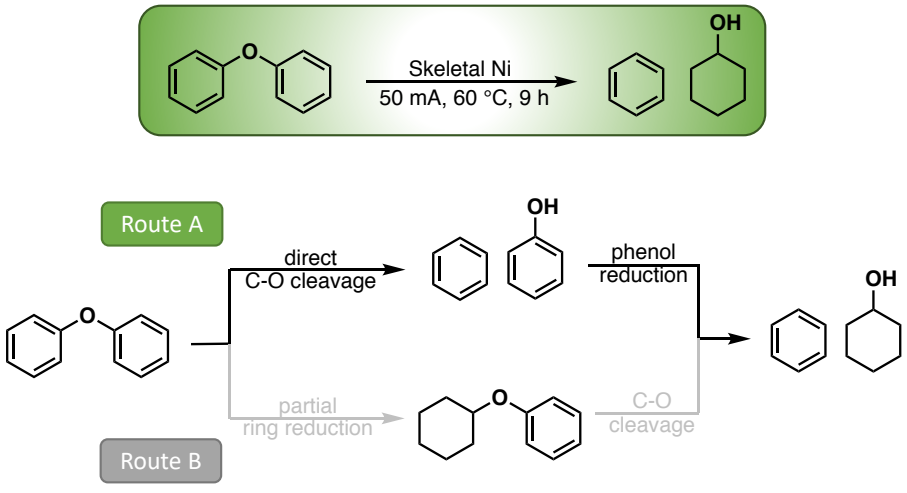

Figure 4.2 Two cleavage pathways of diphenyl ether

to generate cyclohexanol. In Route B, one of the phenyl rings first undergoes ring hydrogenation, converting it into cyclohexyl phenyl ether; C-O cleavage then gives benzene and cyclohexanol.

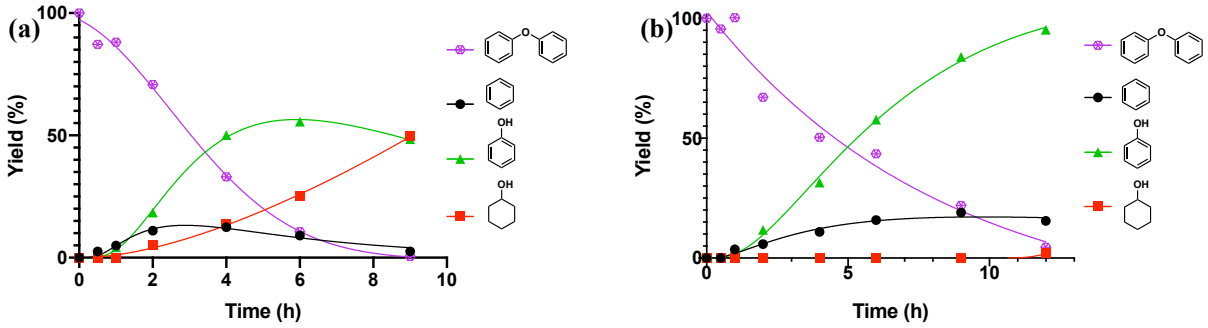

Figure 4.3 (a) Electrocatalyzed hydrogenation (ECH) of diphenyl ether over a skeletal nickel electrode at 50 mA (current density 8 mA/cm^2) in the aqueous mixture of pH 8 borate buffer/IPA (2:1) at 60 °C under ambient pressure (Standard Condition) (b) ECH of diphenyl ether under std. cond. in mixture of buffer/IPA/acetone (40:17:3).

To determine which of paths A or B is preferred, the reaction time sequences were analyzed. As shown in Figure 4.3a, ECH of DPE formed benzene and phenol, with a slower buildup of cyclohexanol. The high hydrophobicity and high vapor pressure of benzene made it difficult to retain in the 60 °C polar aqueous phase. Importantly, however, neither cyclohexane nor cyclohexyl phenyl ether were detected. Importantly, if the latter aryl alkyl ether product were indeed formed, it would not be expected to cleave to cyclohexanol and benzene; other simple alkyl phenyl ethers such as anisole are unreactive under these conditions. These findings rule out route B, consistent

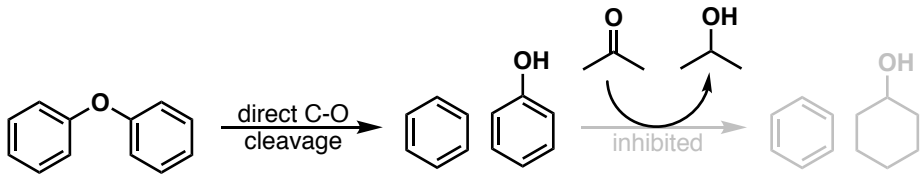

Figure 4.4 Ring reduction inhibited by acetone reduction

with reports from Lercher and co-workers studying more classical catalytic hydrogenation/hydrogenolysis conditions.[34]

In a further test confirming the dominance of route A, a small amount (5%) of acetone was used as a co-solvent in the ECH of DPE under otherwise standard conditions (Figure 4.3b). Our previous study of 2-phenoxyacetophenone cleavage had found acetone to be an inhibitor of phenol ring reduction and explored its use to tune reduction selectivity (Figure 4.4).[39] As shown in Figure 3.3 b, addition of 5% acetone almost completely inhibited phenol reduction, with barely any cyclohexanol seen after 12 hours of continuous ECH at 50 mA. Thus, the direct cleavage pathway A is preferred; if partial or total ring reduction (Route B) preceded ether cleavage, in the presence of acetone as co-solvent, cyclohexanol should arise in parallel with phenol production.

4.2.2 Diphenyl Ether Undergoes Slow Isotope Exchange

To further probe the cleavage mechanism of DPE, isotope labeling experiments were performed. H/D exchange was conducted at 60 °C in a 2:1 mixture of D_2O and nondeuterated 2-propanol (IPA). As shown in Figure 4.5 a, the amount of exchange observed in DPE with discharged nickel catalyst after 12 hours was only ~8%. Exchange occurred ortho to the ether C-O bond, as shown by ^1H NMR (Figure 4.26). Under more vigorous reaction conditions using freshly activated Ni catalyst with applied current, the amount of isotope incorporation was still very low in the recovered DPE, as it was undergoing cleavage into benzene and phenol (Figure 4.28). This suggests that upon the activation of the benzene ring, forward reaction to cleave the C-O ether bond dominates over reversal that would scramble the ortho hydrogens with surface deuterium atoms.

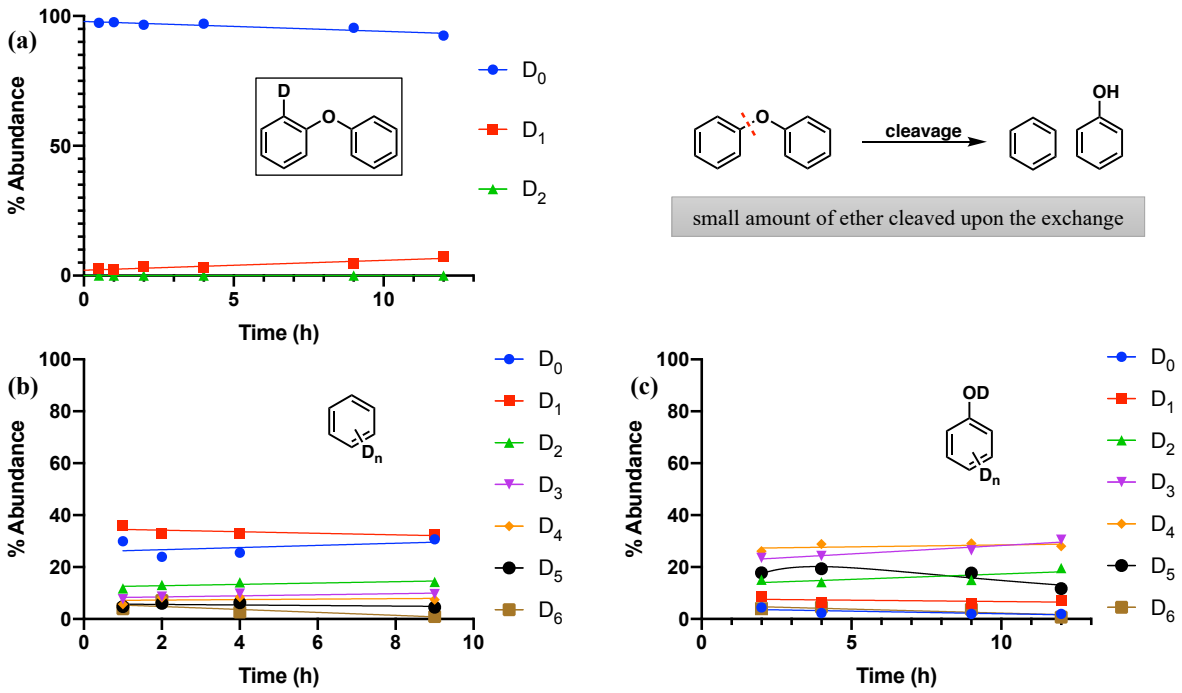

Figure 4.5 Quantified % abundance of D_n in (a) diphenyl ether and cleavage products (b) benzene and (c) phenol, as determined by GC-MS for (MS Spectra Fig. 4.24). The exchange locations in DPE were determined based on NMR evidence (Fig. 4.26). Experiment was run without current flowing, so only a small amount of diphenyl ether underwent cleavage during the exchange experiment.

The location of the H/D exchange suggested the possibility that ether bond cleavage might proceed via ipso-ortho addition of hydrogen and phenol elimination. As shown by the studies above, however, the activated ring of diphenyl ether is not reduced prior to the C-O cleavage. A more attractive alternative exchange pathway is reversible ortho-metallation of a C-H site, pointing to a benzyne pathway for ether cleavage (vide infra).

4.2.3 Proposed C-O Cleavage Mechanisms of Diphenyl Ether

On the basis of the above information, three different direct C-O cleavage mechanisms of diphenyl ether were proposed. In route I, double ring coordination allows ortho C-H insertion on the phenyl ring that is perpendicular to the catalytic surface (Figure 4.6, Route I). Elimination of

the vicinal phenoxide then forms a surface-bound benzyne intermediate, which is rapidly reduced to benzene by reaction with surface hydrogen atoms. This double ring coordination mechanism was proposed based on the appearance of di-deuterated benzene in the cleavage products formed in the H/D exchange experiments (Figure 4.5b). It explains not only the fast reduction of the phenol intermediates, but also the label distribution in the product, and the reaction's sensitivity to substituents (vide infra).

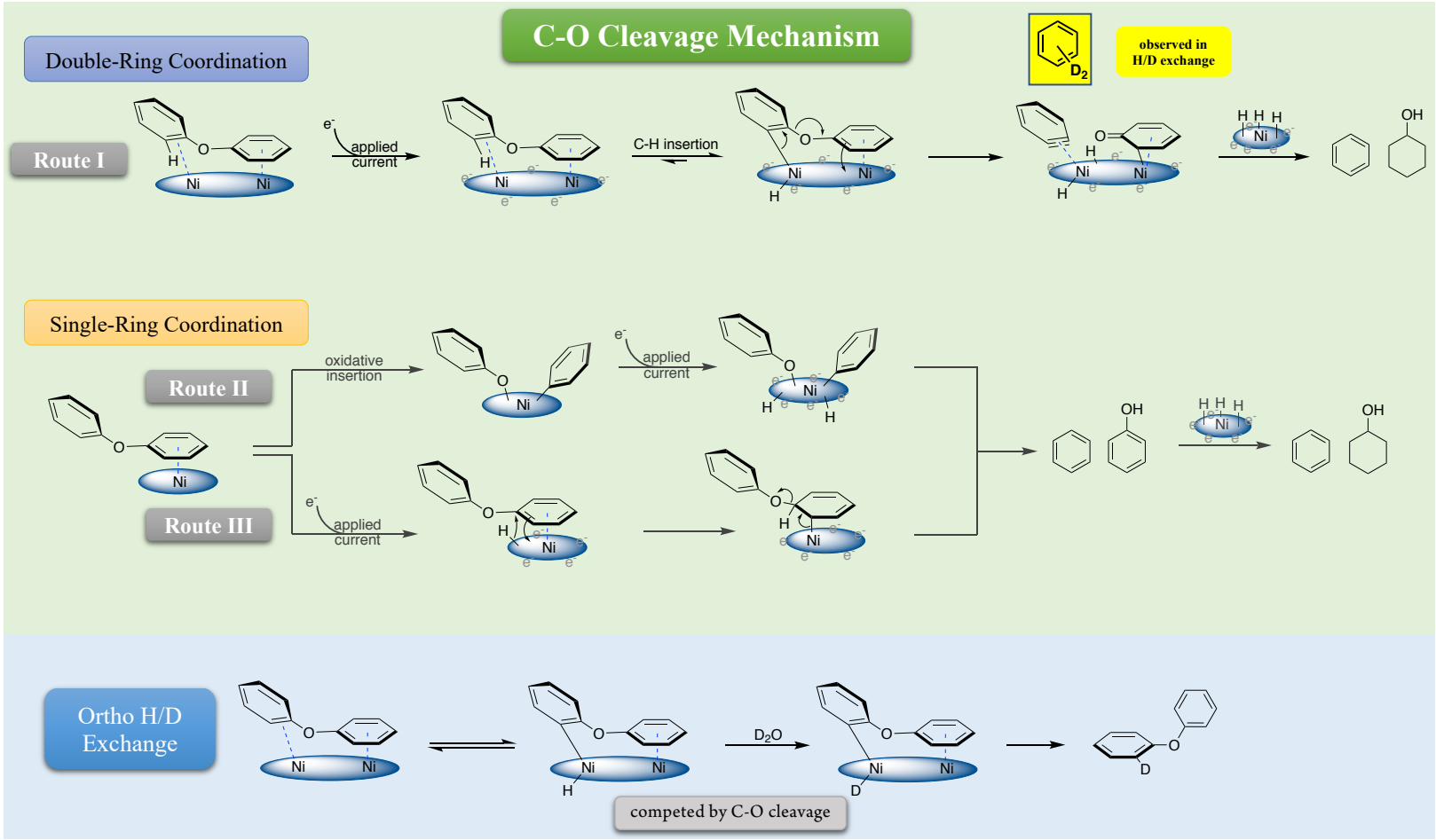

Figure 4.6 Proposed C-O cleavage and H/D exchange mechanisms of diphenyl ether

An alternative candidate cleavage via single ring activation is shown in route II (Figure 4.6). Here, with one of the phenyl rings coordinated to the catalyst, oxidative C-O insertion followed by reductive elimination with hydrogen could directly break the ether bond. This pathway has been demonstrated in several single metal (Ni) molecular catalysis studies, where the nickel center is spatially positioned and electronically modified by its ligand donor set.[27] Lastly, Route III, also beginning with single ring binding, would activate the phenyl ring by delivery of a surface-bound hydrogen atom to the ipso sp^2 carbon of the bound ring, followed by rearomatization of the coordinated ring via cleavage of the C-O bond. As presented in Figure 4.6, the major differences between routes I and II-III are at the ring activation step. To identify the preferred DAE cleavage mechanism, further time-course, substituent effect, and isotopic labeling studies were pursued.

Besides the proposed cleavage paths, Figure 4.6 also outlines a mechanism for the H/D exchange in DPE. In contrast to the fast C-O cleavage, the isotope incorporation is slow. Evidently, if the ortho carbon activation represents the first step in the cleavage process, the forward C-O cleavage predominates over the reverse process, replacing the original hydrogen with deuterium. For this exothermic hydrogenolysis (DPE + H_2 → benzene + phenol; exothermic by 11.6 kcal/mol),[14] presumably the increase in entropy and in solvation upon phenoxide elimination further favors C-O cleavage. Alternative exchange paths such as reversible hydrogenation involving the ortho carbon appear less likely, given the observed resistance of aryl ethers to hydrogenation. Addition would also lead to an anti-relationship between the bound Ni surface and the ortho C-H in the CHD site, complicating the release of the ortho hydrogen and retention of deuterium.

4.2.4 Cleavage Selectivities in DAEs Support Route I as the Main Cleavage Mechanism

A major difference among the above proposed cleavage routes I-III is in the ring activation steps (double vs. single). In fact, the two activations have opposite cleavage selectivity, the dual-ring coordination led to left C-O bond cleavage, and the single-ring coordination generated the right C-O bond cleavage. The symmetrical diphenyl ether could not fully differentiate the mechanisms, since any of the paths lead to the same products (benzene, phenol). However, with a substituent on one of the aryl rings, the different coordination modes would generate different cleavage products (Figure 4.7a).

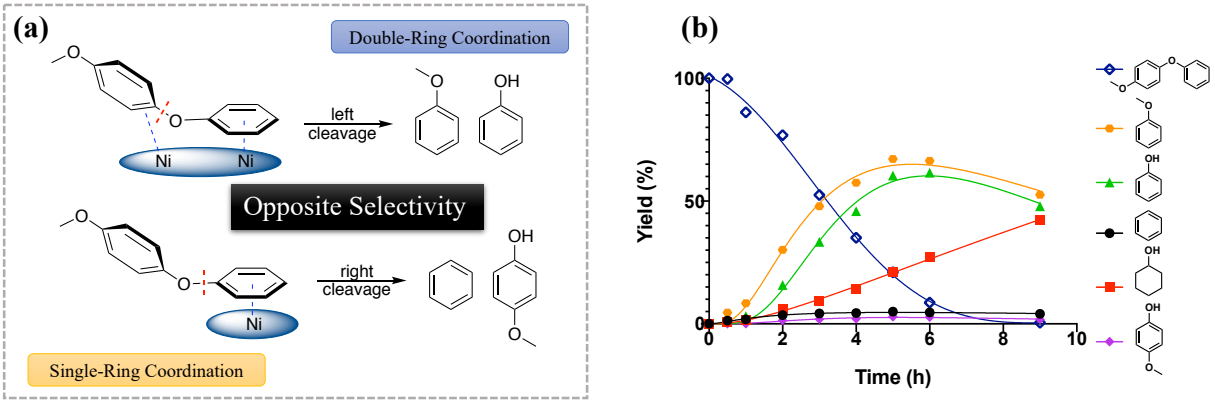

Figure 4.7 (a) Asymmetric diphenyl ethers differentiate the proposed cleavage mechanisms. (b) ECH of para-methoxylated diphenyl ether over skeletal nickel electrode under standard condition (50 mA, 60 °C, 33% v/v IPA).

As noted in our previous report on β-O-4 models, the negatively charged Ni electrode is poor at coordinating and reacting with aromatic rings bearing electron donating substituents such as the methoxy functionality.[39] In this vein, reaction of bis-(4-methoxyphenyl) ether was extremely sluggish (for details, see Figure 4.82). Therefore, 4-phenoxyanisole, the singly para-methoxylated DPE was synthesized and its cleavage regioselectivity was examined. As shown in Figure 4.7b, this substrate was cleaved completely within 7 hours, giving anisole and phenol as the major

cleavage products, consistent with the two-ring coordination mechanism (Figure 4.6, Route I). This cleavage result (anisole and phenol) is also opposite to those seen in previous reports interpreted in terms of oxidative insertion (Route II).[25, 27] Further support for Route I is found in the H/D exchange results (vide infra).

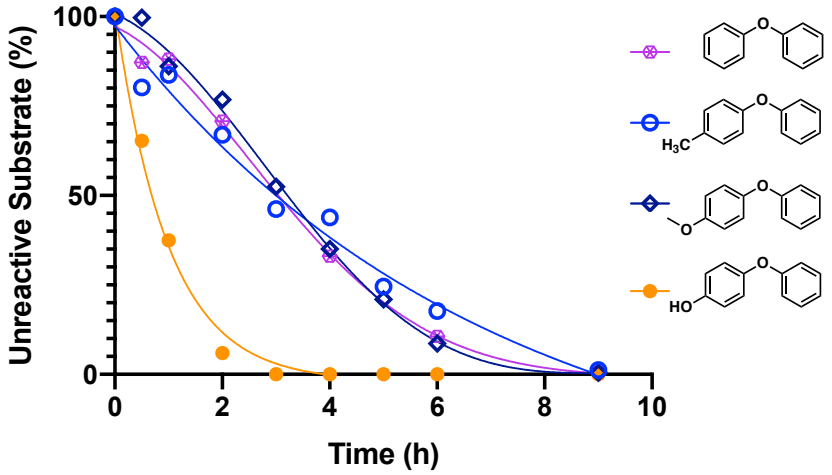

Figure 4.8 C-O ether bond cleavage rate of different electron-donating group substituted diphenyl ether under standard ECH condition. For additional time courses and product analyses see Figure 4.68 a-d.

4.3 Mapping the Cleavage Mechanisms of Diaryl Ethers

4.3.1 Substituent Effects on DAE Cleavage Rates

As shown in Figure 4.8, different substituents on the aromatic ring substantially impact the diaryl ether cleavage rates. As predicted by Route I, the cleavage rates of plain DPE and the para-methoxylated and methylated analogues are similar, suggesting that in the cleavage mechanism these moieties do not directly interact with the catalytic surface in a way that significantly affects the cleavage processes (Figure 4.7a). But, to our surprise, introduction of a para methyl on the diphenyl ether system slightly slowed the cleavage relative to the parent and methoxylated DPE substrates. This was unexpected; typical measures of electronic perturbation such as the Hammett

σ parameter suggest that the methoxy group should be a stronger perturber, and geometrically, the para substituent is expected to be distant from the catalytic surface. But the slower cleavage suggests that the methyl moiety must interfere with the cleavage process in some way.

A strikingly different result was observed in the case of 4-phenoxyphenol, the singly para-hydroxylated analogue of DPE. Here, the presence of the hydroxyl group in the aromatic ring significantly accelerates the C-O cleavage rate. Our previous studies suggested that the electron rich nucleophilic nickel cathode surface has a high affinity for the carbonyl functionality.[39] As with phenol itself, the hydroxyl site on the phenolic ring can equilibrate with the keto form, which binds tightly to the nucleophilic nickel surface, resulting in rapid cleavage.

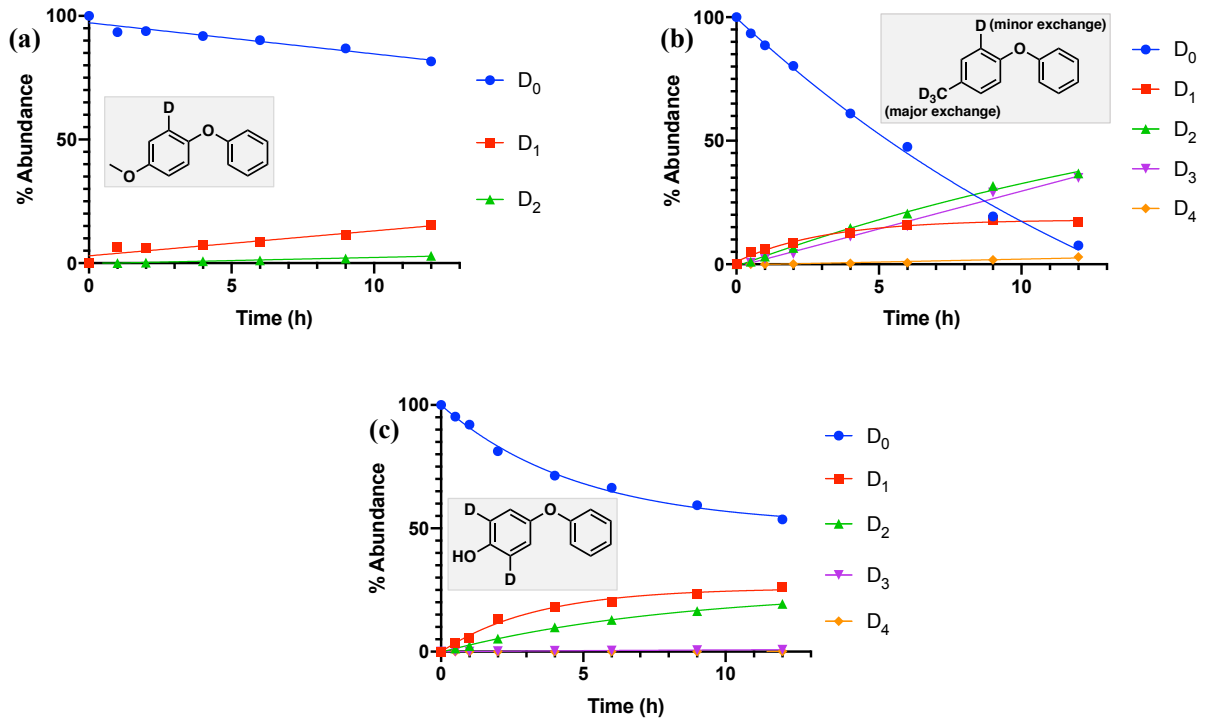

Figure 4.9 H/D exchange time courses and exchange locations for different substituted diphenyl ether: (a) methoxylated diphenyl ether (b) methylated diphenyl ether (c) hydroxylated diphenyl ether (analysis included a H_2O wash to eliminate the rapidly exchangeable hydroxyl H). D_n (n = 0−4) represent numbers of deuterium atoms incorporated. For additional analyses (NMR and MS Spectra) see Figures 4.29-4.43.

4.3.2 Reactivity and Isotope Exchange are Similar in DPE and 4-Methoxylated DPE

As shown in Figure 4.9, the exchange locations of the differently substituted diphenyl ethers were very different. Like the parent DPE, the para methoxylated DPE (Figure 4.9a) had slow deuterium exchange; only ~15% D was incorporated after 12 hours of treatment at 60 °C. Thus, the DPE and 4-methoxylated DPE (Figure 4.8) were similar in two ways: First, in terms of reactivity, these two substrates showed similar, fast C-O ether bond cleavage and slow H/D exchange. Second, the exchange locations were at the same carbon site for both, ortho to the C-O bond being cleaved. Notably, the exchange in the latter substrate occurs on the anisole ring, not the phenyl. Meanwhile, the anisole formed as the cleavage product was doubly deuterated at a level almost independent of the slow deuteration of starting material (for details see Figure 4.29). These similar behaviors imply that these two diaryl ethers react via similar cleavage mechanisms (Figure 4.6, Route I and Figure 4.10a).

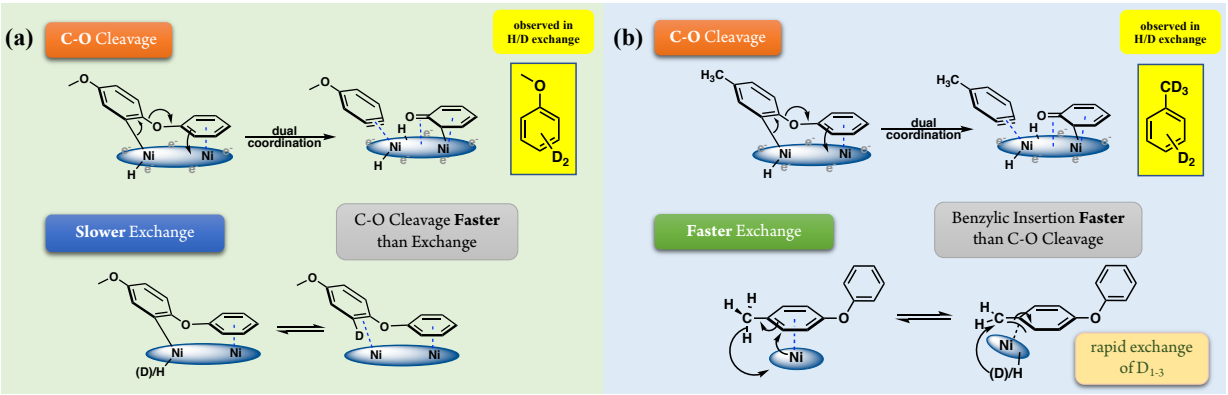

Figure 4.10 Proposed cleavage and exchange mechanisms for (a) methoxylated and (b) methylated diphenyl ethers.

4.3.3 Benzylic Activation on the Methyl Group Distracts from the Ether Cleavage

As mentioned, different from the similarly behaved parent DPE and its electron rich para-methoxylated analogue, introducing a methyl moiety to the diphenyl ether system had in fact slightly brought down the cleavage rate (Figure 4.8). More importantly, it also presented a different H/D exchange behavior. As shown in Figure 4.9b, within 12 hours the methyl group showed nearly complete deuteration, as expected from benzylic C-H insertion by the deuterated nickel catalyst. Similar growth rates of D_1, D_2 and D_3 suggested that once the Ni inserted at the benzylic carbon, the incorporation of D happened rapidly (Figure 4.10b).

The fast H/D scrambling does suggest easy and reversible binding of the methyl group to the catalytic surface; however, this binding does not accelerate the cleavage like the hydroxyl group does. Notably, it also does not activate H/D exchange ortho to the methyl substituent. And in fact, same as the parent and para-methoxylated model, small amount of H/D exchange was detected at the aromatic proton ortho to the C-O ether bond that was being cleaved (exchange locations confirmed by NMR spectra, see Figure 4.37). Thus, on the basis of its cleavage products, toluene and phenol (see Figure 4.68), and the same aromatic C-H activation, we infer that cleavage of para methylated DPE proceeds via the double ring coordination mechanism (Figure 4.6, Route I, and Figure 4.10b) like the parent and methoxylated DPEs. As predicted by this picture, a small amount of penta-deuterated toluene was detected in the exchange experiment (for details, see Figure 4.34b), consistent with the proposed surface-bound methylbenzyne intermediate. Thus, the ether cleavage reaction proceeds via the unsubstituted DPE mechanism (Route I), but with a small slowdown due to competition with the methyl group for binding. Analogous behavior is also seen in the trifluoromethyl-substituted analogue, as detailed below.

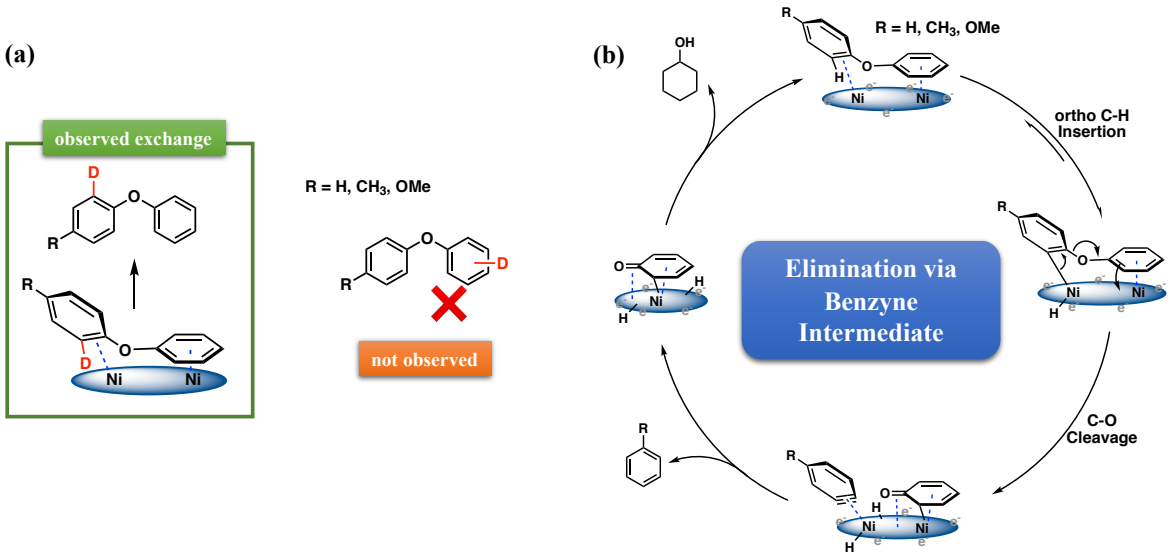

Figure 4.11 (a) Exchange at the ortho C-H of the substituted ring, consistent with the dual-ring coordination (b) proposed cleavage mechanism of DPE, methylated DPE and methoxylated DPE.

4.3.4 Dual-Ring Coordination Results in an Ortho C-H Activation on the Substituted Ring

The location of the H/D exchange of the substituted DPEs (both methoxy and methyl cases), also supports the dual-ring mechanism illustrated in Figure 4.11a. Orienting the substituted ring perpendicular to the Ni surface enables the activation of this ortho aromatic C-H but not those of the unsubstituted phenyl group. Overall, a dual ring coordination mechanism that leads to a surface-bound aryne intermediate is proposed for the cleavage of diphenyl ether (DPE) and its corresponding methoxy and methyl congeners (Figure 4.11b).

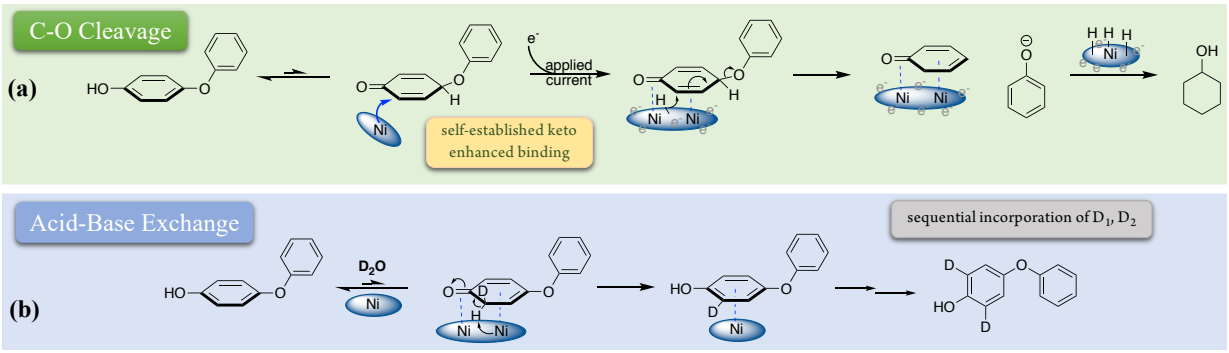

Figure 4.12 Proposed cleavage and exchange mechanisms for hydroxylated diphenyl ethers

4.3.5 The Fast Outlier: Hydroxylated-DPE

Unlike the above three analogues, 4-phenoxyphenol underwent much faster H/D exchange in what appears to be a stepwise sequential process (Figure 4.9c) up to the dideuterated material. This rapid exchange likely reflects the activated keto-enol equilibrium involving the phenol's ortho sites. The $D_{1\text{-}2}$ sequential growth processes in Figure 4.9c appeared similar to classical base-catalyzed phenolic exchange processes, albeit substantially faster. As reported by Miranda and co-workers, at reflux in $NaOD/D_2O$, it required 24 hours to achieve the di-deuteration of the two ortho phenolic protons.[42] Here, at 60 °C without applied current or any inorganic strong base or acid, the catalytic nickel surface achieved 66% ortho D incorporation in 12 hours as shown in Figure 4.9c and Figure 4.12b.

The above rate and labeling site differences strongly suggest that hydroxylated DPE cleaves via a mechanism different from that working in the other three models. As presented in Figure 4.12a, the enhanced binding of the keto ring favors the single-ring coordination, allowing the rapid elimination of the phenoxide leaving group, which explains the dramatic increase of the cleavage rate. After phenoxide removal, the surface-bound dienone would be either rapidly reduced to cyclohexanol or rearomatized via tautomerization back to phenol. Only cyclohexanol

and phenol were observed as the products from ECH of the hydroxylated model (for details, see Figure 4.68). And in fact, compared to the parent DPE, the acetone co-solvent has a larger inhibitory effect towards the hydroxylated model (details see Figure 4.73), which also hints to a different activation mechanism.

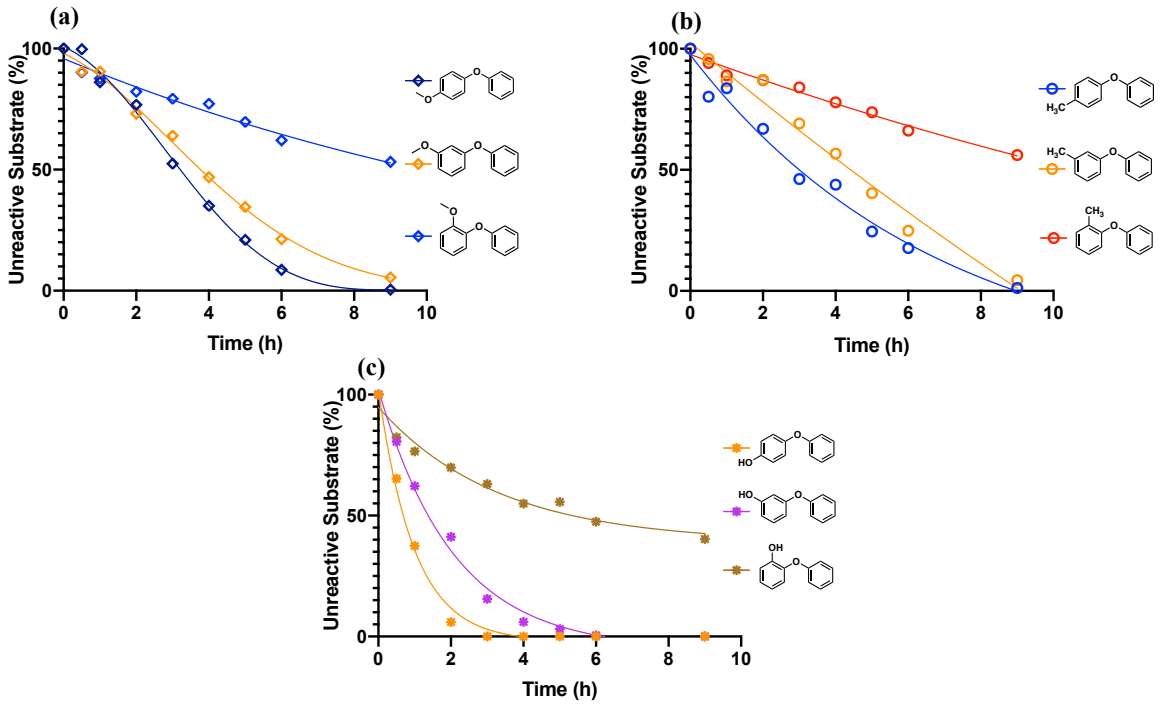

Figure 4.13 C-O bond cleavage rate comparison of DAEs with different substituents at ortho, meta, and para ring positions under standard ECH condition; 50 mA, 60 °C and pH 8 borate buffer/IPA (2:1): (a) methoxylated diphenyl ethers (b) methylated diphenyl ethers (c) hydroxylated diphenyl ethers. For additional time courses and product analyses see Figures 4.69-4.71.

4.3.6 Effects of Substituent Position on Cleavage Rates

Not surprisingly, variations in the positions of the above discussed substituent also exert potent effects on the rates. As shown in Figures 4.13a-c, from para to meta and then to ortho, the closer the functional group is to the C-O ether bond, the slower the cleavage rate. Especially for the methoxy and methyl substituents, the ortho substituted DPEs had very low reactivity.

Importantly, this pattern of rate decreases with changing substituent positions was consistent across all three types of substituents.

These reactivity trends may be attributed to binding and reactivity modulation due to variations in the torsion angle between the biphenyls. It can be envisioned that the closer the R group lies to the ether linkage between the two aromatic rings, the stronger the twisting distortion will be. Compared with a mononuclear molecular catalyst, binding to the heterogenous Ni catalyst surface is presumably more sterically demanding, create a higher barrier to cleavage in those distorted structures. As shown in Figure 4.14a, compared with the para substituted model, the meta methylated/methoxylated diphenyl ether has a slight twist between the rings, which may displace

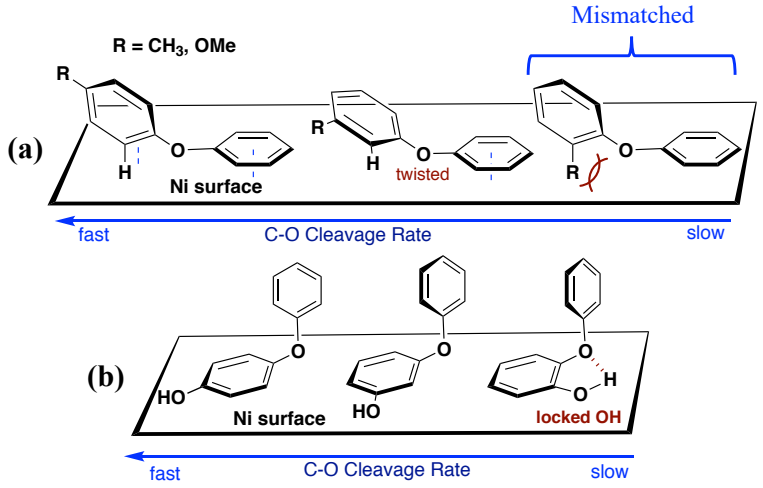

Figure 4.14 Proposed coordination modes of para, meta and ortho substituted diphenyl ethers.

the ortho C-H slightly relative to the catalytic surface. But in the case of ortho substituents, the direct clash between the R group and the catalytic surface generates a mismatch, which significantly inhibits the cleavage. The alternative rotamer would orient the substituent to collide with the π system of the bound ring, also an energetically unfavorable arrangement.

Despite the decreases in cleavage rates with substituent position, for the hydroxylated model, all three structures still react significantly faster than the corresponding methyl and

methoxy systems (Figure 4.13c). This overall faster conversion supports the idea that the hydroxylated DPE analogues react via mechanisms different from those of the methyl and methoxy cases. Evidently, enhanced substrate binding via enol to keto tautomerization is effective for all three isomers, albeit much weaker in the ortho case. We speculate that in the ortho phenoxyphenol (Figure 4.14b), intramolecular hydrogen bonding, together with the above torsional effects, may inhibit formation of the keto form that so strongly favors binding and reaction.

4.4 Cleavage Regioselectivity

4.4.1 C-O Ether Bond Cleavage Regioselectivity in Aryl Phenyl Ethers

With one ring substituted, the two aromatics are no longer identical, setting up an internal competition between the two possible C-O bond cleavage sites (Figure 4.15). Here we examine

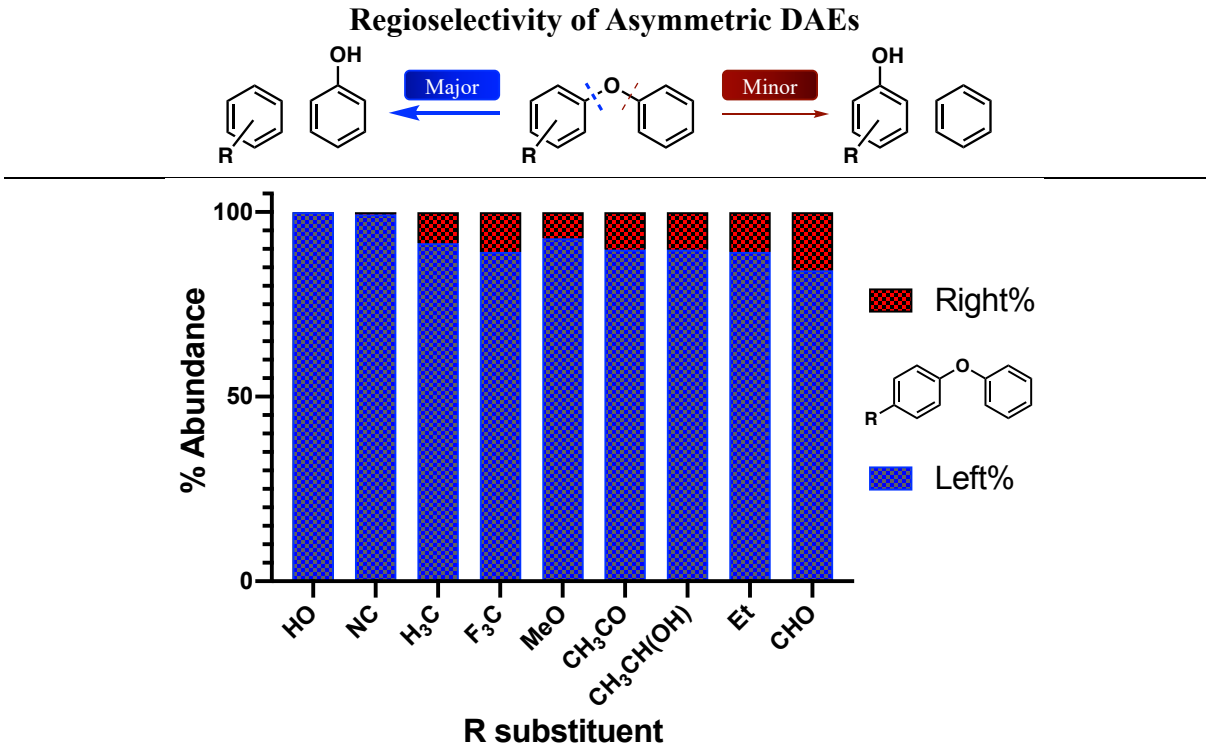

Figure 4.15 Regioselectivity distribution of different para substituted diphenyl ether. For additional time courses and product analyses see Figures 4.74-4.80.

the cleavage regioselectivity of the three models (para-substituted methyl, methoxy, hydroxyl) and several other examples with substituents on the 4 position of one of the benzene rings.

Figure 4.15 summarizes the regioselectivity distribution of all the tested para-substituted aryl ethers. As shown, all of the ethers preferred cleavage on the left-hand side (blue bars), breaking the C-O bond connected to the substituted aromatic ring. Not only various functionalities have no effect in changing the regioselectivity, lowering applied currents with decreased potentials also do not influence the reaction selectivity (details see Figures 4.84-4.85). Lower current with lower applied potential only decreases the cleavage rate, which presumably due to the decreased rate of hydrogen evolution, indeed slowing the reduction.

Interestingly, whether bearing electron donating (MeO, OH, $CH_3CH(OH)$) or highly electron withdrawing substituents (CF_3, NC, CHO), this selectivity was observed. Importantly, in these strongly reducing conditions, most of the electron withdrawing functionalities were reduced prior to aryl C-O cleavage.

For example, the acetyl group was immediately reduced to the corresponding alcohol, which then underwent C-O ether bond cleavage (Figure 4.74). This result accords with the earlier noted strong preference of the Ni to bind and reduce carbonyl compounds. But even strong bonds like the sp^3 C-F in trifluoromethyl were completely reduced to C-H before the C-O ether bond cleavage. No (trifluoromethyl)benzene (the direct cleavage product) was observed, but both toluene and phenoxytoluene, the defluorinated substrate, were easily detected (for details, see Figure 4.79). Thus, all the fluorines were replaced prior to C-O cleavage. This result contrasts with the oxidative insertion cleavage behavior shown by Hartwig's molecular catalyst system, which selectively broke the C-O bond without removing any benzylic fluorine.[27]

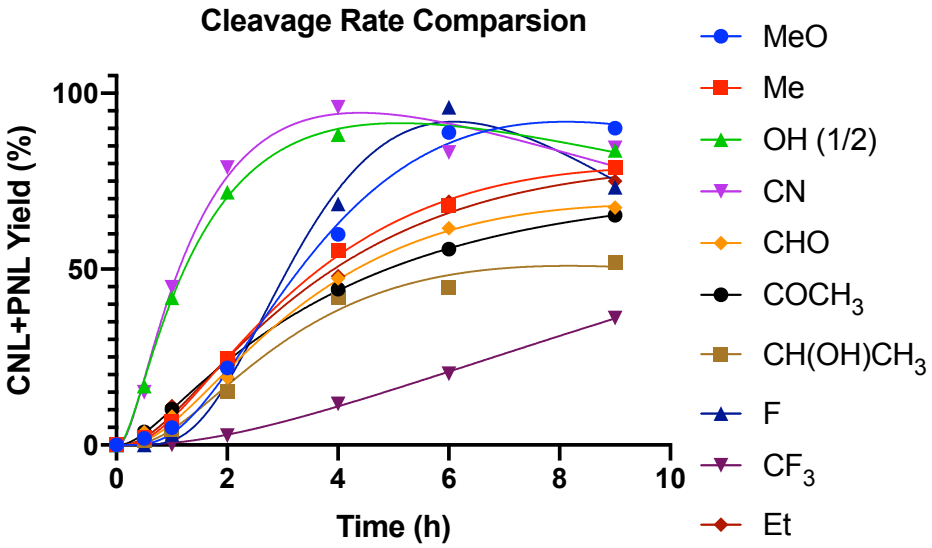

Figure 4.16 Cleavage rate of various para-functionalized diphenyl ethers, under standard ECH condition (50 mA, 60 °C, 33%IPA). Notice, DPE with electron withdrawing functional groups undergoes substituent reduction prior to the C-O cleavage; thus, the sum of cleavage products (cyclohexanol and phenol) was used to represent the actual rate of the cleavage. And since hydroxylated DPE generates two equivalents of phenol and cyclohexanol per cleavage, therefore, 1/2 of the sum of phenol and cyclohexanol was plotted for this rate comparison.

The cleavage rate of the listed functionalized diaryl ethers were also plotted in comparing their cleavage rates (Figure 4.16), which represented by the formation rate of the right-hand cleavage products, phenol and cyclohexanol (all molecules formed the same right-hand cleavage products). Notably, ECH cleavage of the CF_3 substituted aryl ether was the slowest among those studied here. Presumably, this slowness reflected the initial diversion of reducing equivalents required to cleave the three C-F bonds.

In general, our efforts to vary electronic factors via different substituents and to modify the applied currents and potentials had little effect on cleavage regioselectivity; they did, however, impact cleavage rates, presumably due to additional specific interactions between the substituents and the nickel catalyst.

4.4.2 Substituent Position is the Main Factor Controlling Cleavage Regioselectivity

Variation of para substituents from electron withdrawing CF_3 and CN groups to the -OMe donor moiety, led to only minor changes in cleavage regioselectivity. Substituent position was much more important; for both the methoxy and the methyl substituted systems, the closer the R group was to the C-O bond, the more the cleavage preferred to release benzene and the substituted phenol (Figure 4.17a-b).

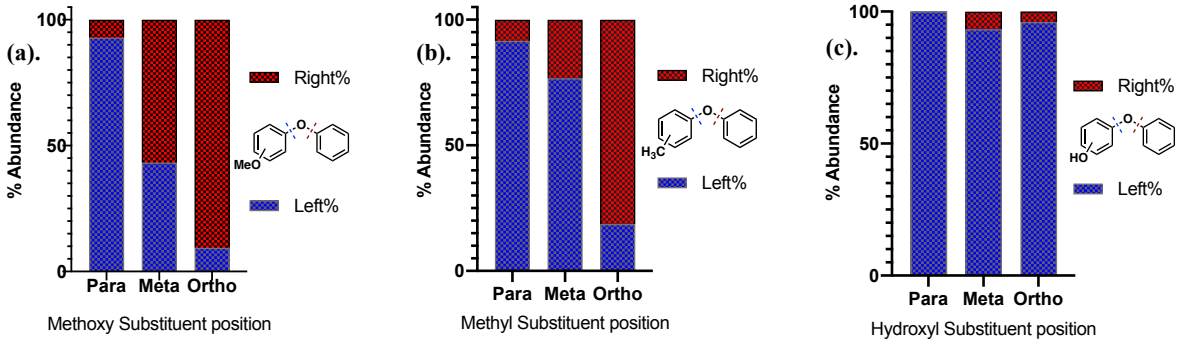

Figure 4.17 Regioselectivity distribution of para, meta and ortho substituted structures of: (a) methoxylated diphenyl ether (b) methylated diphenyl ether. For additional time courses and product analyses see Figures 4.69-4.71.

The strong selectivity effect in the ortho substituted cases was expected; as illustrated in Figure 4.14a, an R group attached to the ortho position would directly clash with either the unsubstituted ring, or the catalyst surface if double ring coordination occurred with the unsubstituted phenyl lying on the surface. Furthermore, with the substituent occupying the ortho

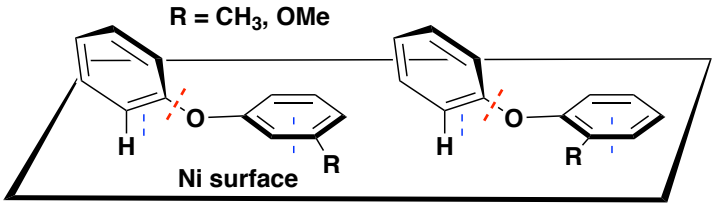

Figure 4.18 Switching of binding conformation of meta and ortho substituted DPE

site, the nickel-activated benzyne-forming phenol elimination is blocked. However, binding by the substituted ring, a much less favorable interaction, does bypass this steric clash (Figure 4.18), resulting in release of substituted phenol and benzene, but much slower reaction.

As with the para substituted substrates, isotope exchange experiments were conducted with the meta and ortho analogues. For the phenoxyanisoles, the fastest-reacting para congener showed only slow isotope exchange (Figure 4.9a). In the more twisted meta and ortho cases, the deuterium incorporation was barely detectable (Figure 4.54). For the phenoxytoluene series, benzylic H/D exchanges in the meta and ortho methyl sites were easily detected (for details, see Figure 4.44), with the less sterically hindered meta isomer showing faster exchange, comparable to that seen in the para case. However, in the ortho phenoxytoluene, benzylic exchange was drastically slower. Thus, the ortho substitution not only redirected the C-O cleavage, but also dramatically slowed direct Ni activation of the benzylic C-H sites.

The hydroxylated DPE series is a key exception to the above regioselectivity switch as a function of substituent position (Figure 4.17c). Though all series show the slowest reactivity in the ortho-substituted cases, the phenoxyphenols do not show reversed cleavage regioselectivity in the ortho-substituted form (Figure 4.71); like its isomers, the *ortho*-phenoxyphenol gives rise only to phenol and ultimately cyclohexanol products. This qualitatively different behavior pattern is additional evidence that phenolic substrates react via a mechanism different from the path followed by all the other substituted DAEs studied here.

4.5 Direct Elimination

4.5.1 Cleavage Selectivity is Controlled by Direct Elimination of Phenoxide Without Disruption of Aromaticity

On the basis of the above labeling, rate, and substituent studies, the direct elimination of the leaving group phenoxide (Figure 4.6, Route I) appears most probable as the cleavage pathway for functionalized diphenyl ethers. This scenario controls the C-O bond broken, and therefore product selectivity, in reductive cleavage of diaryl ethers. Given the choice of which ring prefers to adsorb on the nickel surface, it is clear that essentially any substituent, except for -OH, interferes with surface binding.

A particularly emphatic illustration of this idea comes from study of the bis-4-methoxyphenyl ether (Figure 4.19). Although the monosubstituted 4-phenoxyanisole undergoes cleavage at an essentially similar rate as diphenyl ether, this substrate is almost completely

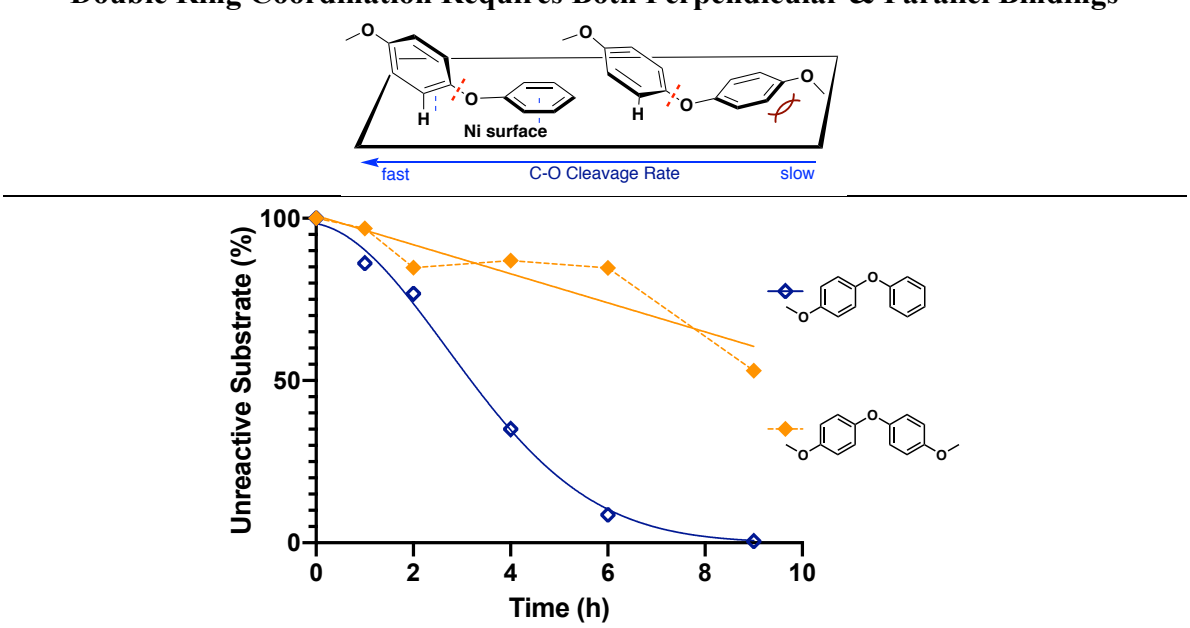

Figure 4.19 Reactivity comparison between 4-phenoxyanisole and bis-4-methoxyphenyl ether. For additional time courses and product analyses see Figure 4.82. Dotted orange line highlights variability in analysis due to borderline solubility of this substrate in the reaction medium.

unreactive (Figure 4.19). Thus, as depicted, we envision surface binding favoring the unsubstituted phenyl ring adsorbing onto a locally flat Ni surface via its π system, placing the ring plane parallel to the surface. Such flat π-bound adsorption geometry has been observed via HREELS in single-crystal adsorption studies, and supported by the computational results of Della Site and co-workers.[43] Analogous, albeit highly constrained, structures have been observed in molecular complexes as well.[44, 45] This positioning leaves the substituted aryl ring roughly perpendicular, but with one of its ortho C-H sites oriented toward the surface. Binding in this manner suggests that C-O cleavage via oxidative insertion by nickel is unlikely, as the C-O bond cleaved is the one not lying on the surface, and therefore poorly positioned for direct insertion.

Further support for the proposed Route I pathway is found in the isotopic labeling in the products of the ether cleavage (for details and discussion, see Figures 4.23, 4.29 and 4.34). Specifically, the benzene, anisole, and toluene formed show essentially fixed ratios over time of di-, mono-, and undeuterated products (D incorporated on the benzene ring after elimination of the phenoxide). Importantly, the benzyne moiety is a potent ligand for Ni and other metals. Benzynes have been observed for over 30 years in structurally characterized molecular complexes with single Ni centers[46, 47] and small Ni clusters[48-51]. Benzyne intermediates have also been identified in LEED and HREELS experiments on metal surfaces, including Ni, that have been dosed with benzene and warmed, with evidence pointing to the benzyne ring plane being tilted from the surface.[52] However, though benzyne-Ni complexes have received some attention as participants in homogeneous processes, there appears little discussion of their possible roles in heterogeneous catalytic reactions.[53]

4.5.2 Selective Inhibition with Acetone Allows Selectivity for Cyclohexanol or Phenol Products

Since the cleavage takes place without immediate reduction of the aromatic products, it is possible to select for phenolic or cyclohexanol products via the use of acetone to prevent phenol reduction, as exploited in the opening discussion that ruled out the formation of cyclohexyl phenyl ether. To illustrate this idea, the para-hydroxylated DPE (4-phenoxyphenol) was chosen, as it is uniformly and rapidly cleaved to two phenol fragments (Figure 4.20), albeit by a mechanism clearly different from the above vicinal elimination path.

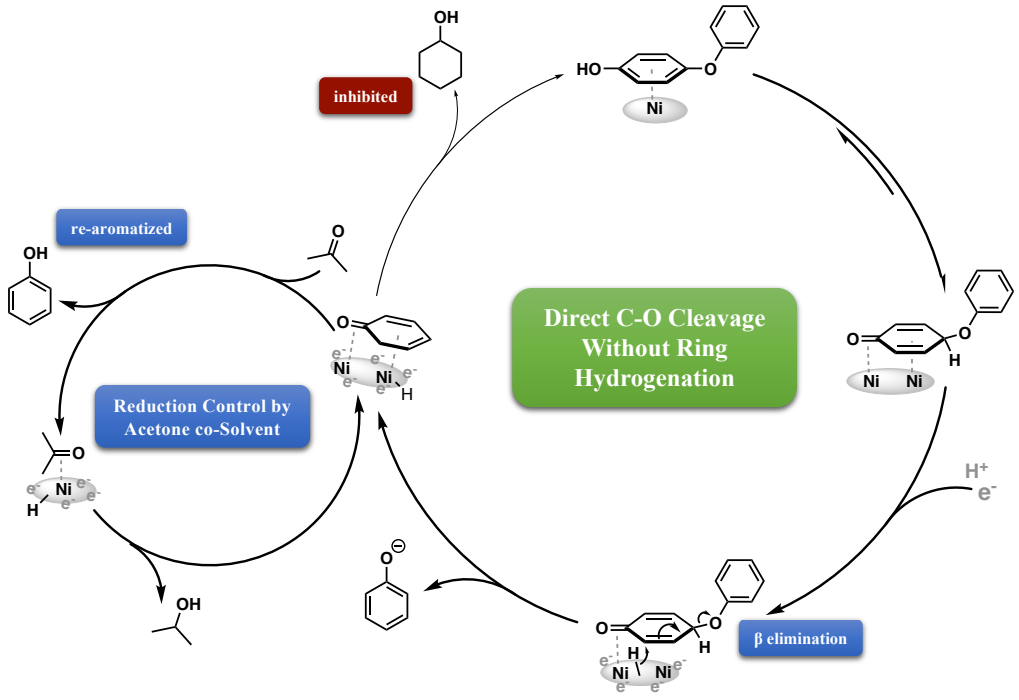

Figure 4.20 Direct elimination of hydroxylated DPE allowing selectivity control

As phenol is produced by phenoxyphenol cleavage, its reabsorption is outcompeted by acetone adsorption, blocking the sites that otherwise convert phenol to cyclohexanol. Present throughout the reaction as a co-solvent, the acetone slows but does not shut down the (also keto-mediated) cleavage of the ether C-O bond as completely as it does the phenol hydrogenation. A

major difference between the two processes could be the energy barrier for reaction; cleavage of the phenoxide only requires one H_2 equivalent and is favored by an increase in entropy. However, reduction of bound phenol requires transfer of three H_2 equivalents, and entails breaking the aromaticity and strong surface binding of the phenol ring. The practical observation is that acetone selectively inhibits phenol monomer reduction, allowing control to target the choice of saturated or aromatic monomer products.

As shown in Table 4.1, by adding only 5% v/v of acetone can significantly inhibit the hydrogenation of phenols to cyclohexanols. Typically, even at low potential and current values, phenol reduction is fast, leading always to substantial amounts of phenol ring saturation. With the acetone additive, however, both water-soluble and insoluble diaryl ethers can be selectively

Table 4.1 co-Solvent study of diphenyl ether (DPE) and para hydroxylated DPE: water insoluble and water-soluble substrates.

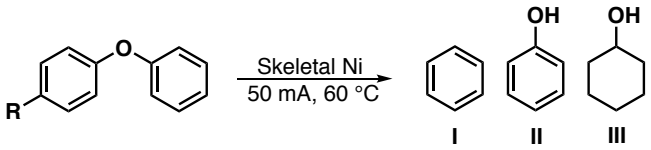

entry	R	co-solv.	conv.	time	yields of products (%)		
					I	II	III
1	H	33%IPA	>99%	9 h	13%	48%	50%
2[a]	H	5%acetone	95%	12 h	19%	95%	2%
3	OH	100%buffer	>99%	1 h	--	90%	82%
4	OH	33%IPA	>99%	3 h	--	117%	40%
5	OH	5%acetone	97%	6 h	--	174%	4%

[a]Besides 5% acetone, 28% of 2-propanol was also added to help dissolving diphenyl ether. The values over 100% reflect the fact that in the case of the phenoxyphenols, cleavage of one ether forms two copies of the product phenol. For additional time courses and product rate analyses see Figures 4.72-4.73.

cleaved into aromatic monomers with minimal ring reduction. At higher acetone concentration (10% v/v), ether bond cleavage continued without phenol reduction to cyclohexanol (Figure 4.73e). As illustrated in Figure 4.20, we envision acetone as a competitive inhibitor, preventing phenol binding in its active keto form but still allowing ether C-O cleavage.

Comparison of the inhibitory effects of acetone on cleavage rates provides additional evidence for the qualitatively different, keto-based path for cleavage of the hydroxylated DPE series, compared to the direct elimination path described above for the parent DPE and other substituted examples. Specifically, DPE cleavage is only slowed by a factor of ca. 1.3 (half-life changes from ca. 3 h to 4 h; compare Figures 4.3a, b) in the presence of 5% acetone, whereas the 4-hydroxy analogue is slowed by a factor of 10 (half-life changes from ca. 10 min to ca. 100 min; compare Figures 4.73a, d), consistent with the potent competition of acetone for the ketone-binding sites needed by phenoxyphenols to cleave, and the parent phenol to undergo ring reduction.

4.5.3 Cleavage of Diaryl Ether Is Not Proceed via Electron Transfer Reduction

Reticulated vitreous carbon (RVC) was also used as electrode for the cathodic electrolysis of diphenyl ether under the same standard ECH condition (50 mA, 60 °C and pH 8 borate buffer/IPA (2:1)). Clearly observed bubbling on the carbon electrode surface suggested the success of hydrogen evolution reaction, but barely any aryl ether cleavage product was detected (Figure 4.21). This indicated such cathodic electron transfer type reduction was not able to achieve the cleavage of this strong aryl ether bond, which is expected; Ni catalyst is required to activation arene rings to enable such C-O cleavage. The critical role of Ni catalyst has also been confirmed in the above H/D exchange studies using the same skeletal Ni catalyst, in the labeling studies no current/potential were applied, but constant isotope exchanges were detected on the aryl ethers. Thus, the important role of Ni metal to enable the activation of such sp^2 C-O ether cleavage was examined.

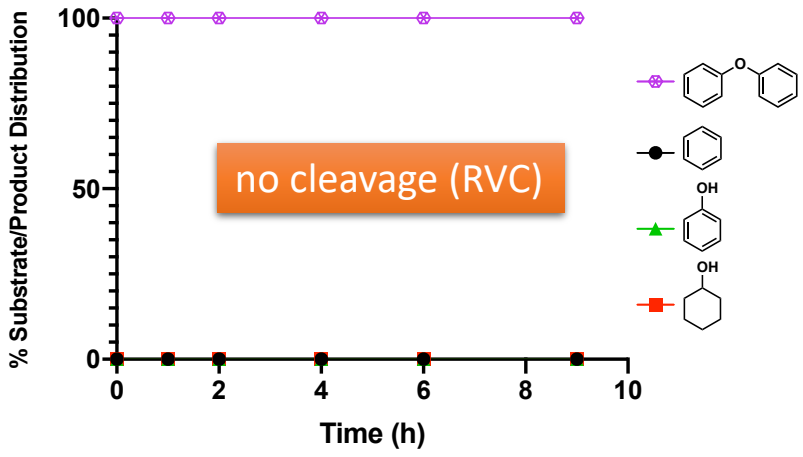

Figure 4.21 ECH measurement of diphenyl ether followed the general ECH experimental procedure with standard condition (50 mA, ~10 V, 60 °C and 33%IPA) using a reticulated vitreous carbon electrode (8 mA/cm^2). Hydrogen evolution was observed, but none of the diphenyl ethers were cleaved.

4.6 Conclusion

A mild aqueous electrocatalytic hydrogenation/hydrogenolysis (ECH) method has been described for selective cleavage of the diaryl ether moiety, catalyzed by skeletal nickel electrodes, to form arene and phenol products. Patterns of reaction rates and cleavage selectivity between the two ether C-O bonds have been mapped out as a function of substituent structure and position. Together with isotopic labeling studies, two distinct cleavage mechanisms were identified: a direct elimination involving a surface-bound benzyne for DPE and its methoxylated and methylated analogues, and a path involving surface binding of the keto form of the phenoxyphenols, the hydroxylated DPE analogues.

We propose that cleavage of the unsubstituted DPE and its methoxy and methyl congeners occurs via a double-ring coordination mechanism. In this route, the nickel catalyst activates an aromatic C-H site vicinal to the C-O bond, which is then eliminated to release phenoxide and form the aryne. Rehydrogenation with surface hydrogen atoms, formed via electrochemical reduction of protons from solution, yields the arene product. Diaryl ethers cleaved via this path were sensitive to changes in substituent position, with cleavage regioselectivity completely switching between para- and ortho-R substitution.

The hydroxylated DPEs are fast outliers, cleaved through a different mechanism which we infer to involve surface binding by the phenol's keto form. This mode significantly enhances the binding of the substituted ring and enables rapid C-O cleavage. Importantly, unlike the dual-ring activation scheme, changes in the hydroxyl position had little impact on the cleavage regioselectivity.

The direct elimination finding successfully enabled the tuning of the cleavage selectivity, via selective inhibition by acetone allows the phenol products to be further reduced to

cyclohexanols or retained as valuable aromatics. The surprising finding of a benzyne intermediate will likely spark interest and further efforts among researchers who study catalysis mechanisms, especially in the growing areas of organic electrochemistry and computational modeling.

4.7 Supplemental Experimental Details

4.7.1 H/D Isotope Exchange Experiments[39]

A one-compartment single cell was equipped with stir bar and rubber stopper with a stainless-steel metal clip. The acetone-treated skeletal Ni catalyst (half size and same preparation as the electrode) was hung on the metal clip and placed inside the one compartment cell, positioned high enough to avoid contact with the stirrer. 10 mL of D_2O with the addition of 3 mL 2-propanol (non-deuterated) was charged inside the cell. As with the ECH studies, another 2 ml of 2-propanol was used to dissolve the weighed diaryl ether substrate (0.125 mmol) in a 4-mL glass vial, before it was added to the D_2O solution. The single cell was maintained at 60 °C, and the skeletal Ni catalyst was allowed to react with the D_2O/2-propanol (2:1) mixture for 1 hour, after which the 2 mL of 2-propanol that contained the dissolved diaryl ether was added into the D_2O solution and allowed to exchange for a maximum of 12 hours at 60 °C under ambient pressure. At each desired time point, 0.25 mL of solution was sampled and analyzed by GC-MS as described earlier.

As previous reported[39], acetone was found to be an excellent organic solvent to discharge the stored reducing power remaining in the skeletal Ni after basic etching of the Al; thus, acetone-treated Ni catalyst was used in the labeling studies to avoid significant cleavage of the diphenyl ethers. Acetone treatment: The fresh activated skeletal Ni catalyst prepared as described above was immersed in pure acetone under nitrogen for a minimum of 24 hours.

Note, an extra step was needed to accurately determine the amount of deuterium that was incorporated in the hydroxylated analogue of diphenyl ether (DPE), since the H/D exchange on –OH functional groups happen instantaneously. The exchanged samples of hydroxylated DPE were extracted as usual with 1 mL of dichloromethane, then the dichloromethane extract was washed

with 1 mL of deionized non-deuterated water to make sure there was no D on the –OH functional group, prior to injection on GC-MS.

4.7.2 MS Quantitative Fitting of Isotope Labeling[39]

The total ion abundance of different mass fragments after H/D exchange was provided by GC-MS representing a mixture of D_n dimer isotopomers. The measured intensity of each ion fragment is a combination of the intensities of the same mass fragments from different D_n incorporated diaryl ether dimers. Therefore, to determine the % abundance of D_n in the exchange results, the proportion of D_n in each mixture is defined as fraction coefficient X_n (n = 0,1,2,3...n). The sum of the products of fraction coefficient X_n times peak fragment intensity I_n should be the total intensity of the corresponding peak in the total ion chromatogram. Meanwhile, the relative fragmentation pattern of different D labeled aryl ethers should not change, only the peak value will shift by one for each H that was replaced by D incorporated inside the compound (Figure 4.22). To avoid complications due to any isotope effects on fragmentation, only the molecular ions were analyzed in this manner.

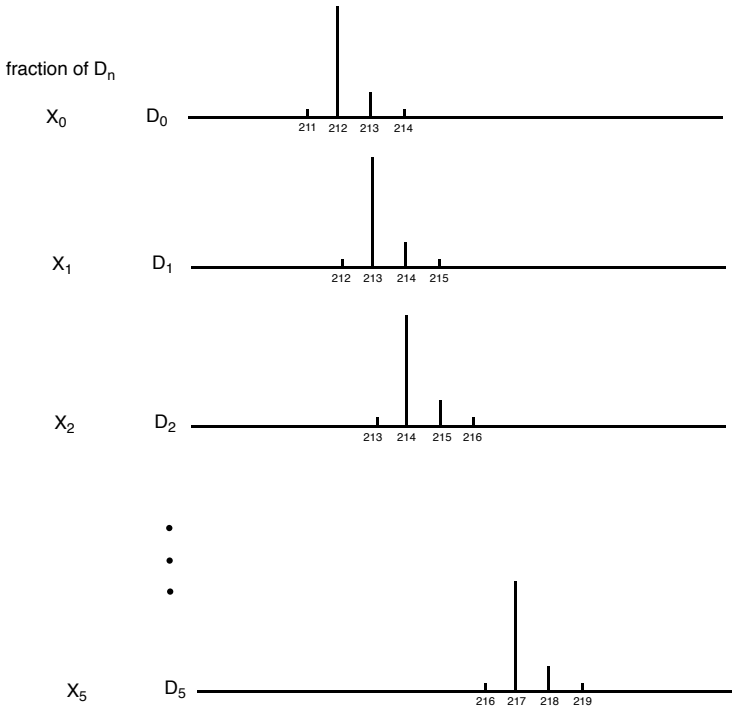

Figure 4.22 As the numbers of D labels in the compound increase, the mass fragmentation pattern and intensity remain the same; only the peak's m/z value will shift. To analyze the molecular ions, fractional coefficients X_n were used as the proportions of D_n in the total ion mixture.

Excel solver was used to fit the corresponding fraction X_n of D_n in the total ion mixture. Below is an example of the solver fitting method of 4-phenoxytoluene H/D exchange at 12 hours. As presented in Table 4.2, column 2 is the intensity distribution of unlabeled 4-phenoxytoluene fragments (parent). Column 3 is the intensity distribution of the D labeled mixture (labeled). The fitted intensity of each ion was calculated by the below **equation 3** and tabulated in column 4-9, where fraction coefficient X_n is tabulated in column 2 (row 13-18). The values of the fractional coefficients X_n were found through excel solver as presented in **equation 5** by minimizing the sum of the square errors. The square error is calculated by **equation 4** and tabulated in column 10, where the smaller the deviation, the closer the fitted intensity to the actual labeled intensity. Based on solved X_n, the percent abundance of D_n is plotted.

$$\%Ion\ Intensity_{fitted} = X_n * \%Ion\ Intensity_{parent} \quad [3]$$

$$Square\ Error = (\sum_{0}^{5} \%Ion\ Intensity_{fitted} - \%Ion\ Intensity_{labeled})^2 \quad [4]$$

$$Solver : \left[minimize \sum_{0}^{5} Square\ error = by\ Varying\ X_n \right] \quad [5]$$

$$\%Abundance\ (D_n) = \frac{X_n}{\sum_0^5 X_n} * 100 \quad [6]$$

Table 4.2 Para-methylated Diphenyl Ether (4-phenoxytoluene) H/D Exchange MS Fitting at 12 hrs

MS Frag. (m/z)	MS Intensity (parent)	MS Intensity (labeled)	Fitted Int. X_0*Parent	Fitted Int. X_1*Parent	Fitted Int. X_2*Parent	Fitted Int. X_3*Parent	Fitted Int. X_4*Parent	Fit. Int. X_5*P	Square Error
180	0.02	0	0.00340395						1.1587E-05
181	1.52	0.37	0.25869992	0.00769147					0.01073474
182	0.72	1.12	0.12254207	0.58455198	0.01638631				0.15722783
183	15.28	4.51	2.600615	0.27689304	1.24535969	0.01558025			0.1380509
184	100	24.61	17.0197317	5.87628564	0.58990722	1.18409914	0.00131766		0.00376276
185	15.34	54.25	2.61082684	38.4573668	12.5191421	0.56088906	0.10014198	0.00019273	2.075E-06
186	1.23	100	0.2093427	5.89936006	81.9315582	11.9033124	0.04743567	0.01464756	3.1997E-05
187	0.07	91.97	0.01191381	0.47302561	12.568301	77.901259	1.00669043	0.00693832	3.5035E-06
188	0	19.72	0	0.02692016	1.00775817	11.9500531	6.58828817	0.14724655	7.0851E-08
189	0	2.99	0	0	0.05735209	0.95818549	1.01064341	0.96365545	2.6755E-08
Deuterium number (D_n)	Fraction Coefficient X_n	% Abundance							∑ Square Errors
D0	0.17019732	7.63696119							0.309825497
D1	0.38457367	17.2562895							
D2	0.81931558	36.7636894							
D3	0.77901259	34.955245							
D4	0.06588288	2.95624525							
D5	0.00963655	0.43240395							

Analogous analyses applied to the fragments, together with NMR evidence, confirm the assigned locations of the D labels.

4.7.3 Fitting Results: % D_n Incorporation During H/D Exchange & Spectra of Aryl Ethers

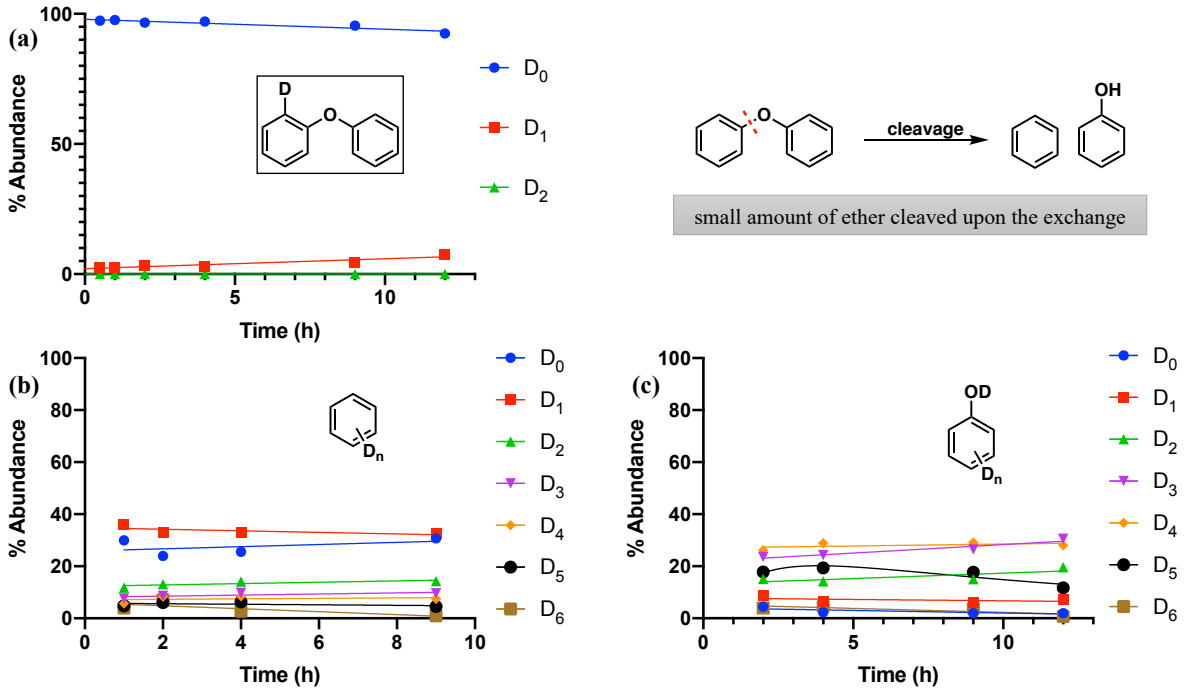

Figure 4.23 Quantified % abundance of D_n in (a) diphenyl ether and cleavage products (b) benzene and (c) phenol, as determined by GC-MS for (MS Spectra shown below in Fig. 4.24). The exchange locations in DPE were determined based on NMR evidence (Figs. 4.26 below). Experiment was run without current flowing, so only a small amount of diphenyl ether underwent cleavage during the exchange experiment.

The formation of di-deuterated benzene points to the proposed cleavage Route I via formation of a benzyne intermediate. The isotope labeling found in the benzene product showed a fixed ratio of di-, mono- and undeuterated products that is essentially fixed over the course of the reaction. Remembering that the skeletal nickel electrodes employed in these studies have been activated via etching in protic media, they are expected to retain substantial H on the surface, some of which exchange with deuterium in the D_2O reaction medium. Presumably, the H atom from the ortho C-H activated by oxidative insertion also remains nearby, so that when two surface hydrogens are donated to reduce the benzyne and release it as benzyne, there is a high probability that one of them will still be protium. However, the dideuterated products appear as a substantial

component of the mixture, in fixed proportion to the monolabeled material (especially in the methoxy and methyl substituted cases below). This clearly indicates the involvement of that ortho C-H site.

Labeling in the phenol is less informative; phenol itself undergoes H/D exchange that is fast on Ni surface, especially at the ortho positions, and it is also rapidly reduced to cyclohexanol.

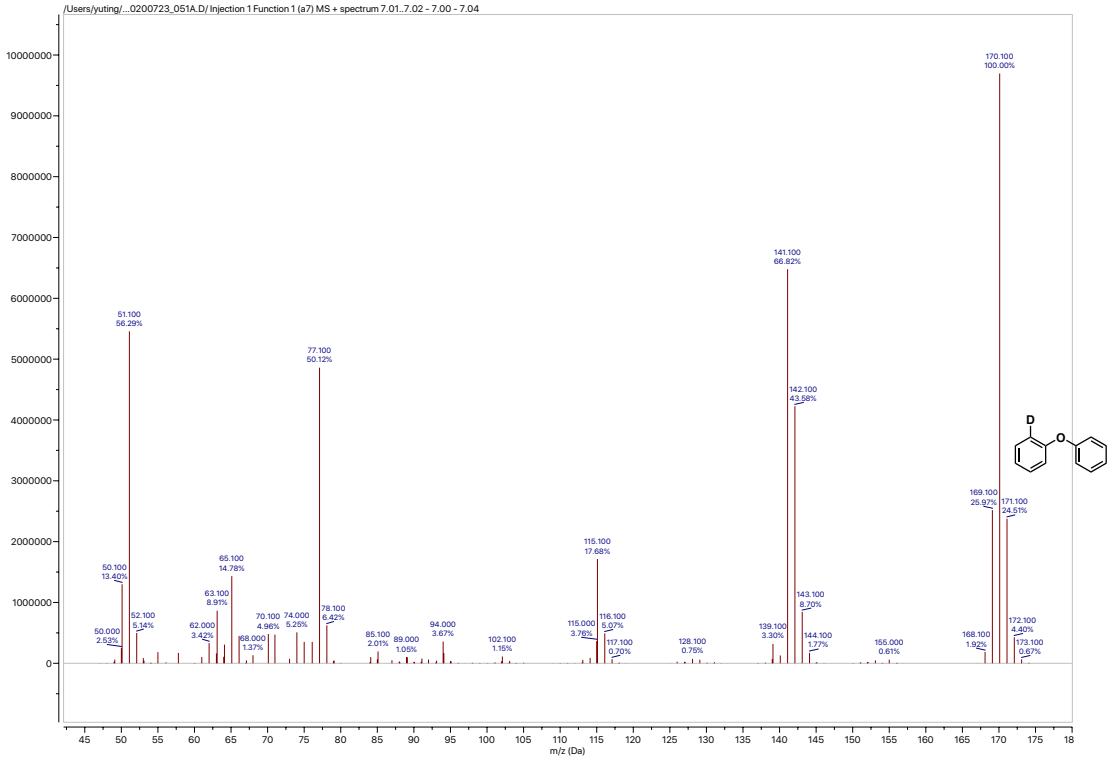

Figure 4.24 Mass spectrum of **labeled** diphenyl ether after 12 hours H/D exchange at 60 °C. Compared to the unlabeled parent (Figure 4.25), no significant increase of m/z 171, which suggested the low D incorporation of diphenyl ether. The location of the exchange was further confirmed by NMR.

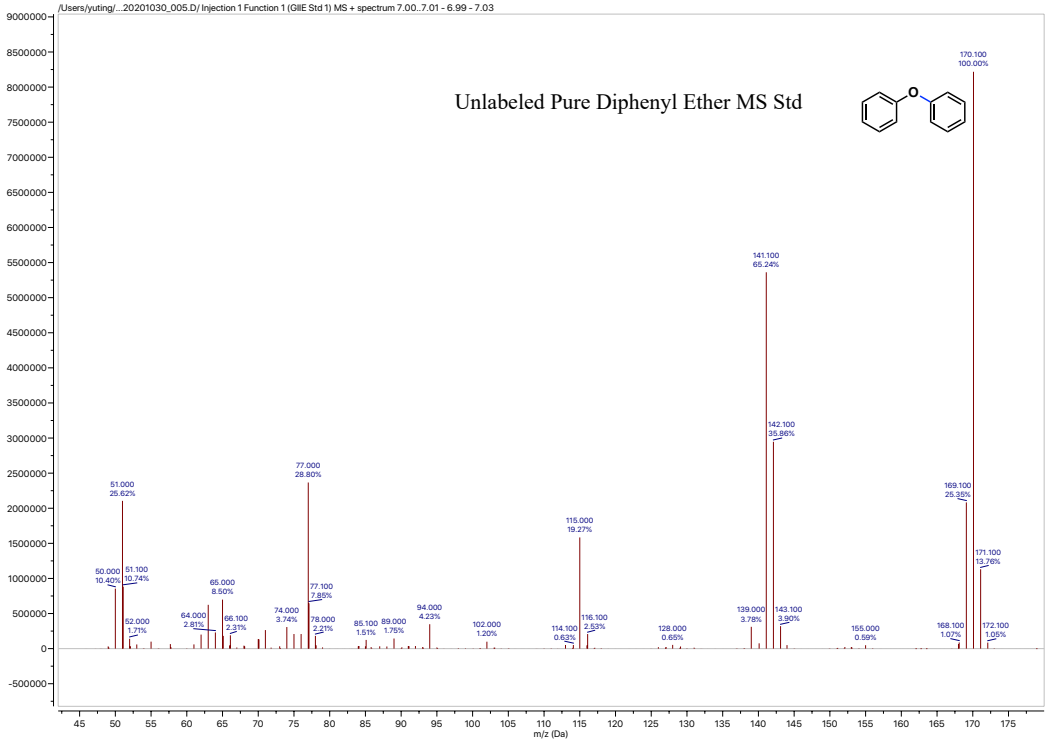

Figure 4.25 Mass spectrum of **unlabeled** diphenyl ether.

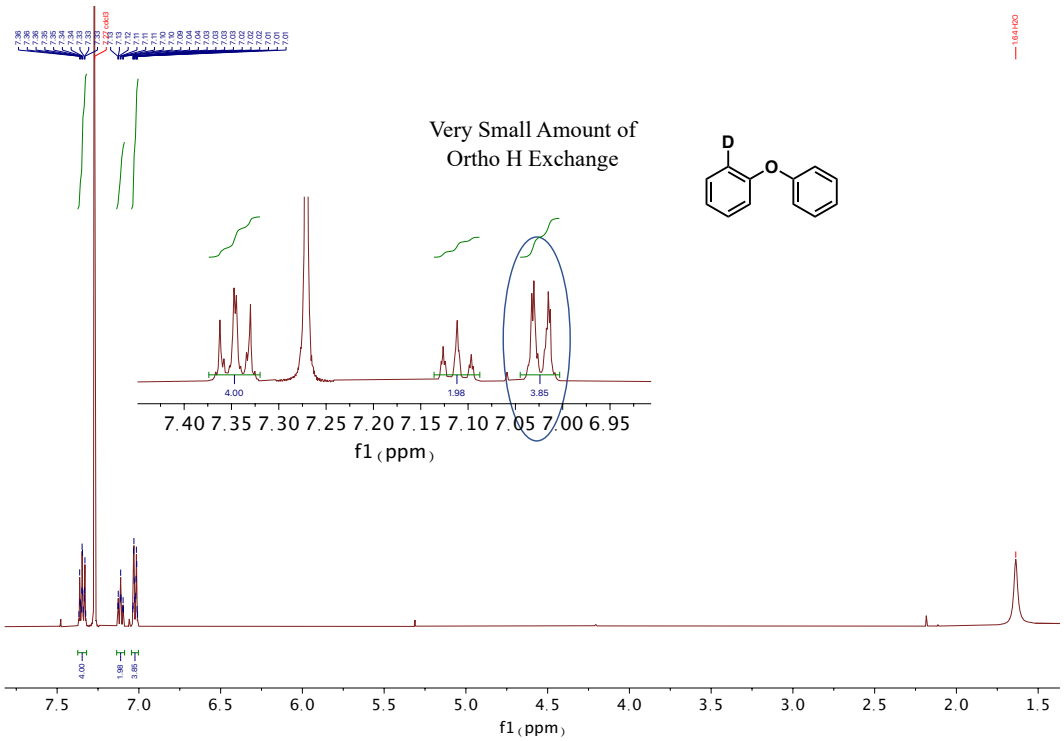

Figure 4.26 NMR spectrum pf **labeled** diphenyl ether after H/D exchange for 12 h. As indicated in the figure, only a small amount of the ortho hydrogens were exchanged, which also matched up with the quantified exchange abundance from the mass spectra result.

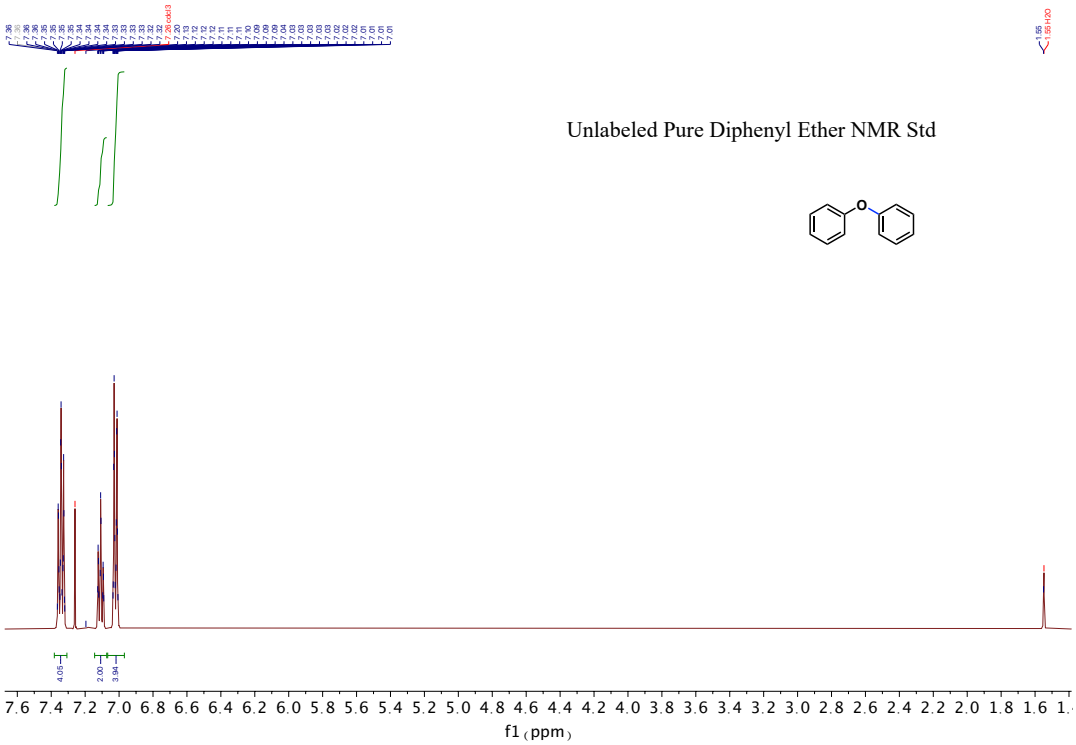

Figure 4.27 NMR spectrum of **unlabeled** diphenyl ether as reference for the labeled spectrum.

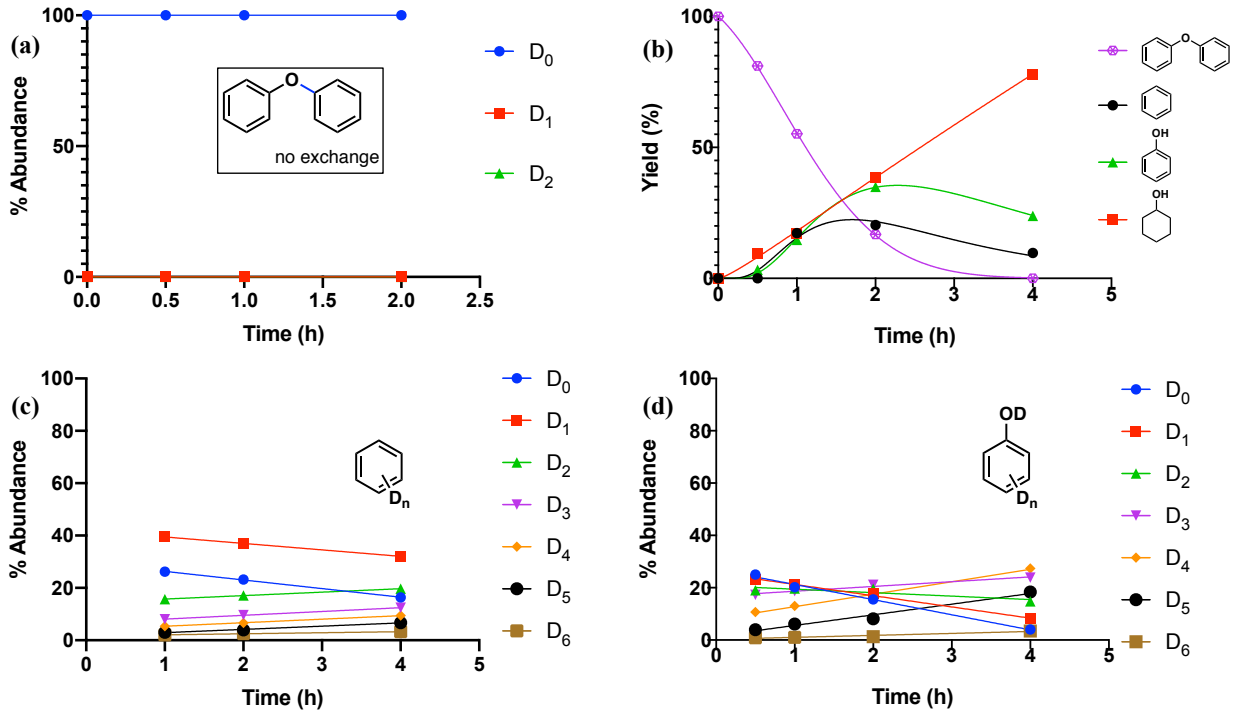

Figure 4.28 (a) Quantified % abundance of D_n in diphenyl ether determined by GC-MS. The H/D exchange experiment with applied current (50 mA) was conducted following the ECH general procedure as described above.

As shown in Figure (a), no deuterium was detected in the remaining diphenyl ether dimer. But as indicated in (b), diphenyl ether was constantly undergoing cleavage into the products, which did contain substantial amounts of D. This finding suggests that the C-O cleavage proceeded immediately once the ortho C-H site was activated. Since the exchange experiment was performed at a smaller scale (1/2 size of the normal ECH reaction), a smaller ECH cell set up was used, which somewhat affects the overall cleavage rate, since the smaller cell has a longer bridge between the two electrodes. (c) Quantified % abundance of D_n in the benzene product. (d) Quantified % abundance of D_n in phenol.

As expected, substantial amounts of D were incorporated in the cleavage products during the fast cleavage under applied current. Free benzene does not undergo H/D exchange itself at significant rates under these reaction conditions; the upward slope in D_2 and more highly labeled

products presumably reflects the increasing proportion of D formed on the cathode surface as residual H atoms are consumed. Isotope effects are unknown, though they would be expected to favor H vs D transfer to the departing benzene.

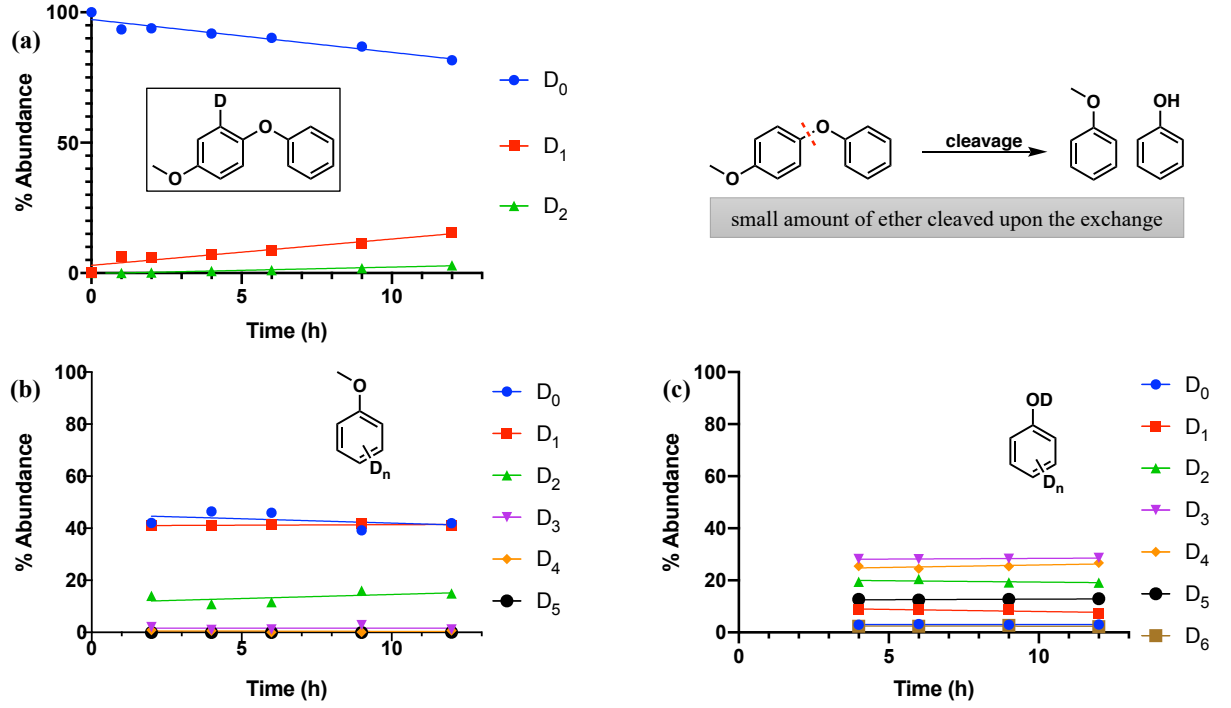

Figure 4.29 (a) Quantified % abundance of D_n of 4-phenoxyanisole determined by GC-MS (MS Spectra shown below Fig. 4.30). The exchange location was determined by NMR (Fig. 4.32 below). Though only a small amount of the ether substrate underwent cleavage during the exchange experiment, the %D of the cleaved products were also determined: (b) Quantified % abundance of D_n in anisole. (c) Quantified % abundance of D_n in phenol.

As in the plain DPE case, the existence of di-deuterated anisole in this case supports for the proposed cleavage Route I via the 4-methoxybenzyne intermediate. The isotope labeling found in anisole also showed a fixed ratio of di-, mono- and undeuterated products in fixed proportions, with the dideuterated products representing a substantial component of the mixture. Again, this clearly indicates the involvement of that ortho C-H site.

As noted above, the phenol product undergoes fast exchange on the Ni surface, and is also rapidly reduced to cyclohexanol.

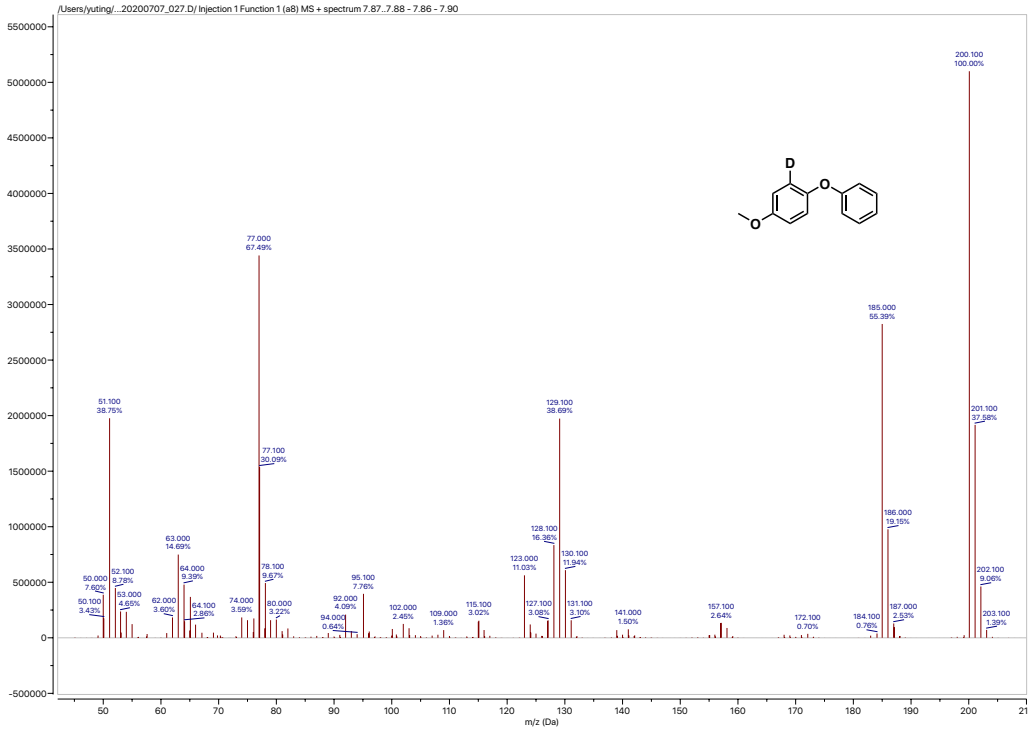

Figure 4.30 Mass spectrum of **labeled** 4-phenoxyanisole after 12 hours H/D exchange at 60 °C. Compared to the unlabeled parent (Figure 4.31), small increases in m/z 201 and 202 peaks are visible, which suggested slow D incorporation. The location of the exchange was further confirmed by NMR.

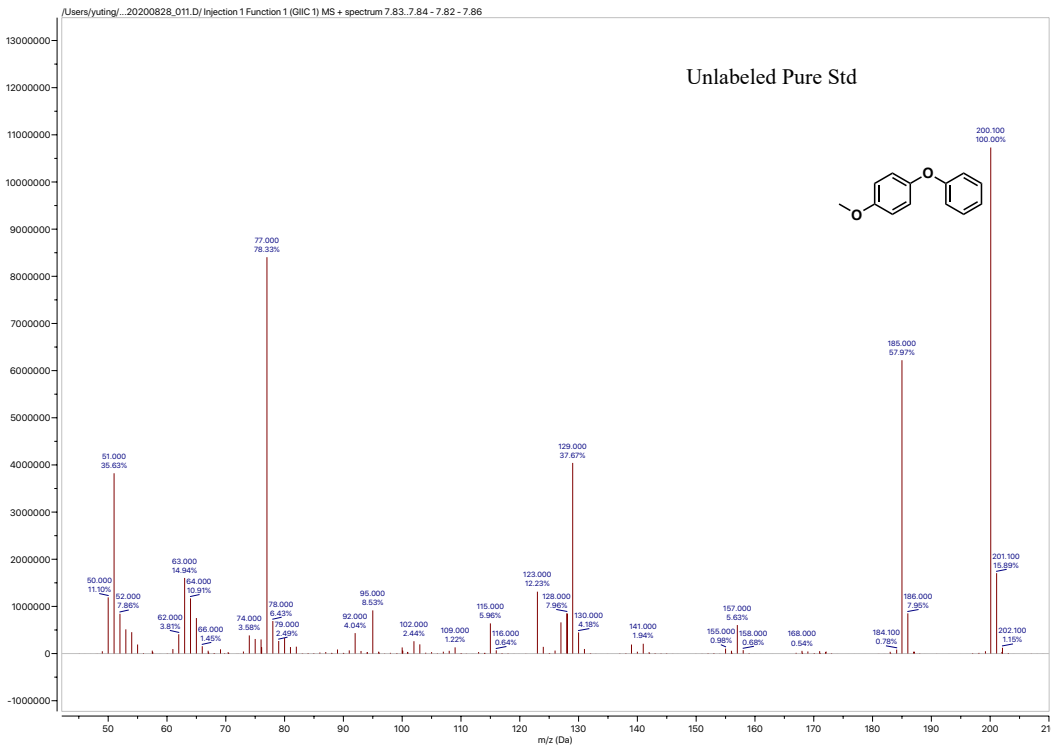

Figure 4.31 Mass spectrum of **unlabeled** 4-phenoxyanisole.

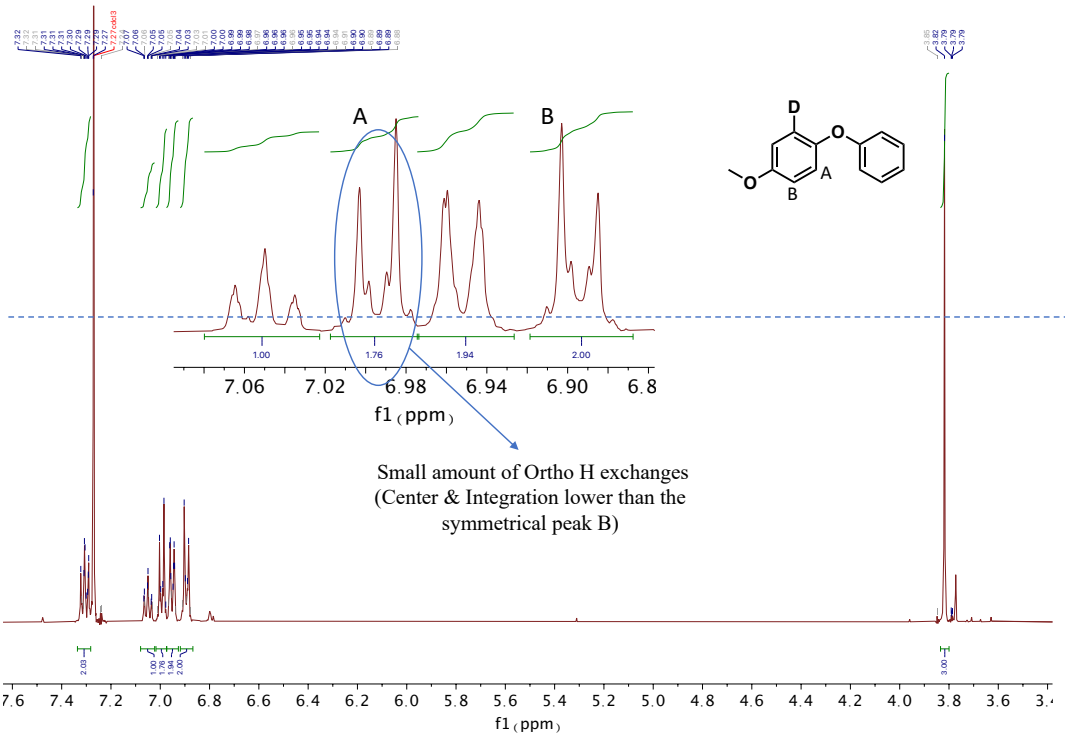

Figure 4.32 NMR spectrum of **labeled** 4-phenoxyanisole after 12 hours exchange. As indicated, the integration of peak A had a mild decrease compared to its symmetrical partner peak B. Despite no significant shape difference between peak A and B, but indicated by the dotted line, the center of peak A is lower than that of B.

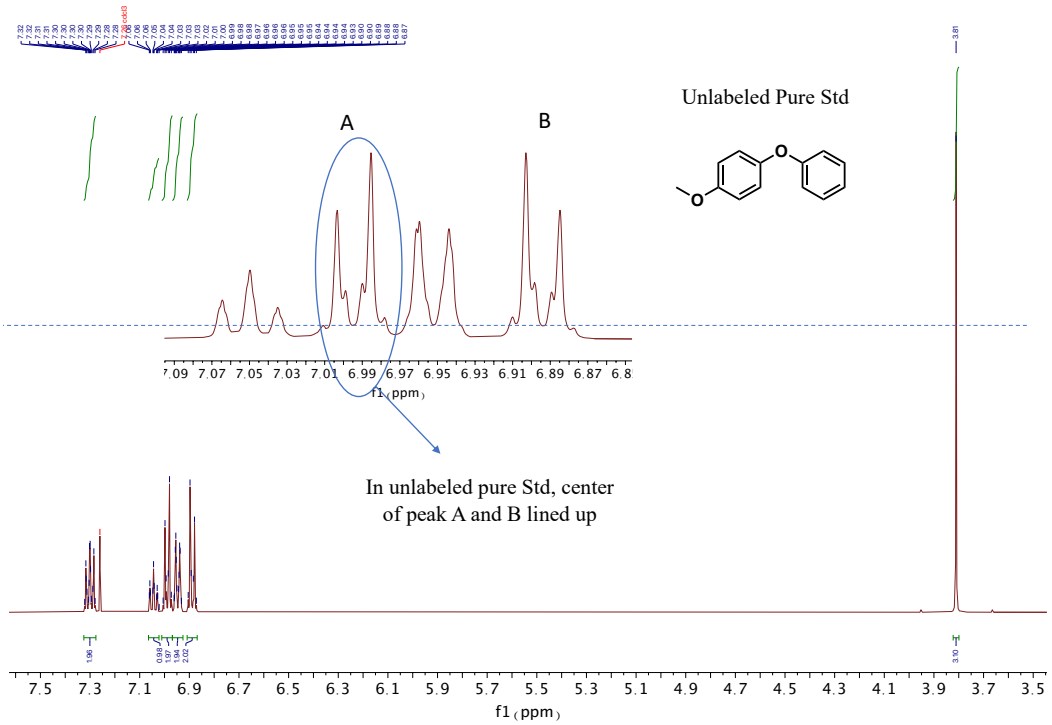

Figure 4.33 NMR spectrum of **unlabeled** 4-phenoxyanisole. Note that in the unlabeled pure compound, the centers of peaks A and B do line up.

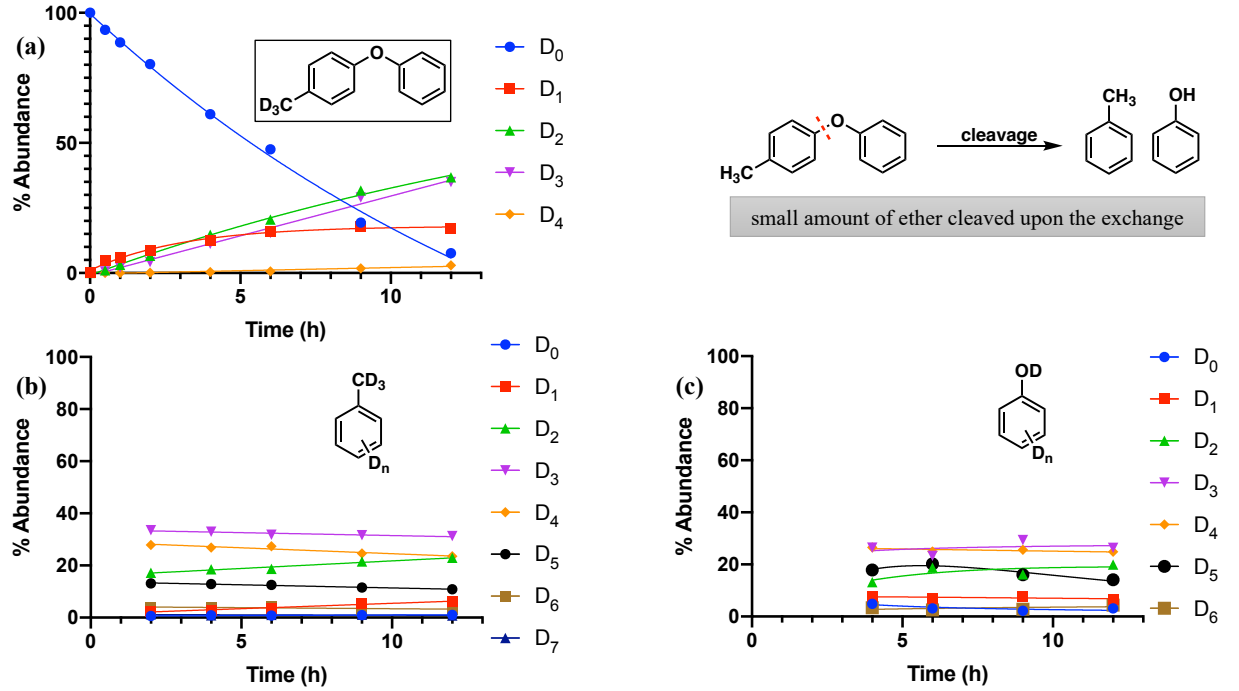

Figure 4.34 (a) Quantified % abundance of D_n in 4-phenoxytoluene determined by GC-MS (MS Spectra shown as Fig. 4.35 below). The exchange location is determined by NMR (Fig. 4.37 below). Though only a small amount of the ether substrate underwent cleavage during the exchange experiment, the %D in the cleaved products were also determined. (b) Quantified % abundance of D_n in toluene. (c) Quantified % abundance of D_n in phenol.

As in the previously analyzed cases, the existence of penta-deuterated toluene in this case was also another supported the proposed cleavage Route I via a 4-methylbenzyne intermediate. The isotope labeling found in toluene also showed essentially fixed ratios among the tri-, tetra- and penta-deuterated products, with the penta-deuterated product appearing as a substantial component of the mixture, in almost fixed proportion to the tri- and tetra-deuterated material. Again, this clearly indicates the involvement of the ortho C-H site in the formation of the toluene product.

As noted in earlier, the phenol product undergoes fast H/D exchange on Ni surface and is also rapidly reduced to cyclohexanol.

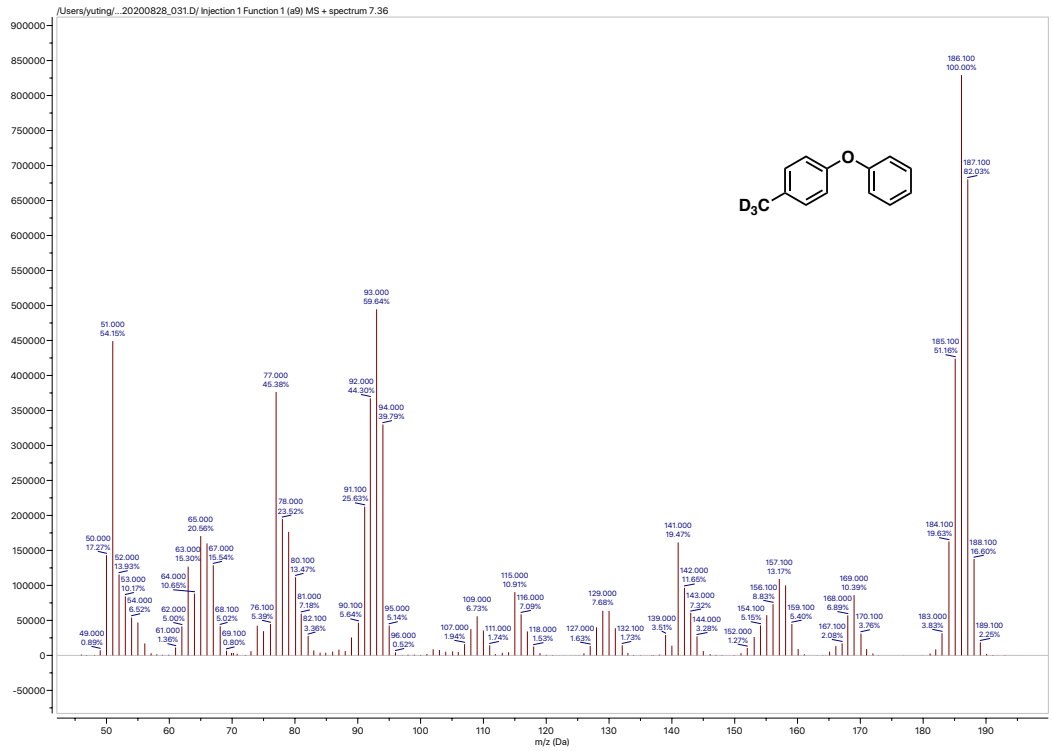

Figure 4.35 Mass spectrum of **labeled** 4-phenoxytoluene after 12 hours H/D exchange.

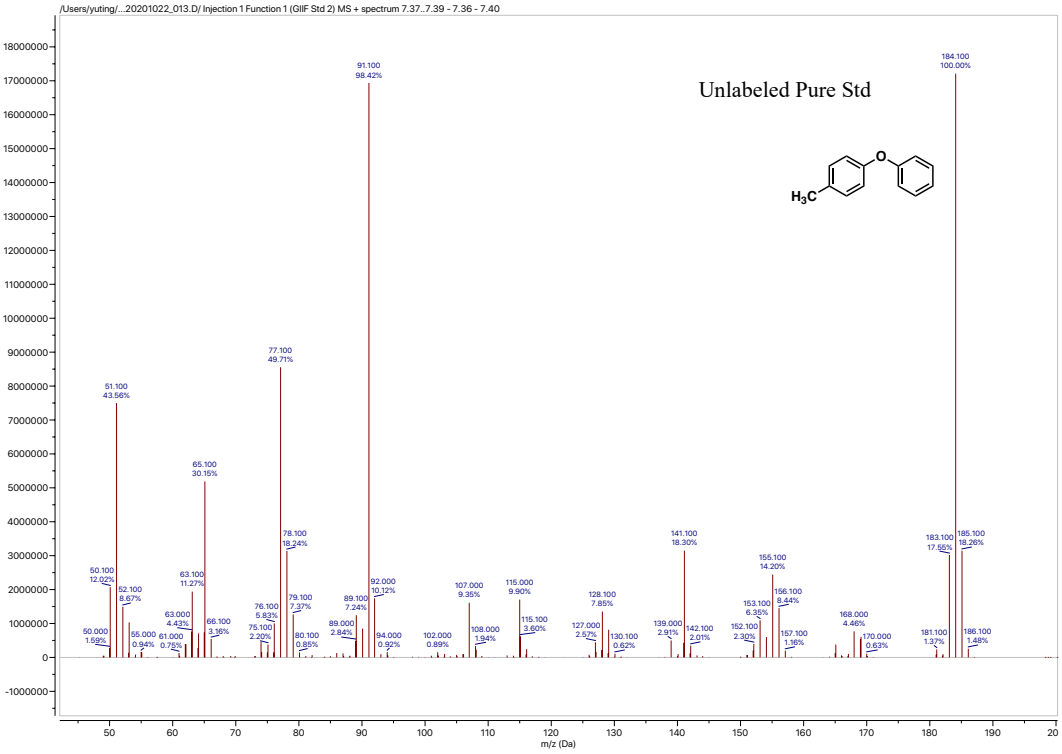

Figure 4.36 Mass spectrum of **unlabeled** 4-phenoxytoluene.

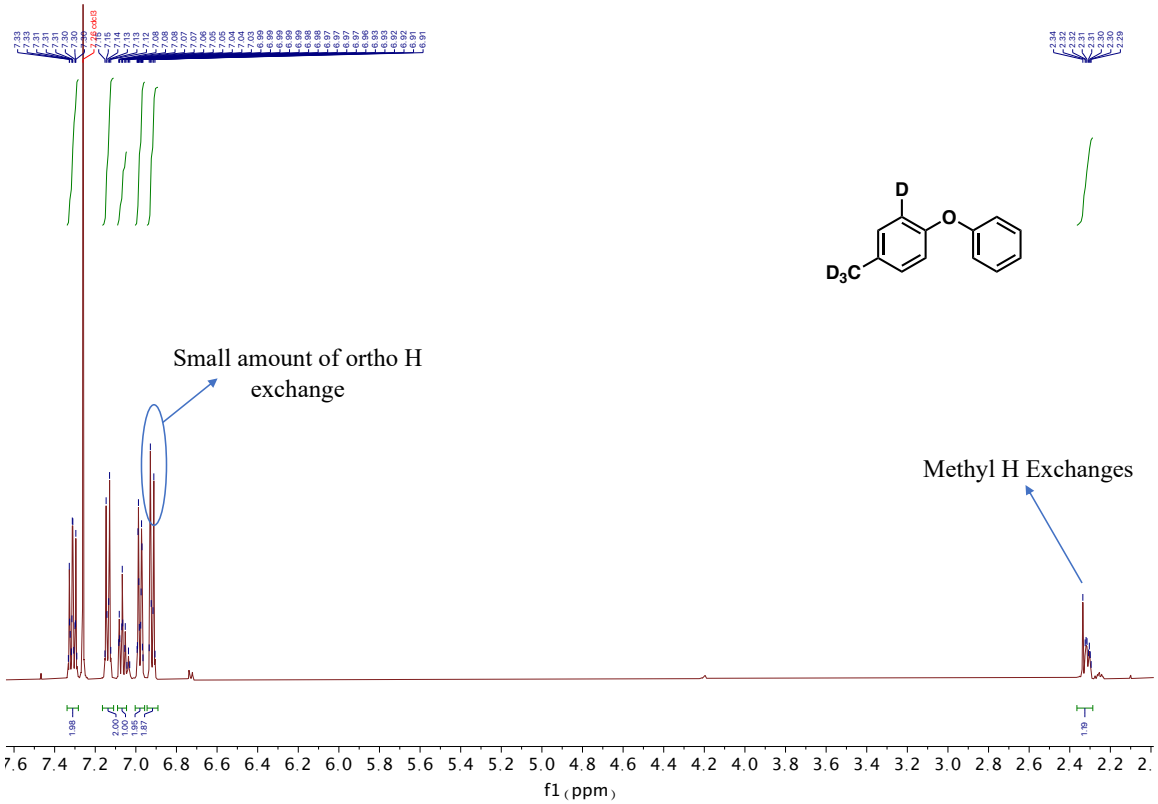

Figure 4.37 NMR spectrum of **labeled** 4-phenoxytoluene after 12 hours exchange.

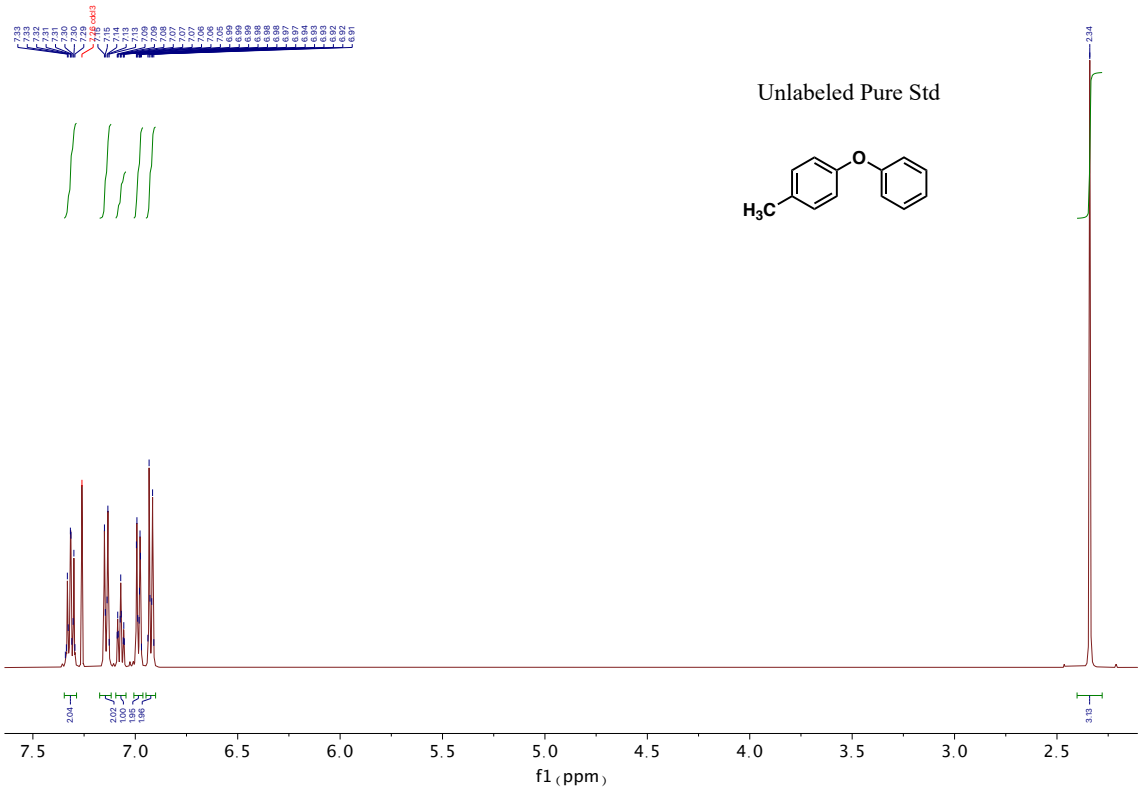

Figure 4.38 NMR spectrum of **unlabeled** 4-phenoxytoluene.

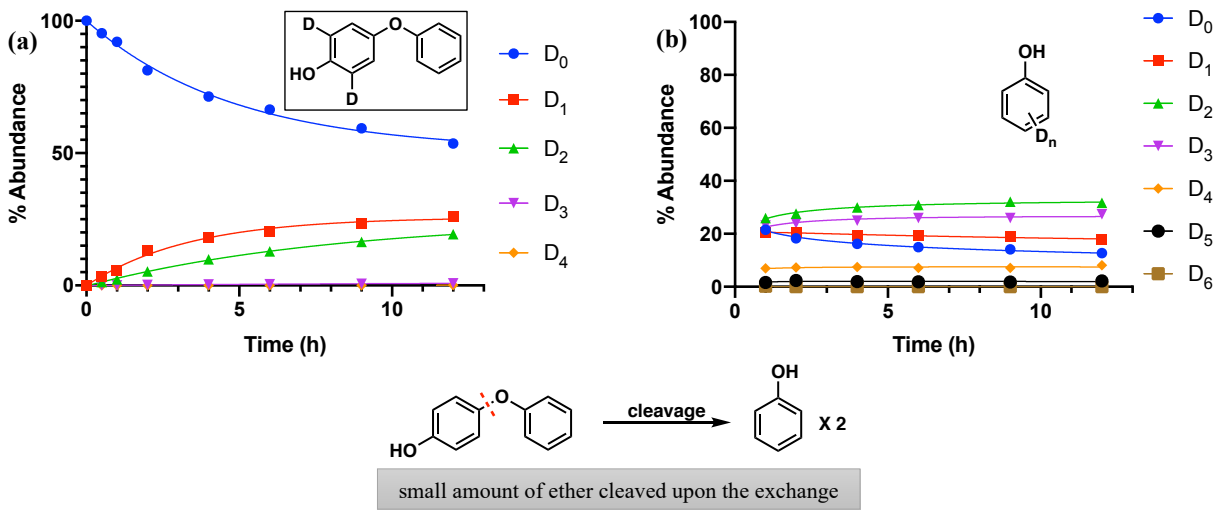

Figure 4.39 (a) Quantified % abundance of D_n of 4-phenoxyphenol determined by GC-MS (MS Spectra shown as Fig. 4.40 below). (b) Quantified % abundance of D_n of phenol, which undergoes fast H/D exchange on the Ni surface.

The D incorporated on the hydroxyl site is exchangeable, so the MS samples of 4-phenoxyphenol had an extra wash using non-deuterated water. The exchange locations in the 4-phenoxyphenol starting material here were determined by NMR (Fig. 4.42 below).

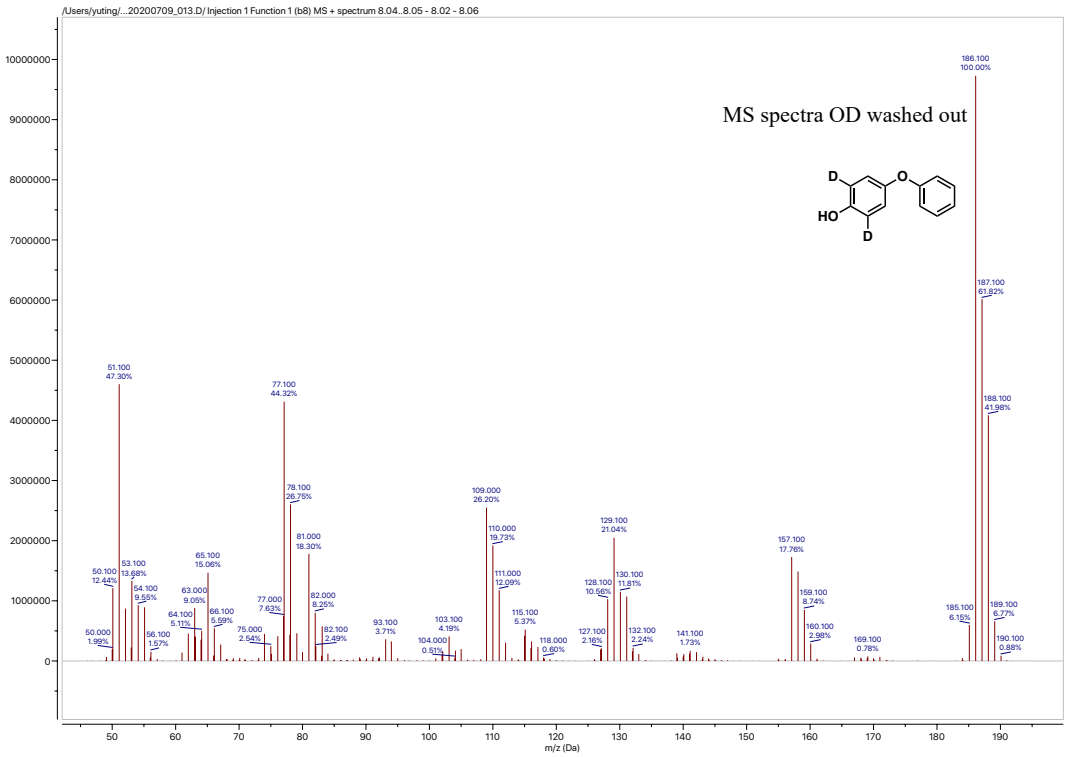

Figure 4.40 Mass spectrum of **labeled** 4-phenoxyphenol after 12 hours H/D exchange. The deuterium in the hydroxyl group was washed off by non-deuterated DI water to properly count the D exchanged in the aromatic protons. The location of the exchange was further confirmed by NMR.

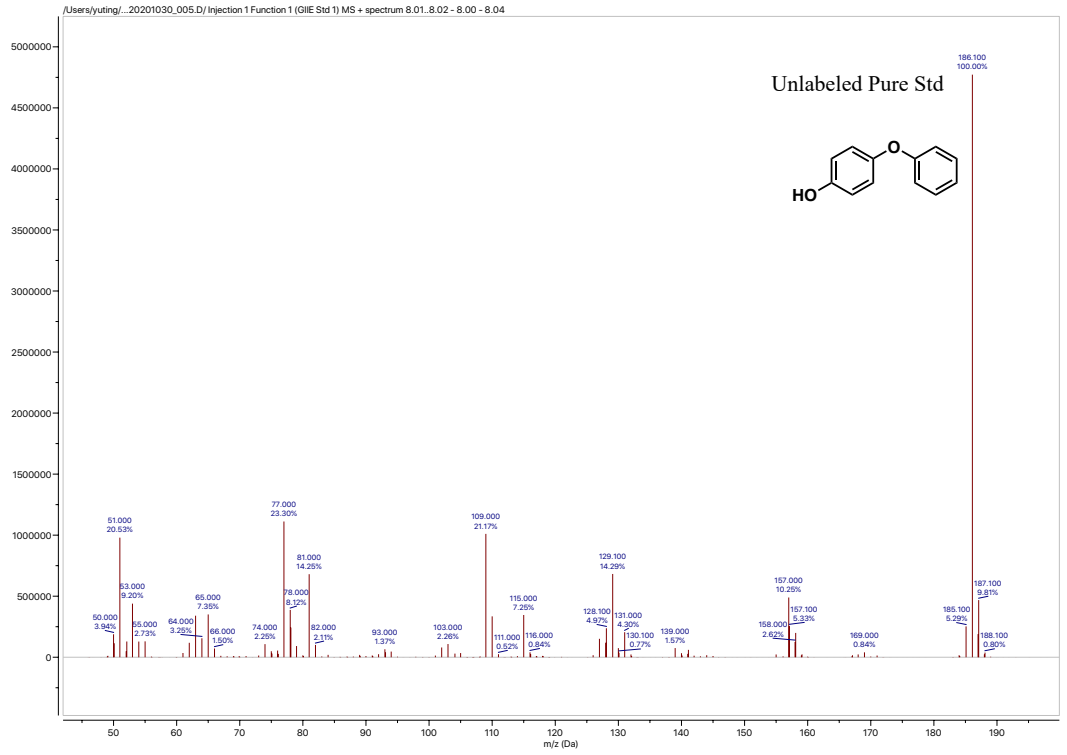

Figure 4.41 Mass spectrum of **unlabeled** 4-phenoxyphenol.

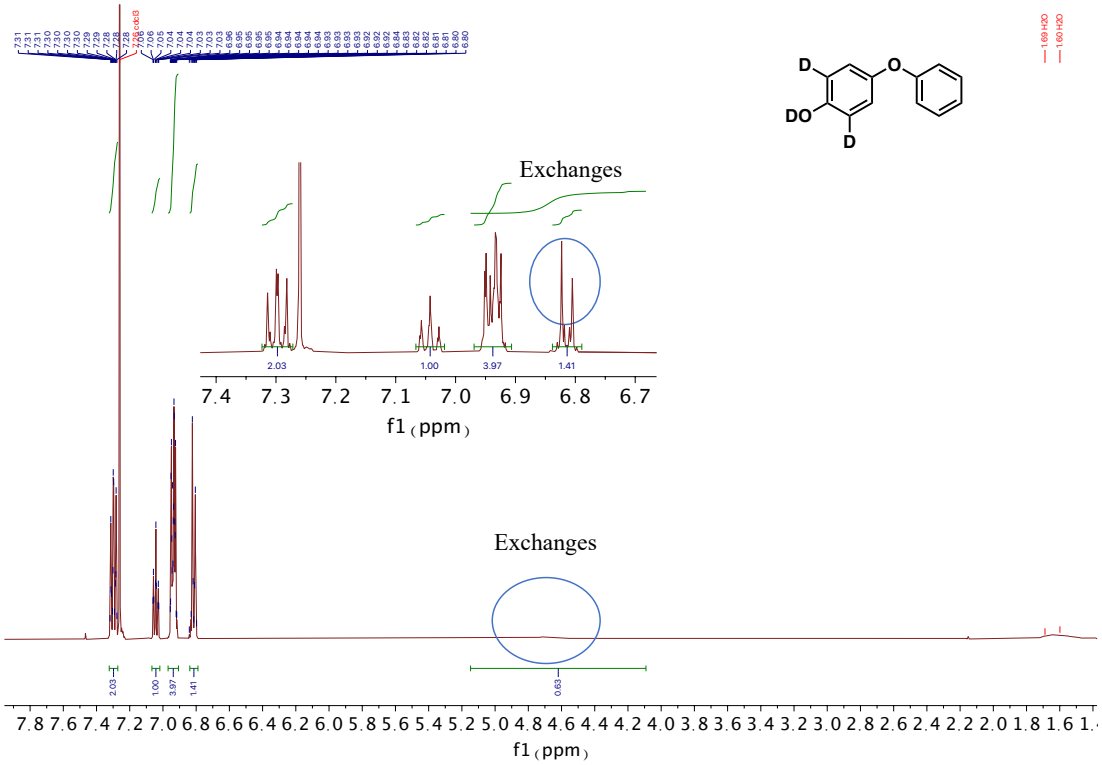

Figure 4.42 NMR spectrum of **labeled** 4-phenoxyphenol after 12 hours exchange. In ^{1}H NMR analysis, OD peak was separated from the aromatic protons, no DI water wash was needed.

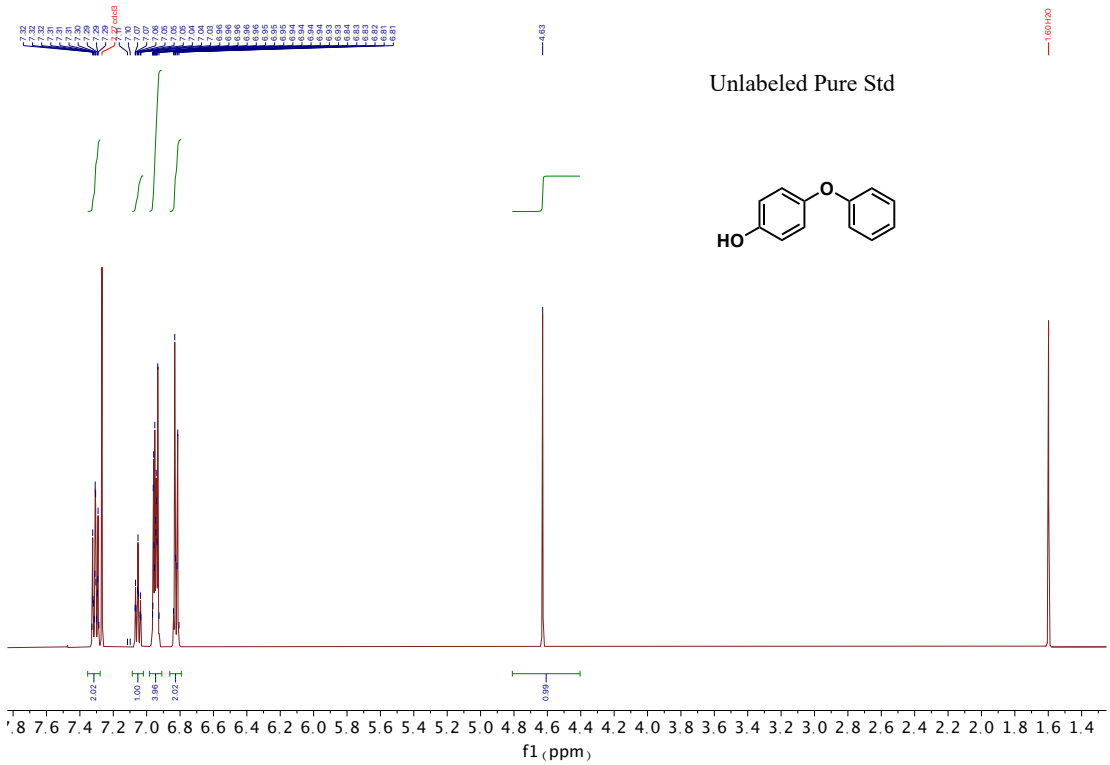

Figure 4.43 NMR spectrum of **unlabeled** 4-phenoxyphenol.

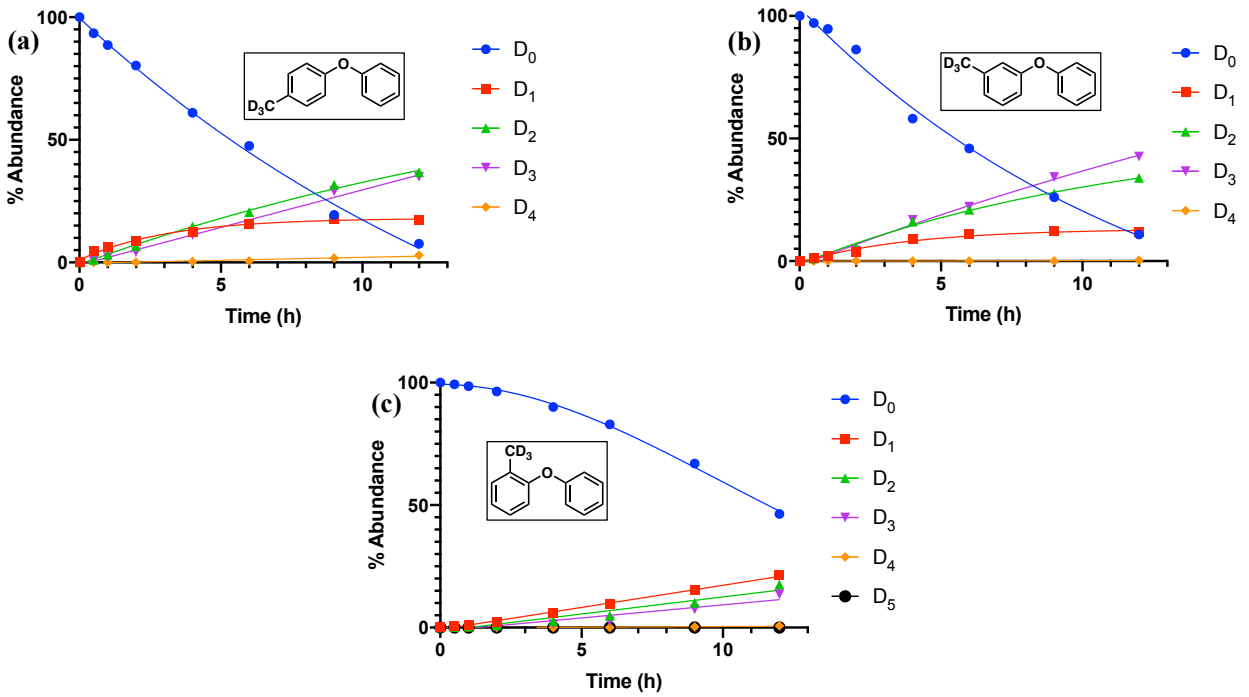

Figure 4.44 Quantified % abundance of D_n of (a) para-methylated diphenyl ether, (b) meta-methylated diphenyl ether and (c) ortho-methylated diphenyl ether.

Isotope distribution were determined by GC-MS. The exchange location is determined by NMR. Spectra of the para isomer are shown above, spectra of the meta (MS Fig. 4.45, NMR Fig. 4.47) and ortho (MS Fig. 4.49, NMR Fig. 4.51) isomers are shown below.

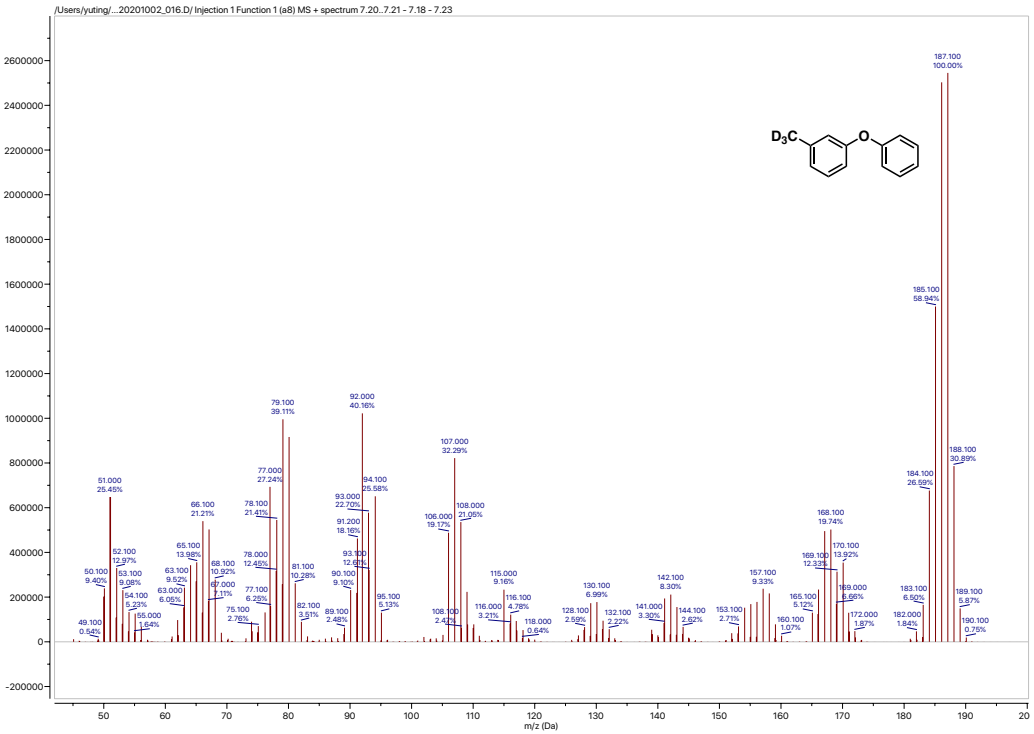

Figure 4.45 Mass spectrum of **labeled** 3-phenoxytoluene after 12 hours H/D exchange. The location of the exchange was further confirmed by NMR.

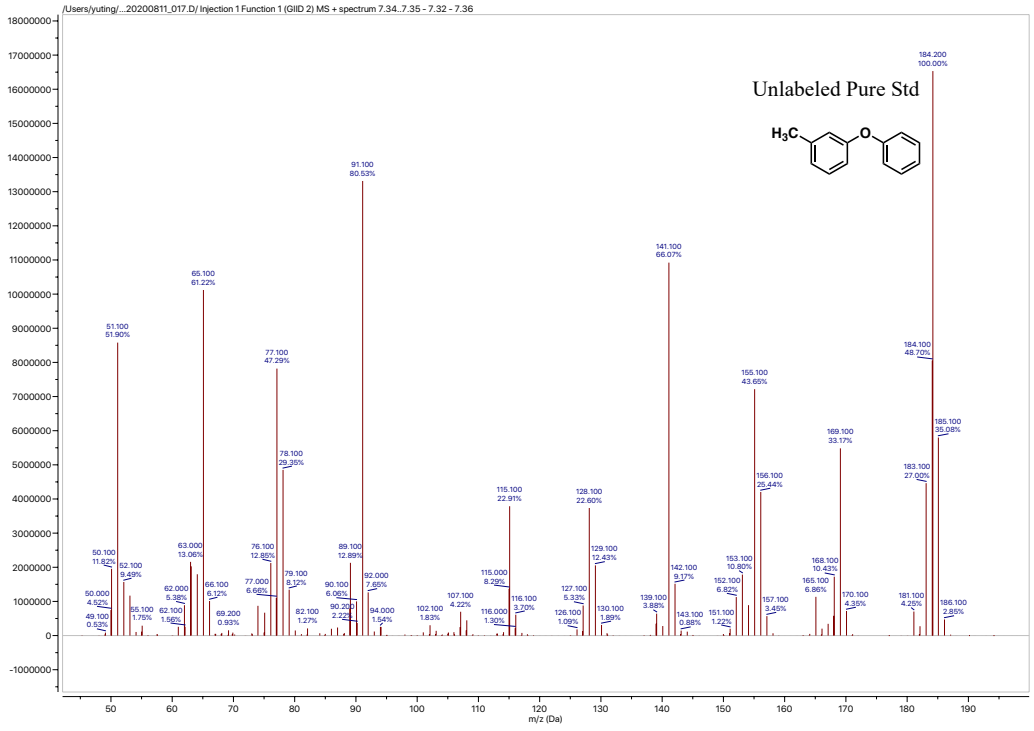

Figure 4.46 Mass spectrum of **unlabeled** 3-phenoxytoluene.

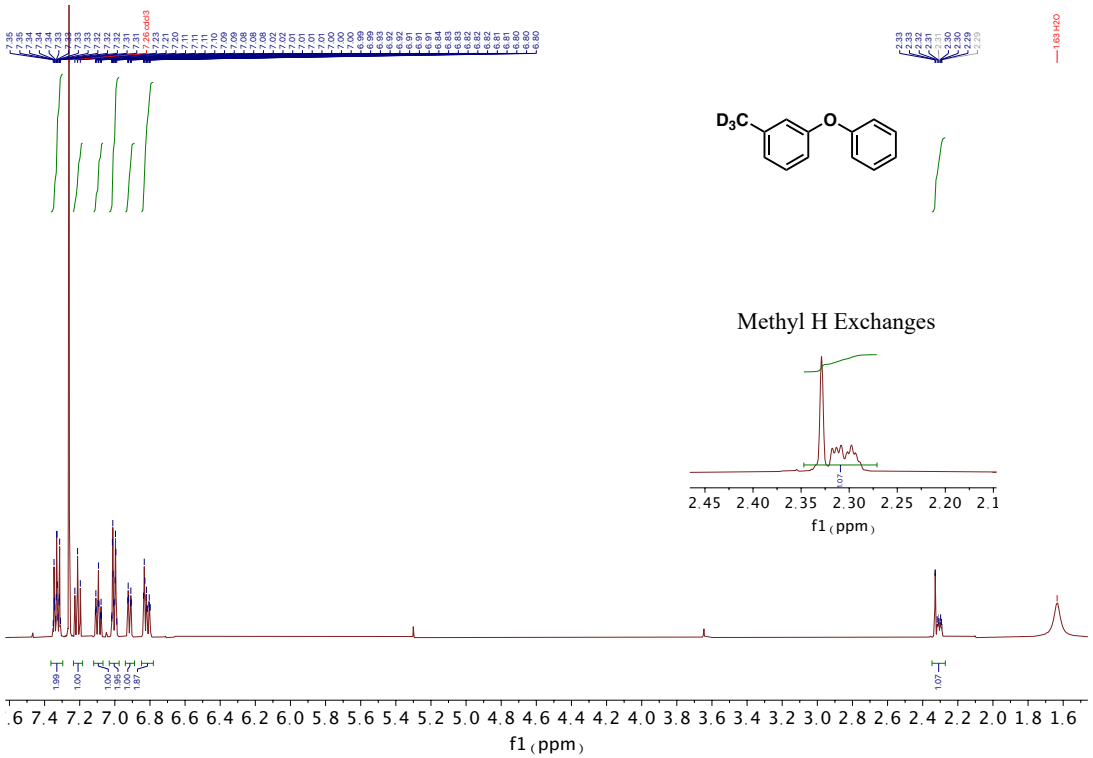

Figure 4.47 NMR spectrum of **labeled** 3-phenoxytoluene after 12 hours exchange. As with the para methyl model, the benzylic methyl showed significant of D incorporation.

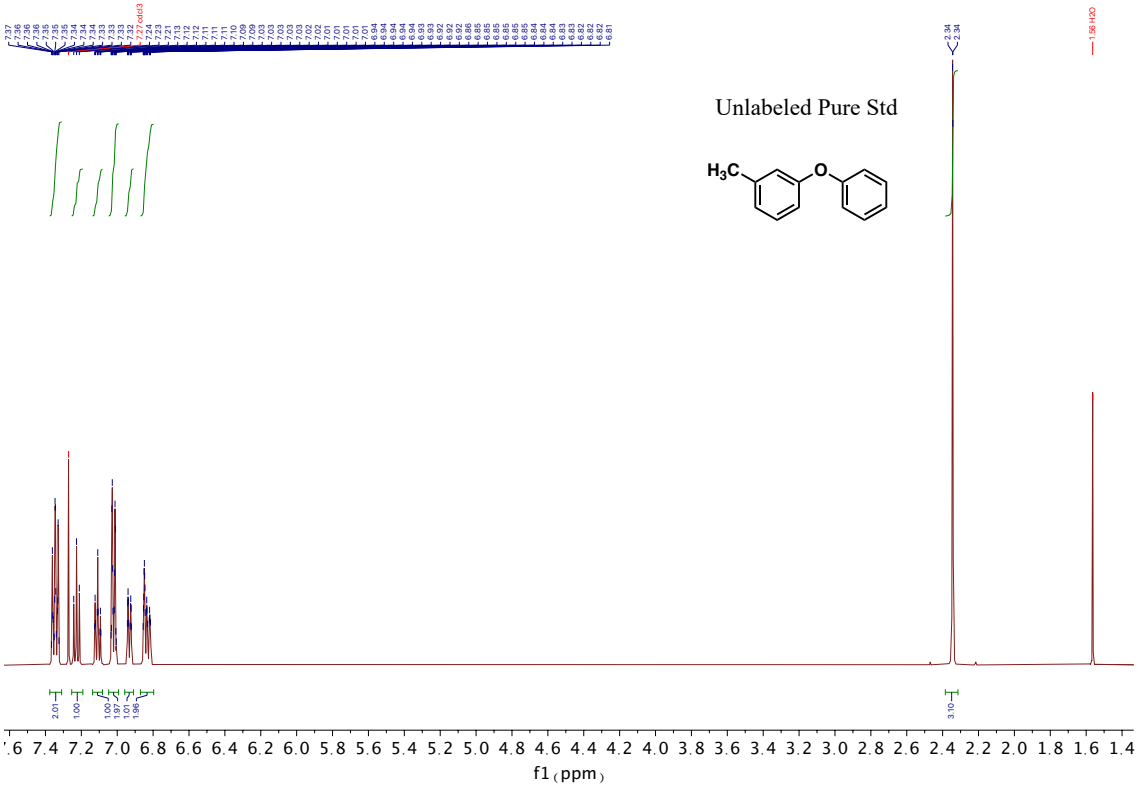

Figure 4.48 NMR spectrum of **unlabeled** 3-phenoxytoluene.

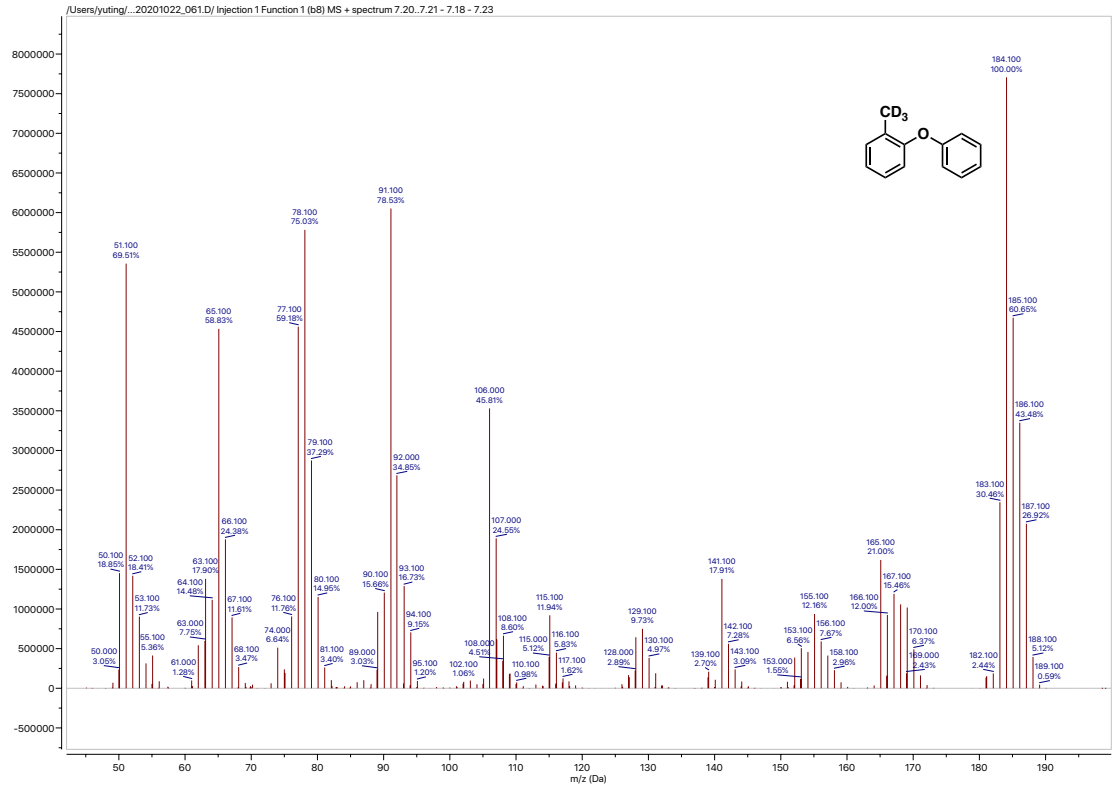

Figure 4.49 Mass spectrum of **labeled** 2-phenoxytoluene after 12 hours H/D exchange. The location of the exchange was further confirmed by NMR.

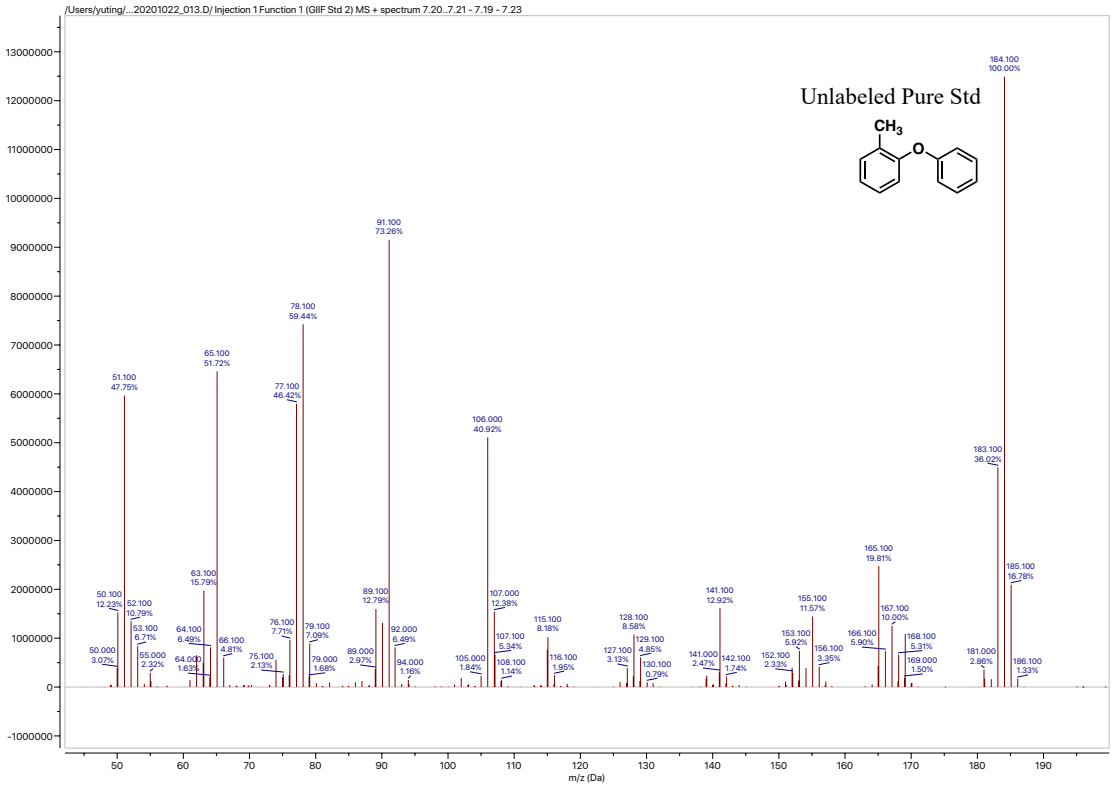

Figure 4.50 Mass spectrum of **unlabeled** 2-phenoxytoluene.

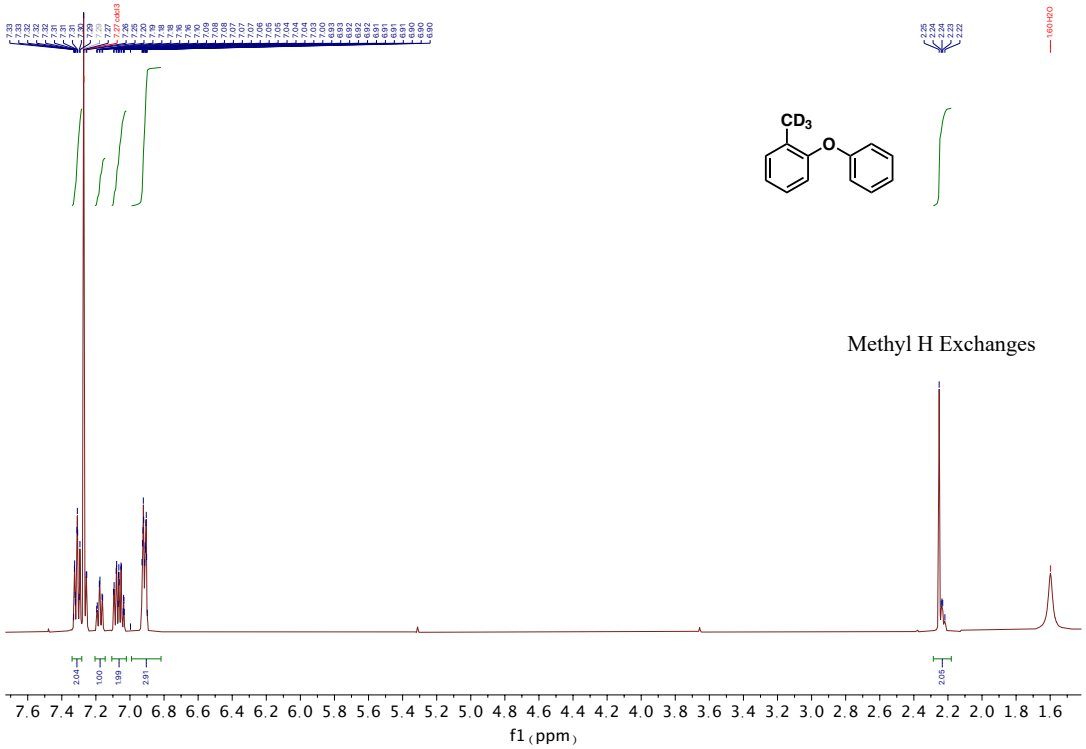

Figure 4.51 NMR spectrum of **labeled** 2-phenoxytoluene after 12 hours exchange. Even the exchange is much slower than the para and meta methyl models, the benzylic methyl still has observable D incorporation.

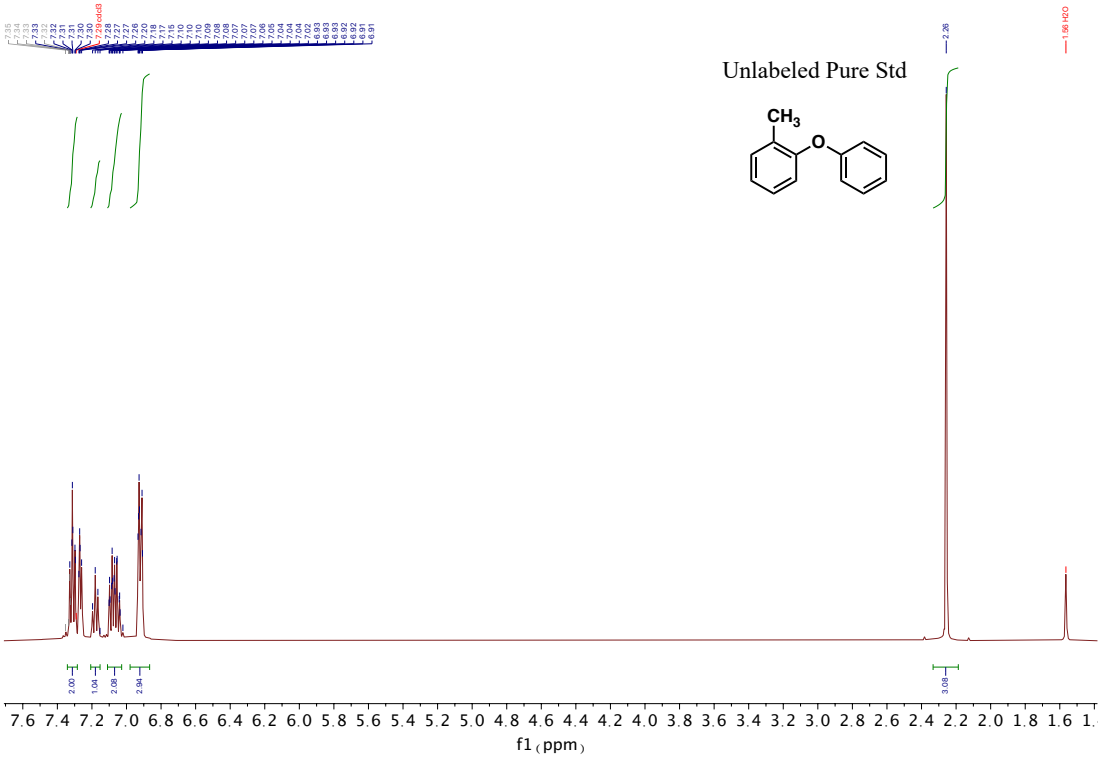

Figure 4.52 NMR spectrum of **unlabeled** 2-phenoxytoluene.

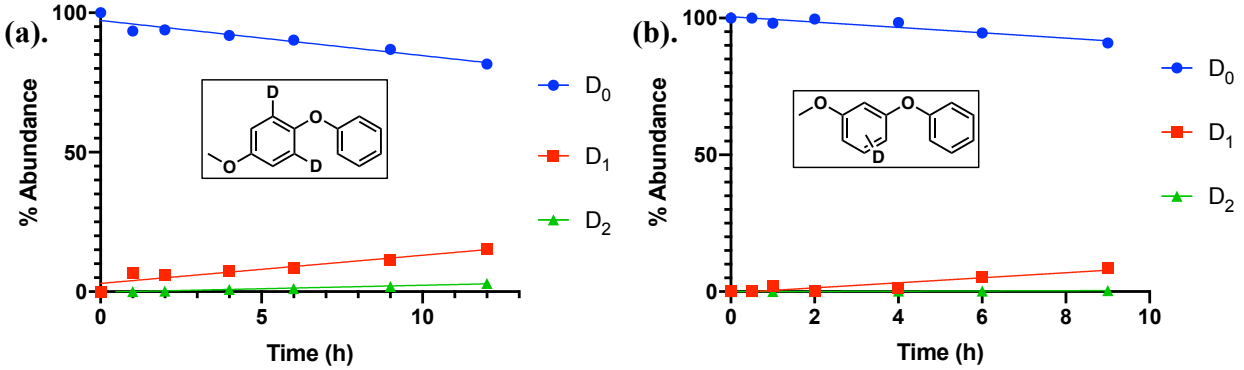

Figure 4.53 Quantified % abundance of D_n of (a) para-methoxylated diphenyl ether and (b) meta-methoxylated diphenyl ether.

Isotope distributions were determined by GC-MS. The exchange locations were determined by NMR. Spectra of the para isomer are shown had above, spectra of the meta isomer are shown (MS Fig. 4.54, NMR Fig. 4.56) below.

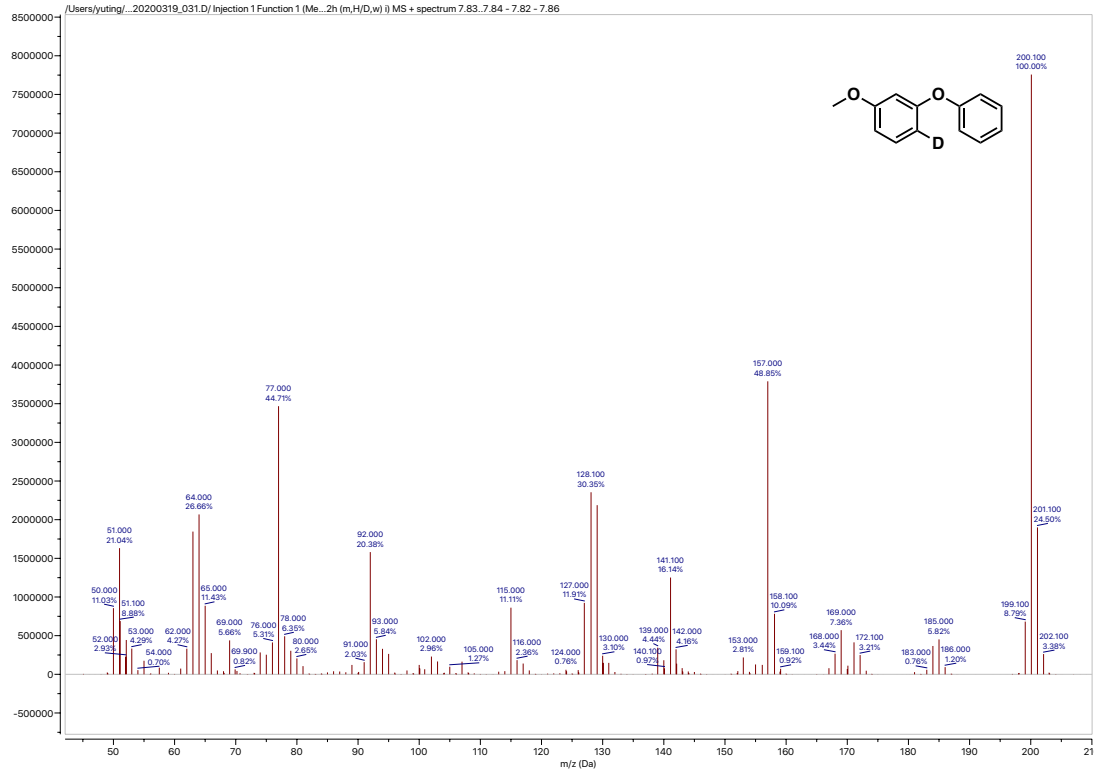

Figure 4.54 Mass spectrum of **labeled** 3-phenoxyanisole after 12 hours H/D exchange. Compared to the spectra of the unlabeled standard (Figure 4.55), only small increases of m/z 201 and 202, and the decreases in m/z 199 are visible.

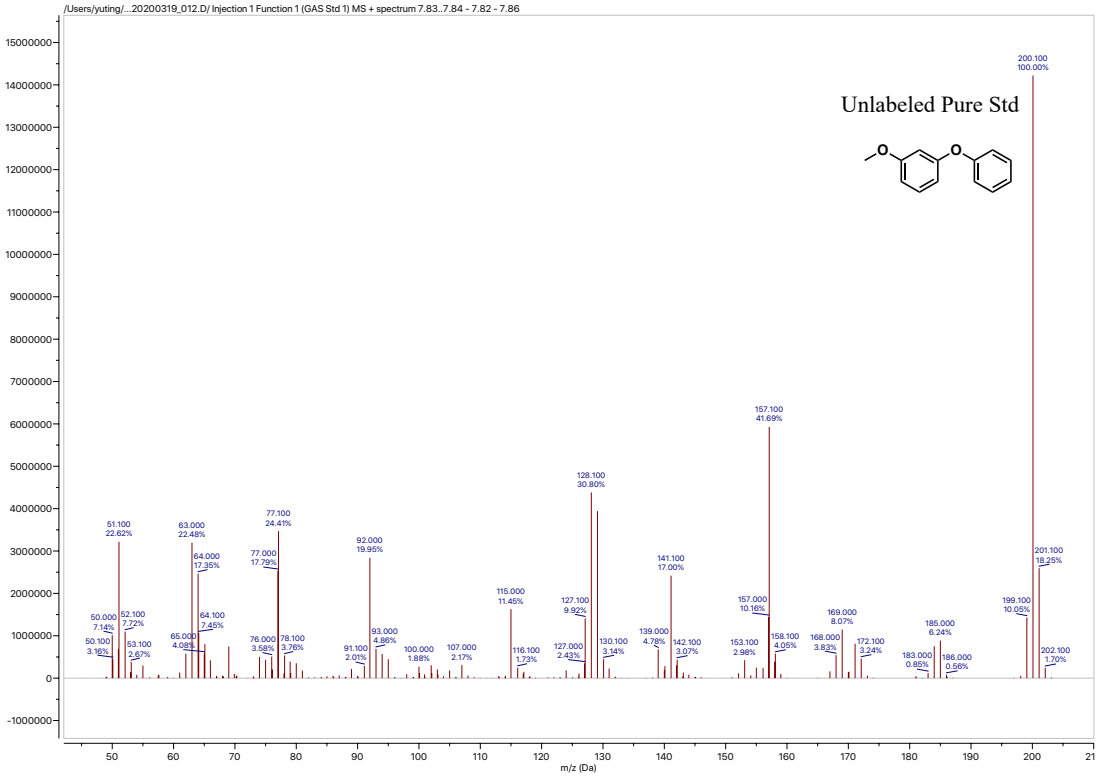

Figure 4.55 Mass spectrum of **unlabeled** 3-phenoxyanisole.

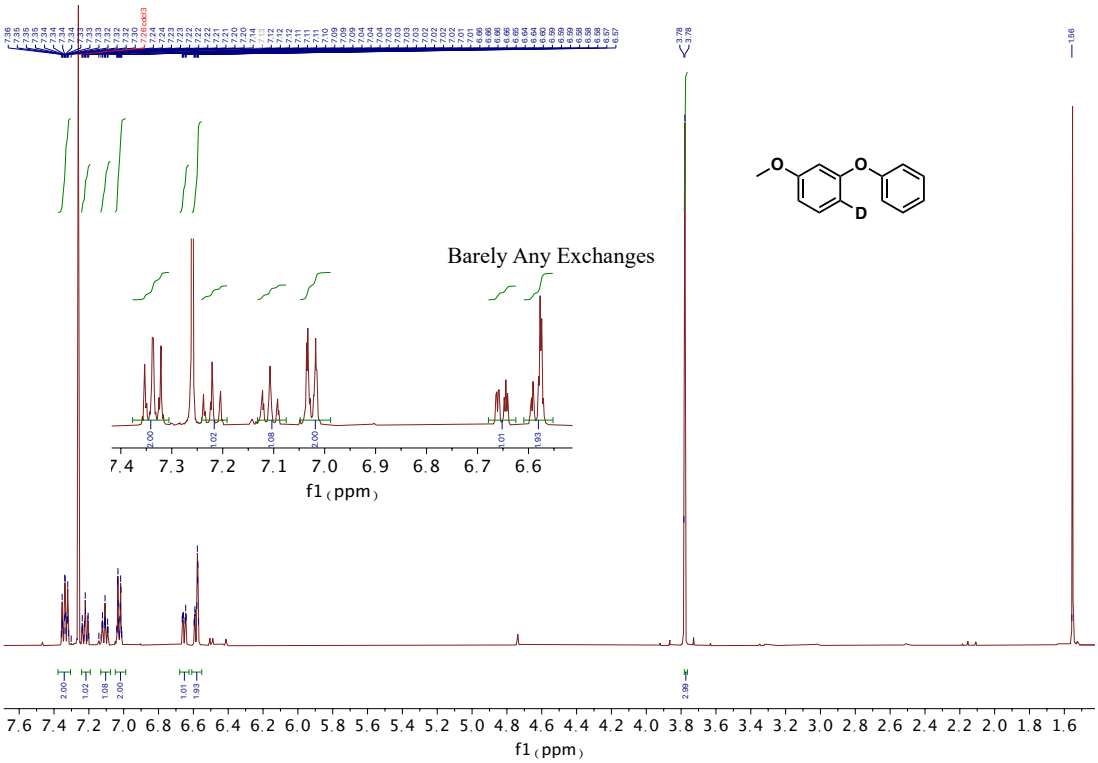

Figure 4.56 NMR spectrum of **labeled** 3-phenoxyanisole after 12 hours exchange. Barely any difference from the unlabeled standard (Fig. 4.57) were detected.

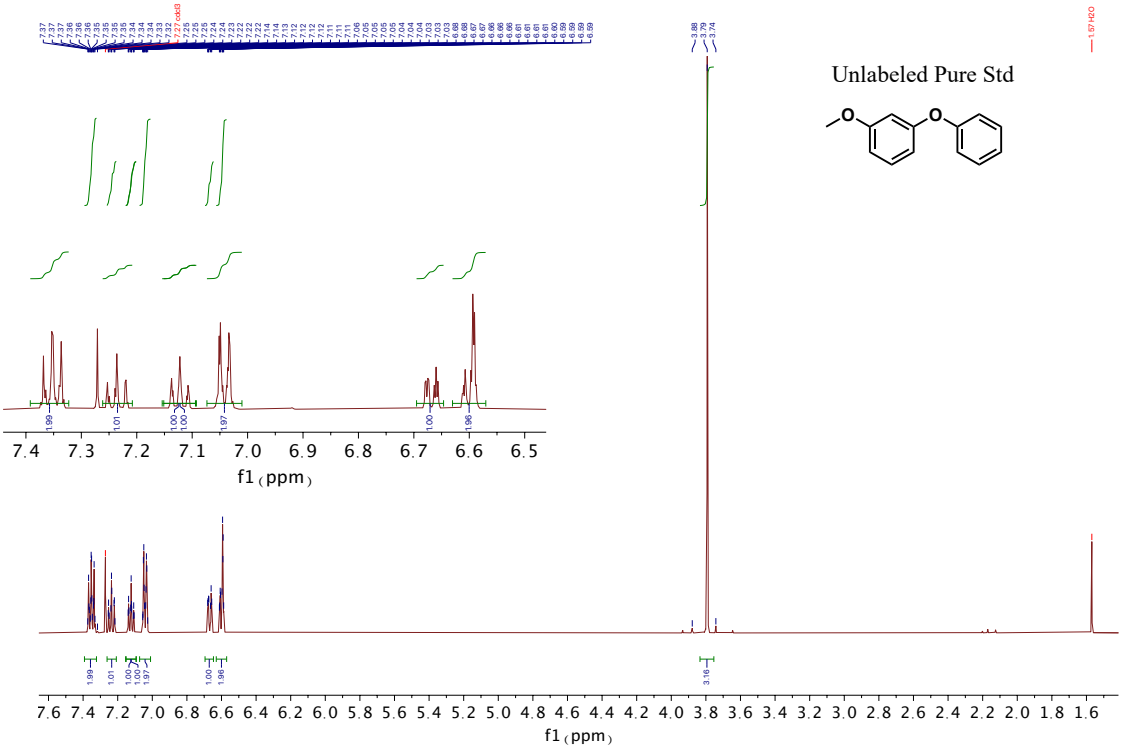

Figure 4.57 NMR spectrum of **unlabeled** 3-phenoxyanisole.

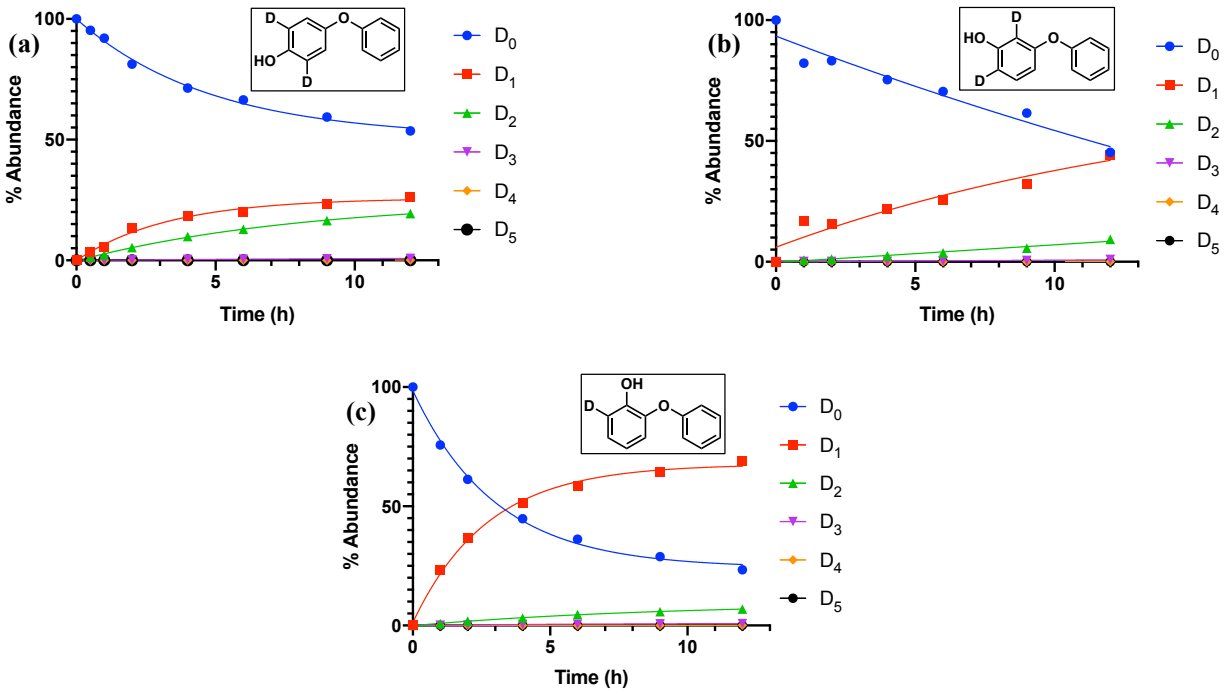

Figure 4.58 Quantified % abundance of D_n of (a) para-hydroxylated diphenyl ether, (b) meta-hydroxylated diphenyl ether and (c) ortho-hydroxylated diphenyl ether. Isotope distributions were determined by GC-MS.

The incorporated D on hydroxyl is easy to lose during the preparation of the analytical sample, therefore, the MS analysis samples had an extra wash using non-deuterated water to remove the OD. The exchange location is determined by NMR. Spectra of the para isomer are shown above, spectra of the meta (MS Fig. 4.59, NMR Fig. 4.61) and ortho (MS Fig. 4.63, NMR Fig. 4.65, 4.67) isomers are shown below.

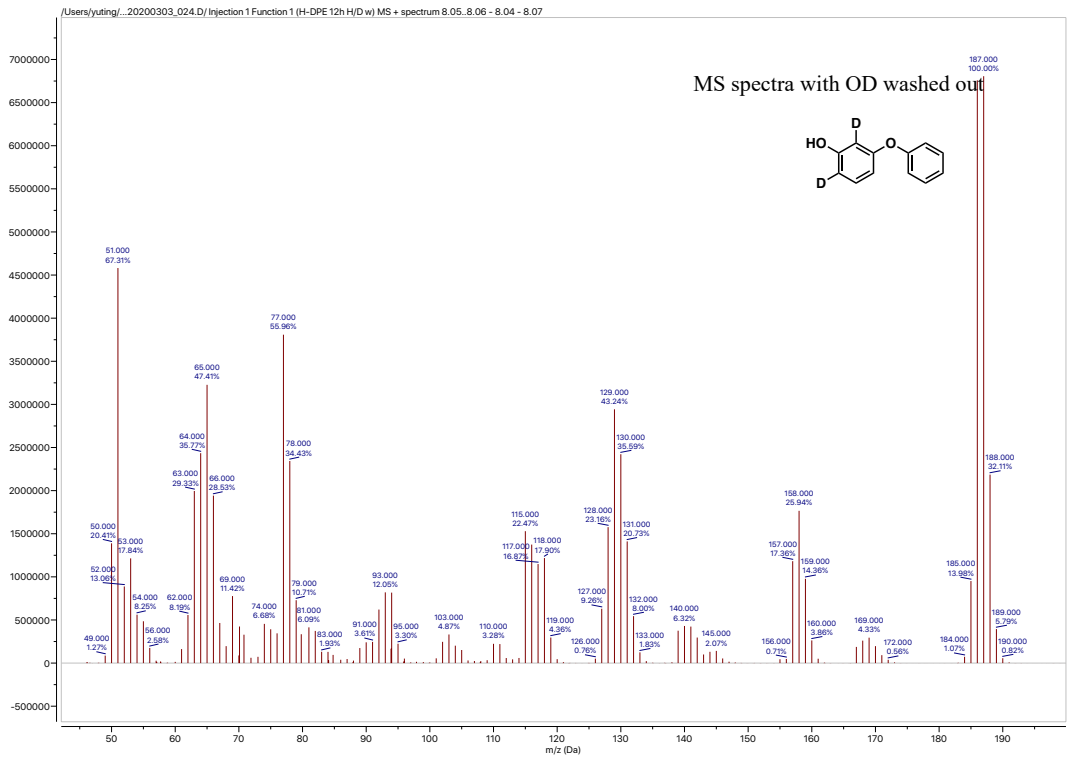

Figure 4.59 Mass spectrum of **labeled** 3-phenoxyphenol after 12 hours H/D exchange. The deuterium on the hydroxyl group was washed off by non-deuterated DI water. The location of the exchange was further confirmed by NMR.

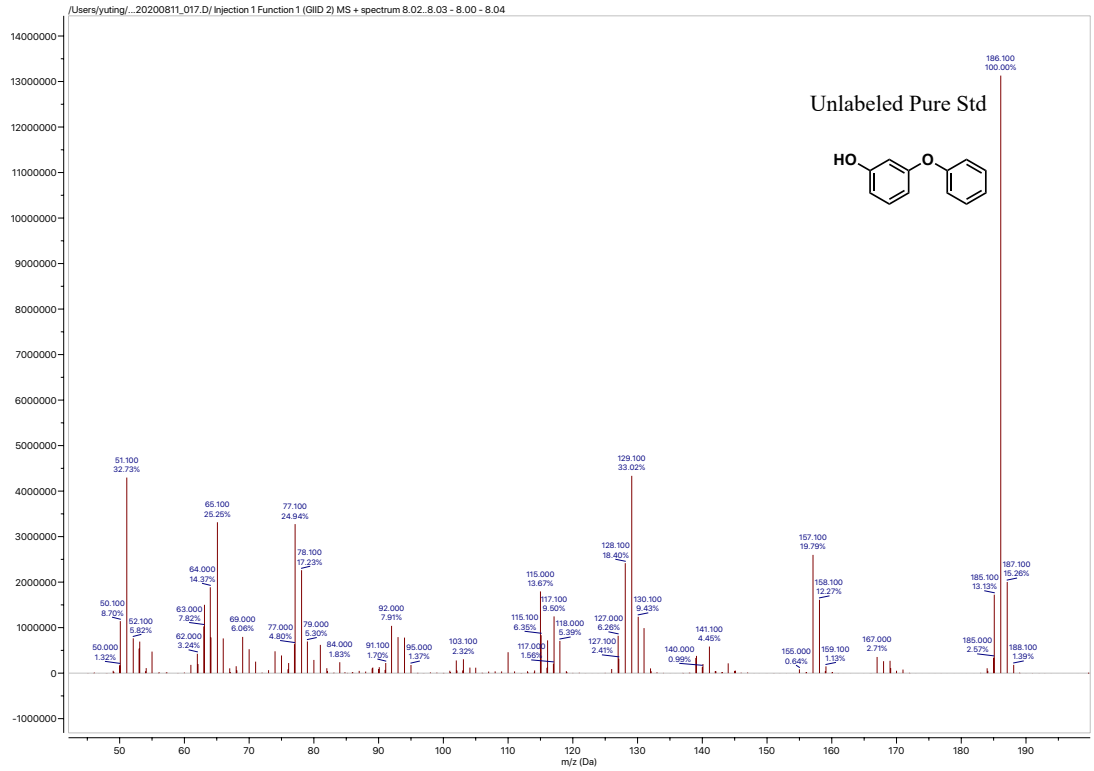

Figure 4.60 Mass spectrum of **unlabeled** 3-phenoxyphenol.

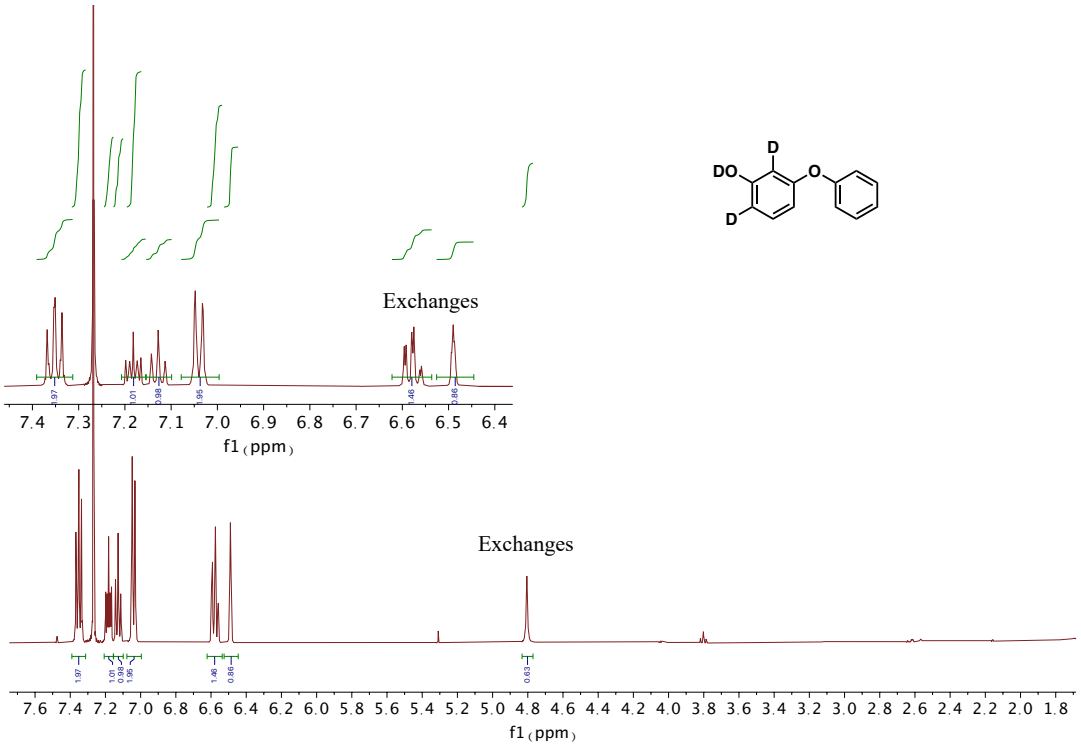

Figure 4.61 NMR spectrum of **labeled** 3-phenoxyphenol after 12 hours exchange. In ^{1}H NMR analysis, OD peak was separated from the aromatic protons, no DI water wash was needed.

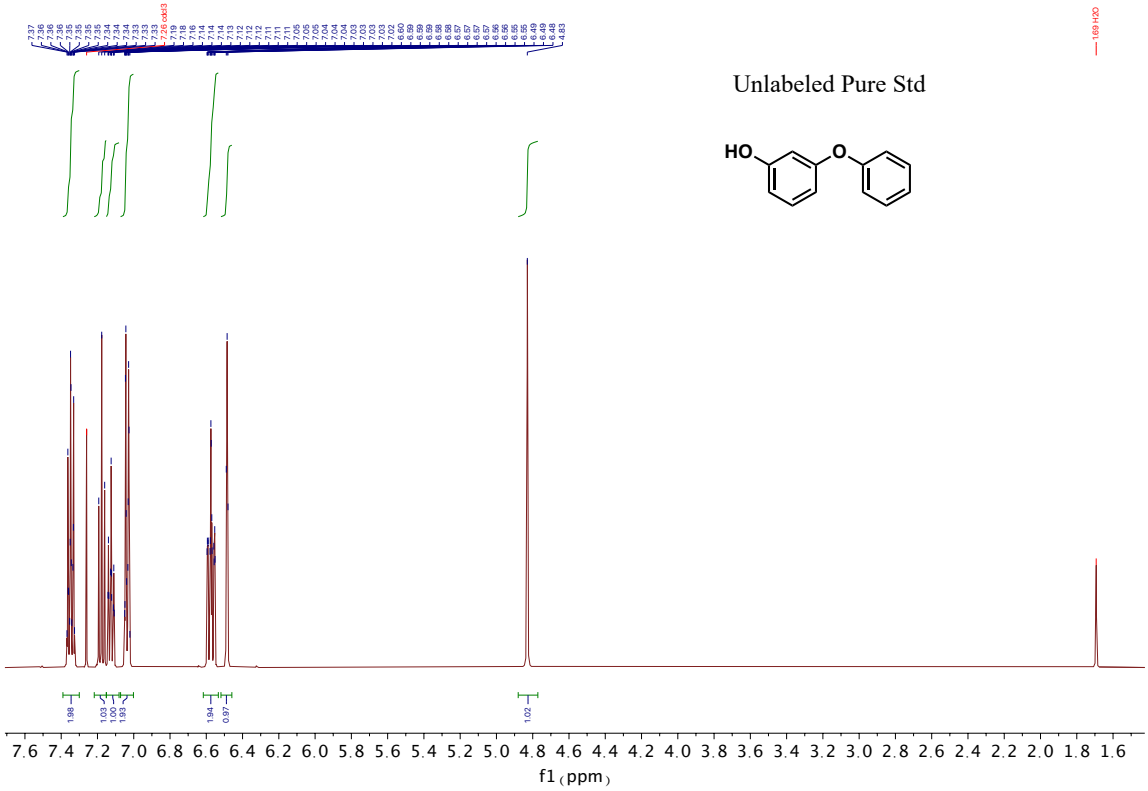

Figure 4.62 NMR spectrum of **unlabeled** 3-phenoxyphenol.

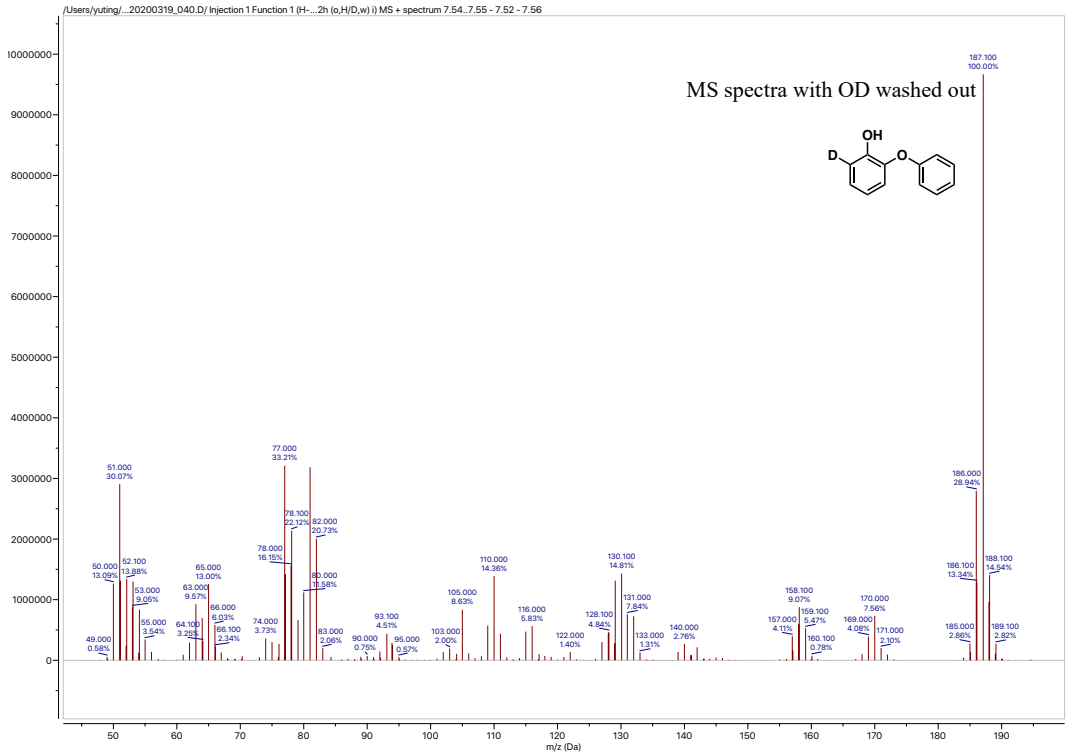

Figure 4.63 Mass spectrum of **labeled** 2-phenoxyphenol after 12 hours H/D exchange. The deuterium on the hydroxyl group was washed off by non-deuterated DI water. The location of the exchange was further confirmed by NMR.

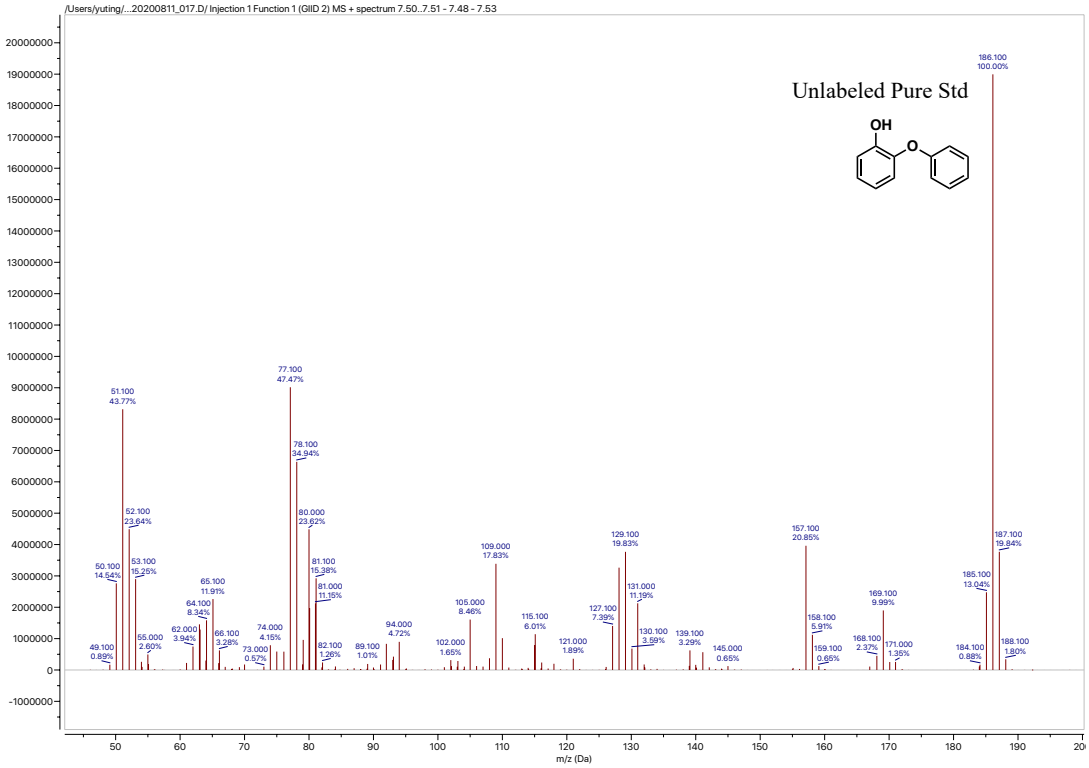

Figure 4.64 Mass spectrum of **unlabeled** 2-phenoxyphenol.

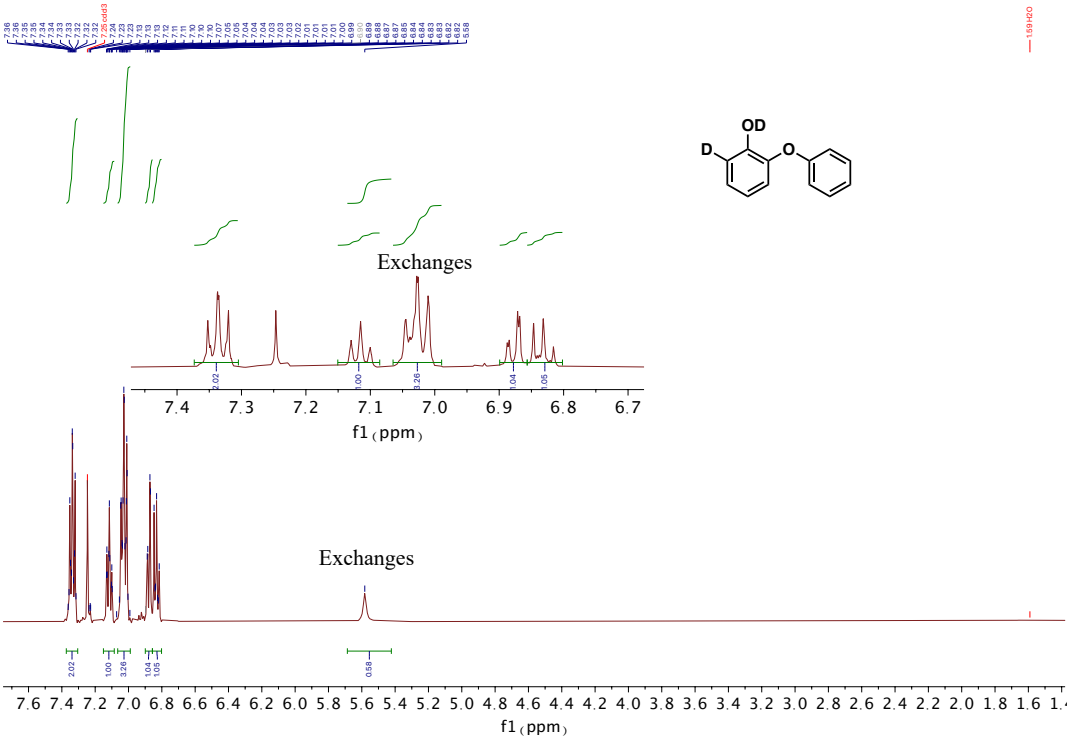

Figure 4.65 NMR spectrum of **labeled** 2-phenoxyphenol after 12 hours exchange. In ^{1}H NMR analysis, OD peak was separated from the aromatic protons, no DI water wash was needed. The exchanged aromatic peak contains different Hs overlapping, to further identify the exchange location, ^{13}C NMR were taken.

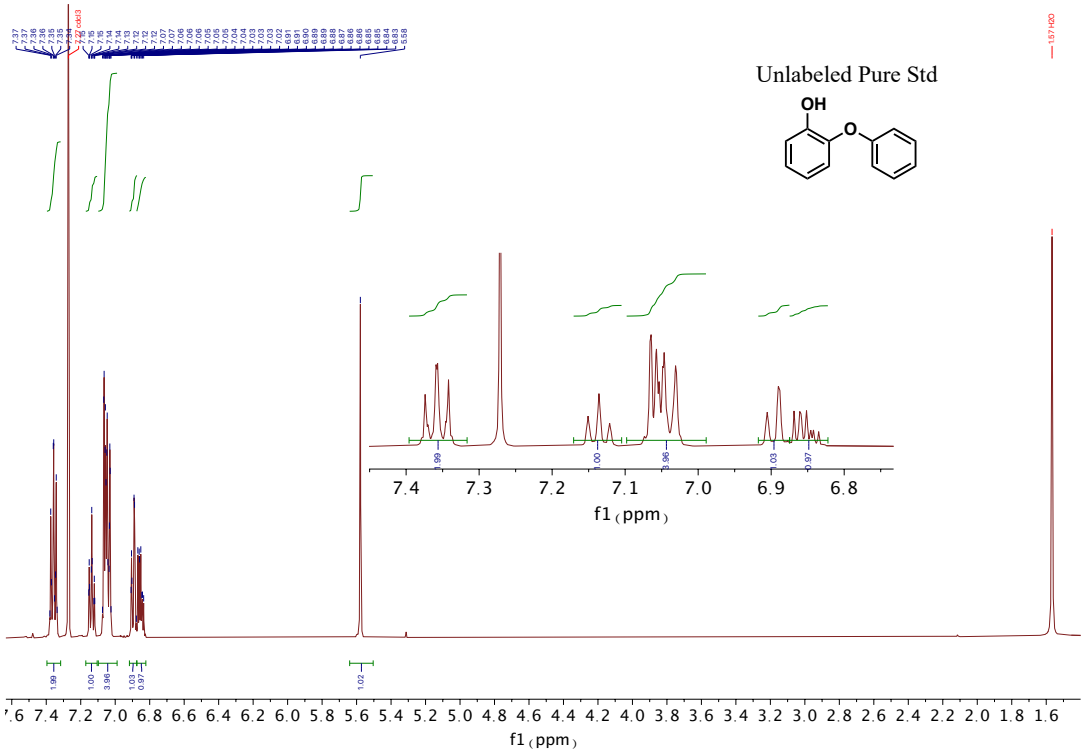

Figure 4.66 NMR spectrum of **unlabeled** 2-phenoxyphenol.

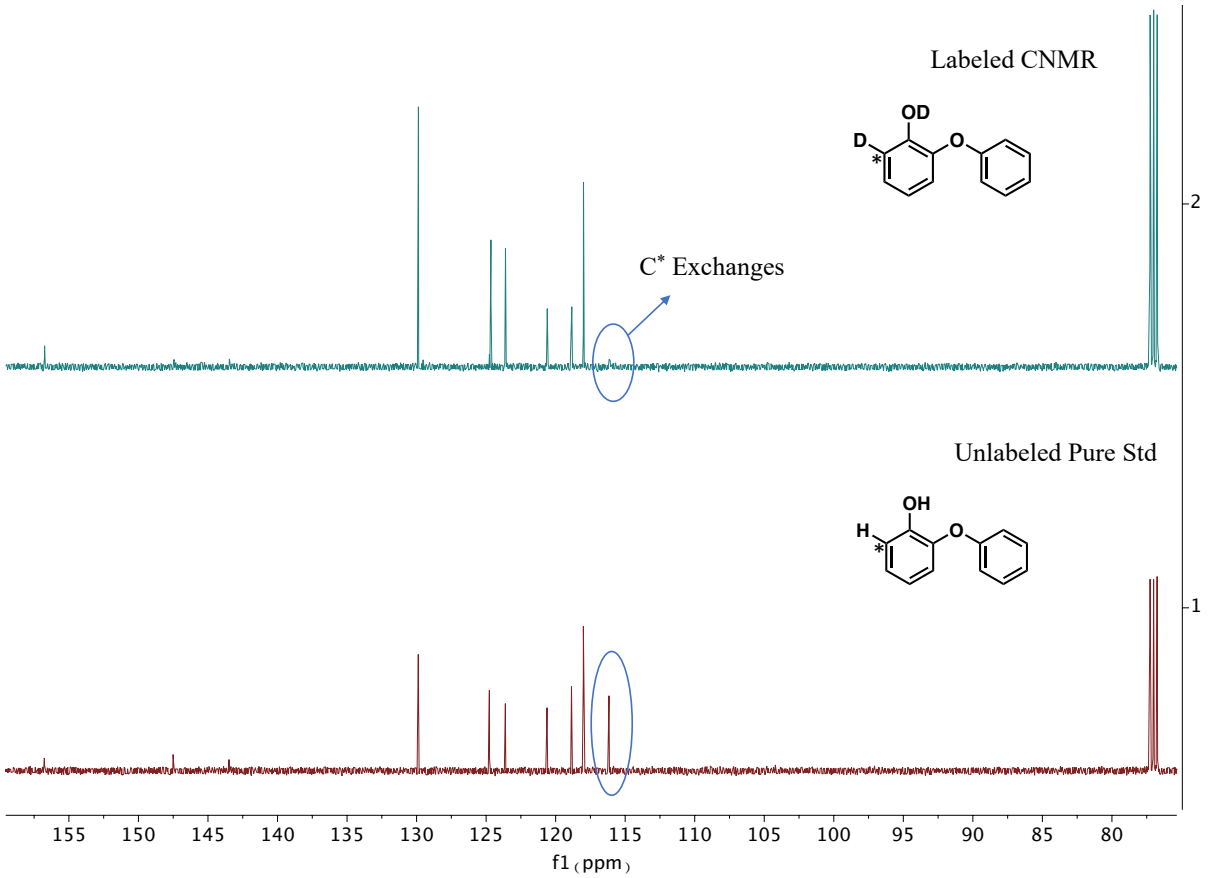

Figure 4.67 Carbon NMR spectrum of **labeled** 2-phenoxyphenol after 12 hours exchange, and the pure unlabeled standard as reference.

As indicated in the spectra, the most upfield carbon had a significant decrease of its intensity. Assignments of ^{13}C resonances were made with the aid of NMR chemical shifts computed at the EDF2/6-31+G* level of theory[54] as implemented in the Spartan '18 code.[16] This DFT method has been specifically optimized to cost effectively predict spectroscopic results.

4.7.4 ***Full ECH Time Courses Measurements***

Full ECH Time Courses for Diphenyl Ether, 4-Phenoxytoluene, 4-Phenoxyanisole and 4-Phenoxyphenol

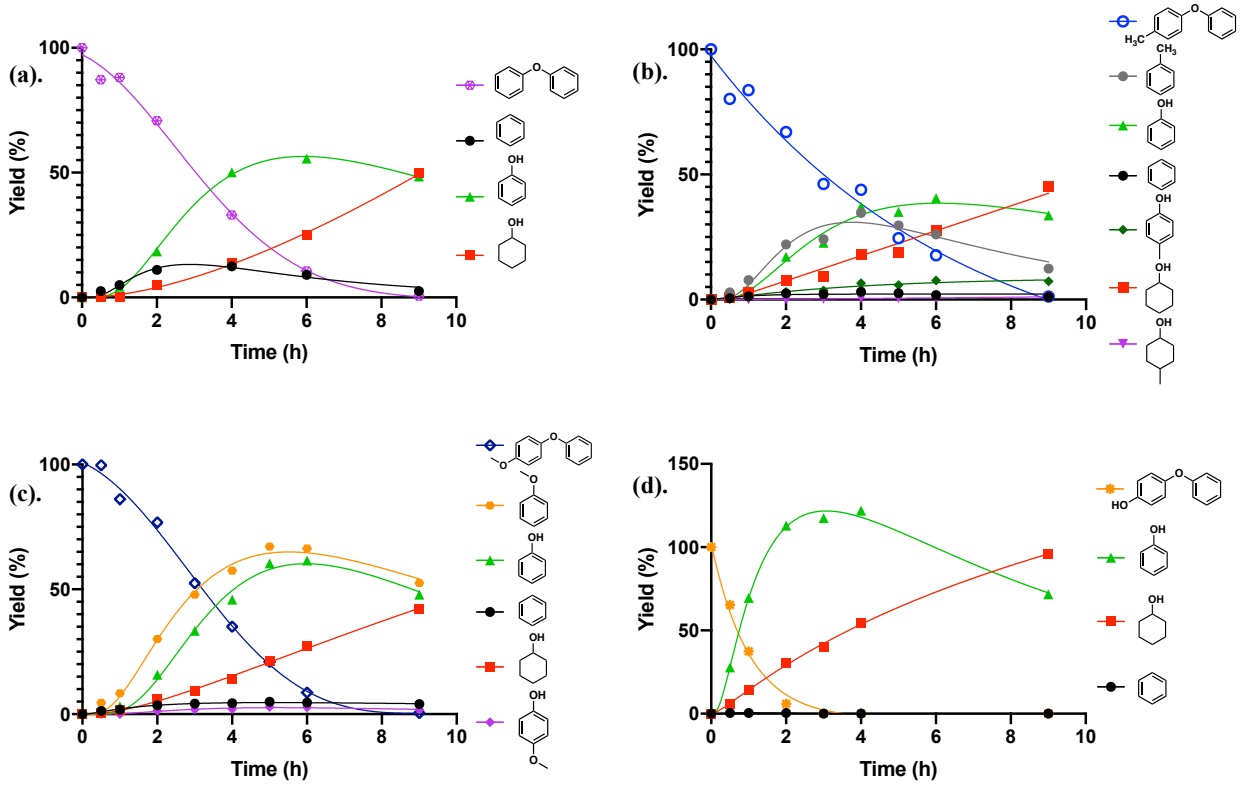

Figure 4.68 Full ECH measurements of diphenyl ether (a), para methylated diphenyl ether (b), para methoxylated diphenyl ether (c) and also para hydroxylated diphenyl ether (d), under standard ECH conditions (50 mA, 60°C, 33%IPA).

The yields of cyclohexanol and phenol were corrected for extraction losses. The yield of 4-methoxyphenol was corrected for extraction loss. The yield of p-Cresol was corrected using the extraction efficiency of phenol. All yield correction details, see chapter 2, section 2.2.5. No yield corrections were applied on the starting diphenyl ethers and the alkyl benzenes.

Full ECH Time Courses for para, meta and ortho Methoxylated Diphenyl Ethers

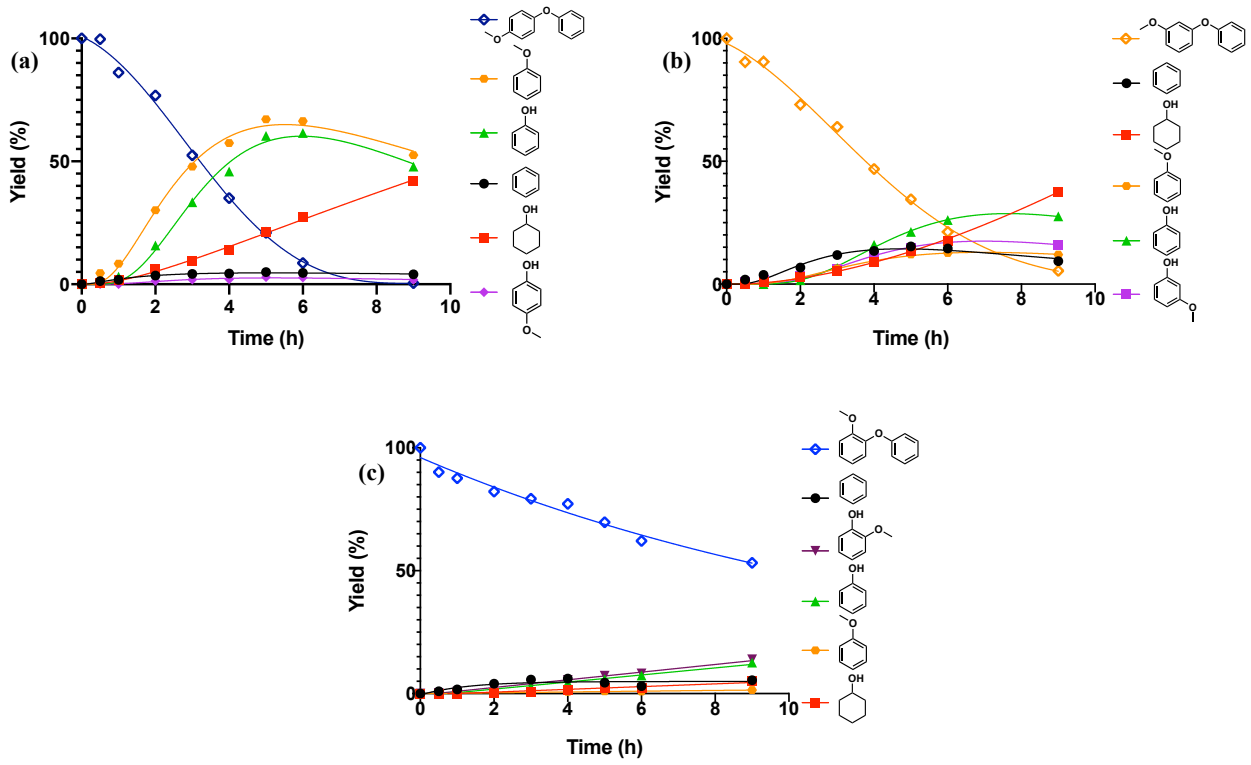

Figure 4.69 Full ECH measurements of (a) para-methoxylated diphenyl ether, (b) meta-methoxylated diphenyl ether and (c) ortho-methoxylated diphenyl ether at standard ECH condition (50 mA, 60 °C and 33%IPA).

The yield of cyclohexanol, anisole and phenol were corrected for extraction losses. The yields of 4-methoxyphenol and 2-methoxyphenol was corrected for extraction loss. The yield of 3-methoxyphenol was corrected using the extraction efficiency of 4-methoxyphenol. All yield correction details, see chapter 2, section 2.2.5. No yield corrections were applied on the starting diphenyl ethers and the benzene.

Full ECH Time Courses for para, meta and ortho Methylated Diphenyl Ethers

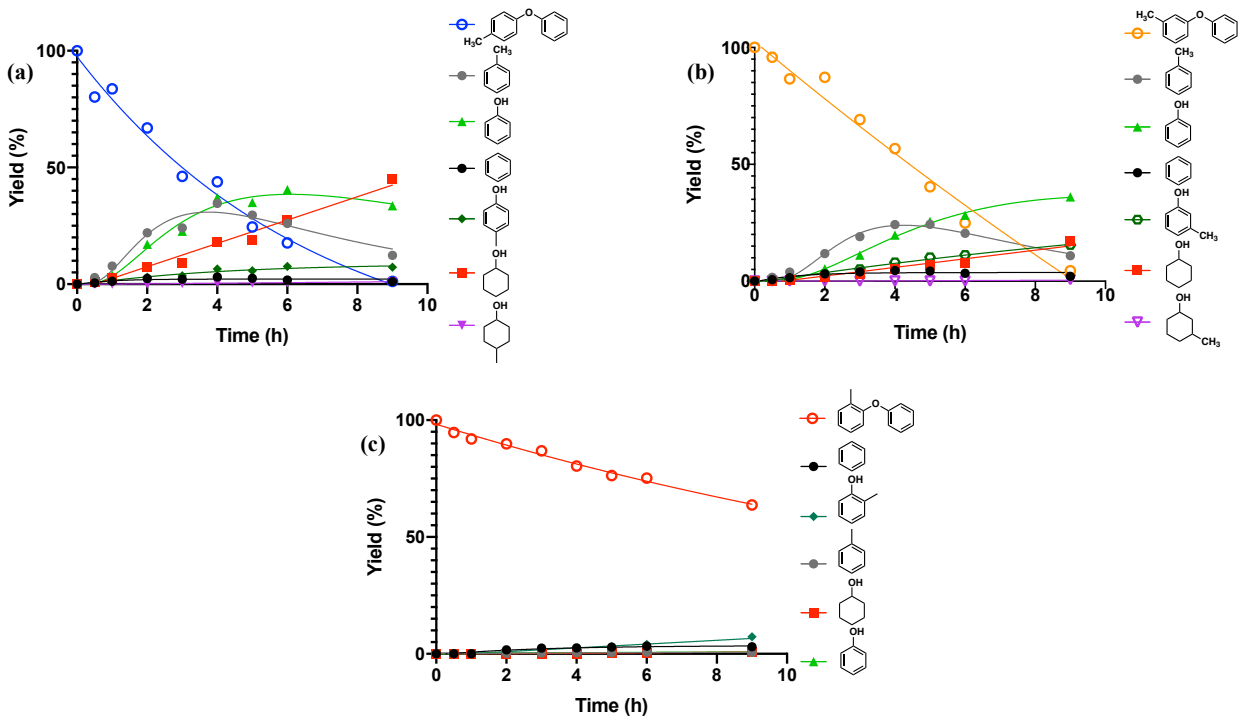

Figure 4.70 Full ECH measurements of (a) para-methylated diphenyl ether, (b) meta-methylated diphenyl ether and (c) ortho-methylated diphenyl ether at standard ECH condition (50 mA, 60 °C and 33%IPA).

The yield of cyclohexanol and phenol were corrected for extraction losses. The yields of cresols were corrected using the extraction efficiency of phenol. All yield correction details, see chapter 2, section 2.2.5. No yield corrections were applied on the starting diphenyl ethers, methyl cyclohexanols or alkyl benzenes.

Full ECH Time Courses for para, meta and ortho Hydroxylated Diphenyl Ethers

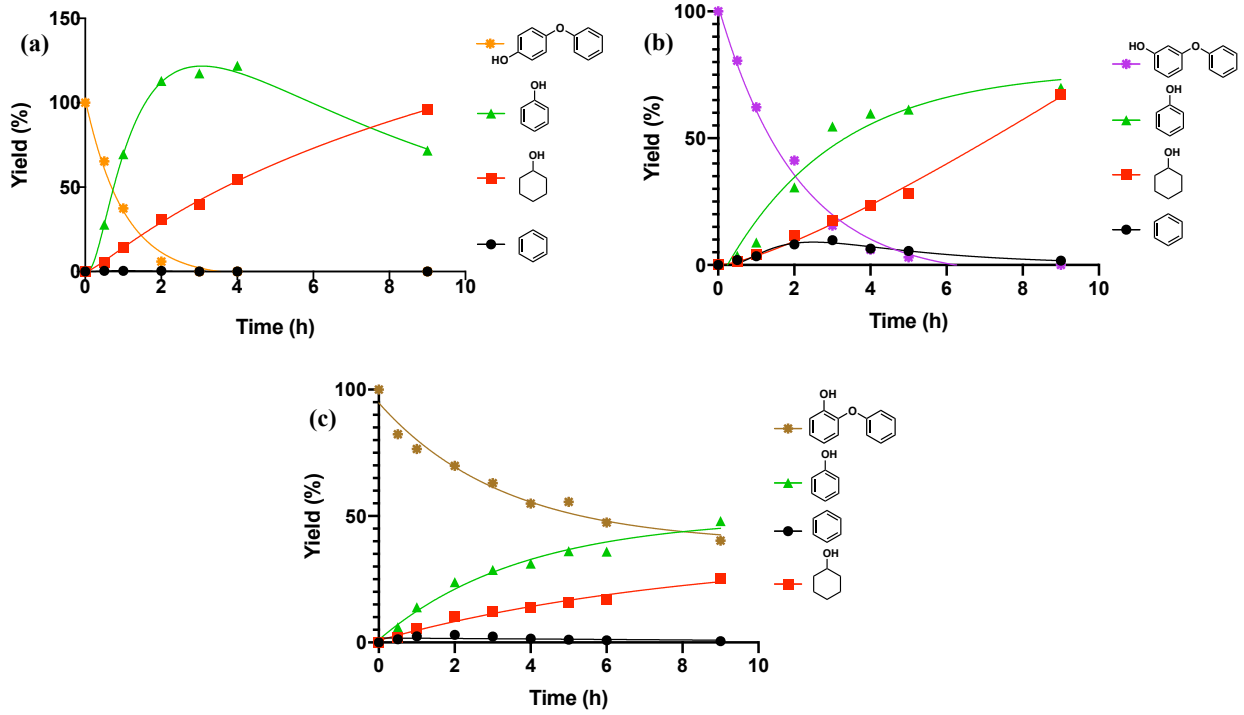

Figure 4.71 Full ECH measurements of (a) para-hydroxylated diphenyl ether, (b) meta-hydroxylated diphenyl ether and (c) ortho-hydroxylated diphenyl ether at standard ECH condition (50 mA, 60 °C and 33%IPA).

The yield of cyclohexanol and phenol were corrected for extraction losses. All yield correction details, see chapter 2, section 2.2.5. No yield corrections were applied on the starting diphenyl ethers and the benzene. Note that for meta-hydroxylated DPE, small amounts of 1,3-dihydroxylbenzene were formed (also implied by the benzene observed) as the reaction progressed, but due to its high hydrophilicity, it was difficult to extract that diol product into dichloromethane for GC-MS analysis.

Full ECH Time Courses for Diphenyl Ether using Different Organic Co-Solvents

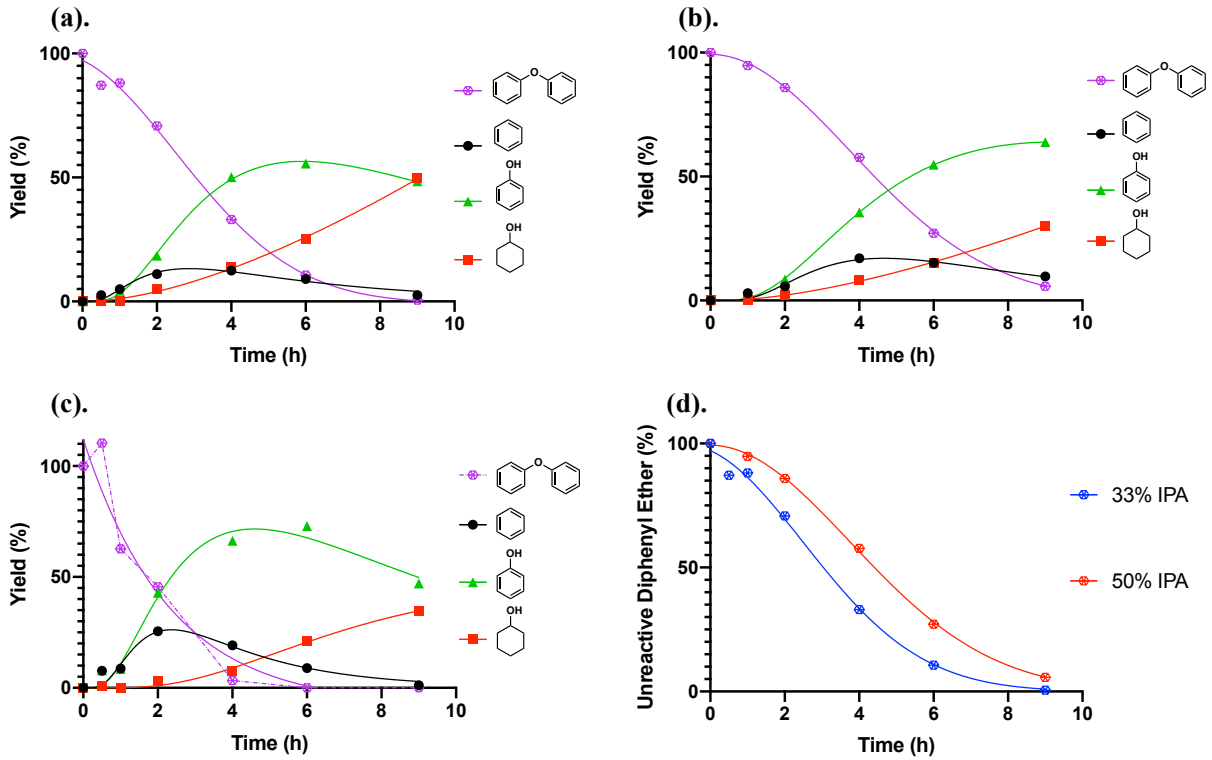

Figure 4.72 Full ECH measurements of (a) diphenyl ether under standard conditions (50 mA, 60 °C) with 33% v/v IPA as co-solvent, (b) diphenyl ether under reaction condition (50 mA, 60 °C) with 50% v/v IPA as co-solvent, (c) diphenyl ether under reaction condition (50 mA, 60 °C) with 33% v/v EtOH as co-solvent, (d) plot of diphenyl ether cleavage rate comparison between 33% v/v IPA and 50% v/v IPA.

The yield of cyclohexanol and phenol were corrected for extraction losses. All yield correction details, see chapter 2, section 2.2.5. No yield corrections were applied on benzene and the starting materials. Notice, 33% v/v EtOH buffer mixture can also achieve complete cleavage, but it's less amphiphilic than IPA that made the starting material diphenyl ether less soluble, which fluctuated the quantification during the analysis (as noted by the dotted line).

Full ECH Time Courses for 4-phenoxyphenol (Hydroxylated DPE) using Different Organic Co-Solvents at ***Different Time Scales***

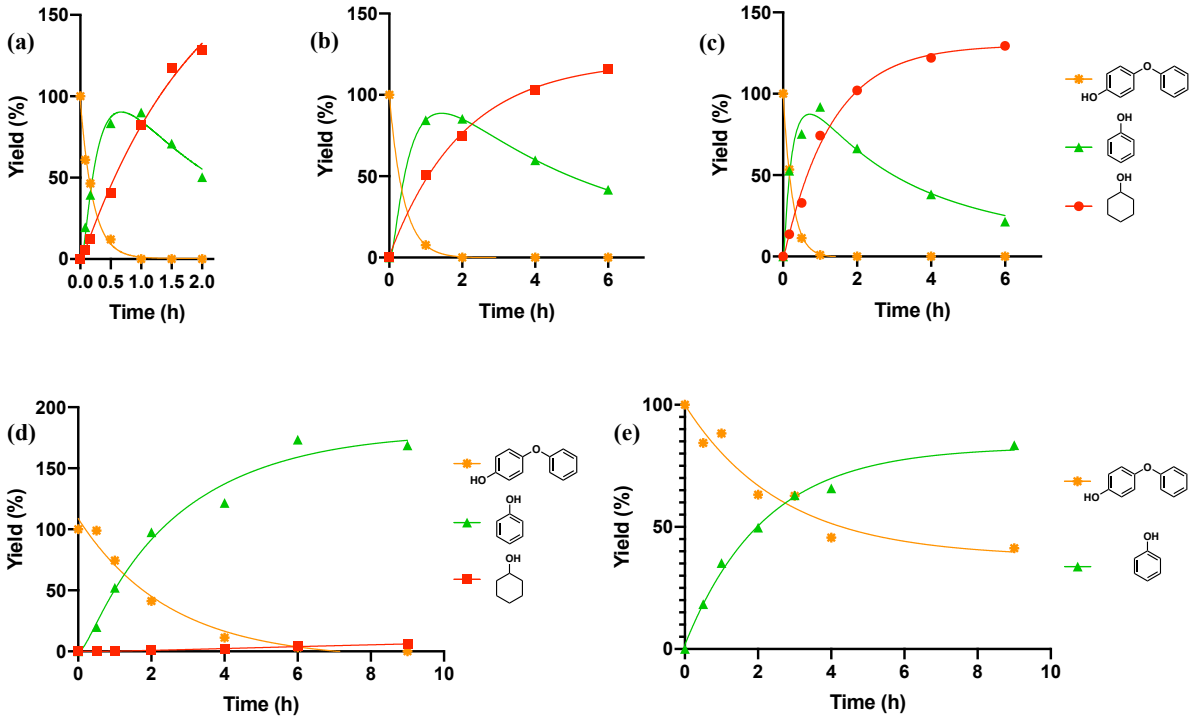

Figure 4.73 Full ECH measurements of 4-phenoxyphenol under standard conditions (50 mA, 60 °C) with (a) 100% pure buffer, (b) 10% v/v IPA as co-solvent, (c) 10% v/v EtOH as co-solvent, (d) 5% acetone as co-solvent and (e) 10% acetone as co-solvent. Low percentage of organic co-solvent were used, no yield correction was applied.

Full ECH Time Courses for 1-(4-phenoxyphenyl)ethan-1-one

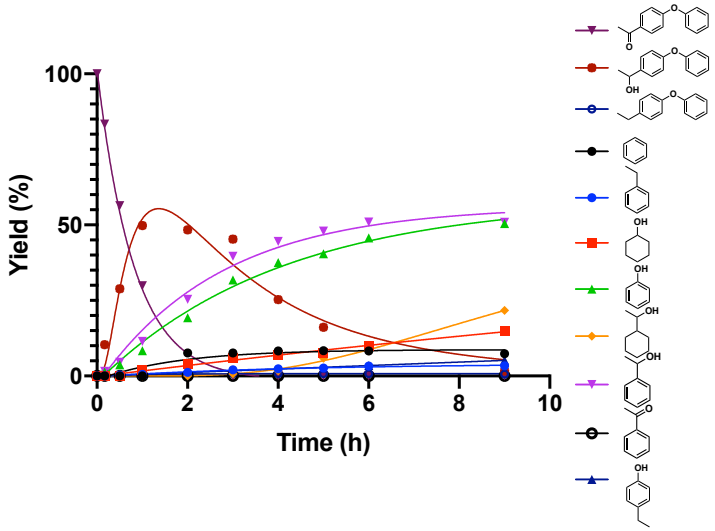

Figure 4.74 ECH measurement of 1-(4-phenoxyphenyl)ethan-1-one at standard condition (50 mA, 60 °C and 33% IPA).

The yields of phenol, cyclohexanol, 1-phenylethanol and 1-cyclohexylethanol were corrected for extraction losses. The yield of 4-ethylphenol was corrected using the extraction efficiency of phenol. All yield correction details, see chapter 2, section 2.2.5. No yield correction was applied for benzene, ethylbenzene or the starting material 1-(4-phenoxyphenyl)ethan-1-one.

Full ECH Time Courses for 1-(4-phenoxyphenyl)ethan-1-ol

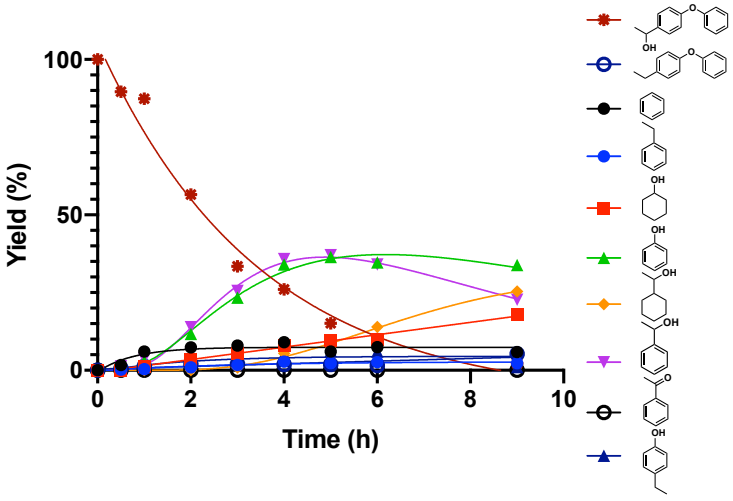

Figure 4.75 ECH measurement of 1-(4-phenoxyphenyl)ethan-1-ol at standard condition (50 mA, 60 °C and 33% IPA).

The yields of phenol, cyclohexanol, 1-phenylethanol and 1-cyclohexylethanol were corrected for extraction losses. The yield of 4-ethylphenol was corrected using the extraction efficiency of phenol. All yield correction details, see chapter 2, section 2.2.5. No yield correction was applied for benzene, ethylbenzene or the starting material 1-(4-phenoxyphenyl)ethan-1-ol.

Full ECH Time Courses for 4-phenoxybenzonitrile

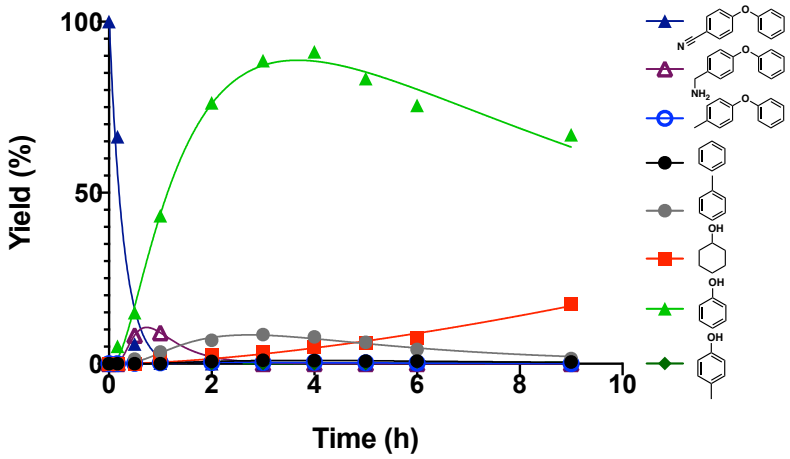

Figure 4.76 ECH measurement of 4-phenoxybenzonitrile at standard condition (50 mA, 60 °C and 33% IPA).

The yields of phenol and cyclohexanol were corrected for extraction losses. All yield correction details, see chapter 2, section 2.2.5. No yield correction was applied for benzene, toluene, p-cresol or the starting material 4-phenoxybenzonitrile. The more polar primary amine product phenylmethanamine was not quantified due to limitations of the GC column.

Full ECH Time Courses for 4-phenoxybenzaldehyde

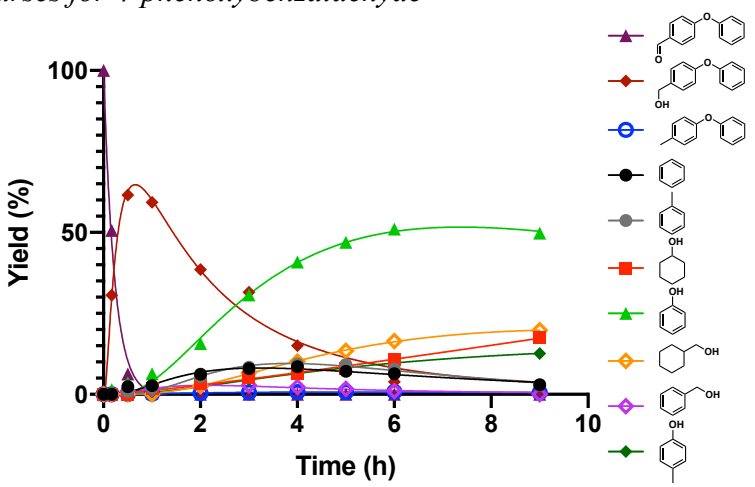

Figure 4.77 ECH measurement of 4-phenoxybenzaldehyde at standard condition (50 mA, 60 °C and 33% IPA).

The yields of phenol and cyclohexanol were corrected for extraction losses. The yield of cyclohexylmethanol was corrected using the extraction efficiency of cyclohexanol. The yield of phenylmethanol and p-cresol were corrected using the extraction efficiency of phenol. All yield correction details, see chapter 2, section 2.2.5. No yield correction was applied for benzene, toluene or the starting material 4-phenoxybenzaldehyde.

Full ECH Time Courses for 1-fluoro-4-phenoxybenzene

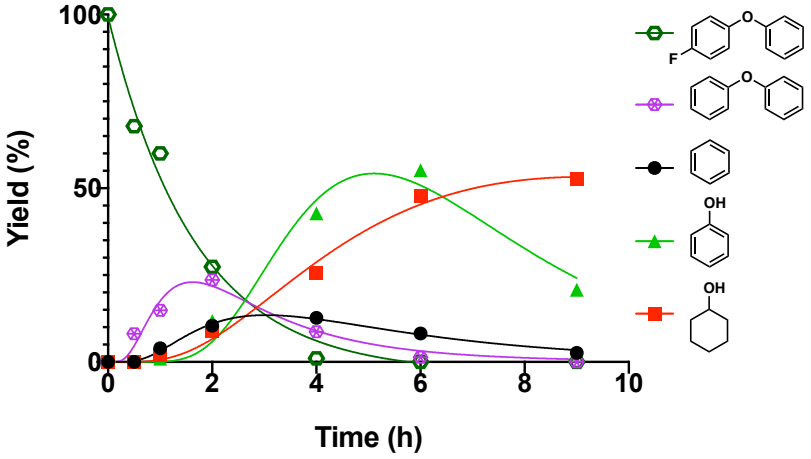

Figure 4.78 ECH measurement of 1-fluoro-4-phenoxybenzene at standard condition (50 mA, 60 °C and 33% IPA).

The yields of phenol and cyclohexanol were corrected for extraction losses. All yield correction details, see chapter 2, section 2.2.5. No yield correction was applied for benzene, diphenyl ether or the starting material 1-fluoro-4-phenoxybenzene.

Full ECH Time Courses for 1-phenoxy-4-(trifluoromethyl)benzene

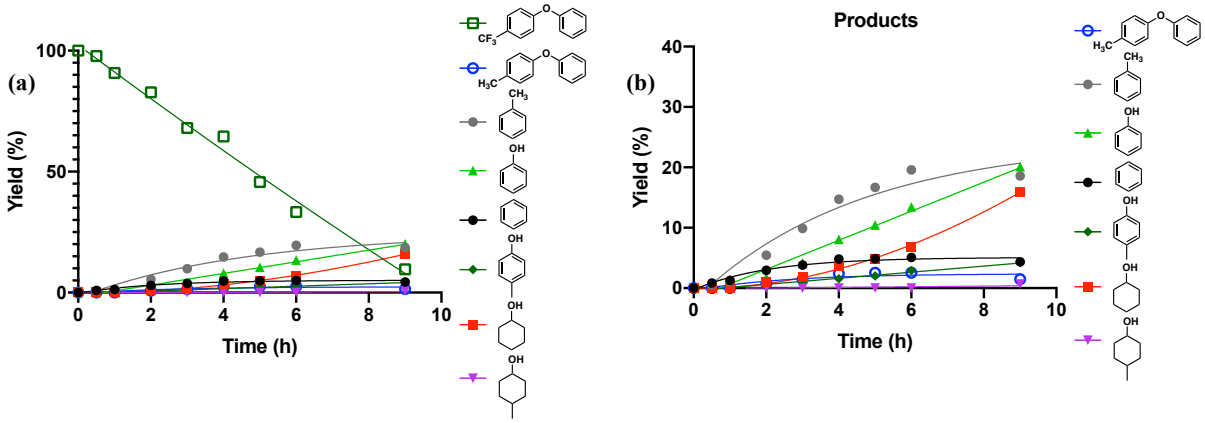

Figure 4.79 (a) ECH measurement of 1-phenoxy-4-(trifluoromethyl)benzene at standard condition (50 mA, 60 °C and 33% IPA). (b) Time courses of product formation. As shown in figure (b), none of the cleavage products contained any F, confirming that defluorination proceeded prior to the C-O cleavage.

Yields of phenol and cyclohexanol were corrected for extraction losses. The yield of p-cresol was corrected using the extraction efficiency of phenol. The yield of 4-methylcyclohexanol was corrected using the extraction efficiency of cyclohexanol. All yield correction details, see chapter 2, section 2.2.5. No yield corrections were applied for benzene, toluene or the starting material 1-phenoxy-4-(trifluoromethyl)benzene.

Full ECH Time Courses for 1-ethyl-4-phenoxybenzene

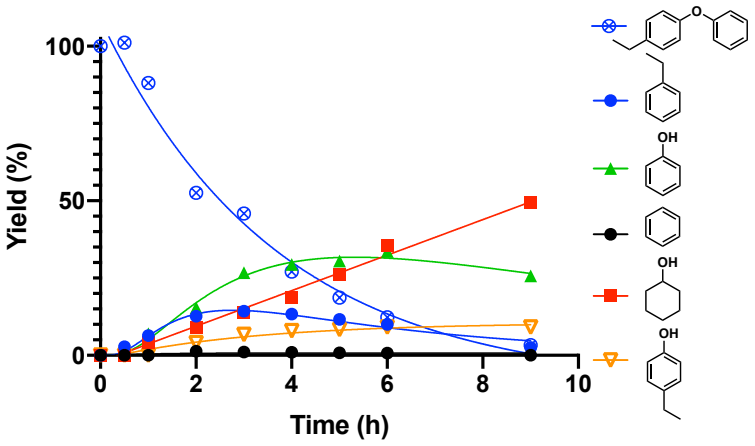

Figure 4.80 ECH measurement of 1-ethyl-4-phenoxybenzene at standard condition (50 mA, 60 °C and 33% IPA).

The yields of phenol and cyclohexanol were corrected for extraction losses. The yield of 4-ethylphenol was corrected using the extraction efficiency of phenol. All yield correction details, see chapter 2, section 2.2.5. No yield correction was applied for benzene, ethylbenzene or the starting material 1-ethyl-4-phenoxybenzene.

Full ECH Time Courses for 1-phenoxy-4-(trifluoromethyl)benzene

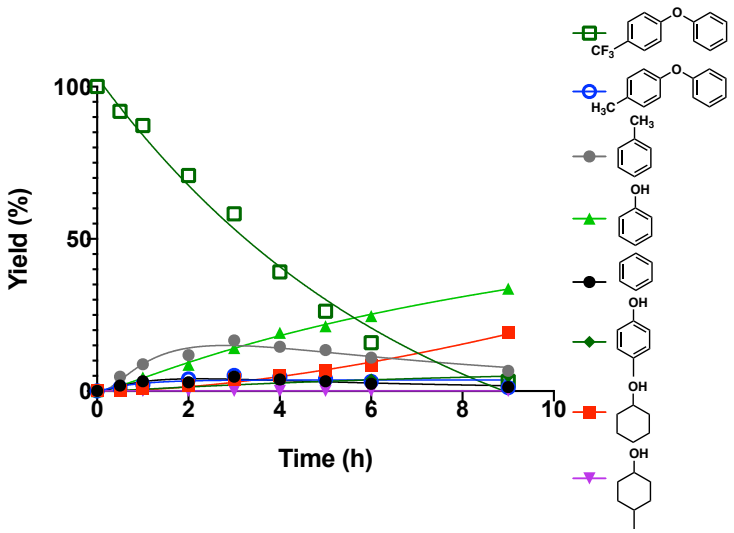

Figure 4.81 ECH measurement of 1-phenoxy-4-(trifluoromethyl)benzene at **80 mA**, 60 °C and 33% IPA.

The yields of phenol and cyclohexanol were corrected for extraction losses. The yield of p-cresol was corrected using the extraction efficiency of phenol. The yield of 4-methylcyclohexanol was corrected using the extraction efficiency of cyclohexanol. All yield correction details, see chapter 2, section 2.2.5. No yield corrections were applied for benzene, toluene or the starting material 1-phenoxy-4-(trifluoromethyl)benzene.

Full ECH Time Courses for 4,4'-oxybis(methoxybenzene)

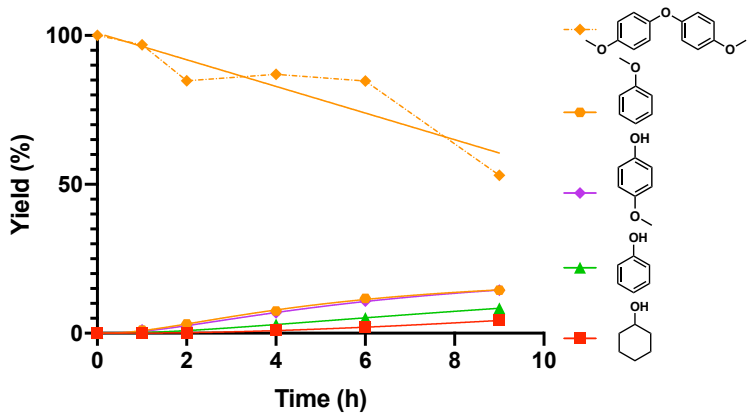

Figure 4.82 ECH measurement of 4,4'-oxybis(methoxybenzene) at standard condition (50 mA, 60 °C and 33% IPA).

The yields of phenol, cyclohexanol and anisole were corrected for extraction losses. The yield of 4-methoxyphenol was corrected for extraction losses. All yield correction details, see chapter 2, section 2.2.5. No yield correction was applied for the starting material 4-phenoxybenzaldehyde.

4.7.12 Cleavage Regioselectivity of Asymmetric Diaryl Ethers

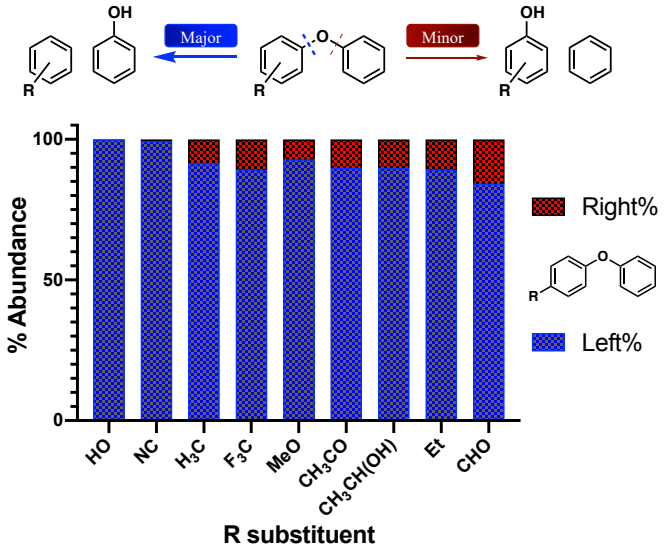

Figure 4.83 Cleavage regioselectivity of various para-functionalized diphenyl ethers.

Example of Regioselectivity Calculation (4-phenoxytoluene):

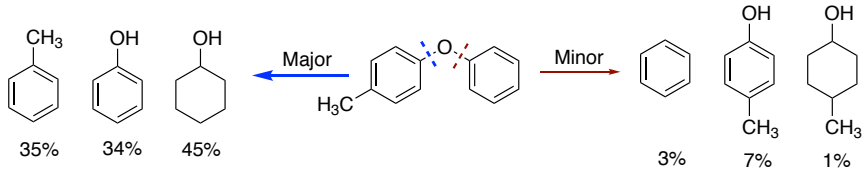

In both major and minor cleavage, the highly non-polar and volatile products benzene and toluene were gradually lost as reaction progressing (S1c). Thus, the regioselectivity % Abundance was calculated based on the more stable polar products (cyclohexanol, phenol, p-cresol and 4-methylcyclohexanol).

$$Right\ Cleavage\ \% = \frac{\sum right\ polar\ products}{\sum total\ polar\ products} = \frac{7+1}{34+45+7+1} * 100 = 9.2\%$$

$$Left\ Cleavage\ \% = \frac{\sum left\ polar\ products}{\sum total\ polar\ products} = \frac{34+45}{34+45+7+1} * 100 = 90.8\%$$

Regioselectivity of all listed substituted diphenyl ethers were calculated as this general procedure.

Cleavage Regioselectivity Is Not Significantly Influenced by Applied Current/Potential or Temperature

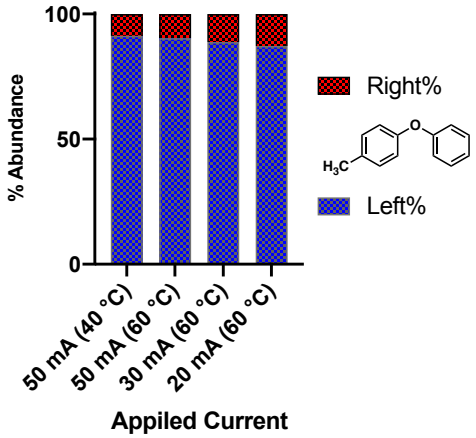

Figure 4.84 Regioselectivity distribution of para methylated diphenyl ether cleavage under different currents and temperatures.

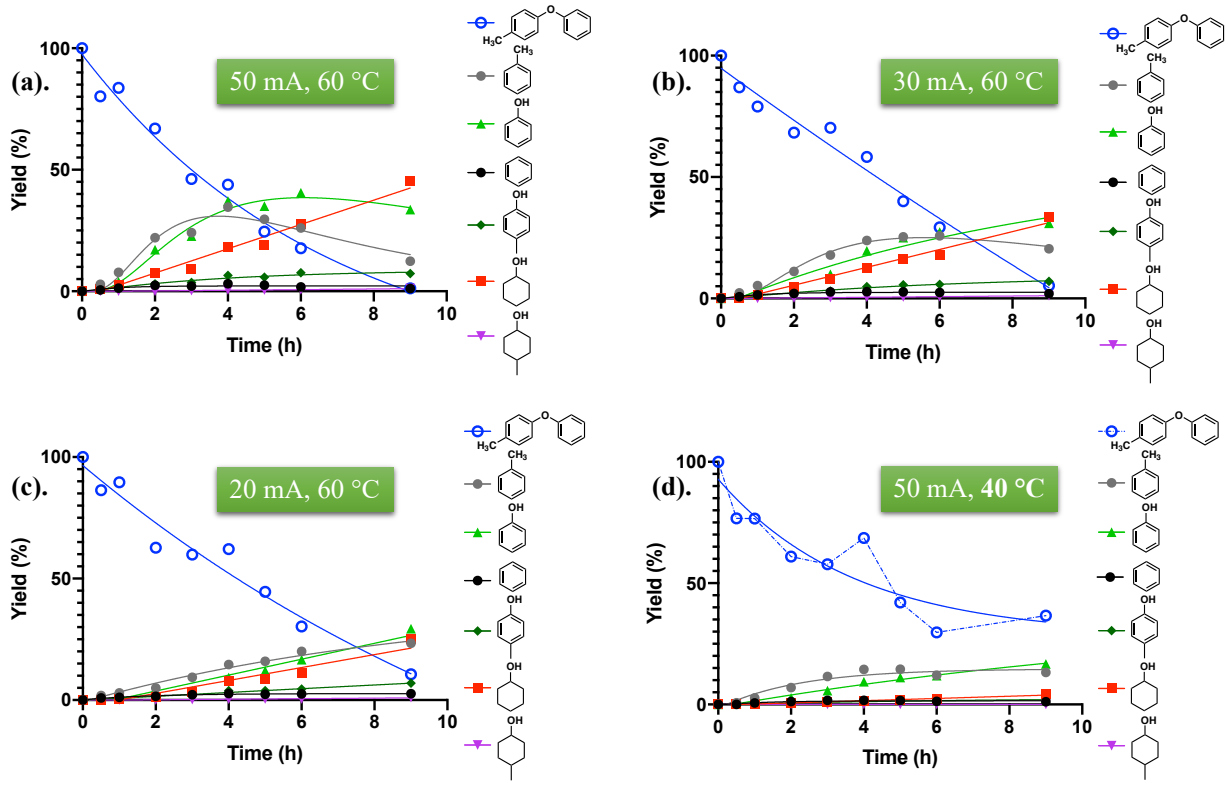

Figure 4.85 Full ECH measurements of para-methylated diphenyl ether with different applied currents and temperatures (a) 50 mA (~10 V), 60 °C and 33% IPA (b) 30 mA (~7 V), 60 °C and 33% IPA (c) 20 mA (~5.7 V), 60 °C and 33% IPA (d) 50 mA, 40 °C (decreased DPE solubility at this lower temperature) and 33% IPA.

The yields of cyclohexanol and phenol were corrected for extraction losses. The yields of cresols were corrected using the extraction efficiency of phenol. All yield correction details, see chapter 2, section 2.2.5. No yield corrections were applied on the starting diphenyl ethers, methyl cyclohexanols or alkyl benzenes.

Both the cleavage products and regioselectivity were not impacted by the lower current and applied potential; only the C-O cleavage rate was significantly slower under the decreased current and temperature conditions, presumably due to the lower rate of hydrogen formation on the Ni metal surface.

REFERENCES

REFERENCES

1. Samanta, P.; Desai, A. V.; Let, S.; Ghosh, S. K., Advanced Porous Materials for Sensing, Capture and Detoxification of Organic Pollutants toward Water Remediation. *ACS Sustainable Chemistry & Engineering* **2019,** *7* (8), 7456-7478.

2. Bolong, N.; Ismail, A. F.; Salim, M. R.; Matsuura, T., A review of the effects of emerging contaminants in wastewater and options for their removal. *Desalination* **2009,** *239* (1-3), 229-246.

3. Rodrigo, M. A.; Oturan, N.; Oturan, M. A., Electrochemically Assisted Remediation of Pesticides in Soils and Water: A Review. *Chemical Reviews* **2014,** *114* (17), 8720-8745.

4. Klinger, G. E. *et al.* Biomimetic Reductive Cleavage of Keto Aryl Ether Bonds by Small-Molecule Thiols. *ChemSusChem*, **12**, 4775-4779 (2019).

5. Rafiee, M.; Alherech, M.; Karlen, S. D.; Stahl, S. S., Electrochemical Aminoxyl-Mediated Oxidation of Primary Alcohols in Lignin to Carboxylic Acids: Polymer Modification and Depolymerization. *Journal of the American Chemical Society* **2019,** *141* (38), 15266-15276.

6. Dabral, S.; Hernandez, J. G.; Kamer, P. C. J.; Bolm, C., Organocatalytic Chemoselective Primary Alcohol Oxidation and Subsequent Cleavage of Lignin Model Compounds and Lignin. *ChemSusChem* **2017,** *10* (13), 2707-2713.

7. Zhang, C. F.; Li, H. J.; Lu, J. M.; Zhang, X. C.; MacArthur, K. E.; Heggen, M.; Wang, F., Promoting Lignin Depolymerization and Restraining the Condensation via an Oxidation-Hydrogenation Strategy. *ACS Catalysis* **2017,** *7* (5), 3419-3429.

8. Rahimi, A.; Ulbrich, A.; Coon, J. J.; Stahl, S. S., Formic-acid-induced depolymerization of oxidized lignin to aromatics. *Nature* **2014,** *515* (7526), 249-252.

9. Deuss, P. J.; Scott, M.; Tran, F.; Westwood, N. J.; de Vries, J. G.; Barta, K., Aromatic Monomers by in Situ Conversion of Reactive Intermediates in the Acid-Catalyzed Depolymerization of Lignin. *Journal of the American Chemical Society* **2015,** *137* (23), 7456-7467.

10. Shuai, L.; Amiri, M. T.; Questell-Santiago, Y. M.; Heroguel, F.; Li, Y. D.; Kim, H.; Meilan, R.; Chapple, C.; Ralph, J.; Luterbacher, J. S., Formaldehyde stabilization facilitates lignin monomer production during biomass depolymerization. *Science* **2016,** *354* (6310), 329-333.

11. Amiri, M. T.; Dick, G. R.; Questell-Santiago, Y. M.; Luterbacher, J. S., Fractionation of lignocellulosic biomass to produce uncondensed aldehyde-stabilized lignin. *Nature Protocols* **2019,** *14* (3), 921-954.

12. Nguyen, J. D.; Matsuura, B. S.; Stephenson, C. R. J., A Photochemical Strategy for Lignin Degradation at Room Temperature. *Journal of the American Chemical Society* **2014,** *136* (4), 1218-1221.

13. Wu, X. J.; Fan, X. T.; Xie, S. J.; Lin, J. C.; Cheng, J.; Zhang, Q. H.; Chen, L. Y.; Wang, Y., Solar energy-driven lignin-first approach to full utilization of lignocellulosic biomass under mild conditions. *Nature Catalysis* **2018,** *1* (10), 772-780.

14. P.J. Linstrom and W.G. Mallard, Eds., **NIST Chemistry WebBook, NIST Standard Reference Database Number 69**, National Institute of Standards and Technology, Gaithersburg MD, 20899, https://doi.org/10.18434/T4D303.

15. Chen, T.; Xiong, H.; Yang, J.-F.; Zhu, X.-L.; Qu, R.-Y.; Yang, G.-F., Diaryl Ether: A Privileged Scaffold for Drug and Agrochemical Discovery. *Journal of Agricultural and Food Chemistry* **2020,** *68* (37), 9839-9877.

16. Le, T. G.; Kundu, A.; Ghoshal, A.; Nguyen, N. H.; Preston, S.; Jiao, Y. Q.; Ruan, B. F.; Xue, L.; Huang, F.; Keiser, J.; Hofmann, A.; Chang, B. C. H.; Garcia-Bustos, J.; Wells, T. N. C.; Palmer, M. J.; Jabbar, A.; Gasser, R. B.; Baell, J. B., Structure-Activity Relationship Studies of Tolfenpyrad Reveal Subnanomolar Inhibitors of Haemonchus contortus Development. *Journal of Medicinal Chemistry* **2019,** *62* (2), 1036-1053.

17. Yang, Q.; Cai, S.; Dong, S. W.; Chen, L. L.; Chen, J. F.; Cai, T. M., Biodegradation of 3-methyldiphenylether (MDE) by Hydrogenophaga atypical strain QY7-2 and cloning of the methy-oxidation gene mdeABCD. *Scientific Reports* **2016,** *6*, 10.

18. Manzetti, S.; van der Spoel, E. R.; van der Spoel, D., Chemical Properties, Environmental Fate, and Degradation of Seven Classes of Pollutants. *Chemical Research in Toxicology* **2014,** *27* (5), 713-737.

19. Jones, K. C.; de Voogt, P., Persistent organic pollutants (POPs): state of the science. *Environmental Pollution* **1999,** *100* (1-3), 209-221.

20. Yamaguchi, K.; Hikiji, W.; Takino, M.; Saka, K.; Hayashida, M.; Fukunaga, T.; Ohno, Y., Analysis of Tolfenpyrad and its Metabolites in Plasma in a Tolfenpyrad Poisoning Case. *Journal of Analytical Toxicology* **2012,** *36* (7), 529-537.

21. Dong, M. F.; Wen, G. Y.; Tang, H. X.; Wang, T.; Zhao, Z. H.; Song, W. G.; Wang, W. M.; Zhao, L., Dissipation and safety evaluation of novaluron, pyriproxyfen, thiacloprid and tolfenpyrad residues in the citrus-field ecosystem. *Food Chemistry* **2018,** *269*, 136-141.

22. Ambrus, A. TOLFENPYRAD (269) Report, Food and Agriculture Organization of the United Nations. http://www.fao.org/fileadmin/templates/agphome/documents/Pests_Pesticides/JMPR/Evaluation13/Tolfenpyrad.pdf (accessed 05/29/2021).

23. Alvarez-Bercedo, P.; Martin, R., Ni-Catalyzed Reduction of Inert C-O Bonds: A New Strategy for Using Aryl Ethers as Easily Removable Directing Groups. *Journal of the American Chemical Society* **2010,** *132* (49), 17352-17353.

24. Kelley, P.; Lin, S. B.; Edouard, G.; Day, M. W.; Agapie, T., Nickel-Mediated Hydrogenolysis of C-O Bonds of Aryl Ethers: What Is the Source of the Hydrogen? *Journal of the American Chemical Society* **2012,** *134* (12), 5480-5483.

25. Sergeev, A. G.; Hartwig, J. F., Selective, Nickel-Catalyzed Hydrogenolysis of Aryl Ethers. *Science* **2011,** *332* (6028), 439-443.

26. Sergeev, A. G.; Webb, J. D.; Hartwig, J. F., A Heterogeneous Nickel Catalyst for the Hydrogenolysis of Aryl Ethers without Arene Hydrogenation. *Journal of the American Chemical Society* **2012,** *134* (50), 20226-20229.

27. Saper, N. I.; Hartwig, J. F., Mechanistic Investigations of the Hydrogenolysis of Diary! Ethers Catalyzed by Nickel Complexes of N-Heterocyclic Carbene Ligands. *Journal of the American Chemical Society* **2017,** *139* (48), 17667-17676.

28. Dong, L.; Xin, Y.; Liu, X. H.; Guo, Y.; Pao, C. W.; Chen, J. L.; Wang, Y. Q., Selective hydrodeoxygenation of lignin oil to valuable phenolics over Au/Nb2O5 in water. *Green Chemistry* **2019,** *21* (11), 3081-3090.

29. Zhao, C.; Kou, Y.; Lemonidou, A. A.; Li, X. B.; Lercher, J. A., Hydrodeoxygenation of bio-derived phenols to hydrocarbons using RANEY (R) Ni and Nafion/SiO2 catalysts. *Chemical Communications* **2010,** *46* (3), 412-414.

30. Zhao, C.; Lercher, J. A., Upgrading Pyrolysis Oil over Ni/HZSM-5 by Cascade Reactions. *Angewandte Chemie-International Edition* **2012,** *51* (24), 5935-5940.

31. Guo, M.; Peng, J.; Yang, Q. H.; Li, C., Highly Active and Selective RuPd Bimetallic NPs for the Cleavage of the Diphenyl Ether C-O Bond. *ACS Catalysis* **2018,** *8* (12), 11174-11183.

32. Bulut, S.; Siankevich, S.; van Muyden, A. P.; Alexander, D. T. L.; Savoglidis, G.; Zhang, J. G.; Hatzimanikatis, V.; Yan, N.; Dyson, P. J., Efficient cleavage of aryl ether C-O linkages by Rh-Ni and Ru-Ni nanoscale catalysts operating in water. *Chemical Science* **2018,** *9* (25), 5530-5535.

33. Chen, L.; Fink, C.; Fei, Z. F.; Dyson, P. J.; Laurenczy, G., An efficient Pt nanoparticle-ionic liquid system for the hydrodeoxygenation of bio-derived phenols under mild conditions. *Green Chemistry* **2017,** *19* (22), 5435-5441.

34. He, J. Y.; Zhao, C.; Lercher, J. A., Ni-Catalyzed Cleavage of Aryl Ethers in the Aqueous Phase. *Journal of the American Chemical Society* **2012,** *134* (51), 20768-20775.

35. Molinari, V.; Giordano, C.; Antonietti, M.; Esposito, D., Titanium Nitride-Nickel Nanocomposite as Heterogeneous Catalyst for the Hydrogenolysis of Aryl Ethers. *Journal of the American Chemical Society* **2014,** *136* (5), 1758-1761.

36. Dabo, P.; Cyr, A.; Lessard, J.; Brossard, L.; Menard, H., Electrocatalytic hydrogenation of 4-phenoxyphenol on active powders highly dispersed in a reticulated vitreous carbon electrode. *Canadian Journal of Chemistry* **1999,** *77* (7), 1225-1229.

37. Cyr, A.; Chiltz, F.; Jeanson, P.; Martel, A.; Brossard, L.; Lessard, J.; Menard, H., Electrocatalytic hydrogenation of lignin models at Raney nickel and palladium-based electrodes. *Canadian Journal of Chemistry* **2000,** *78* (3), 307-315.

38. Lam, C. H.; Lowe, C. B.; Li, Z. L.; Longe, K. N.; Rayburn, J. T.; Caldwell, M. A.; Houdek, C. E.; Maguire, J. B.; Saffron, C. M.; Miller, D. J.; Jackson, J. E., Electrocatalytic upgrading of model lignin monomers with earth abundant metal electrodes. *Green Chemistry* **2015,** *17* (1), 601-609.

39. Zhou, Y. T.; Klinger, G. E.; Hegg, E. L.; Saffron, C. M.; Jackson, J. E., Multiple Mechanisms Mapped in Aryl Alkyl Ether Cleavage via Aqueous Electrocatalytic Hydrogenation over Skeletal Nickel. *Journal of the American Chemical Society* **2020,** *142* (8), 4037-4050.

40. Jiang, S.; Chen, Z.; Chen, X.; Nguyen, D.; Mattei, M.; Goubert, G.; Van Duyne, R. P., Investigation of Cobalt Phthalocyanine at the Solid/Liquid Interface by Electrochemical Tip-Enhanced Raman Spectroscopy. *Journal of Physical Chemistry C* **2019,** *123* (15), 9852-9859.

41. Wu, H. R.; Song, J. L.; Xie, C.; Wu, C. Y.; Chen, C. J.; Han, B. X., Efficient and Mild Transfer Hydrogenolytic Cleavage of Aromatic Ether Bonds in Lignin-Derived Compounds over Ru/C. *ACS Sustainable Chemistry & Engineering* **2018,** *6* (3), 2872-2877.

42. de Aguiar, V. M.; Silva, R. E.; Leao, R. A. C.; de Souza, R.; Goncalves, R. S. B.; Miranda, L., Studies on the laccases catalyzed oxidation of norbelladine like acetamides. *Molecular Catalysis* **2020,** *485*, 8.

43. Delle Site, L.; Alavi, A.; Abrams, C. F., Adsorption energies and geometries of phenol on the (111) surface of nickel: An ab initio study. *Physical Review B* **2003,** *67* (19), 3.

44. Suseno, S.; Horak, K. T.; Day, M. W.; Agapie, T., Trinuclear Nickel Complexes with Metal-Arene Interactions Supported by Tris- and Bis(phosphinoaryl)benzene Frameworks. *Organometallics* **2013,** *32* (23), 6883-6886.

45. Shoshani, M. M.; Johnson, S. A., Cooperative carbon-atom abstraction from alkenes in the core of a pentanuclear nickel cluster. *Nature Chemistry* **2017,** *9* (12), 1282-1285.

46. Bennett, M. A.; Drage, J. S.; Griffiths, K. D.; Roberts, N. K.; Robertson, G. B.; Wickramasinghe, W. A., Stablization of 1,2,4,5-tetradehydrobenzene by complexation at 2 nickel(0) centers. *Angewandte Chemie-International Edition in English* **1988,** *27* (7), 941-942.

47. Bennett, M. A.; Wenger, E., The reactivity of complexes of nickel(0) and platinum(0) containing benzyne and related small-ring alkynes. *Chemische Berichte-Recueil* **1997,** *130* (8), 1029-1042.

48. Keen, A. L.; Johnson, S. A., Nickel(0)-catalyzed isomerization of an aryne complex: Formation of a dinuclear Ni(I) complex via C-H rather than C-F bond activation. *Journal of the American Chemical Society* **2006,** *128* (6), 1806-1807.

49. Keen, A. L.; Doster, M.; Johnson, S. A., 1,4-shifts in a dinuclear Ni(I) biarylyl complex: A mechanistic study of C-H bond activation by monovalent nickel. *Journal of the American Chemical Society* **2007,** *129* (4), 810-819.

50. Buchalski, P.; Jadach, P.; Pietrzykowski, A.; Suwinska, K.; Jerzykiewicz, L.; Sadlo, J., Products of the reaction of 9-nickelafluorenyllithium complexes with water. *Organometallics* **2008,** *27* (14), 3618-3621.

51. Bennett, M. A.; Griffiths, K. D.; Okano, T.; Parthasarathi, V.; Robertson, G. B., An electronically unsaturated trinickel complex containing triply bridging benzyne and 2,2'-biphenylyl groups. *Journal of the American Chemical Society* **1990,** *112* (19), 7047-7048.

52. Huntley, D. R.; Jordan, S. L.; Grimm, F. A., Adsorption and thermal-decomposition of benzene on Ni(110) studied by chemical, spectroscopic, and computational methods. *Journal of Physical Chemistry* **1992,** *96* (3), 1409-1417.

53. Hsieh, J.-C.; Cheng, C.-H., O-Dihaloarenes as aryne precursors for nickel-catalyzed 2+2+2 cycloaddition with alkynes and nitriles. *Chemical Communications* **2008,** (26), 2992-2994.

54. Lin, C. Y.; George, M. W.; Gill, P. M. W., EDF2: A density functional for predicting molecular vibrational frequencies. *Australian Journal of Chemistry* **2004,** *57* (4), 365-370.

Chapter 5 Defluorination (C-F Activation) and Surface Topology of Skeletal Nickel

5.1 Introduction

5.1.1 Literature review on metal catalyzed C-F activation

Due to their high chemical and thermal stabilities, large hydrophobicity and weak intermolecular interactions, C-F bonds have been widely incorporated in a vast range of organic molecules, especially in pharmaceuticals and industrial products.[1] Production of such fluorinated compounds is growing at an accelerating rate. Also owing to their high stability, fluorinated molecules are significantly resistant to natural degradation, as mentioned in the aryl ether studies in previous chapters, perfluoroalkyl substances (PFAS) also are a major class of persistent and bioaccumulative organic pollutants.[2, 3]

Along with the mechanistic investigation of aryl ether cleavage, activation of C-F bonds was discovered in the course of studies of electrocatalytic hydrogenolysis of diaryl ethers. The highly porous skeletal nickel (Raney® Ni) electrode was not only able to activate sp^2 C-F bonds in these aromatic systems, but it was also found to enable the cleavage of more inert sp^3 C-F bonds. This finding is important; heterogeneous catalytic defluorination (via classic hydrogenation)[4-6] of fluoroarenes have been reported before, but reports of defluorination of perfluoroalkyl groups are rare. In fact, even for more reactive and versatile homogeneous molecular catalysis, activation of aromatic sp^2 C-F bonds has been more commonly seen than activation of more stable sp^3 C-F bonds.[7-9] Therefore, the a wide variety of aryl ether substrates explored did lead to a critical discovery: electrocatalytic activation of one of the most unreactive functionalities—C-F bonds—by a heterogeneous solid metal catalyst.

5.2 Defluorination: Discovery of C-F Bond Activation

5.2.1 sp^2 C-F activation of Phenolic Monomer

From the previously reported ECH studies of different lignin-derived aromatic monomers, phenol was found to be an easy target that can undergo fast ring reduction to become cyclohexanol. Meanwhile, compared to the unreactive aromatics (like benzene or anisole), we have concluded that phenol's high reactivity was mainly owing to the introduction of the hydroxyl functionality. Importantly, based on the mechanistic findings from the previous ether dimer studies (chapters 3-4), the presence of the hydroxyl group on the benzene ring enables equilibration with the keto form of such aromatic alcohols. This keto tautomer can activate the aromatic system by enhancing the binding between the substrate and the metal surface, which accelerates both C-O cleavage and ring saturation.

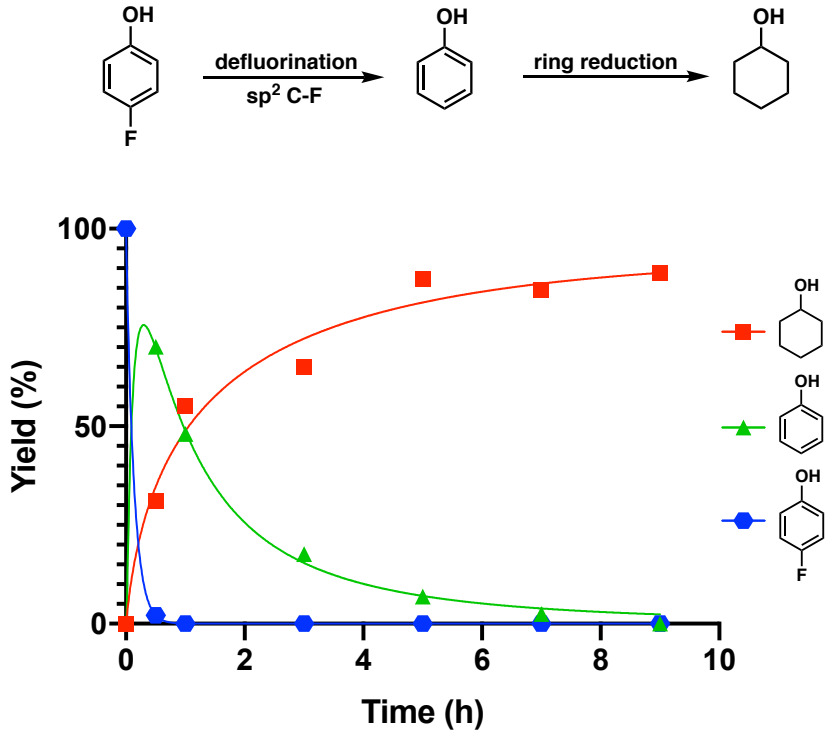

Figure 5.1 Electrocatalytic hydrogenation of 4-fluorophenol over skeletal nickel electrode under 50 mA at 60 °C, and with 100% pH 8 borate buffer.

As shown in Figure 5.1, 4-fluorophenol undergoes fast defluorination to phenol, which then undergoes the familiar ring reduction to become cyclohexanol. At high current (50 mA), reduction of the aryl C-F bond was fast; phenol only began to be reduced after most of the 4-fluorophenol was defluorinated. Base the previous investigations of the role of the hydroxyl moiety, we also hypothesize that this fast sp^2 C-F reduction of 4-fluorophenol is due to the formation of the corresponding keto tautomer of this phenolic fluoroarene (Figure 5.2).

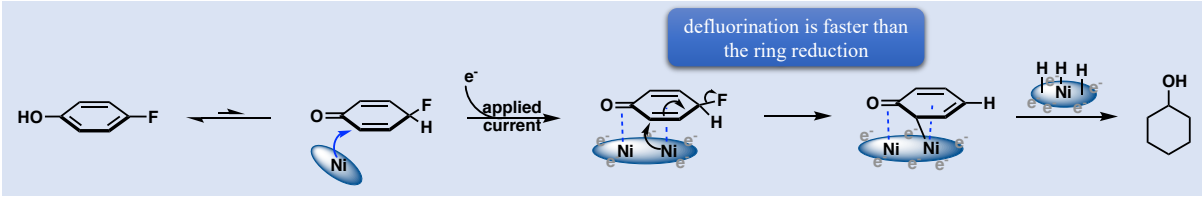

Figure 5.2 Proposed electrocatalytic defluorination mechanism of 4-fluorophenol.

5.2.2 C-F activation in diaryl ether system

Comparable with the reduction of 4-fluorophenol, electrocatalytic hydrogenation of para-fluorinated diphenyl ether (DPE) also begins with defluorination prior to its C-O ether cleavage. As shown in Figure 5.3, the C-F bond in para-fluoro DPE was reduced prior to the breakdown of its C-O ether bond. Fluorinated DPE was first reduced to plain diphenyl ether (DPE), which was then cleaved into benzene and phenol. No 4-fluorophenol or 4-fluorobenzene was observed during the ECH of para-fluorinated DPE. Meanwhile, compared with the fast defluorination rate of 4-fluorophenol, the sp^2 C-F reduction in the fluorinated diphenyl ether showed a slower cleavage rate. However, the hydrodefluorination is still significantly faster than the diaryl ether cleavage, consistent with the notion that in water, fluoride is a better leaving group than phenoxide.

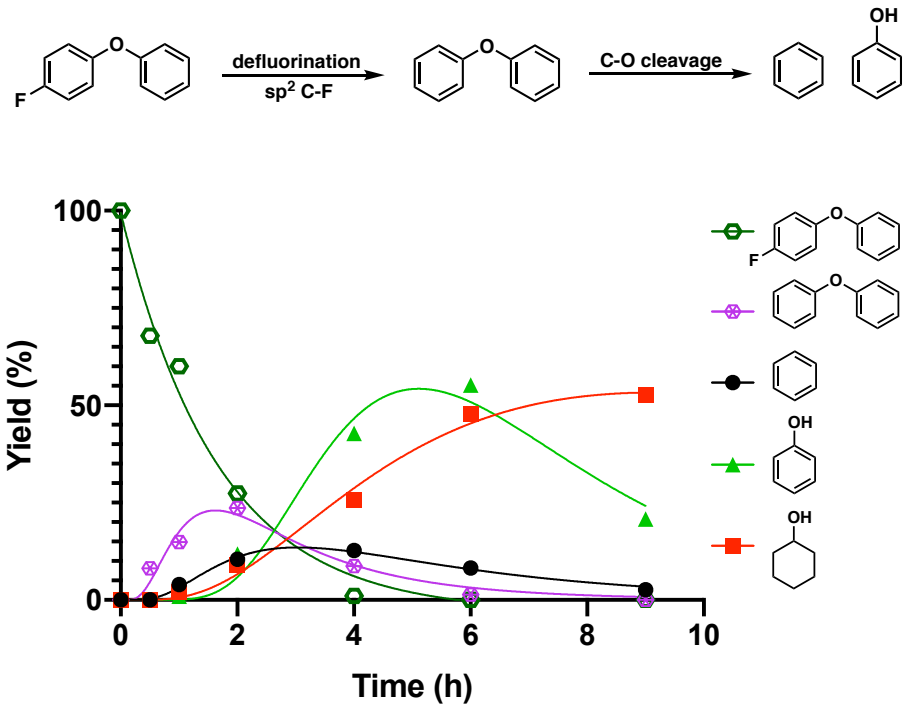

Figure 5.3 Electrocatalytic hydrogenation of para-fluorinated diphenyl ether over a skeletal nickel electrode at 50 mA in the aqueous mixture of pH 8 borate buffer/IPA (2:1) at 60 °C under ambient pressure.

In the reaction mechanism proposed in chapter 4, dual ring coordination is required for the activation of C-O cleavage in the diphenyl ether system. But as shown in Figure 5.3, the C-F reduction happens much faster than the C-O cleavage, which suggests a different substrate binding mode for the activation of this para C-F bond. Thus, as shown in Figure 5.4, we propose a reductive defluorination mechanism with a partial ring coordination mode for the catalytic C-F cleavage of this para-fluoro diphenyl ether. Importantly, compared with the dual ring activation binding geometry for the C-O ether bond cleavage, the partial ring coordination is more likely to be established, thus, leading to faster defluorination via a conventional oxidative insertion, reductive elimination sequence.

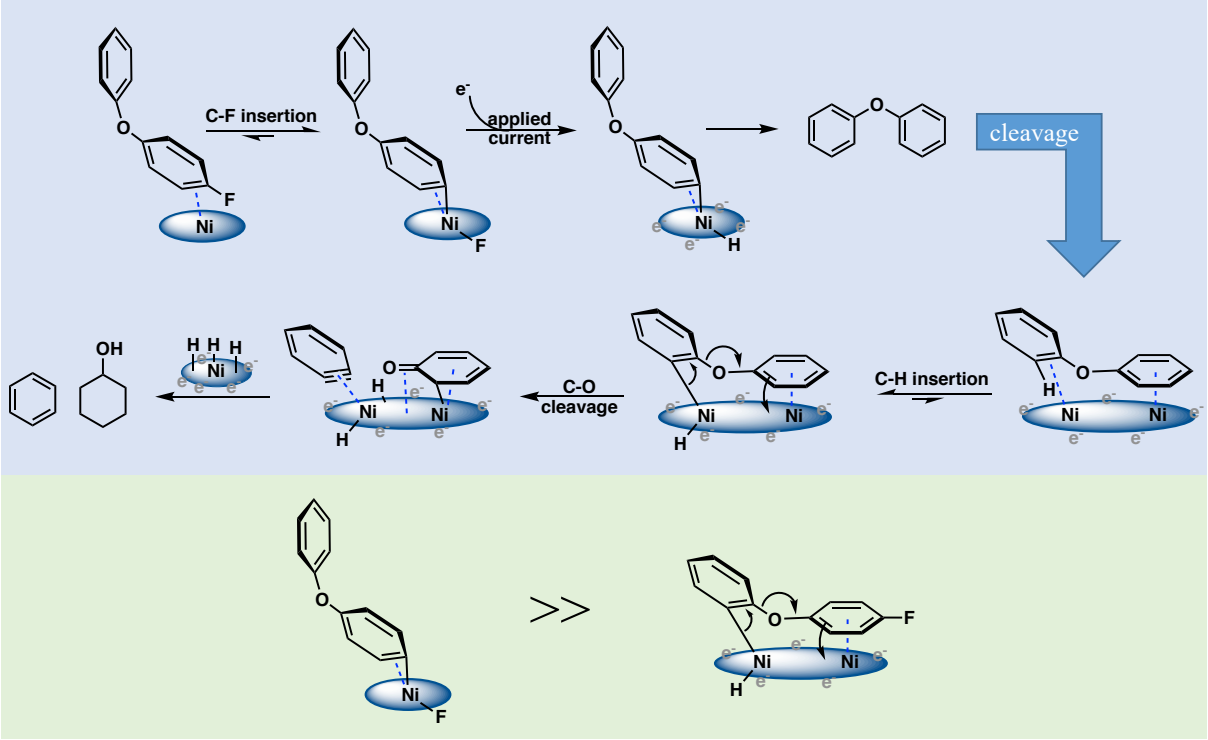

Figure 5.4 Proposed electrocatalytic defluorination mechanism of 4-fluoro DPE.

Activation of fluoroarenes has received substantial attention in both homogeneous and heterogeneous catalysis, but activation of perfluoroalkyl groups were rarely found in both approaches. During the substrate mapping of diaryl ethers, defluorination of benzylic C-F bonds was also discovered (Chapter 4, Figure 4.79). As with the 4-fluoro DPE, all of the sp^3 C-F bonds in para-trifluoromethylated DPE were reduced and replaced with C-H bonds prior to the C-O ether cleavage (Figure 5.5). No partially defluorinated products were observed. In the exchange study of methylated DPE (Chapter 4), we observed fast H/D scrambling of the benzylic C-Hs, and similarly, in the case of CF_3, once nickel was inserted into the benzylic carbon, reduction of the sp^3 C-F bonds appears to be fast. Importantly, the cleavage rate of para-trifluoromethyl DPE is the slowest among all of the tested DPE substrates. This indicates nickel is more favored to bind with

the benzylic CF_3 and the presence of the fluorines further enhanced this binding, indeed, led to a much slower ether cleavage.

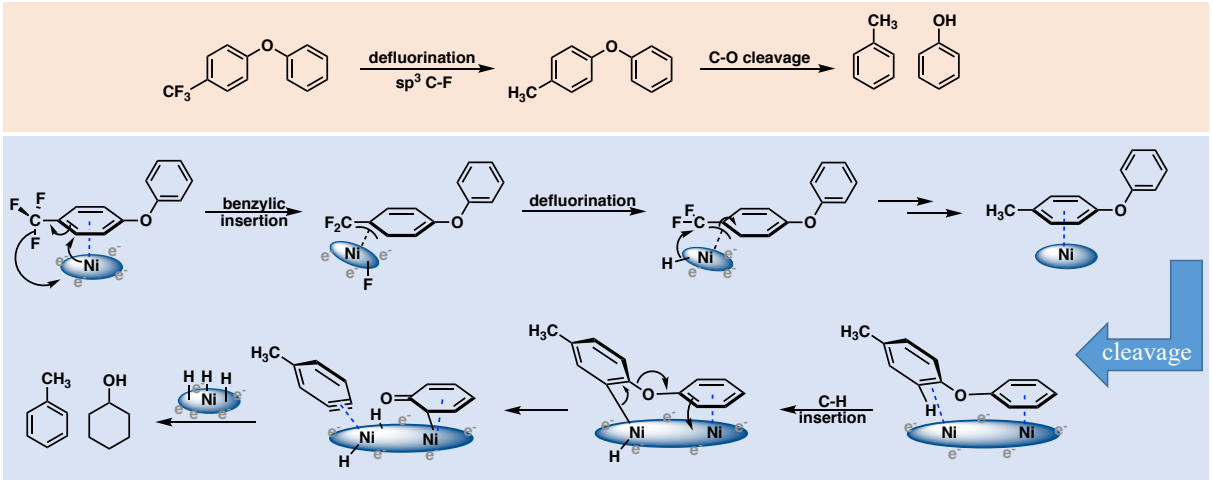

Figure 5.5 Proposed electrocatalytic defluorination mechanism of para-trifluoromethyl DPE.

5.2.3 ECH of α-O-4 and C-F activation in α-O-4 type aryl ether system

A distinct observation was found in the case of a trifluoromethylated α-O-4 type aryl ether (a minor linkage of lignin polymer). All of the organofluorides discussed above had their C-F bonds reduced before the ring reduction or the ether cleavage. But as shown in Figure 5.6a, the trifluoromethylated benzyl phenyl ether has its C-O ether bond cleaved without removal of any fluorines. Importantly, different from the above ether cases, benzyl phenyl ether has a weaker and more reactive benzylic sp^3 C-O bond. Instead of stripping off the benzylic fluorines, the benzylic phenoxide is a better leaving group. For the fluorinated diaryl ethers, we infer that although phenoxide is a better leaving group, the sp^2 C of the C-O ether bond between the two diphenyls is a worse site, both sterically and electronically for direct attack. However, in the case of the benzyl phenyl ether, the C-O cleavage is easier, which results in rapid C-O breakdown without any defluorination. Figure 5.6b illustrates this favored cleavage mechanism of the trifluoromethylated

benzyl phenyl ether. Defluorination of the resulting 4-trifluoromethyl toluene to form para xylene appears to occur only in trace amounts.

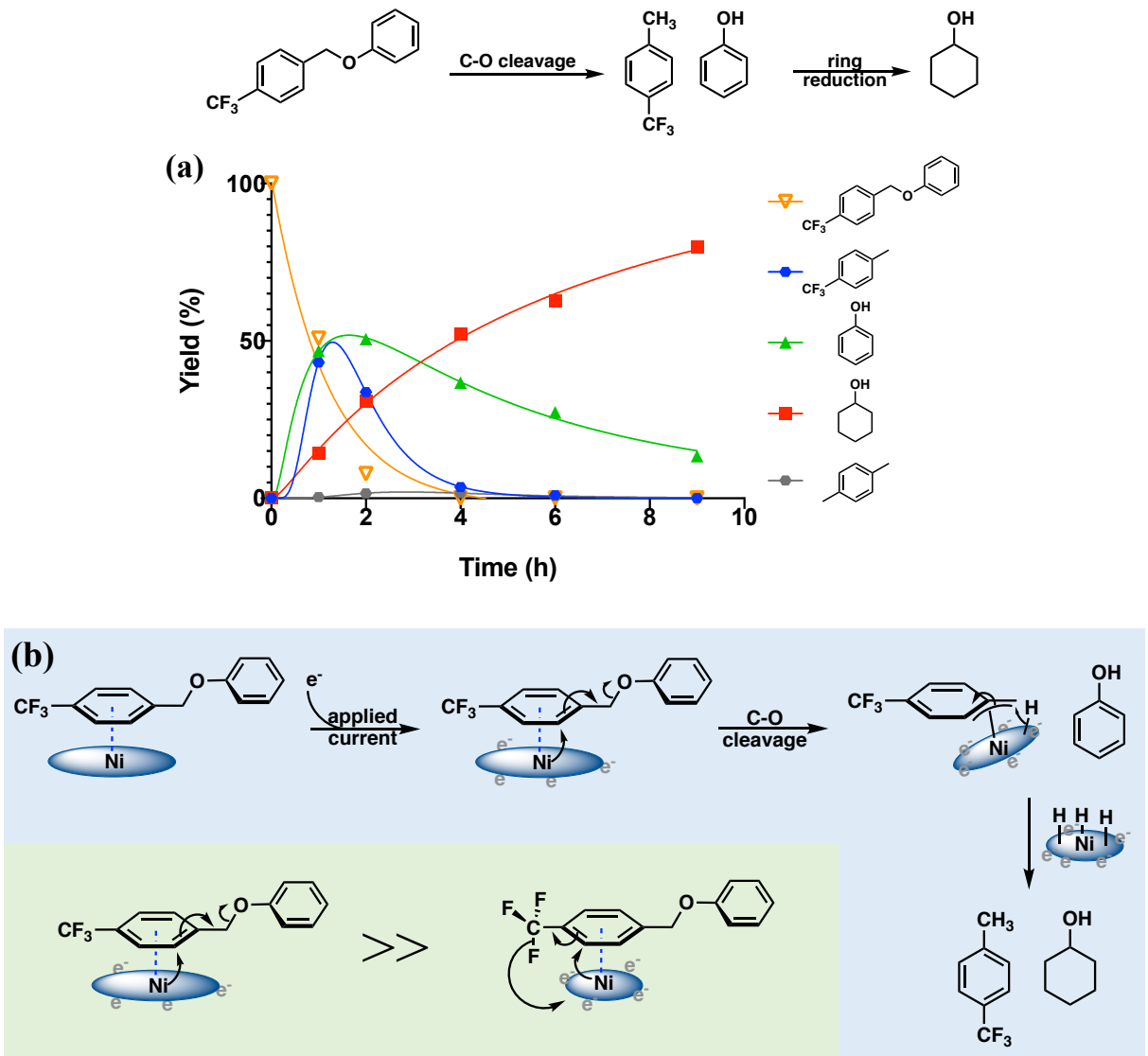

Figure 5.6 (a) Electrocatalytic hydrogenation of para-perfluorinated benzyl phenyl ether over a skeletal nickel electrode at 50 mA in the aqueous mixture of pH 8 borate buffer/IPA (2:1) at 60 °C under ambient pressure. (b) Proposed electrocatalytic cleavage mechanism of para-perfluorinated benzyl phenyl ether.

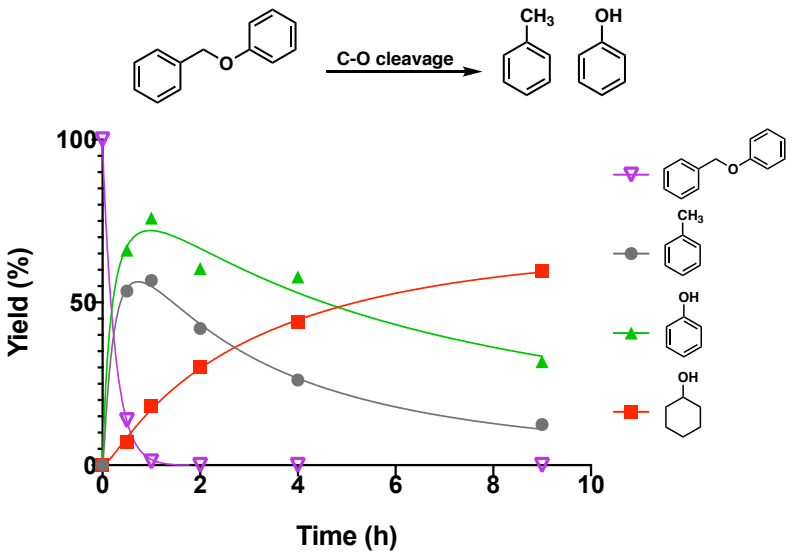

Figure 5.7 Electrocatalytic hydrogenation of benzyl phenyl ether over a skeletal nickel electrode at 50 mA in the aqueous mixture of pH 8 borate buffer/IPA (2:1) at 60 °C under ambient pressure.

ECH of simple benzyl phenyl ether was also tested (Figure 5.7). This substrate undergoes C-O ether cleavage to form toluene and phenol substantially faster than the trifluoromethylated case shown in Figure 5.6. When compared its cleavage rate with other previously examined ethers, benzyl phenyl ether shows the fastest cleavage rate among all these simplest unfunctionalized aryl ethers (Figure 5.8).

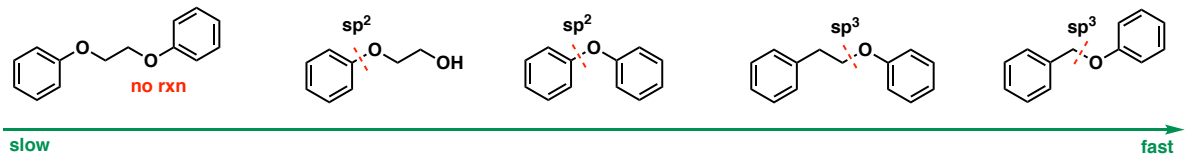

Figure 5.8 Cleavage hierarchy of different aryl ethers.

5.3 Surface Topology of Plated Skeletal Nickel Electrode

As previously reported by Hao, catalyst characterization via Scanning Electron Microscopy (SEM) was used to analyze the surface topology of plated Raney® nickel electrode.[10] A spiky polycrystalline morphology was found, which is significantly different from reported electron micrographs of the conventional activated Raney® nickel powders.[5, 11, 12] Meanwhile, as reported by Bao and co-workers, structural variations of Raney® nickel particles have a crucial on the catalytic reactivity.[12] As shown in Figure 5.9, highly porous skeletal nickel offers various types of aryl ether cleavage in the ECH context. The high surface area of Raney® nickel ensures its high reactivity, which enables cleavage of the strong diaryl ether C-O bonds.

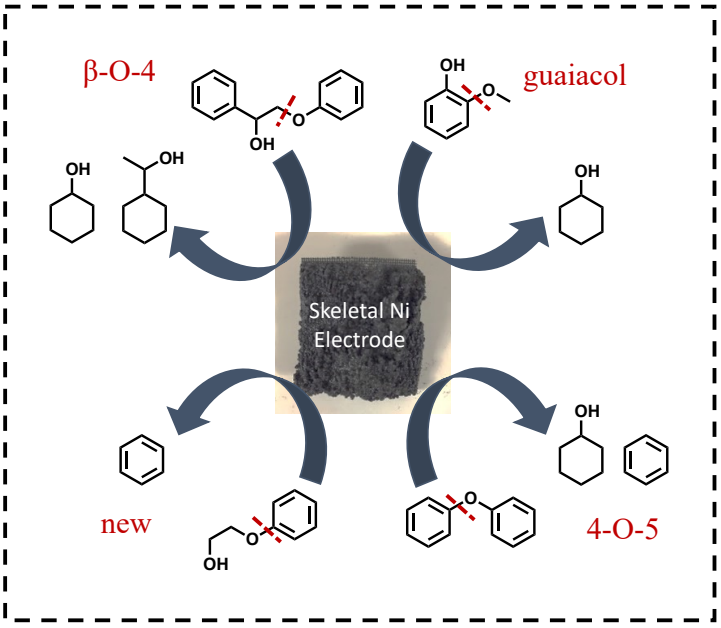

Figure 5.9 Skeletal nickel electrode enabled various ether cleavages.

SEM images taken by Hao suggested that the high reactivity of this plated and activated electrode is correlated with the sharpness and spikiness of its surface crystallinity (Figure 5.10).

Notably, commercially available activated Raney® nickel powder does not display such sharp spiky features.[5]

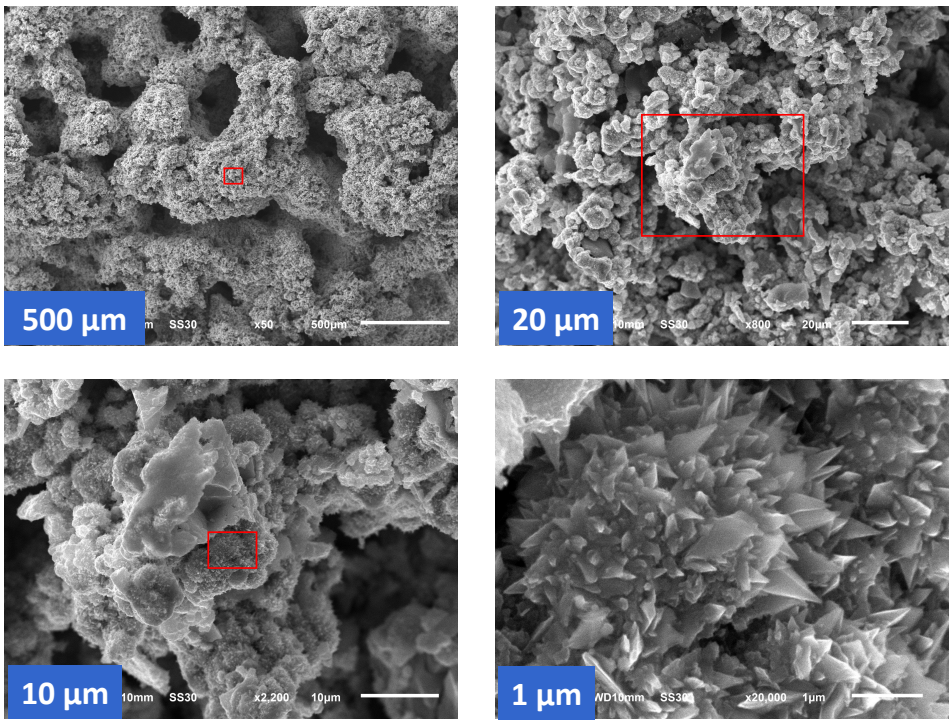

Figure 5.10 High resolution SEM images of fresh activated skeletal nickel electrode taken by Hao.

Therefore, it is natural to believe that the spiky form of the surface clusters may come from the electro-plating process. The composition and nano-variations of these sharp spikes were analyzed through transmission electron microscopy (TEM). The TEM samples were prepared by scraping off some of the surface clusters from the plated electrode; these scraped off surface clusters were then crushed into smaller particles and dispersed on the copper grid (lacey carbon film support). Figure 5.11 shown a general view of the dispersed particles on the sample grid. Evidently, the scraping and crushing processes resulted in significantly variable particle sizes. The larger particles were difficult to analyze by transmission electron microscope, so subsequent analysis focused on the smaller particles.

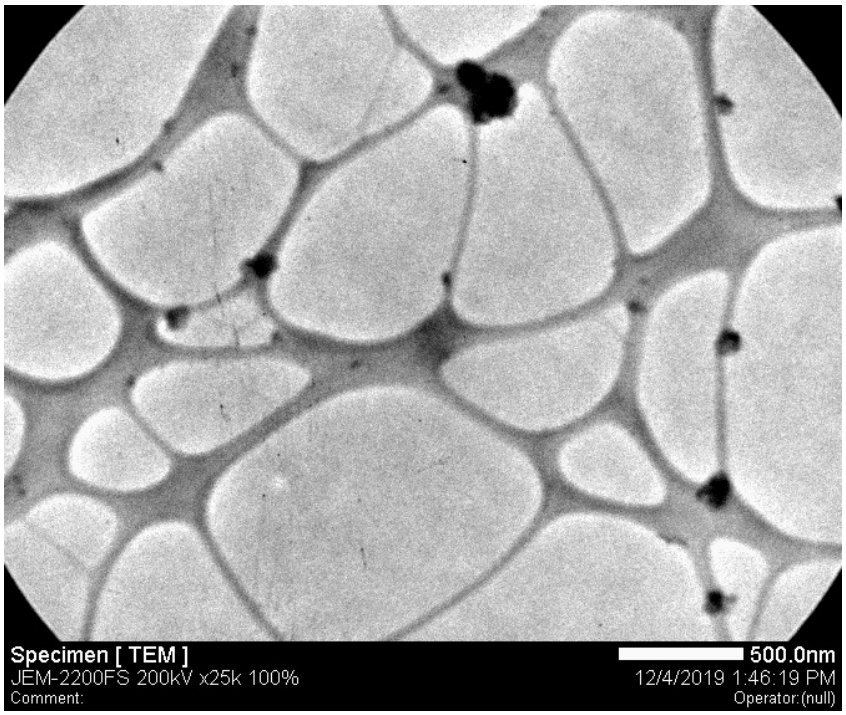

Figure 5.11 Dispersed metal particles of freshly prepared skeletal Ni electrode. Particle size varied significantly from the TEM sample preparation processes. As shown, black metal particles in variable sizes were spread on the lacy carbon support (grey).

Two distinct nickel particles were examined under high resolution. Particle 1 (Figure 5.12) has a defined tip in contrast to particle 2 (Figure 5.13). Significantly different from the denser particle 2, particle 1 seems to be composed of numerous smaller Ni nanoparticles, as reflected from by white voids between the small nano-units. Meanwhile, at higher focus (Figure 5.12 c), the morphological variations of this single particle were more obvious. However, different from particle 1, particle 2 was mostly composed of Ni, showing no voids or pores on its bulk surface. At higher magnification the atomic layout of the Ni metal is more uniform when compared with particle 1. Thus, the atomic microstructures of the plated skeletal Ni surface are complicated. If only determined by the shapes of these two selected particles, particle 1 may more likely be a nano-representation of the spiky tips in the SEM image.

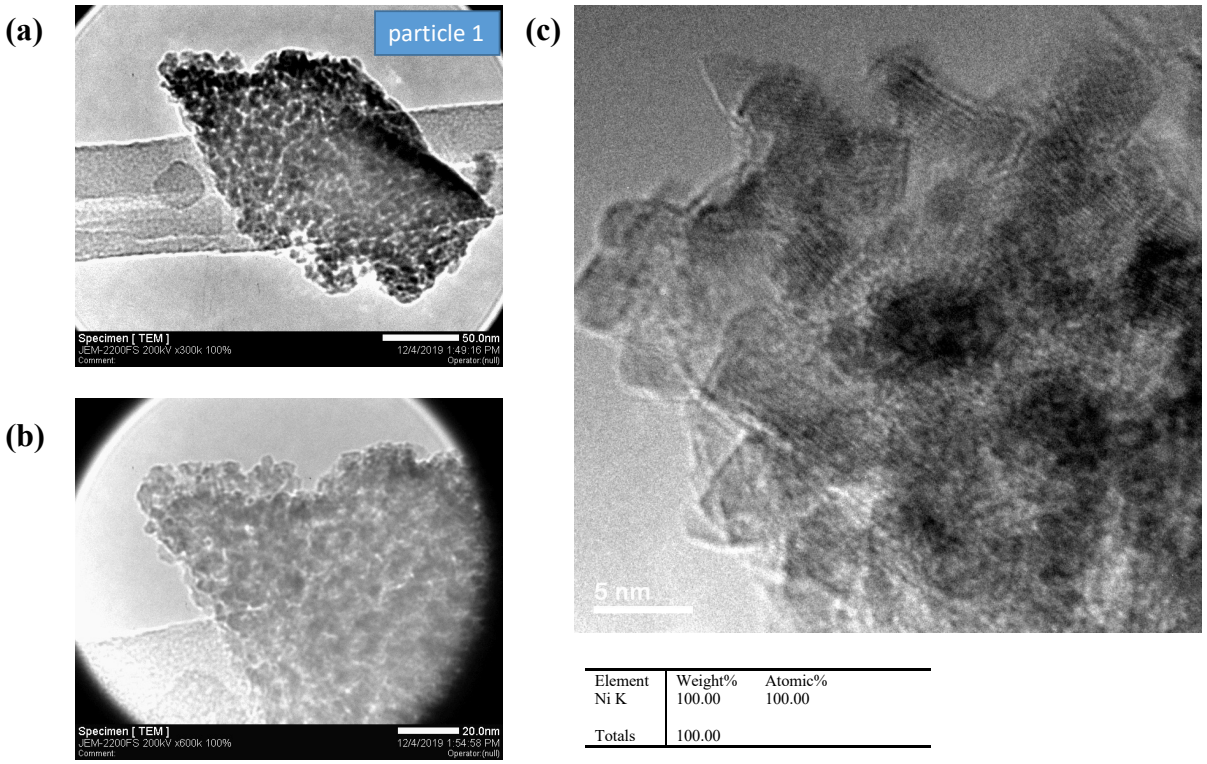

Figure 5.12 TEM images of particle from freshly activated skeletal nickel electrode (a) particle 1 (b) magnified of the tip of particle 1 (c) high resolution focused image of the tip of particle 1

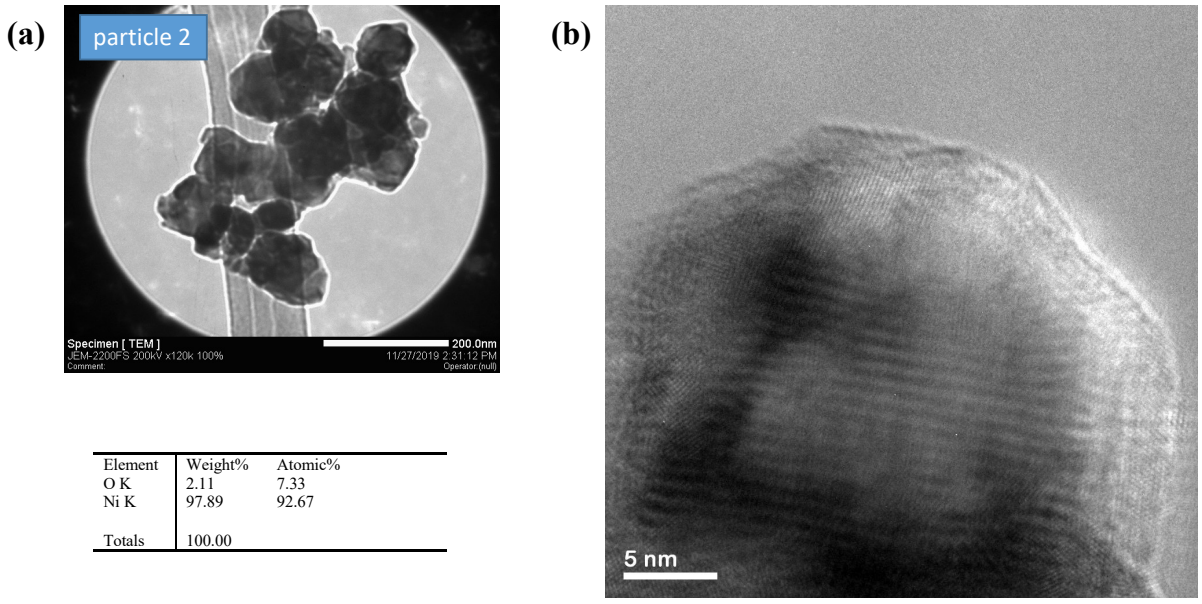

Figure 5.13 TEM images of particle 2 from fresh activated skeletal nickel electrode (a) particle 2 (b) high resolution focused image of particle 2

5.4 Conclusion

Along with the catalytic cleavage mapping of various functionalized diaryl ethers, the skeletal nickel catalyzed aqueous electrocatalytic hydrogenation/hydrogenolysis (ECH) method was also found to effect the defluorination of both perfluoromethyl and fluoro substituted aryl ethers. Thus, skeletal Ni electrodes are able to activate of both sp^2 and sp^3 C-F bonds. In the fluorinated arene ethers, defluorination always occurred prior to the cleavage of C-O ether bond. However, in the case of the trifluoromethylated benzyl phenyl ether, the C-O ether bond broke before reduction of the C-F bonds. On the basis of both aryl ether cleavage mechanistic findings and the observations of the C-F reduction, defluorination mechanisms were proposed for the corresponding organofluorides.

The detailed microcrystalline morphology of electroplated skeletal nickel surface was analyzed via transmission electron microscope. Under high magnification, distinct morphologies were also found between small nickel clusters. Some were agglomerated from numerous smaller nanoparticles, while some shown a denser uniform bulk surface.

REFERENCES

REFERENCES

1. Purser, S.; Moore, P. R.; Swallow, S.; Gouverneur, V., Fluorine in medicinal chemistry. *Chemical Society Reviews* **2008,** *37* (2), 320-330.

2. Samanta, P.; Desai, A. V.; Let, S.; Ghosh, S. K., Advanced Porous Materials for Sensing, Capture and Detoxification of Organic Pollutants toward Water Remediation. *ACS Sustainable Chemistry & Engineering* **2019,** *7* (8), 7456-7478.

3. Coleman, N. V.; Rich, D. J.; Tang, F. H. M.; Vervoort, R. W.; Maggi, F., Biodegradation and Abiotic Degradation of Trifluralin: A Commonly Used Herbicide with a Poorly Understood Environmental Fate. *Environmental Science & Technology* **2020,** *54* (17), 10399-10410.

4. Baumgartner, R.; McNeill, K., Hydrodefluorination and Hydrogenation of Fluorobenzene under Mild Aqueous Conditions. *Environmental Science & Technology* **2012,** *46* (18), 10199-10205.

5. Ma, X. X.; Liu, S. J.; Liu, Y.; Gu, G. D.; Xia, C. H., Comparative study on catalytic hydrodehalogenation of halogenated aromatic compounds over Pd/C and Raney Ni catalysts. *Scientific Reports* **2016,** *6*, 11.

6. Baumgartner, R.; Stieger, G. K.; McNeill, K., Complete Hydrodehalogenation of Polyfluorinated and Other Polyhalogenated Benzenes under Mild Catalytic Conditions. *Environmental Science & Technology* **2013,** *47* (12), 6545-6553.

7. Clot, E.; Eisenstein, O.; Jasim, N.; Macgregor, S. A.; McGrady, J. E.; Perutz, R. N., C-F and C-H Bond Activation of Fluorobenzenes and Fluoropyridines at Transition Metal Centers: How Fluorine Tips the Scales. *Accounts of Chemical Research* **2011,** *44* (5), 333-348.

8. Colomban, C.; Kudrik, E. V.; Afanasiev, P.; Sorokin, A. B., Catalytic Defluorination of Perfluorinated Aromatics under Oxidative Conditions Using N-Bridged Diiron Phthalocyanine. *Journal of the American Chemical Society* **2014,** *136* (32), 11321-11330.

9. Young, R. J.; Grushin, V. V., Catalytic C-F bond activation of nonactivated monofluoroarenes. *Organometallics* **1999,** *18* (3), 294-296.

10. Hao, P., Electrocatalytic Hydrogenation of Monomeric, Dimeric, and Polymeric Lignin Model Compounds with Raney Nickel: Chemistry, Mechanistic, and Product Toxicity Studies. Michigan State University, East Lansing, MI, 2018.

11. Gao, X. L.; Mo, W. L.; Ma, F. Y.; Noritatsu, T.; Wu, H. L.; Fan, X., Effects of a forming process on the properties and structure of RANEY (R)-Ni catalysts for the hydrogenation of 1,4-butenediol. *RSC Advances* **2020,** *10* (10), 5516-5524.

12. Lei, H.; Song, Z.; Tan, D. L.; Bao, X. H.; Mu, X. H.; Zong, B. N.; Min, E. Z., Preparation of novel Raney-Ni catalysts and characterization by XRD, SEM and XPS. *Applied Catalysis a-General* **2001,** *214* (1), 69-76.

Chapter 6 Conclusions and Future Directions

The goal of this project was to further explore and improve the electrocatalytic strategy to depolymerize lignin and convert both lignin and aryl ether derived organic pollutants into valuable chemicals. An important motivation is the completion of the cycle of carbon and energy, which will help mitigate the increasing challenges of climate change, energy shortage, and surface water pollution. To achieve this objective, this document demonstrated a mild, effective and water compatible electrocatalytic hydrogenolysis/hydrogenation approach to convert a large set of aryl ethers and alkyl aryl ethers into small molecules (saturated higher energy units or valuable aromatic monomers). Both water soluble and water insoluble ether substrates were explored. Importantly, several distinct electrocatalytic cleavage mechanisms of different structurally varied aryl ethers were identified, by examining the mechanistic variations induced by the various substituents. These efforts led to the discovery of C-F activation by the Ni cathode (Figure 6.1). The insights from this work also offer guiding principles for rational catalytic design.

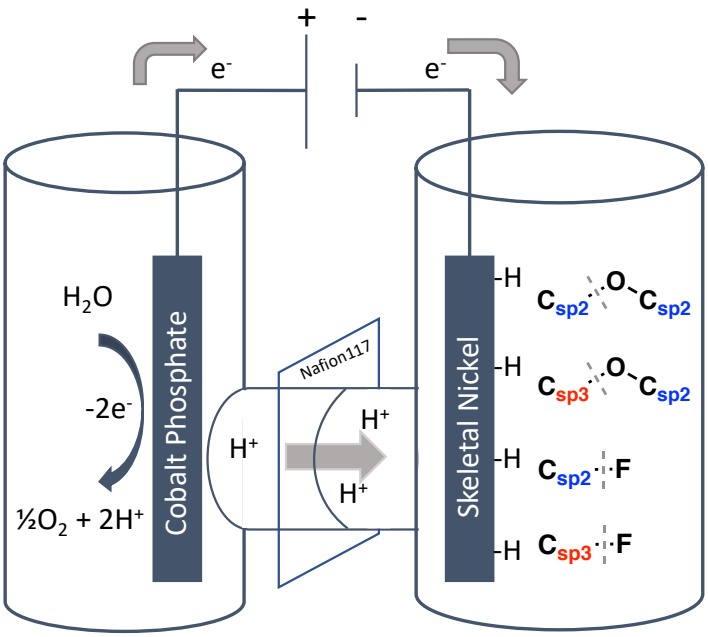

Figure 6.1 This electrocatalytic hydrogenation (ECH) approach offered four different types of carbon-oxygen/carbon-fluorine bond cleavage in aqueous media.

Future directions of electrocatalytic hydrogenation include:

1) Somewhat unexpectedly, electrocatalytic C-F activation of perfluoroalkyl aryl ether was discovered occurring over the surface of skeletal nickel electrodes. Per- and polyfluoroalkyl substances (PFAS, Figure 6.2) are one of the major and highly persistent contaminations in water systems, and they accumulate over time in both the environment and the human body. Preliminary studies have shown that long term exposure of PFOS and PFOA can lead to adverse health issues in humans (such as problems for reproduction, liver and kidney issues, and immunological effects). The ability of skeletal Ni electrode to activate inert C-F bonds in the aryl ethers studied here suggests that such approach in the activation of C-F bond in PFAS might offer a strategy for their mitigation by reductive defluorination.

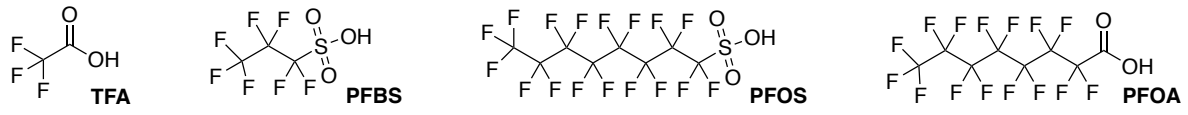

Figure 6.2 Chemical structures of trifluoroacetic acid and three common per- and polyfluoroalkyl substances (PFAS).

2) Chapter 4 has demonstrated the successful cleavage of diaryl ethers from ECH via skeletal Ni electrode. And in both chapters 3 and 4, this Ni electrode has shown high reactivity toward the activation of benzylic C-Hs. Thus, it is reasonable to hypothesize that this approach could be

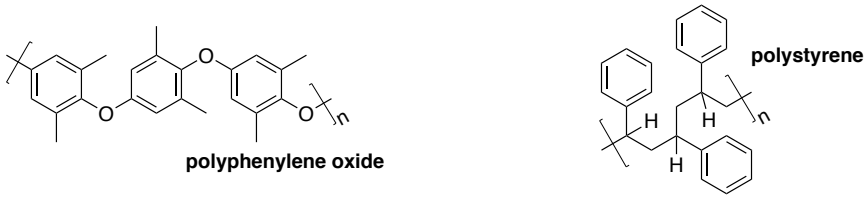

Figure 6.3 Structures of polyphenylene oxide and polystyrene.

applied in the depolymerization of polyphenylene oxide (PPO) and possibly polystyrene (Figure 6.3), addressing plastic pollution, which is another serious global crisis for this century.

3) As described in chapter 2, water-insoluble substrates required addition of the amphiphilic 2-propanol as co-solvent (up to 33% v/v) to assist substrate dissolution. Under this high organic co-solvent content, to reach the desired current (for example 50 mA) higher applied voltage was required (~10 V). Thus, to increase the energy efficiency of ECH, addition of additional salt ions (for example NaCl) can lower the voltage. A list of buffer salt combinations can be searched to further optimize the reaction conditions.

4) In 2014, Esposito reported heterogeneous TiNi bimetallic solid catalyst for the hydrogenolysis of aryl ethers. This bimetallic Ti containing metal catalyst showed the opposite cleavage regioselectivity from our Ni catalyst. Therefore, investigation of bimetallic electrodes (such as TiNi, CuNi) will be important for further study of the relationships between the cleavage selectivity and the metal composition. The second metal ion can be introduced during the plating process by addition of another metal ion source to the plating solution.